AN ESCHER AWARE PATTERN ANALYSIS: SYMMETRY BEYOND SYMMETRY GROUPS

A THESIS SUBMITTED TO
THE GRADUATE SCHOOL OF NATURAL AND APPLIED SCIENCES
OF
MIDDLE EAST TECHNICAL UNIVERSITY

BY

VENERA ADANOVA

IN PARTIAL FULFILLMENT OF THE REQUIREMENTS
FOR
THE DEGREE OF DOCTOR OF PHILOSOPHY
IN
COMPUTER ENGINEERING

SEPTEMBER 2015

Approval of the thesis:

AN ESCHER AWARE PATTERN ANALYSIS: SYMMETRY BEYOND SYMMETRY GROUPS

submitted by **VENERA ADANOVA** in partial fulfillment of the requirements for the degree of **Doctor of Philosophy in Computer Engineering Department, Middle East Technical University** by,

Prof. Dr. Gülbin Dural Ünver
Dean, Graduate School of **Natural and Applied Sciences** ________________

Prof. Dr. Adnan Yazıcı
Head of Department, **Computer Engineering** ________________

Prof. Dr. Sibel Tarı
Supervisor, **Computer Engineering Dept., METU** ________________

Examining Committee Members:

Prof. Dr. Kemal Leblebicioğlu
Electrical and Electronics Engineering Department, METU ________________

Prof. Dr. Sibel Tarı
Computer Engineering Department, METU ________________

Prof. Dr. Ahmet Coşar
Computer Engineering Department, METU ________________

Assoc. Prof. Dr. Tolga Can
Computer Engineering Department, METU ________________

Assoc. Prof. Dr. Mine Özkar Kabakçıoğlu
Architecture Department, ITU ________________

Date: ________________

I hereby declare that all information in this document has been obtained and presented in accordance with academic rules and ethical conduct. I also declare that, as required by these rules and conduct, I have fully cited and referenced all material and results that are not original to this work.

Name, Last Name: VENERA ADANOVA

Signature :

ABSTRACT

AN ESCHER AWARE PATTERN ANALYSIS: SYMMETRY BEYOND SYMMETRY GROUPS

Adanova, Venera
Ph.D., Department of Computer Engineering
Supervisor : Prof. Dr. Sibel Tarı

September 2015, 211 pages

Ornaments constructed by repeating a base motif, timeless and ubiquitous, link culture, art, science and mathematics. To this date, the mathematical study of the ornaments has been the study of discrete symmetry groups and permutations. As such, the study merely focuses on the mechanical side of repetition, ignoring the artistic aspects (symmetry breaking strategies via intriguing choices of form and color permutations) that make ornaments such bewildering objects. Taking our inspiration from Escher's art, we study all aspects of ornamental patterns not only considering the usual mathematical properties but also other idiosyncratic features that are often more important in perception, aesthetics, art and design and as well as in appreciating cultural heritage.

Our novelty is to replace the structure extraction problem with a content attenuation or suppression problem. When content is suppressed, clues to the repetition structure emerge. We show that based on content-suppressed images, unit cells and fundamental regions of planar ornaments can be robustly extracted even for ornaments with peculiar color permutations. Moreover, using tools of deep learning, we perform key validation tests showing that our coding via content-suppression makes it possible to construct content-dependent, subjective and more importantly continuous characterizations of the underlying symmetry behavior.

Keywords: Symmetry, ornament, content/style, wallpaper groups, color symmetry

ÖZ

ESCHER TARZI BEZEMELERİN ANALİZİ: SİMETRİ GRUPLARIN ÖTESİNDE SİMETRİ

Adanova, Venera
Doktora, Bilgisayar Mühendisliği Bölümü
Tez Yöneticisi : Prof. Dr. Sibel Tarı

Eylül 2015 , 211 sayfa

Baz motiflerin tekrarlanması sonucunda oluşan bezemeler, zaman ve mekandan bağımsız olarak, kültür, sanat, bilim ve matematiği bağlamaktadır. Bu güne kadar, bezemelerin matematiksel modelleri ayrık simetri gruplarının ve permütasyonlar ile sınırlanmıştır. Bu tür çalışmalar tekrarlanmış yapıların mekanik yönlerine odaklanmış olup, bezemelerin sanatsal yönleri (ilgi çekici form ve renk permütasyonların aracılığıyla simetri kırma yöntemleri) ihmal edilmiştir. Escher'in sanatından esinlenerek, biz bezemelerin sadece klasik matematiksel özelliklerini incelemekle sınırlı kalmayıp, algı, estetik, sanat ve tasarımda daha da önemli olan özelliklerini araştırmaktayız.

Bizim önerdiğimiz yeni yaklaşım, yapı çıkarma problemini içerik bastırma problemiyle değiştirmektir. İçeriğin bastırılması bezemelerin tekrarlama yapısına dair ipuçları ortaya çıkarır. İçeriği bastırılmış görüntüleri kullanarak tuhaf renk permütasyonları olan düzlemsel bezemelerin bile temel bölgeleri sağlam olarak çıkarılabileceğini göstermekteyiz. Üstelik, derin öğrenim araçlarını kullanarak, bizim içerik bastırma yöntemimizin simetri davranışının içeriğe bağlı, subjektif ve daha da önemlisi devamlı niteliğini kurma imkanını verdiğini gerçekleştirdiğimiz deneylerle göstermekteyiz.

Anahtar Kelimeler: Simetri, bezeme, içerik/stil, simetri grupları, renk simetri

To my family

ACKNOWLEDGMENTS

Foremost, I would like to thank my advisor Prof. Dr. Sibel Tari for her constant support, guidance, enthusiasm and patience. Every meeting with her has been a contribution to my self-confidence and desire to explore unexplored.

I would like to thank jury committees: Prof. Dr. Kemal Leblebicioğlu, Prof. Dr. Ahmet Coşar, Assoc. Prof. Dr. Tolga Can and Assoc. Prof. Dr. Mine Özkar Kabakçıoğlu, for their encouragement and insightful comments.

My sincere thanks go to my husband, Maksat. This thesis would not be possible without his support and help. I thank my son, Amir, for giving meaning to my life.

TABLE OF CONTENTS

LIST OF TABLES

TABLES

LIST OF FIGURES

FIGURES

LIST OF ABBREVIATIONS

SMDS	Spectral Multidimensional Scaling
SIFT	Scale-Invariant Feature Transform
tSNE	t-Stochastic Neighbor Embedding

CHAPTER 1

INTRODUCTION

Symmetry is a language of nature. It introduces order and proportionality. People with symmetric faces are considered aesthetically pleasing, people with symmetric bodies considered to be the ones with the right genes; even the music is perceived as more pure and beautiful, when it is symmetric. People are used to symmetry and tend to reflect it in their daily life. The buildings, decorations, furniture, vehicles, to name the few, are all symmetrical. In the scientific world, the symmetry is irreplaceable in the study of crystals. It can explain violent structures in microbiology, such as viruses. This all motivate scientists to study symmetry.

The theory on symmetry, as we know it today, began with the group theory introduced by Évariste Galois [19]. With his theory motion became a characterizing feature of symmetry. Adopting the group theory, several researchers [59, 54, 55] came up with the symmetry group classifications. Though not directly, Galois produced a language that enables to see the similarities and differences of symmetries underlying visually different patterns.

The symmetry is defined as a distance-preserving transformation (isometric operations) on some object that leaves that object unchanged. If we restrict ourselves to a single object, then there are only two isometries that can be applied upon it: rotations and reflections. Extending the definition to a multiple copies of the same object in the plane by introducing more freedom in movement gives four planar isometries that leave the object unchanged. Those four planar isometries are known as translation, rotation, reflection, and glide reflection.Figs. 1.1-

1.3 illustrate four isometries. An object has translational symmetry, when a copy of it is moved in a certain direction by a certain distance (See Fig. 1.1).

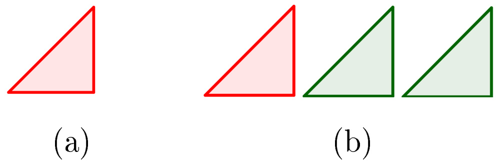

Figure 1.1: Translational symmetry. (a) Original object. (b) Translational symmetries of original object.

Reflection symmetry of an object can be achieved by reflecting a copy of it across certain axis, whereas the glide reflection is achieved by reflecting a copy of an object across certain axis and then moving the reflected copy in a certain direction by a certain distance (Fig. 1.2).

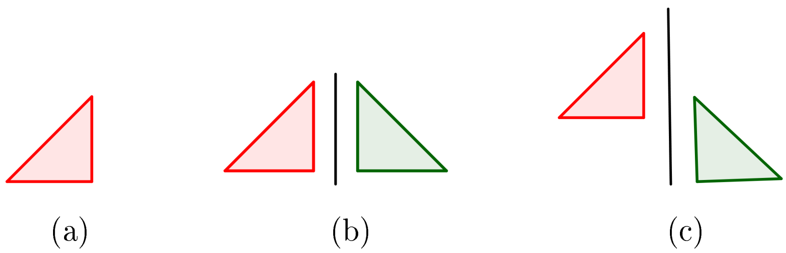

Figure 1.2: Reflectional and glide reflectional symmetries. (a) Original object. (b) Reflectional symmetry. (c) Glide reflectional symmetry.

If one chooses any point on an object and rotates a copy of it around that point by a certain degrees, a rotational symmetry for that object is obtained. Depending on the amount of degrees chosen to rotate, two-fold, three-fold, four-fold or six-fold rotational symmetries are obtained (Fig. 1.3).

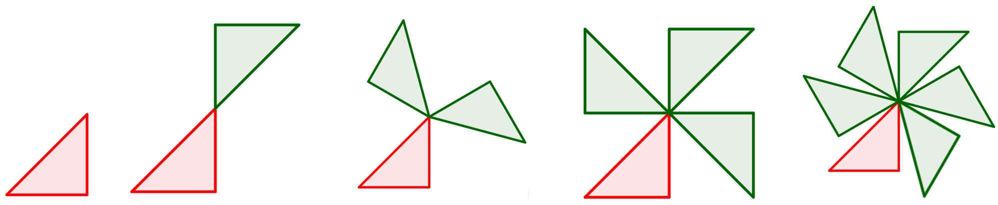

Figure 1.3: Rotational symmetry. (a) Original object. (b) Two-fold rotational symmetry. (c) Three-fold rotational symmetry. (d) Four-fold rotational symmetry. (e) Six-fold rotational symmetry.

1.1 Tilings

If we choose some motif (tile) and repeat it infinitely many times in two directions, using aforementioned four planar isometries, we obtain a tiling (an ornament). The plane should be filled so that no gaps or overlaps introduced. In Fig. 1.4 only Fig. 1.4(a) illustates a true tiling, while the second and the third ones are not tilings due to overlaps introduced in the second one (on the second row second tile overlaps the first tile), and the gaps introduced in the third one (on the second row there is a gap between first and second tiles). It should be noted that no matter what isometries being used to fill the plane, translational symmetry is always one of them. In other words, not all the tilings have reflectional, rotational or glide reflectional symmetries, however, all of them contain a translational symmetry. This is natural, since without translational symmetry it would be impossible to repeat a motif infinitely many times to fill the plane.

Periodic Tilings. For a tiling to be periodic, it should have a finite region, which can recreate the entire tiling only by translating the copies of that region. Also, the periodic tiling has a translational vector of a minimum length in two different directions that maps it onto itself. Consider two tilings given in Fig. 1.5. The tiling in Fig. 1.5(a) has translational vector of minimal length in vertical direction, but not in horizontal direction. See how the number of square tiles increased by one each time the thin rectangle tile is encountered. Hence, this

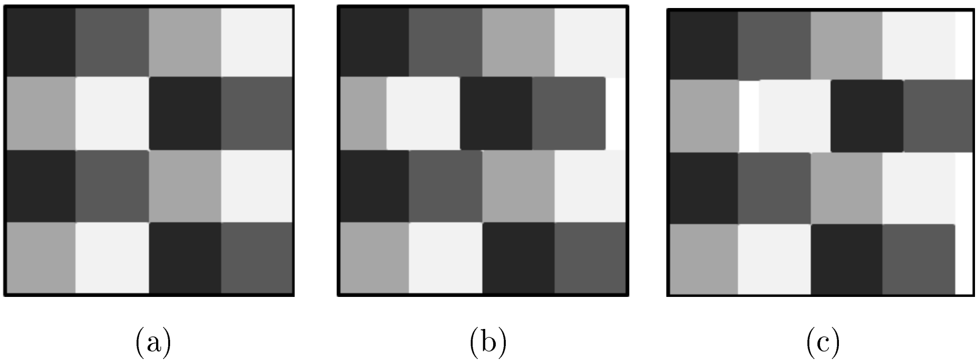

Figure 1.4: Tiling vs. non-tilings. (a) True tiling. (b) Not a tiling due to overlaps. (c) Not a tiling due to gaps.

tiling is not periodic, while the second one is periodic.

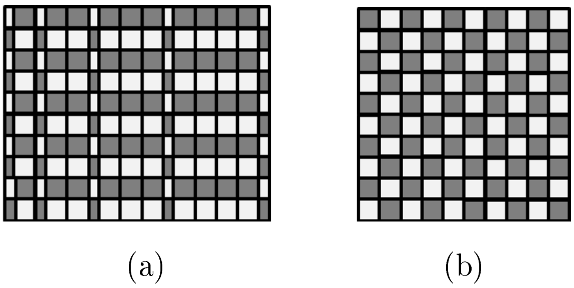

Figure 1.5: Periodic vs. non-periodic tilings. (a) Non periodic tiling. (b) Periodic tiling.

Symmetries of Cultures. Ornaments are found in every culture. Various works of anthropologists and art historians [80] reveal that different cultures prefer different symmetries when creating their ornaments. They come to believe that the preference of a culture for specific symmetries is not random, and that these symmetries symbolize cultural ideas and social structures within a culture. In [71], Shepard pointed out that the symmetry analysis can help distinguish the subtle and varied changes of styles between art designs of different cultures. Based on this, the study of ornaments has become one of the tools to study different cultures and cultural relations.

One of the major cultural art designs lie in the walls of Alhambra palace. There, we can observe various ornaments that are representatives of Islamic

Art. Though being highly symmetrical structures, those ornaments are created by non-mathematicians, who were not aware of the theories behind the symmetry. Fig. 1.6 illustrates some of the ornaments found in Alhambra palace.

Figure 1.6: Examples of ornaments found in Alhambra palace

Beautiful examples of ornaments from modern art are found in the works of M. C. Escher. What makes his work unique is the presence of meaning introduced via recognizable figures that are interlocked to form repeating patterns (See Fig. 1.7). Accompanied with interesting color permutations, his ornaments are the bewildering samples of visions of symmetry. Although Escher never considered himself as a mathematician, his works have been alluring scientific minds for decades.

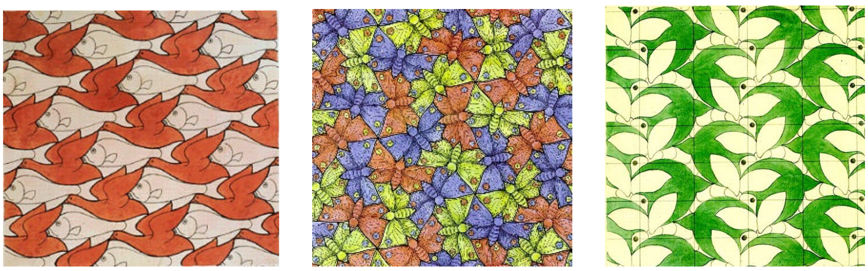

Figure 1.7: Some examples from M. C. Escher's works

1.1.1 Lattices

Each periodic tiling is associated with a *lattice*, which can be put on a tiling so that all units of a lattice are repeated copies of each other. To obtain an underlying lattice of a tiling, the easiest way would be to choose any point in the tiling, mark its translated copies with dots and connect those dots. The marked dots are *lattice points*, and each unit of the lattice is known as *unit cell*.

It is worth mentioning that, usually, the centers of highest order of rotations are chosen as lattice points. One can reconstruct the entire tiling only by translating the unit cell in two different directions. There are only five types of different lattices: *parallelogram*, *rectangular*, *square*, *rhombic*, and *hexagonal*. Fig. 1.8 illustrates five lattices on different tilings. For each tiling, a few red dots are shown to represent lattice points. The simplest one of all five is the square lattice, which has equal sides (a) and an angle of 90° between two sides. A rectangular lattice is similar to square lattice, but the sides are not of equal length (a, b). Another type of lattice of interesting name is a hexagonal lattice. It represents a rhombus that is constructed by two equilateral triangles. The name hexagon comes from the fact that for each lattice point the closest lattice points lie on the hexagon. A rhombic lattice has equal sides (a) but the angle between sides is other than 60° or 90°. A parallelogram lattice is a rhombic lattice with the sides of different length (a, b).

Notice that the symmetries that a tiling exhibit restricts possible lattice types that might be associated with it. For example, if a tiling has reflectional symmetry, then its lattice must be rhombic, rectangular or square. A tiling with 90° rotational symmetry has a square lattice, while the tilings with 60° or 120° rotational symmetries have a hexagonal lattice.

1.1.2 Symmetry Group and Fundamental Domain

Given a tiling, defining the set of all the isometries that maps the tiling onto itself, gives the *symmetry group* of the tiling. Knowing the symmetry group of a tiling enables the recreation of the entire tiling from a small portion of it. Such small portion is known as *fundamental domain* or the *generating region* of a tiling. It is a smallest region on the tiling that would be enough to recreate the entire tiling by applying all the isometries that the symmetry group of the original tiling exhibit. The size of a fundamental domain is always a rational part of the unit cell. Fig. 1.9 shows a tiling with two different motifs, the unit cell and the fundamental domain of the tiling. The fundamental domain is 1/4 part of the unit cell. Another example is shown in Fig. 1.10 but this time for the tiling

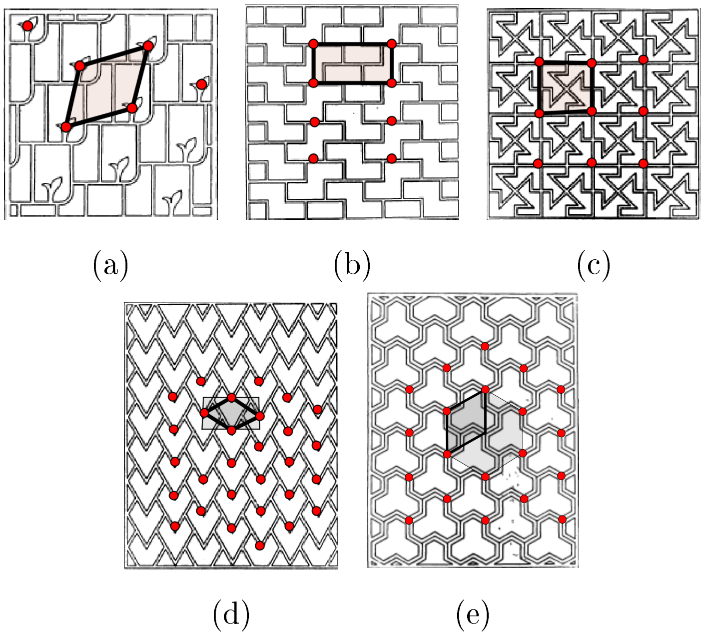

Figure 1.8: Five lattice types. Tilings taken from [66]. (a) Parallelogram lattice. (b) Rectangular latice. (c) Square lattice. (d) Rhombic lattice. (e) Hexagonal lattice.

that consists of one motif of different colors. This is an interesting example. The tiling remains in the same symmetry group both when the colors are ignored and when the colors are considered. However, the unit cell and, hence, the fundamental domain differ depending on whether the color is considered or not. Top row of Fig. 1.10 (b) shows the unit cell obtained ignoring the colors, while the bottom row illustrates the one obtained taking the colors into account. The fundamental domains for both unit cells are given in Fig. 1.10 (c), which are 1/4 part of the unit cells. Fig. 1.10 (d) shows the results of tile recreation from two different unit cells. Observe that for the first case the colors interchange, while for the second we recreate the exact copy of the original tiling. Observe also that the fundamental domain for the first case contain smaller portion of a tiling.

Note that, by translating the unit cell obtained for tilings in two different directions, we can recreate the entire tiling. However, using the fundamental domain we can recreate the entire tiling by apply all the isometries upon it that are in the symmetry group of a tiling.

(a) (b) (c)

Figure 1.9: Fundamental domain. (a) Two motif tiling with glide reflections. (b) Unit cell. (c) Fundamental domain.

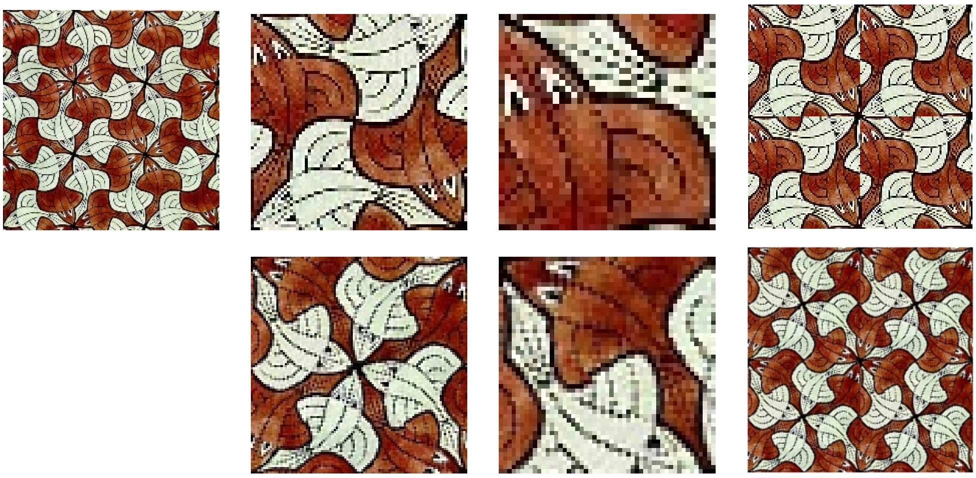

(a) (b) (c) (d)

Figure 1.10: Fundamental domain. (a) A single motif tiling with four-fold rotations. (b) (Top row) Unit cell obtained ignoring the colors. (Bottom row) unit cell obtained considering the color permutation. (c) Fundamental domains. (d) Recreation of the tiling using translational copies of the unit cell.

One might think that given a fundamental domain, constructing an entire tiling using its symmetry group is impossible since it can be applied in infinitely many ways. For example, consider a triangular fundamental domain given in Fig. 1.11 (a). If the given symmetry group contains reflections, one would think that the reflections can be done in many different ways. One way would be to choose some reflection axis within the triangle as given in Fig. 1.11 (b) , and reflect the triangle along that axis. This situation is illustrated in Fig. 1.11 (c). Clearly, in this manner, recreation of the original tiling would be impossible. However, such situations are not possible for several reasons. First, the definition of tiling does not permit overlaps. Second, by doing so we obtain entirely new motif that has a reflection within itself as shown in Fig. 1.11 (d). Finally, to recreate a tiling that is filled with the new motif, we need completely different fundamental domain that is shown in Fig. 1.11 (e).

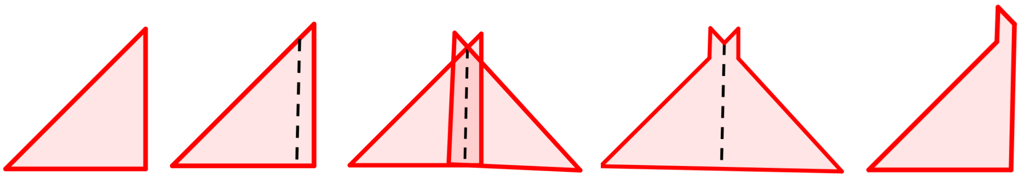

(a) (b) (c) (d) (e)

Figure 1.11: A new motif vs. funadamental domain

1.1.3 Wallpaper Groups

Recall five lattice types defined above. A lattice defines the underlying structure of a tiling. When a tiling is associated with a lattice type, it means that the tiling cannot have symmetry more than the underlying lattice has. Thus, a tiling has a symmetry, which is less, or equals the symmetry of a lattice. This fact eases the way of considering all possible symmetry groups a tiling can have. Considering all possible combinations of isometries on five lattice types reveals that there are only seventeen different symmetry groups. This fact has been known for nearly a century after the works published by [59, 54, 55], though the enumeration of seventeen symmetry groups dates back long before it became publicly known. The seventeen groups are known as *Wallpaper Groups*. The first column of Table 1.1 enumerates the seventeen Wallpaper Groups. A notation used for naming different symmetry groups is the short version of the one in [28]. Each letter on the symmetry group name describes the group properties. The letter p stands for *primitive cell* and the letter c stands for *centered cell*. The primitive cell is a unit cell with the centers of highest order of rotation at the vertices. The centered cell is encountered only in two cases (cm and cmm symmetry groups), and is chosen so that the reflection axis is normal to one or both sides of the cell. An example for centered cell is shown Fig. 1.8 (d), where the centered cell is shown as an outline for the rhombic lattice. The number that comes after one of those two letters is the highest order of rotation that the ornament exhibits. The third and fourth letters can be m, which stands for mirror reflection, g, which stands for glide reflection, and 1, which denotes no symmetry axis. The symmetry axis for the third letter is normal to $x - axis$ and for the forth is at angle α to the $x - axis$. No symbols in the third and fourth position indicate that the group contains no reflection or glide reflection. The second letter in notation representing the highest order of rotation in a symmetry group can take only values 1, 2, 3, 4, and 6. This restriction is introduced by the *crystallographic restriction theorem*, which states that the patterns repeating in two dimension can only exhibit 180°, 120°, 90°, and 60° rotations. The simple proof for this theorem can be found in [73]. Fig. 1.12 illustrates unit cells with symmetries for seventeen Wallpaper Groups. The darker regions represent fundamental domains.

Table1.1: Wallpaper Groups

Type	Lattice	Highest Order of Rotation	Fundamental Domain
p1	parallelogram	1	1 unit
p2	parallelogram	2	1/2 unit
pm	rectangular	1	1/2 unit
pg	rectangular	1	1/2 unit
cm	rhombic	1	1/2unit
pmm	rectangular	2	1/4 unit
pmg	rectangular	2	1/4 unit
pgg	rectangular	2	1/4 unit
cmm	rhombic	2	1/4 unit
p4	square	4	1/4 unit
p4m	square	4	1/8 unit
p4g	square	4	1/8 unit
p3	hexagonal	3	1/3 unit
p3m1	hexagonal	3	1/6 unit
p31m	hexagonal	3	1/6 unit
p6	hexagonal	6	1/6 unit
p6m	hexagonal	6	1/12 unit

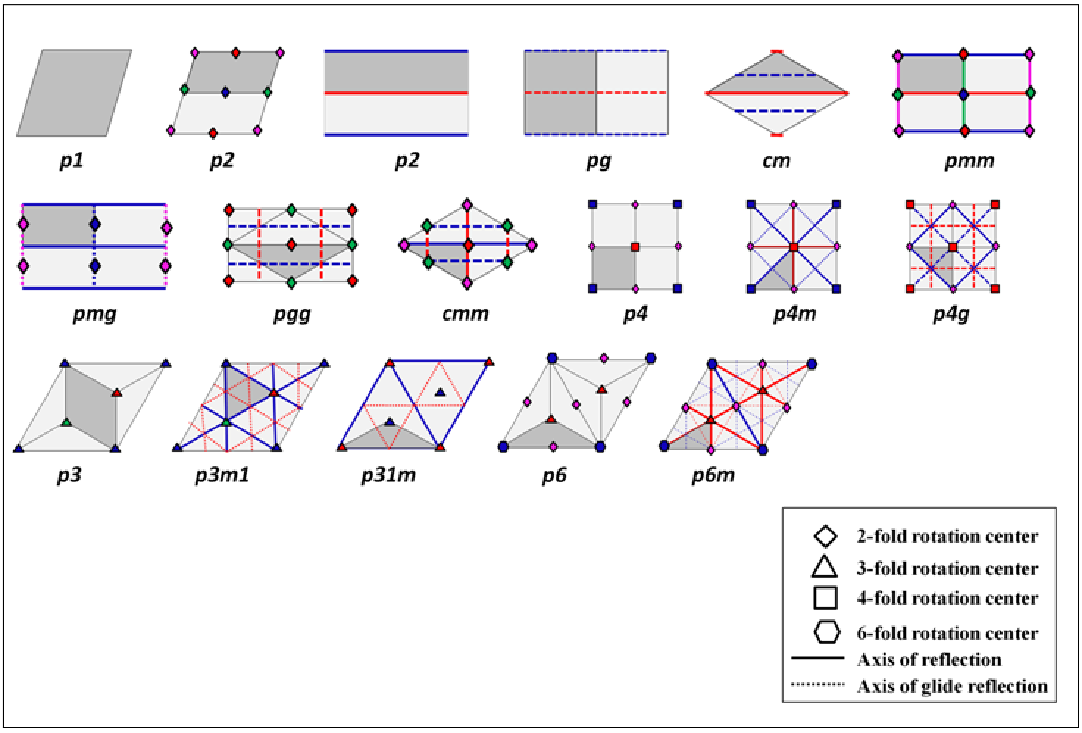

Figure 1.12: Unit cell structures for 17 Wallpaper Groups. The darker regions indicate fundamental domains.

The decision tree shown in Fig. 1.13 describes the algorithm of defining the symmetry group of a tiling. One can arrive to one of the seventeen symmetry groups each time answering to yes/no questions.

There are also other notations defining seventeen groups. There is an *orbifold* notation, which is in one-to-one correspondence with symmetry groups. There is also a *Heesch* type, where the type of a tiling is described according to the moves done by a basic shape that fills the plane. However, Heesch type considers only the tilings where only a single shape is used (*monohedral tilings*). Escher used his own notation to classify his tilings. Beside the symmetry group classification, there are also color symmetry groups. We will talk of them in the next section.

1.1.4 Color Symmetry

So far, we have been talking about the symmetry of figures only. In other words, we considered uncolored tilings. However, tilings often come with the

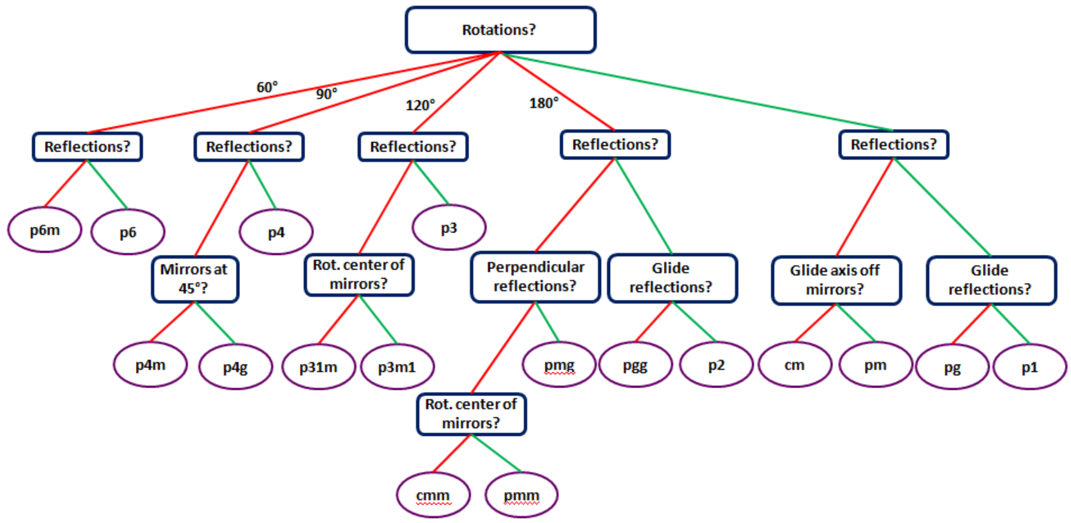

Figure 1.13: Decision Tree

colors. Introducing colors in a tiling may only preserve or decrease symmetry of an underlying tiling (a tiling where colors are ignored). In order for a tiling to have symmetry, the coloring should be performed in a regular way. It is said that a tiling has certain symmetry, if applying that symmetry on a tiling maps all the motifs of one color to the same motifs of a single color. Such symmetries are said to be *consistent with colors*. For two-colored tilings a mapping might be either color reversing or color preserving, while for tilings with more colors, reversing means mapping to the other color.

The seventeen symmetry groups described earlier are used for uncolored tilings and are taken as base groups for further classification of color symmetry groups. There are only finite ways of coloring a single symmetry group using n colors. See an example for possible colorings, using two colors, of a tiling with underlying group $p4g$ in Fig. 1.14. The underlying tiling of the colored ones shown in Fig. 1.14 has one center of four-fold rotation in the middle of each tile (red square), one two-fold rotation center at the point where four tiles meet (yellow diamond). There are mirror reflection axes passing through the centers of two-fold rotations, and glide reflection axes passing through four-fold centers and lying halfway between four-fold and two-fold rotation centers. There are only three possible colorings with two colors for this symmetry group. In the first coloring (Fig. 1.14(a)) the four-fold rotation preserves colors, while the two-fold rotation is color reversing. All reflection axes are color reversing. All glide reflections are also color reversing. Second coloring type is shown in Fig. 1.14(b). Notice that all three have the same symmetries as the underlying tiling has. The differences come with different color permutations. In the second coloring type the four-fold rotation is color reversing, while the two-fold rotation is color preserving. All mirror reflections are color preserving, while all glide reflections are color reversing. The last type (Fig. 1.14(c)) is the same as the second one, however, now mirror reflections are color reversing and the glide reflections are color preserving. It should be noted that this type of colored tilings are called *perfectly colored* tilings. A tiling is perfectly colored when all the symmetries of underlying tiling are associated with unique color permutation [69].

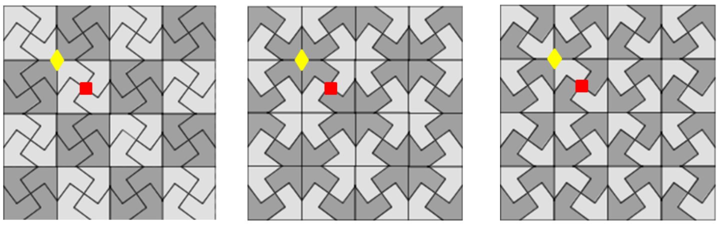

(a) (b) (c)

Figure 1.14: Three possible colorings of a tiling with two colors of underlying group $p4g$.

See another example for two-colored versions of a tiling with underlying symmetry group of $p6m$ in Fig. 1.15. Again, there are three possibilities only. Without going into details, just by choosing a center of six-fold rotations in the middle of hexagons (red dots), we can list the differences between these three. In the first one, the six-fold rotation is color preserving (black triangle goes to black one, and the gray triangle goes to gray one). There are reflections, which are typical for hexagons, and they are all color reversing (black triangle maps to gray one). The second coloring contains color reversing six-fold rotations. Both color reversing and color preserving reflections are encountered: vertical reflection axes are color preserving, and the horizontal axes are color reversing. The third one is the same as the second coloring type, however, here horizontal reflection axes are color preserving, and the vertical axes are color reversing.

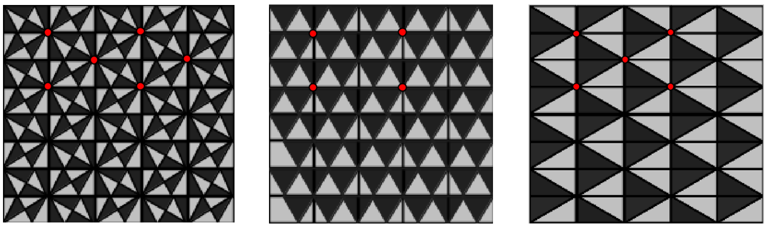

(a) (b) (c)

Figure 1.15: Three possible colorings of a tiling using two colors of underlying group $p6m$.

Two possible colorings for a tiling of symmetry group pmg with three colors are illustrated in Fig. 1.16. The tiling of pmg symmetry group have two different centers of two-fold rotations (red and yellow diamonds), mirror reflection all parallel to each other, and a glide reflection axes passing though the centers of two-fold rotations and perpendicular to mirror reflection axes. In the first case none of the mirror reflections are color preserving. Neither are the rotations. While in the second all mirror reflections are color preserving. One of two rotations is partly color preserving (yellow diamond), while the other is color reversing.

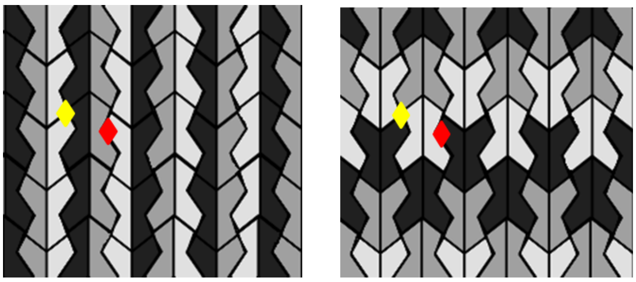

(a) (b)

Figure 1.16: Two possible colorings of a tiling with three colors of underlying group pmg.

Considering all possible colorings using n colors for each of these seventeen symmetry groups gives the total number of possible color symmetry groups of n-colored tilings. Table 1.2 shows all the possibilities of coloring a tiling of particular symmetry group with n colors. The sum of the coloring possibilities for a given number of color, gives the number of color symmetry groups that are possible with n colors. The results up to $n = 8$ are shown. Thus. from the results, one can see that two-colored tilings are classified into 46 groups. There are 23 groups for three-colored tilings, 96 for four-colored tilings , and so on. The list of possible colorings of symmetry groups up to $n = 60$ can be found in [79].

Table1.2: Color Symmetry Groups

Group	Number of Colors						
	2	3	4	5	6	7	8
p1	1	1	2	1	1	1	2
p2	2	1	3	1	2	1	4
pm	5	2	10	2	11	2	16
pg	2	2	4	2	5	2	7
cm	3	2	7	2	7	2	13
pmm	5	1	13	1	9	1	21
pmg	5	2	11	2	11	2	19
pgg	2	1	11	2	11	2	19
cmm	5	1	11	1	8	1	21
p4	2	0	5	1	2	0	9
p4m	5	0	13	0	2	0	28
p4g	3	0	7	0	2	0	13
p3	0	2	1	0	1	1	0
p3m1	1	2	1	0	4	0	1
p31m	1	2	1	0	5	0	1
p6	1	2	1	0	5	1	1
p6m	3	2	2	0	11	0	3
Total	46	23	96	14	90	15	166

Two-colored tilings are studied the most and are most available in literature. There are 46 color symmetry groups for two-colored tilings. There are also cases when a two-colored tiling has no color symmetry. This occur when none of the symmetries of the underlying tiling, when applied on colored tiling reverses colors, *i.e.* the symmetry of the underlying tiling is preserved. Then there are $46 + 17 = 63$ possibilities of coloring a tiling with two colors. The details on these 63 possibilities of two-colored tilings is shown in [6]. The list of possible colorings with illustrations for two- and three-colored tilings is given in [25], while 96 possible colorings of four-colored tilings are illustrated in [79].

There is no internationally accepted notation for the colored symmetry groups. Moreover, the existing notations do not go beyond the three-colored tilings. The notation of Belov and Tarkhova [7] is widely used for two-colored tilings. Their notation is much similar to the notation used for the seventeen one-colored symmetry groups. A prime ($'$) symbol is used to represent a color reversal for corresponding symmetry operation. Thus, if a translation reverses colors, then p'_b is used if the translation is along the edge of primitive cell, while p'_c is used for the translations along a diagonal of primitive cell. When either of these symbols used, no other symbol has a prime attached in the notation even if it also reverses colors. m' is used to indicate a color reversal in mirror reflections, and g' is used for color reversals in glide reflection. We revisit the example of three two-colored versions of $p4g$ given in Fig. 1.14. Fig. 1.17 shows primitive cells for all three colored tilings (red square). Observe that the translation is along the edge of primitive cell. For all three the translation does not reverse the color. For the first tiling (Fig. 1.17 (a)) the four-fold rotation preserves colors but all reflections (along the yellow axes indicated by yellow lines) and glide reflections (along the axes indicated by dotted yellow lines) reverse colors. Then, this tiling according to notation of Belov and Tarkhova [7] belongs to group $p4g'm'$. For the next two tilings the four-fold rotation reverses colors, then the letter '4' should be primed. In the second tiling, all mirror reflections are color preserving while the glide reflections are color reversing. This tiling belongs to $p4'g'm$ group. The last tiling belongs to group $p4'gm'$, since all glide reflections preserve colors, and all mirror reflection reverse colors.

Coxetre [12] introduced his own "*type/subtype*" (T/T^*) notation for two-colored tilings. This notation comes from his observation that two-colored tilings are produced by two one-color tilings of the same type. T indicates the symmetry group of an underlying tiling (when colors ignored) and T^* indicates the symmetry group of a tiling when one of the colors kept fixed and the other is considered. Returning to our example in Fig. 1.17, we can classify the first tiling as of group $p4g/p4$. This indicates that the underlying tiling is of group $p4g$, and it consists of two one-color tilings of group $p4$. The second and third tilings are of group $p4g/cmm$ and $p4g/pgg$, respectively. Notice that, in this notation, the color reversals break the symmetry, reducing it to a tiling with lower symmetry. The second and third tiling (Fig. 1.17 (b-c)) have four-fold rotations that reverse colors. Hence, the subtypes of a tiling are of lower symmetry group (no four-fold rotations). This notation describes all two-colored tilings, except for two cases: p'_b1m and p'_bm. It describes both as pm/pm. [80] suggests to distinguish these two cases by using two different notations: $pm/pm(m')$, to indicate that mirror reflections reverse colors, and $pm/pm(m)$ when no color reverses occur from mirror reflections.

Grünbaum and Shephard [25] have suggested their own notation for both two-colored and three-colored tilings. They listed and illustrated all possibilities of colorings of tiling using two and three colors. Their notation is not descriptive of the types of symmetry the tiling exhibits. The notations used are as $pg[3]_1$ indicating the first version of coloring for pg tiling using three colors. If we are to classify the examples in Fig. 1.17, then the first tiling is of group $p4g[2]_1$, indicating the first version of coloring for $p4g$ tiling using two-colors, while the second and the third tilings are of group $p4g[2]_2$ and $p4g[2]_3$, respectively.

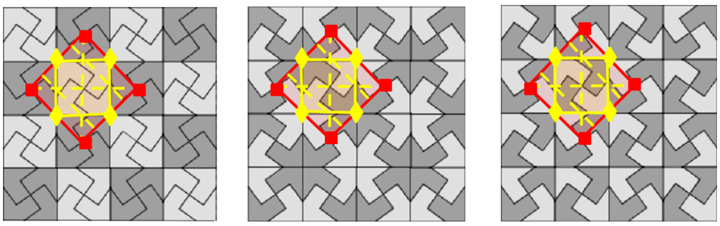

(a) (b) (c)

Figure 1.17: Three possible colorings of a tiling with two colors of underlying group $p4g$.

A table comparing these three notations for two-colored tilings can be found in Appendix A. In order to define the color symmetry of a tiling using two-colors, one can refer to a decision tree similar to the one shown in Fig. 1.18. Since it is not possible to fit all 46 color symmetry groups in one page, we show only the branches that define the color symmetry of two-color tilings that contain six-fold and three-fold rotations. Note that considering color symmetries requires treatment of each case for n colors separately. Increase in number of colors n used in ornaments, makes the classification problem non-trivial. The problem with more colors was mentioned by Senechal in [68, 69], where the author discusses the difficulty of finding unambiguous classification schemes for perfectly colored ornaments of three or more colors.

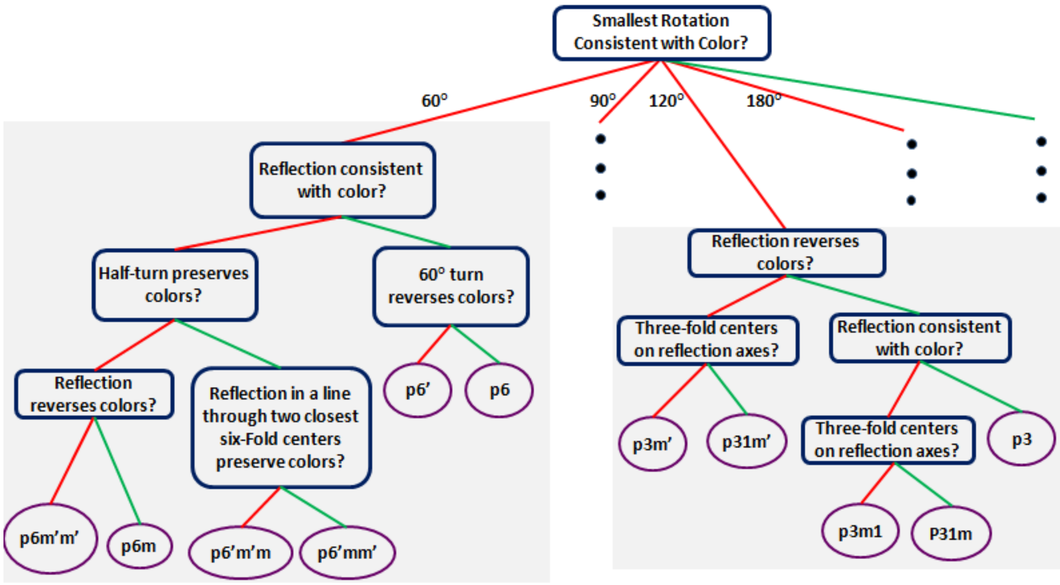

Figure 1.18: Decision Tree for Color Symmetry

1.2 Thesis Overview

1.2.1 Motivation

To this end, the only way of studying ornaments involves finding repeating elements, then, according the rules applied to repeat these elements, associating an ornament with some predefined group. Being a completely mechanical approach, it leaves the artistic side of the ornaments unattended. Privileged by artistic freedom, the artists tend to break the symmetry by introducing interesting color permutations and playing with the shapes. This important factor is being ignored by classical approach. The other limitation of classical approach, is the abundance of notations, which are listed separately for different number of colors being used in an ornament. Furthermore, classifying ornaments according to their symmetry groups, give inflexible, strict, and discrete clusters. From these clusters, we cannot infer the relations between different clusters.

Consider two images given in Fig. 1.19. The first ornament contains two different birds that are translated in two directions to fill the plane. The symmetry group of this ornament is $p1$. The second one contains one bird in two different colors that are related by glide reflection. Hence, its symmetry group is pg. However, those two images are perceptually very close to each other. Close investigation of the first image reveals that, if we ignore the colors, the only thing preventing the blue bird to be the exact reflection of the white bird is the subtle change at their tail. While the tail of a blue bird looks downward, the tail of the white bird looks upward. Otherwise, those two birds would be related by glide reflection, which would imply that two ornaments in Fig. 1.19 were created using the same production rules. By adding a minor change to the first image, the artist broke the symmetry. Finding the symmetry groups of these two ornaments, by ignoring the colors, classifies them into two different groups ($p1$ and pg). If we consider colors, then the first ornament contains no color symmetry, while the second one is assigned to the group of one of the colorings of pg group. In either of the two different ways, the closeness of these two ornaments is not captured.

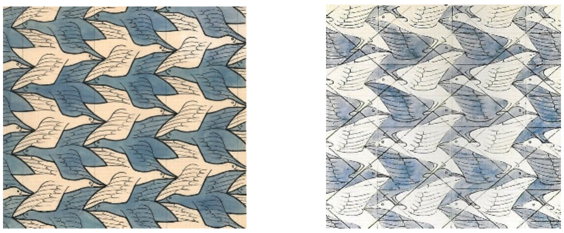

(a) (b)

Figure 1.19: Two quite similar ornaments produced using two different repetition rules. (a) An ornament of $p1$ group. Produced by translating two distant figures, which are almost similar. (b) An ornament of pg group. Contains only one bird figure of two different colors. One bird of one color is a glide reflection of a bird of another color.

Fig. 1.20 illustrates three ornaments. An attempt to define which symmetry groups they belong introduces complications. Are we considering the symmetry group of underlying uncolored ornament or trying to define the color symmetry of the ornament? If the color permutations are ignored, all three belong to group $p6$. This is not true, when the colors enter the scene. First two are assigned to two different groups of possible colorings using three colors of an ornament with underlying symmetry group of $p6$, and the last one is assigned to one of the groups of possible colorings using two colors of an ornament with underlying symmetry group $p6$. Thus, in one way all three are always classified into one group, in another they always belong to different groups. This situation brings ambiguity. Moreover, when all three are classified according to color symmetry, they are never seen in one cluster, despite the fact that they share some common properties.

(a) (b) (c)

Figure 1.20: Three ornaments of group $p6$. When color permutations are considered the ornaments in (a) and (c) contain three-fold rotations, while the ornament in (b) contains two-fold rotations. Also observe that two ornaments in (a) and (c) differ in number of colors used.

An interesting example is illustrated in Fig.1.21. The underlying symmetry group of an ornament (*horseman*) in Fig.1.21 (a) is pg. Enumerating possible colorings of an ornament with underlying symmetry group pg using two colors, give two groups, pg' and p'_b1g (Belov and Tarkhova notation). The first group contains ornaments with color-reversing glide reflections only, while the latter group contains ornaments with both color-reversing and color-preserving translations and glide reflections. The color symmetry of the given ornament (Fig.1.21 (a)) is pg'. However, visually it is more similar to p'_b1g. We conducted an experiment containing eight people. We first showed the original image given in Fig.1.21(a) to participants, then demonstrated three ornaments of different color symmetry groups. These three are shown in Fig.1.22 (b)-(d). The first one (Fig.1.21 (b)) is of group $p_b'1$ (a group containing only color-reversing and color-preserving translations), the second one (Fig.1.21 (c)) is of pg' group and the last one (Fig.1.21 (d)) is of $p_b'1g$ group. The participants were asked to choose the most similar ornament to the original ornament. All participants chose the ornament shown in Fig.1.21 (d), which is of $p_b'1g$ group, as most similar one. We assume that this visual similarity of horseman ornament to the ornament of $p_b'1g$ group occurs due to the nature of a motif in the horseman ornament, which contains an illusion of glide reflection within itself. As it is shown in Fig.1.22 (a) a motif (horseman) consist of two parts (red and green shapes), where the lower part (shown in green) looks like a glide reflection of the upper part (shown in red). We have simplified the ornament to a binary image in Fig.1.22 (b) in order to get rid of details. Cut out and zoomed upper and lower parts are illustrated in Fig.1.22 (c), while in Fig.1.22 (d) we reflect the upper part along the x-axis. Observe that the upper body of a man is almost related by glide reflection to the back leg of a horse. Also, both shapes are in V shape, where the V shape for upper part looks upward and downward for the lower part giving an illusion of glide reflection. This all give an impression that the ornament is the repetition of the upper (or lower) part of a motif with color-reversing and color-preserving translations and rotations, which makes it similar to the ornament in Fig.1.21 (d).

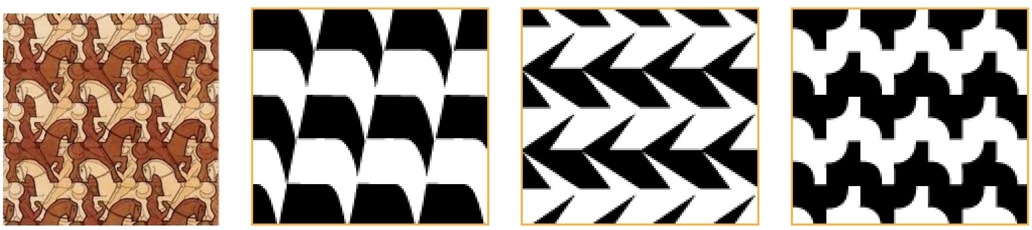

(a) (b) (c) (d)

Figure 1.21: (a) Horseman ornament. (b) An ornament of $p_b'1$. (c) An ornament of pg' group. (d) An ornament of $p_b'1g$ group. Although the horseman is of pg' color symmety group, all participants marked the ornament of $p_b'1g$ group as the most similar one to the horseman ornament.

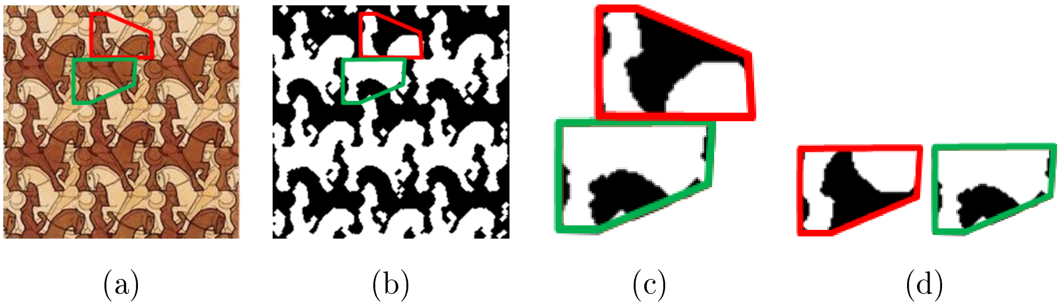

Figure 1.22: (a) A single horseman motif consists of two shapes which are glide reflections of each other. (b) Simplified horseman ornament. (c) Cut out and zoomed upper and lower parts of a motif. (d) The upper part of a horseman motif reflected along the x-axis.

The examples given above suggest that we need a different approach to study ornaments. The purpose of this thesis is to provide a more flexible approach, which would consider both symmetries and artistic intention made in an ornament, and make it possible to measure the similarities between different ornaments with different symmetries.

1.2.2 Overview of the Approach

In this thesis, we approach the study of ornaments from different perspective. We gradually suppress the content of an ornament. Since the study of symmetric patterns is more interested in detecting how the elements repeat rather than the nature of the elements, we consider the explicit shapes (horses, birds, dog, *etc.*) and colors (red, blue, green, *etc.*) used in ornaments as content. Once the content is suppressed, what is left is the information on how different nodes in an ornament are repeated using different color permutations. The content suppression consists of two stages. First stage is a binarization stage, where the ornament is divided into several binary masks. Each mask contains the information on how a motif of certain color is permuted. However, the information on exactly what colors being used is lost. At this stage, we suppress the color information. In order to suppress the shape information, in the second stage, we apply a linear transform on each of the masks of an ornament. The linear transform suppresses the peripheral regions of individual shapes and highlights the node centers. Thus, given an image of precise shapes like dogs, birds, *etc*, the linear transform outputs the repetition rules of node centers. The node centers join based on the symmetry type that an ornament exhibit to represent different abstract structures like triangles, three-leaved roses, four-leaved roses, hexagons, *etc*. For example, if an ornament contains three-fold rotations, then the repetitions of node centers of an individual shape join to form three-leaved roses or triangles. The content suppression process is illustrated in Fig. 1.23.

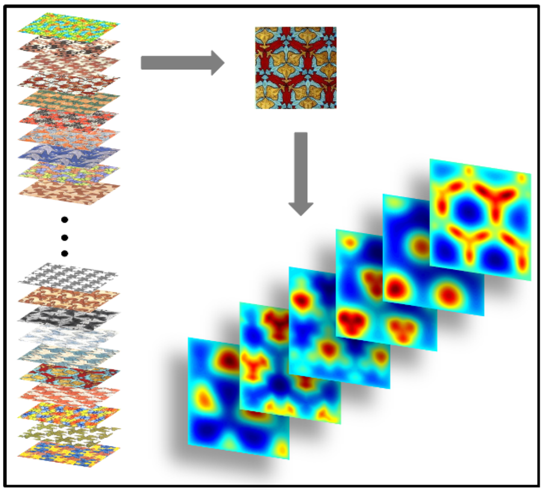

Figure 1.23: Content Suppression

The major advantage of suppressing the content of images is that it enables to measure the similarities between ornaments with different symmetries. This allows to treat the symmetry as a continuous feature using which rather than assigning each ornament to discrete groups we let for different organizations to emerge joining ornaments with close symmetries. In this manner, the relationships of different symmetry groups are inferred. Fig. 1.24 shows the main steps of our approach. Each time we consider a group of ornaments. For each of the ornaments the content suppressed images are computed using which the similarity matrix is obtained. For visualization purposes, we then reduce the dimensionality of similarity matrix using one of the existing dimensionality reduction techniques. An ornament joins another ornament with the closest symmetries in the current context. Thus, depending on the context the relations between ornaments change. Emerging organizations are not necessarily in agreement with wallpaper group classification.

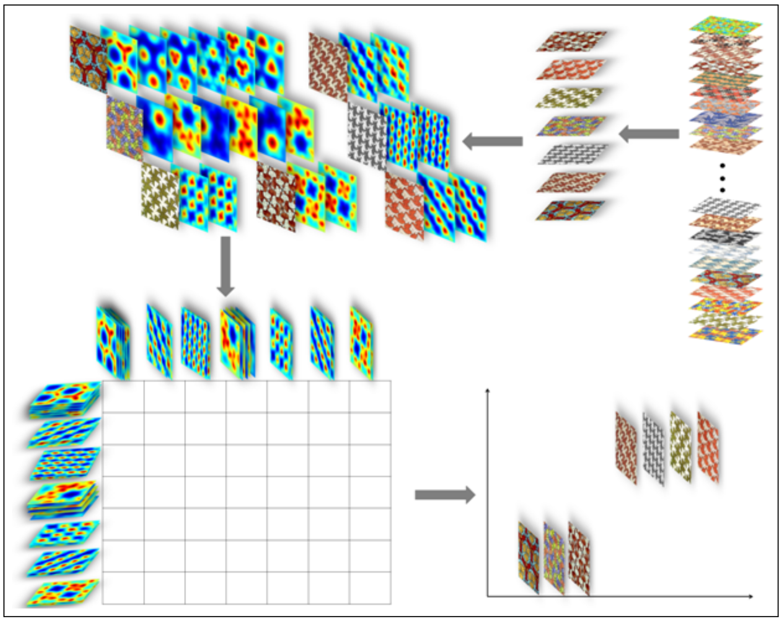

Figure 1.24: Group approach

Beside the group approach described above, it is also possible to analyze ornaments in an individual level using the content suppressed images. Recall that when the content of ornaments is suppressed the individual node centers are enhanced. Detecting the maximal values within the content suppressed images, we find the repetitions of individual nodes of certain color. We then extract several connections between the maximal nodes. These connections are further clustered into groups depending on connection sizes and orientations. As a result, each connection group defines certain symmetry of an ornament. Combining all symmetries inferred from different connection groups, we obtain the lattice and define the symmetry group of an ornament. Main steps for the approach are illustrated in Fig. 1.25.

1.2.3 Contribution

This thesis introduces a novel thinking and methods to study ornaments and symmetries in ornaments. We achieve this via:

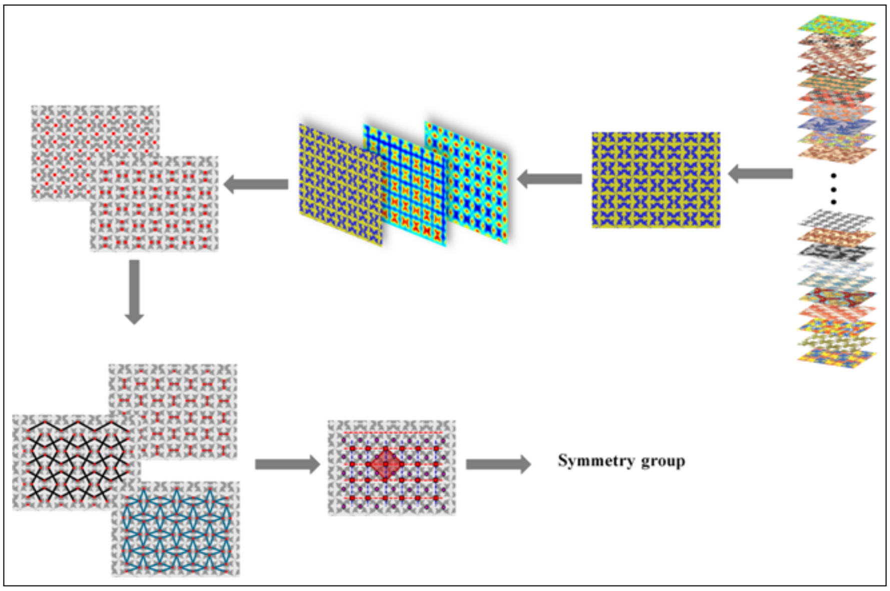

Figure 1.25: Single tile approach

- introducing a method to measure stylistic similarities of different ornaments with varying symmetries.
- performing style-based clustering in a given context, which reveal relations between different symmetry groups.
- introducing a new way of finding symmetries in an individual ornament, without explicitly searching for repeating elements.

1.2.4 Organization

The thesis is organized as following. In Chapter 2, we review works that are related to our work. In Chapter 3, we address the content suppression problem. The binarization and linear transform stages are described. We then present the content suppressed results for various ornaments. In this chapter, we retrieve the style of ornaments. In Chapter 4, we perform style-based clustering in a given context. Various clustering results are given, which are divided into multiple experiments. We, then, present quantitative analysis for the experiments performed. Comparison of clustering results of different levels of content suppression is given in Chapter 5. Analysis of individual ornaments are done in

Chapter 6. Finally, in Chapter 7, we summarize and conclude our work.

CHAPTER 2

PREVIOUS WORK

The importance of symmetry in perception has been argued by several researchers. One of the earliest works is by Attneave [3, 4]. He argued that symmetric figures are easier to reproduce than asymmetric ones because the symmetric figures, as they consist of repeating units, contain less information, making them more memorable and visually pleasing as a result of their simplicity due to reduced information. In [17], Eisenman and Rappaport argued that symmetry-asymmetry dimension is important in its own right and deserve an investigation separate than simplicity-complexity dimension. Over the years, several researchers presented empirical evidence for the influence of symmetry of shapes and/or visual compositions on visual attention, exploration and physiological arousal. For example, the results in [48] indicate that people tend to fixate first on the symmetry axis (suggesting that symmetry "catches the eye"), and then proceed on visual exploration, and visual expolaration of symmetric forms are linked to aesthetic judgements. In computational literature, symmetry is proposed as an alternative saliency measure, i.e., interesting regions in visual forms are defined as the regions with symmetry be it in form or color, e.g. [38, 63, 27].

In the computational literature, the works on symmetry is mainly restricted to finding symmetry axes in a single object in 2D or 3D. Since a single object can have only mirror reflections and rotational symmetries, the effort is mainly focused on reflections and rotations [51, 74, 36, 34, 35, 58, 65, 37, 60, 57, 61, 51, 36, 52, 39, 40], while the glide reflection (as it requires considering of multiple copies of an object) is to a large extent ignored and addressed in few works only [41, 43]. Further interestingly, a misconception by people is to associate mirror reflection as a synonym to symmetry [80]. This makes the mirror reflection the most studied type of symmetry while even the rotational symmetry is much less explored. An interesting and important work on rotational symmetry is by Zabrodsky and Peleg [84, 85], where the continuous nature of rotational symmetry has been brought to attention. Treating symmetry as a continuous feature enables to compare two shapes with different symmetries and to obtain the relations between different shapes.

The group theoretical approach to the study of ornaments, lists all the symmetries contained in an ornament. Then according to the symmetries that an ornament contains, it is assigned to one of the predefined symmetry groups (e.g. the 17 plane symmetry groups if color variations are ignored). The plane symmetry group based classification takes the form of a binary decision tree.

In the computer vision pattern recognition literature, Liu et al [44, 45, 46, 62] addressed the classification of repeated patterns according to the 17 plane symmetry groups. They first obtain the peaks of the autocorrelation function and then connect those peaks to obtain the underlying lattice. Recall that the possible lattice types that can be associated with an ornament are restricted by the symmetries it exhibits. For example, if an ornament has mirror reflection, then its lattice must be rhombic, rectangular or square. An ornament with 90° rotational symmetry has a square lattice, while the ornaments with 60° or 120° rotational symmetries have a hexagonal lattice. Thus, once the lattice type is known, the number of possible symmetry groups to which an ornament can be assigned is decreased. The next step would be to check all possible symmetries that are associated with a given lattice type, answering several yes/no questions, until the correct wallpaper group is identified.

The most thorough work on Escher's ornaments can be found in Schattschneider's book on *Visions of Symmetry* [67]. The author listed more than hundred and fifty Escher ornaments and contents from Escher's notebook, together with the symmetry groups of the ornaments according to various classification systems. According to Schattschneider, Escher's own notes indicate that as an artist, he produced his ornaments using a layman's local view rather than following globally defined seventeen plane symmetry groups. In his early work on Moorish ornaments [24], Grünbaum also mentioned that the scientific approach to study symmetry is concerned about the global symmetry, while the artisans, when creating their ornaments, are concerned about the local view, in which each part of an ornament is related to its immediate neighbors in some specific way. Later, in his work on the symmetry groups present in Alhambra [23], Grünbaum points out that the artist of that time had no knowledge of symmetry groups, and that the present approach of scientist to study ornaments is rather irrelevant. He suggests that a new, more flexible, approach is needed, which would be more consistent with the minds of people that created these ornaments. In [53], the author also suggests that when studying symmetry in ornaments, the artistic intention should be considered as much as possible.

Classifying objects based on their stylistic differences is a rapidly developing approach. Recently, a fine-grained classification become of more interest. In this type of classification, rather than classifying unrelated classes, the objects of the same class are classified. Since objects of the same class have common general features, the key point is to find discriminative elements on the different subclasses of the same class. Those discriminative elements represent the style of the subclass. This type of problems are addressed in [42, 82, 8, 9, 29], where objects of the same class are classified based on style. The content-style separation problem, in general setting, is addressed by Tenenbaum and Freeman [76], by formulating it via bilinear models.

Works classifying art images and decorations based on their style also take their share in the recent literature [16, 49, 70, 83, 47, 20]. Authors in [16] perform a classification of geographical places according to stylistic elements which are discriminative elements of a particular place. Yang et al [83] analyze Chinese wash paintings and the foreign art paintings in terms of their aesthetic style differences, while Liu et al [47] address stylistic differences for particular artists, specifically for Van Gogh and Monet. Though these works aim to capture stylistic similarities and differences between art images, their definition of *style* is not applicable to the study of highly symmetrical structures, the ornaments. What defines style, in the mentioned works, is highly influenced by color, texture, and shape; while the study of symmetry involves studying how design elements repeat rather than the nature of design elements.

In computational literature, there is a growing interest in understanding the human creativity. This is achieved by constructing a program capable of human-level creativity. Several researchers [33, 32, 78] address the synthesis problem in the setting of Escheresque tiles. In [33, 32], the authors tackled the problem of finding the best approximation of a given arbitrary shape that tiles a plane in order to produce Escheresque tiles with arbitrary forms. A method to transform Euclidean ornaments to hyperbolic ones in order to produce hyperbolic Escheresque tiles are proposed by von Gagern and Richter-Gebert [78].

The problem of synthesizing an artwork in a certain style is addressed in [86, 72, 2]. [72] presented an approach of shape simplification to the regions of given photographs, creating paintings similar to the works of Matisse and Kandinsky. [86] introduced abstract painting system named Sisley that creates abstract paintings from photographs adding some level of ambiguity. Cubist rendering approach is proposed by [2]. Given 3D input scenes they are synthesized into cubist paintings with artistic effects.

Another area of our interest is the knowledge discovery, which is defined by [18] as "*The non-trivial process of identifying valid, novel, potentially useful, and ultimately understandable patterns in data*". It contains works that seek for alternative ways of classifying data, which would give results that are new and interesting. Such approach can be found in the works of alternative clustering [26, 13, 14, 15, 5, 21, 22] and concept discovery problem [10, 11, 81, 30, 31].

CHAPTER 3

CONTENT SUPPRESSION

Typically, the study of symmetries in an ornament implies an explicit search for repetitive structures in an ornament. Based on the relations of those repetitive structures a decision on the symmetry group of an ornament is made. A decision that is to be made is limited to some predefined rules, and introduces no flexibility. Furthermore, defining a symmetry group of some ornament leads to ambiguous results, raising questions like, are we talking about the color symmetry or just ignoring the colors; which notation do we use for classification (since there are so many of them) and why do we think it is the most appropriate one. Most importantly, those approaches do not consider the share of an artist, who is the actual creator of ornaments in question. Artists tend to break symmetries by introducing different color usage or by slight change in shape details. All those shortcomings appeal to approach the study of symmetries in ornaments from different perspective. Instead of searching for repetitive structures, we aim to see the underlying structure of an ornament. The underlying structure defines the style of an ornament, implying that the ornaments with the similar underlying structures are similar style-wise, and were created using the same production rules. The style must reflect not only the symmetry group, but also the artistic intention, and color symmetry. Think of looking at the city from above. One can see the underlying structure of the city, understanding the order of buildings in terms of their locations. While the explicit forms and specific colors of buildings are not visible, the rules by which those buildings are organized can be inferred. Furthermore, one can see how the roof colors of the buildings alternate throughout the city. Just like the analogy given above, we aim to see the underlying structure of ornaments by ignoring explicit forms and specific color usage in an ornament. This leads to content-style separation concept. Once we suppress the content of an ornament, the rest must reveal its underlying structure, which, in fact, is a style of an ornament.

In this chapter, we define what aspects of an ornament we consider as a part of content, and what aspects we leave as a style of an ornament. Once the content is defined, next we perform content suppression. We give technical details on the content suppression stages. Finally, we give the content suppressed results for various ornaments.

3.1 Content-Style Separation

Before starting to suppress the content of an ornament, we should decide on what do we consider as content. An ornament consists of motifs, repetitions of which, obeying some rules, form an entire ornament. A choice of an artist for a precise shape as a motif should not cloud our judgment on underlying structure of an ornament. The artist could use different shapes to fill the plane using the same repetition rules. Thus, a shape of a motif is a part of content. However, the information on how the artist repeated those shapes throughout the ornament is a part of style. The artist also chooses specific color to fill a motif. We neglect the information on specific color choices in an ornament; however, we care about the permutation of different colors in an ornament, and consider them as a part of style. Fig. 3.1 shows two ornaments with the same style. Observe that the first one is a hand drawn ornament from Escher's collection, while the second one is a computer-generated ornament. Hence, the types of colors used are completely different. In addition, the number of colors in two ornaments differ: three and five respectively. Furthermore, the shapes used to fill the plane are different, while the first one contains recognizable figures; the second one contains abstract structures. Despite all those distinctions, both have the same underlying structure. This fact shows the unimportance of precise shape and specific color choice information, adding them to the content. The importance of color permutations are shown in Fig. 3.2. Fig. 3.2(a) shows two ornaments with the dots representing the center of highest order of rotation in them. Both of them contain three colors, and both of them are of group $p6$ according to symmetry group classification. However, when one rotates the copies of these ornaments around the given center of rotation point, it is possible to see that actually the order of rotations for those two ornaments differ. Thus, for the ornament in first row, if one rotates it for 60° , the shapes match up, however the colors do not match. The same goes to 120° rotation. Observe that both shapes and colors of shapes match up only when the tile is rotated for 180° . For the second ornament, shown in second row, a match of both shapes and shape colors occur when one rotates it for 120° and 240°. Although both of those ornaments are considered to belong to p6 group according to symmetry group, their color-symmetry groups differ: first ornaments contains only two-fold rotations, and the second ornament contains only three-fold rotations. This shows that the color permutation can influence the underlying structure of an ornament. Therefore, we consider the color permutation as a part of ornament style.

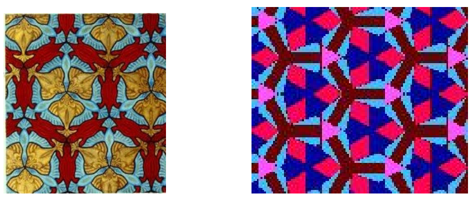

Figure 3.1: Two ornaments with different color types but the same production rules. (Left) Hand-drawn ornament. (Right) Computer-generated ornament.

We take an ornament and gradually suppress the content. It contains of two levels. The first level is a binarization level. At this stage, we extract several binary masks for a given ornament that encode different aspects of color usage. The extracted binary masks have no information of specific colors used in an ornament; however, they carry information of how colors were permuted in an ornament. While we succeed to suppress the color information at binarization level, the explicit forms of motifs still present in masks. The next aim would be to suppress the shape information. The second level takes as input extracted masks for an ornament, and diffuses shapes. For that purpose, we use a linear

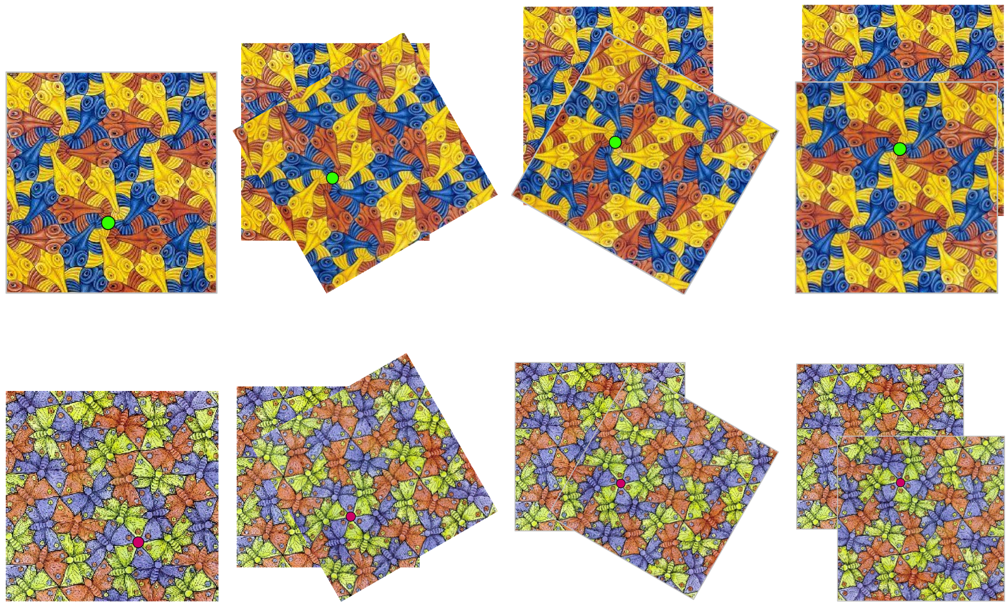

(a) (b) (c) (d)

Figure 3.2: Two ornaments of the underlying group $p6$. Green and red dots represent the centers of rotations. (a) 60° rotation. For both images shapes match but not the colors. (b) 120° rotation. The match on both shapes and colors occur only for the ornament at the bottom. (c) 180° rotation. The match on both shapes and colors occur only for the ornament at the top.

transform, which is a scale invariant diffusion operator. The linear transform takes images with precise shapes and outputs images with abstract shapes like triangles, tiskelions, swastika, crosses, hourglasses, etc. Those structures give clues on what symmetries exhibit in a particular ornament. In addition, they give visual similarities between different tiles that are similar style-wise. For a summary of levels we pass in a pursuit of content suppression see Fig. 3.3. We give technical details on binarization and linear transform in the following sections.

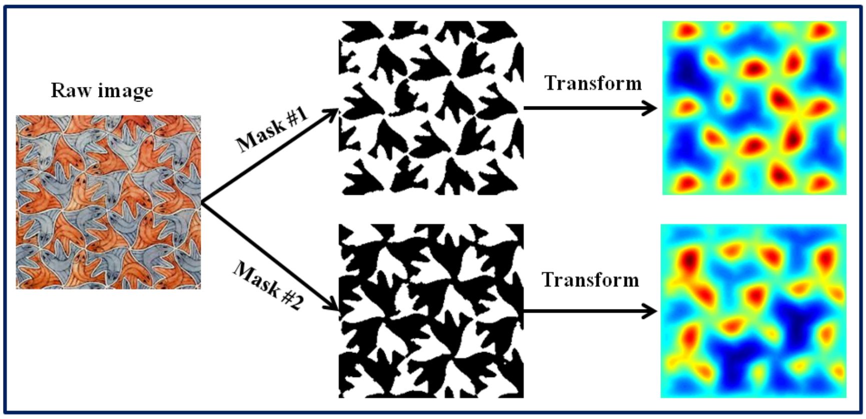

Figure 3.3: An illustration of the content suppression levels.

3.2 Binarization

The first step of content suppression is a binarization stage. Here, given an ornament, we extract several binary masks for it. First, the row image is converted into HSV color space. We, then, for each of the three channels extract several binary masks. The binarization process is based on thresholding method. For each channel, we automatically define n numbers of threshold values. Thus, given an image (channel), the binarization produces first mask by assigning black to regions where the corresponding values (color feature) in image is less than the first threshold $n1$, and white to all other regions. The second mask gets black regions where the color feature is greater than or equal to threshold $n1$ and less than threshold value $n2$. The third mask is produced by assigning black regions where the color feature is greater than or equal to threshold $n2$ and less than threshold $n3$. This process goes on in this manner, and the last mask gets black regions where the color feature is greater than or equal to nn. Thus, for each channel we obtain $(n+1)$ masks. However, since the inverses of each mask also contain important information, we include them too. The overall number of masks for each channel is $2*(n+1)$. If $n=1$, we obtain only two masks for an image. The inverses of masks are not considered in this case, since two masks are already inverses of each other. Note that, after the binarization process the final number of masks equals $6*(n+1)$, for all three channels of an image.

However, not all of them will be useful. Most of the masks will be redundant. We discard the masks that contain no information but the noise. We, then, perform morphological operations (opening, closing) on the masks that are left. The masks, that still contain disturbing noises after morphological operations, are also discarded. Generally, for one of the HSV channels we get acceptable set of binary masks that have a well captured information of color permutations. One can also create new masks by combining different masks through and/or operations. Thus, after discarding redundant masks, and combining different masks, we obtain a new set of masks. Of course, it is desirable to have minimal set of masks. Ideally the mask size equals to twice the number of colors that the image contains: one mask for each color and their inverse. However, defining the thresholds for binarization automatically, does not always give good results, leading to explore more possibilities. For example, we assign $n = 1$, and automatically define a threshold value. This value may not give good separation of colors. Then we assign $n = 2$, and perform another binarization, this time considering two threshold values. This situation increases the number of masks for each image. For an example of binarization results for particular ornaments, see Fig. 3.4–3.5. Observe the mask inverses in the second row of Fig. 3.5. Recall that one mask carries permutation information of one color. Had we ignored the mask inverses, we would lose the information on how the given color is related to other color permutations. In the given example, keeping the mask inverses hints on the permutation of two other colors with respect to the given color permutation in particular mask.

Figure 3.4: Two masks obtained for two-colored ornament of group p4g.

The threshold values are obtained using Otsu's method [56]. This method gives only one threshold at a time, since it assumes that the image contains

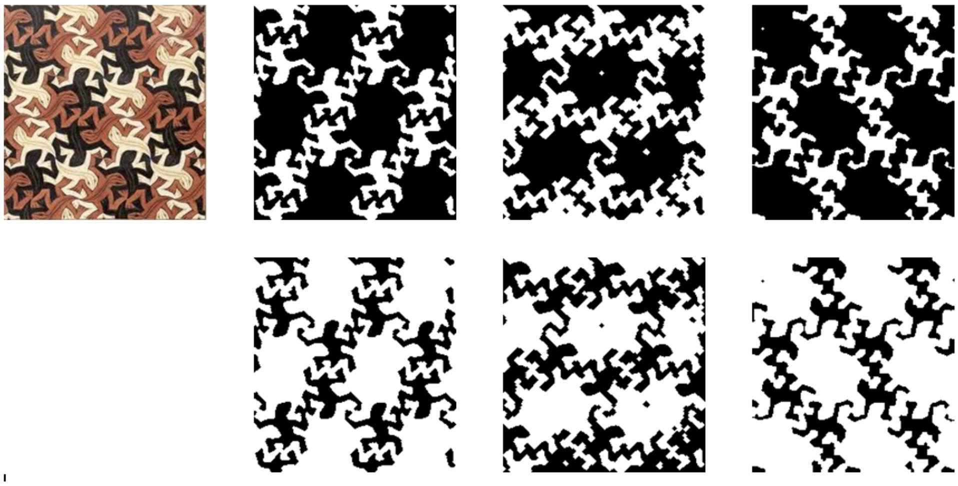

Figure 3.5: Six masks obtained for a three-colored ornament of group p6.

two classes of pixels, which yield a bi-modal histogram. In order to obtain n threshold values, we call the method recursively. Given an image, we get a threshold value, which divides it into two regions. Then those two regions are treated as two independent images, and the threshold value is defined for each of them. Then for each image, we get two regions, which then call the same method recursively. If $n = 1$, then we have only one threshold value. If $n = 2$, then we will get 3 threshold values. For $n = 3$, we get 7 thresholds, and so on. As one can see, the number of threshold values is more than we need. We select only the top n effective ones, where the effectiveness is defined by the threshold effectiveness measure in Otsu method. Otsu's method can be invoked via *graythresh()* function in Matlab.

3.3 Linear Transform

The binarization stage suppresses the color information. We perform this stage in order to avoid the choice of an artist for specific colors to cloud our judgment in perceiving style of an image. The thresholded masks carry information of shapes used in ornament and color permutations applied on it. While the latter one is considered as a part of an ornament style, the shape information is another aspect of an image that we desire to get rid of. The shapes lose their forms if we blur them using an appropriate filter size. Hence, any diffusion filter, e.g. convolving the masks via Gaussian, gives the desired solution. The solution that we desire is that after the filtering, the image shapes are suppressed, but the repetition rules of those shapes are highlighted. We face some difficulties with the diffusion filters. The first question that comes in mind would be how much diffusion is required? What information in an image should be kept, and what should be suppressed? The diffusion filters highly rely on parameters that we will have to deal with. Thus, our attention turns toward a shape transform recently proposed by [75]. This transform is originally proposed for shapes. When the transform is applied on a shape, it yields a diffuse field, which contains both positive and negative values. The positive regions are separated from negative regions by an emergent zero-crossing curve that divides a shape into central and peripheral regions. The central region takes positive values, and contains the least deformable part of a shape. For an example see Fig. 3.6, where the transform of dog shape is shown. Observe the blue curve separating central part from peripheral regions. The central part of a transform takes positive values, while the peripherals take negative values. The field result shown in the figure is the absolute value of the field, which we use solely for visualization purposes.

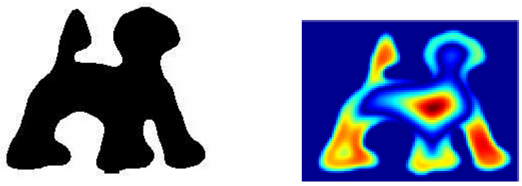

Figure 3.6: Linear transfrom computed for a dog shape. (Left) Original shape. (Right) Linear transform. The central part is separated from peripheral regions via the blue curve which is the zero-crossing curve.

We adapt this transform to our problem, so that it is applied to entire tile domain. The transform suppresses the peripheral regions of individual shapes in an ornament, after which only the central, least deformable coarse structures of motifs remain. In this manner, we suppress the shapes, making the explicit forms unimportant. What remains is the underlying center repetition. The details of our approach are as follows. Let S denote the set of pixels of tile image and $M : S \rightarrow \{0, 1\}$ be a binary mask obtained via thresholding the tile image as described above. Let us define an external function $g : S \rightarrow R$. Then, let

$$f(p) = \begin{cases} g(p) & ifM(p) = 0 \\ 0 & ifM(p) = 1 \end{cases} \tag{3.1}$$

The shape suppressed image satisfies the following relation at any $p \in S$ whose four neighbors are denoted by p_N, p_S, p_W, p_E:

$$term_1(p) - term_2(p) - term_3(p) + f(p) = 0$$

where

$term_1(p) = \omega(p_N) + \omega(p_S) + \omega(p_W) + \omega(p_E) - 4\omega(p)$

$term_2(p) = \frac{1}{|S|} \sum\limits_{q \in S} \omega(q)$

$term_3(p) = \frac{1}{|S|} \omega(p)$

We numerically solve the linear system using an iterative scheme:

$$\begin{aligned} \omega^{t+1}(p) &= \omega^t(p) + \triangle^t(p) \\ \triangle^t(p) &= \alpha(term_1^t(p) - term_2^t(p) - term_3^t(p) + f(p)) \end{aligned} \tag{3.2}$$

Here, $\alpha < 0.25$ is a step size that ensures convergence. Initial value of ω^0 is set to 0. The iteration stops whenever $\triangle^t$ is less than a fixed threshold (0.001 for all our results). In all the results we set the external function g as the distance transform of the mask using the Matlab command $bwdist(M)$. From now on, we will call the results obtained from this transform as ω field of an image.

See Fig. 3.7 for an example of the ω field result for sample image. Fig. 3.7(b) shows one of the masks of a tile in Fig. 3.7(a). Computing the ω field only for foreground objects of a mask (black regions) attenuates the shape peripherals and highlights the node centers (Fig. 3.7(c)). When we compute the ω field for the entire mask, we observe the relation between the node centers (Fig. 3.7(d)). Observe that from the last image we have no clue on the shapes depicted in the original image. What we see, is an underlying structure of an original image that shows how a particular node is being repeated in a tile. For more results on ω field, see the next section.

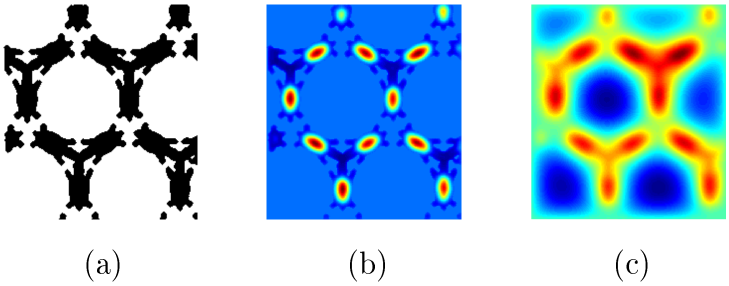

Figure 3.7: ω field computed for one of the masks of an ornament. (a) Mask. (b) ω field computed only for foreground objects (black regions). (c) ω field computed for entire mask.

3.4 Results for Content Suppressed Ornaments

We present ω fields obtained for ornaments with different underlying structures. The results will show different abstract structures that emerge in the ornament fields. Those structures represent the symmetries that the ornaments exhibit, and help perceive similarities and differences in various ornaments. Let us summarize what stages we pass in order to obtain content suppressed images, with highlighted underlying structures. We pass thorough two stages: binarization and filtering. After the binarization stage, we have several masks for a particular ornament. Then we compute ω fields of those masks, and get the images where the shapes are suppressed. For each ornament we show both the masks and the corresponding ω fields.

Fig. 3.8 illustrates field results for five ornaments of pure translational group. Observe that the masks of each ornament (second column) have no information about the specific colors used in ornaments. However, the number of masks gives a hint on the number of colors used in ornaments. Here, all ornaments contain two colors. Hence, all five ornaments have two masks. Recall that, however, the number of masks is not limited to the number of colors. Also, observe that from the masks one can still tell what shapes are used in ornaments, like birds, Pegasus, fishes, etc. When the ω fields for each of the masks are computed, the shapes are suppressed leaving only the arrangements of node centers (third column). Since five ornaments in question have only translational symmetry, the ω fields of each ornament show translated copies of node centers. The node centers are arranged in vertical and diagonal lines. Here, the line structures indicate translational symmetry.

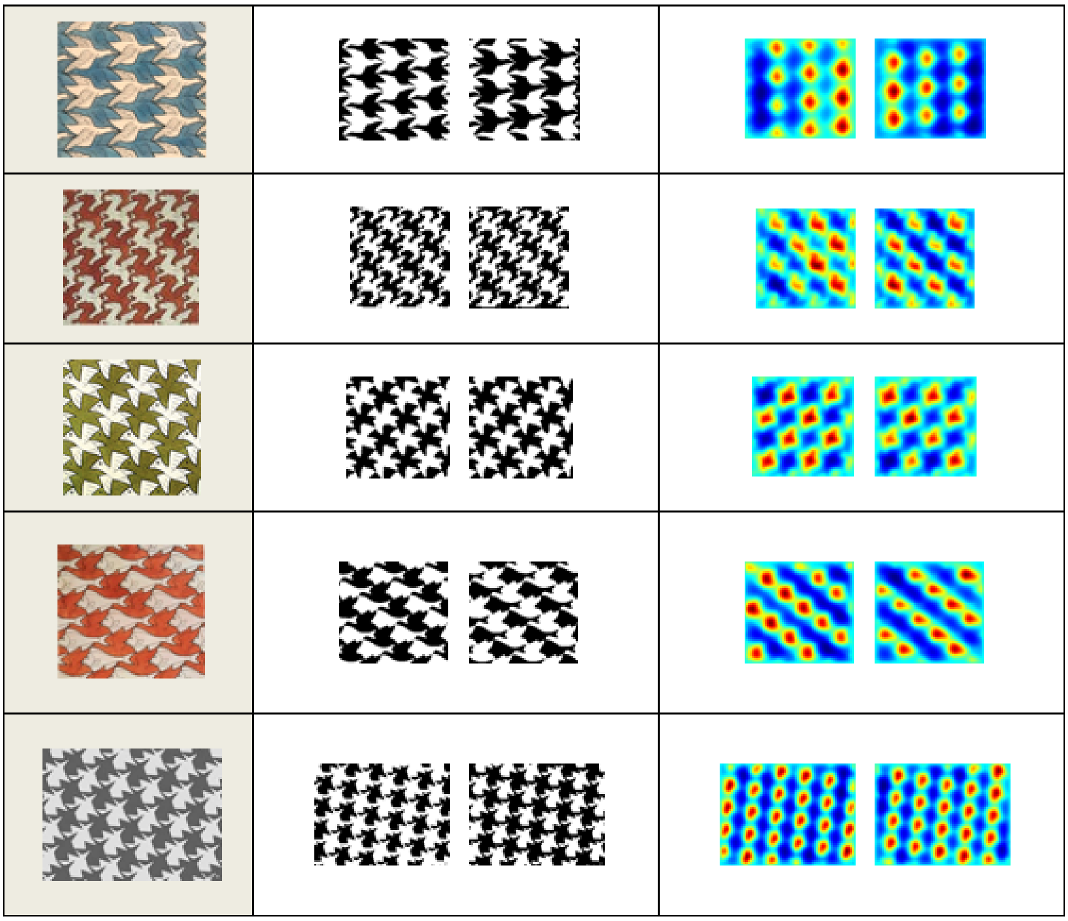

Figure 3.8: Five ornaments of pure translational group. All five exhibit line structures in the transform domain.

Another set of ornaments are given in Fig. 3.9. Those ornaments are of glide group, first two of which belong to group pgg and last three belong to group pg. The transformed results for those images exhibit zigzag structures. In the third ornament, the glide reflection of a motif goes to another color so that when we extract the masks the glide reflection is lost. That is why the ω field of this ornament is expected to exhibit line structures, just like the ones that occur for pure translational group. However, as we discussed in introductory chapter, this ornament contains hidden glide reflection in a horseman shape. This internal glide reflection adds "zigzagness" to the field of the ornament, distinguishing it from the ornaments of pure translational group. We also perceive dumbbell-like structures in the fields of first image, which is of pgg group. Observe that there are zigzag structures, but the nodes come in pairs. Those dumbbell-like structure occur due to rotations that the ornament exhibit. The second tile is also of pgg group; however, its rotation goes to the other color, leading to the loss of two-fold rotations. Observe Fig. 3.10 for two-fold rotations on those first two ornaments . As one can see, for the first ornament (Fig. 3.10(a)) after the half-turn rotation there is a perfect match up both in shapes and colors, while for the second ornament only shapes match.

Fig. 3.11 illustrates two three-color ornaments of $p6$ symmetry group. When colors are considered each turn of a six-fold rotation leads to the same shape of different color. Thus, the maximum order of rotation that both ornaments exhibit is two. These two ornaments are the good examples on how the color permutation can change symmetries in an image. The ω fields computed for both ornaments reveal dumbbell-like structures. We have already encountered them in the field of pgg ornament of previous set. These dumbbell-like structures represent two-fold rotations and occur when two node centers join in a two-fold rotation. Rectangular structures in the fields of both images represent the combination of two-fold rotations of shapes that belong to other two colors.

The ω fields computed for four ornaments with three-fold rotations and mirror reflections are given in Fig. 3.12. The first column in a figure shows the original images, the second column shows the masks obtained for that particular ornament, and the third one contains corresponding ω fields computed for

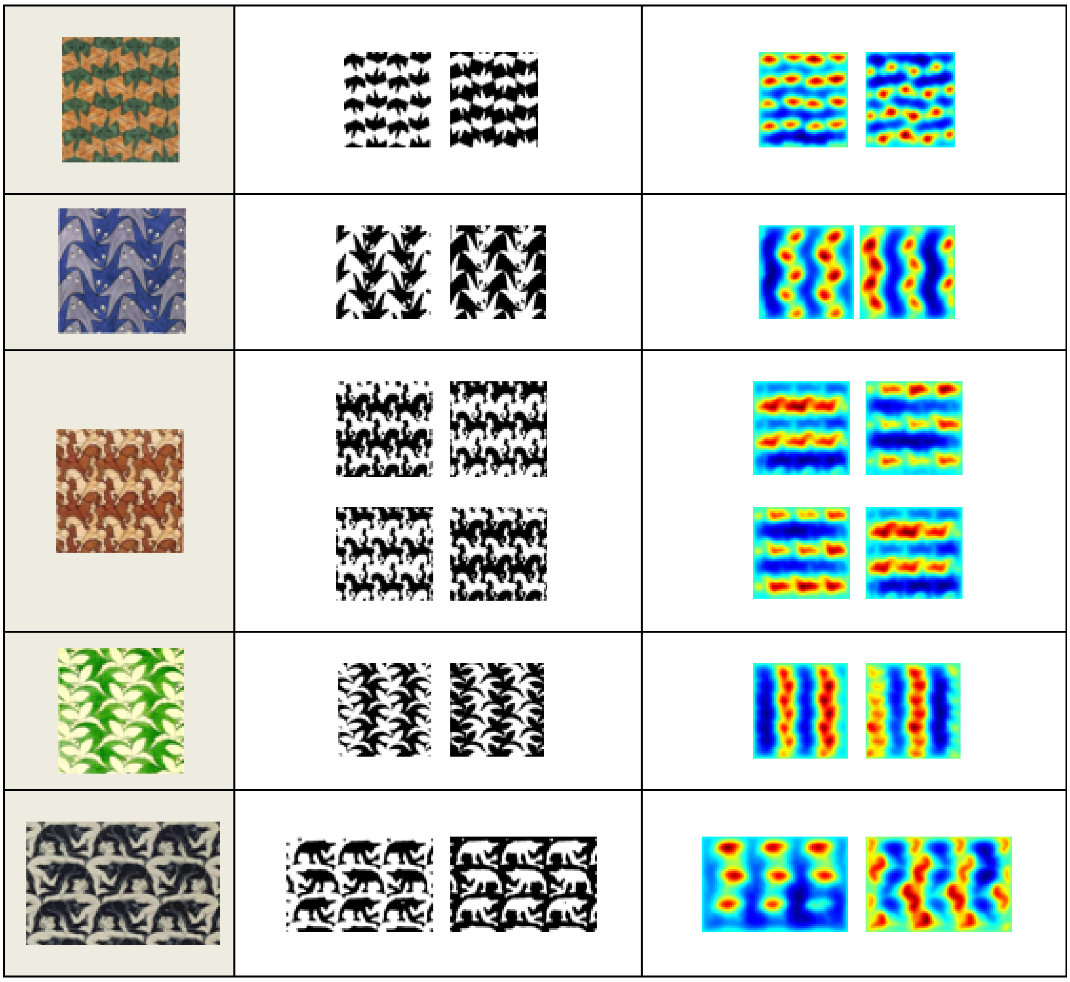

Figure 3.9: Five ornaments of glide group. First two are of group pgg and the rest are of group pg. Observe that the glide reflectional symmetry is represented by zigzag structures in all five ornaments.

the masks. First three tiles are from Escher's collection, and the last one is a computer-generated ornament. Although first three ornaments have the same number of colors in original images, the number of masks of each ornament differs (6, 8 and 12 respectively). First two ornaments from Escher's collection belong to $p3m1$ group and the last one is of group $p31m$ according to symmetry group classification. According to Escher's system, all three are of triangle system. Last computer-generated ornament is of $p3m1$ symmetry group. Observe that the filtered images for all four ornaments exhibit similar structures,

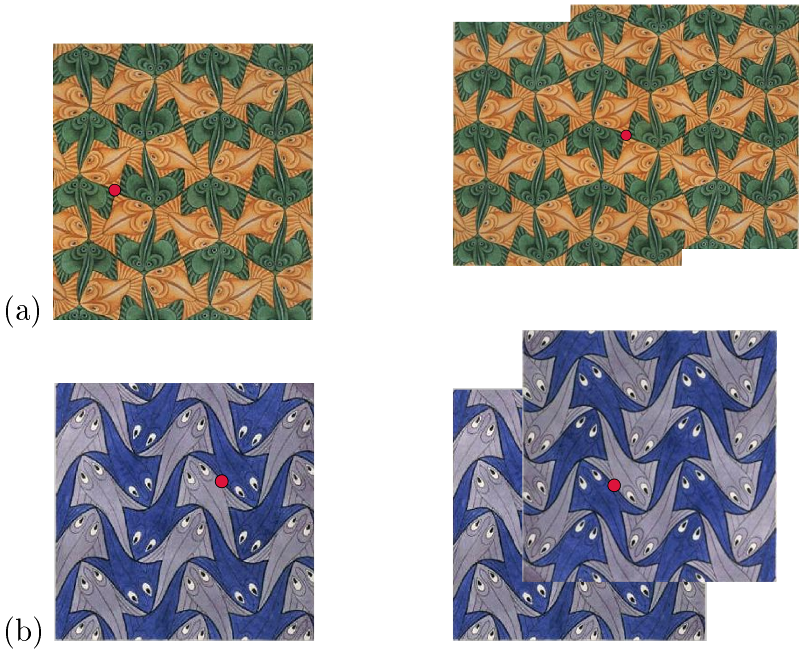

Figure 3.10: Two-fold rotation in two ornaments of group *pgg*. (a) The rotation is to the same color. (b) The rotation is to the other color.

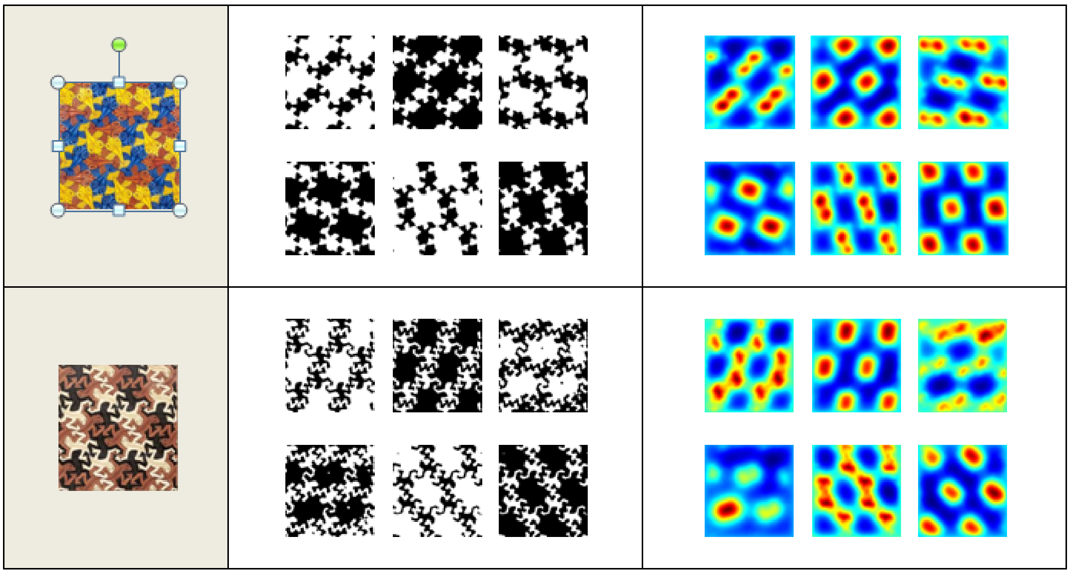

Figure 3.11: Two ornaments of group $p6$. Due to color permutations the maximum order of rotation reduces to two. This is represented by dumbell-like structures in the ω fields computed for masks.

like triangles and three-leaved roses. These rosette structures occur when the repetitions of node centers join in a three-fold rotation. Some of the fields also contain hexagonal structures, which represent the arrangement of nodes of other colors with respect to the current color. The structures emerged represent the symmetries contained in ornaments. All four ornaments contain three-fold rotations, and so do the three-leaved rose and triangle structures of the fields. Those ornaments also contain mirror reflections, and so do the abstract structures of the field.

Consider another set of ornaments given in Fig. 3.13. First two are two-color ornaments of group $p6$, the third one is a three-color ornament, known as mariposas, of group $p6$, and the last one is a two-color ornament of group $p3$. Although first three tiles are of group $p6$ according to symmetry group, when the color permutations are considered, the maximum order of rotation they exhibit is three. What makes those four ornaments similar is that they all exhibit three-fold rotations. The difference between this and the previous four ornaments is that this set contains no mirror reflections. Observe that the ω fields of the ornaments reveal this distinction. All of them contain structures like three-leaved roses just as the structures observed from the results of previous set. However, this time the three-leaved roses are more cyclic (*triskelions*). This implies the lack of mirror reflections in the ornaments. From the ω fields of the mariposas masks we can also observe hexagonal structures. They represent six-fold rotations, which occurs due to color permutations. The six-fold rotation in its entirety kept in a mask inverse, since two other colors that are not representatives of the current mask are considered as one colored six-fold rotation.

In Fig. 3.14, we illustrate five ornaments that exhibit four-fold rotational symmetry. The first four images are of group p4 and the last one is of group p4g. From the ω fields of first two images, we see how four-leaved roses replace three-leaved roses. Here, the whole rotation is kept in one color, thus enabling the field to capture the rotation in its entirety. The third ornament's ω fields exhibit cross structures, which also show that the nodes in an ornament are related by four-fold rotations. The forth ornament contains both four-leaved roses and square structures. Observe that the four-leaved roses are more cyclic, implying

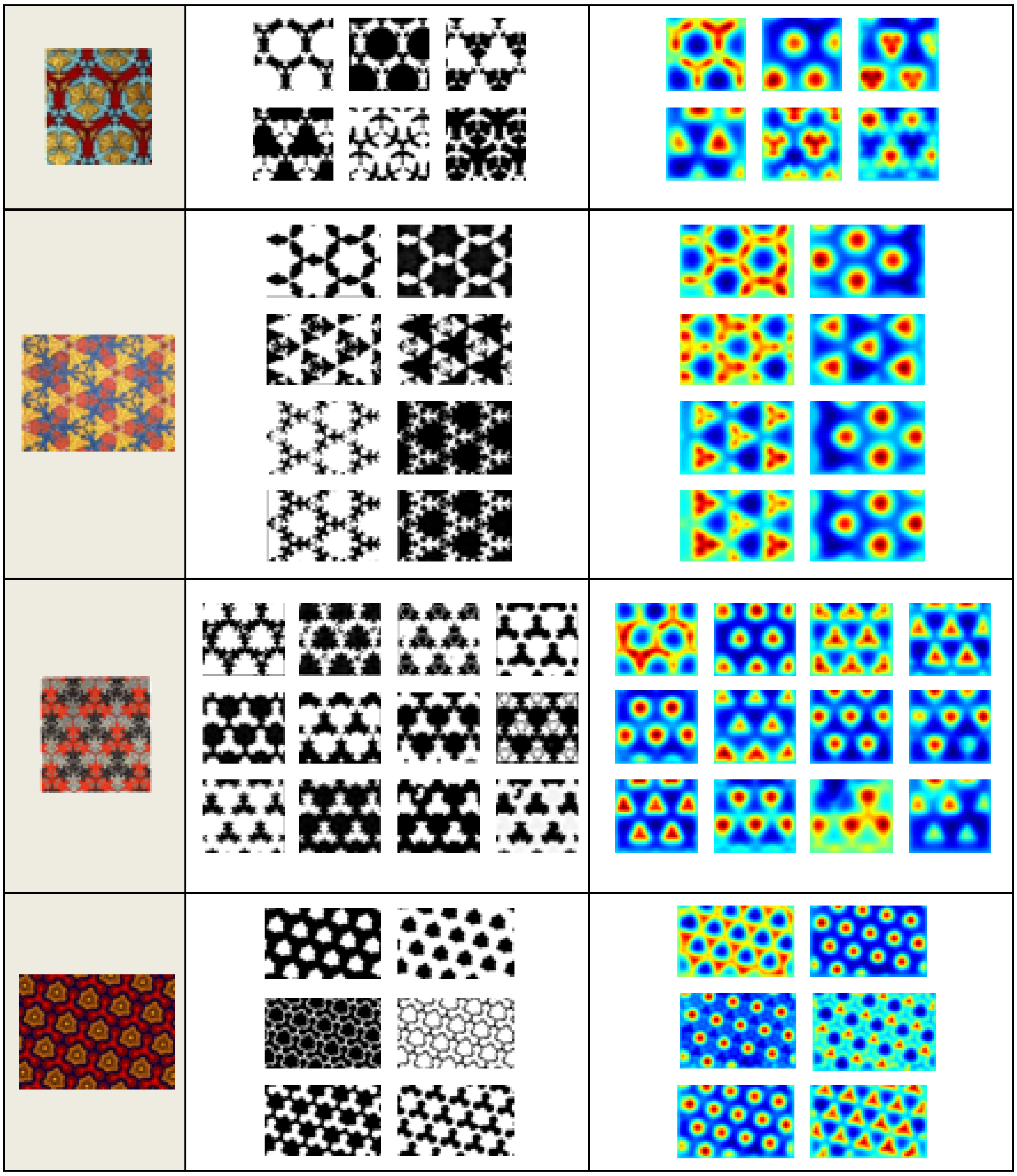

Figure 3.12: (a) Four ornaments with three-fold rotations and mirror reflections. (b) Masks obtained for each ornament. (c) ω field computed for each of the masks of the ornament. All four exhibit similar abstract structures, like triangles and three-leaved roses.

lack of mirror reflections. The interesting result is illustrated for the last ornament. There is a four-fold rotation center in the middle, which is captured by a swastika-like structure shown in blue in the second mask of an ornament. Here,

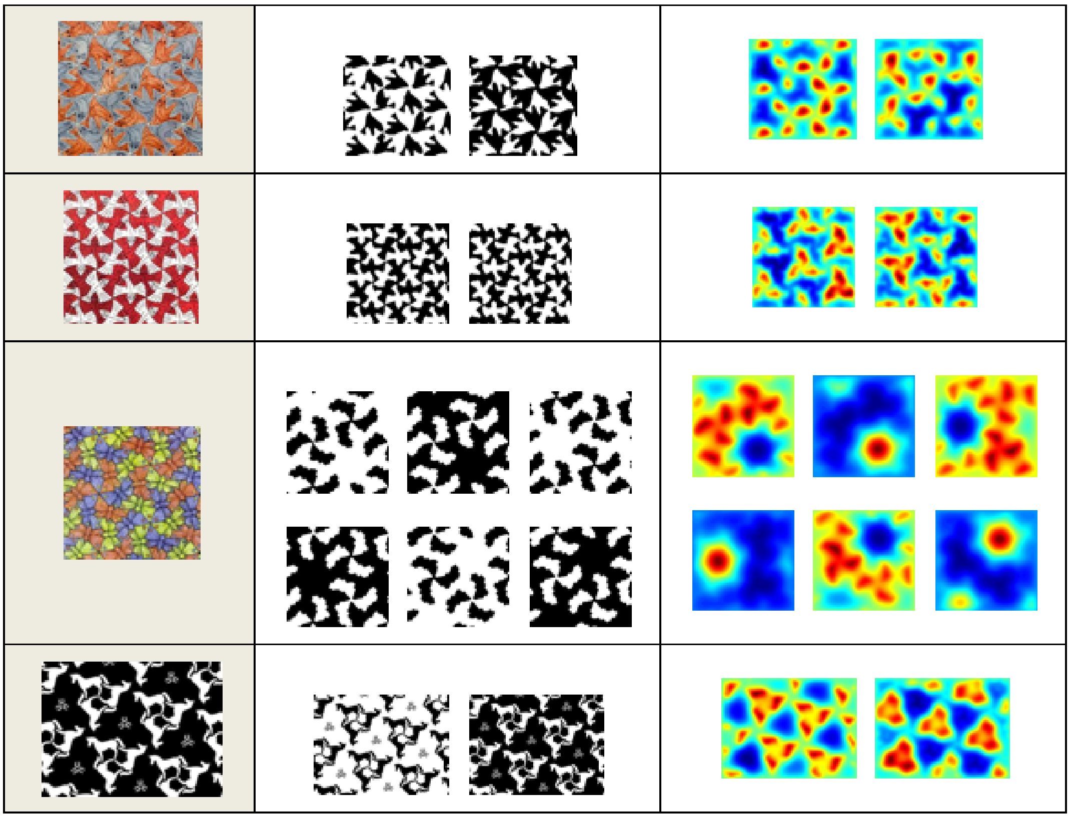

Figure 3.13: Four ornaments with three-fold rotations without mirror reflections. First three ornaments belong to $p6$ group. However, due to color-permutations the maximum order of rotation they exhibit is three. All four exhibit three-leaved roses that are more cyclic.

again the whole rotation is kept in one color. Beside the four-fold rotations, there are also mirror reflections in the last image. Those reflections are represented by hour-glass-like structures. The mirror reflections are what distinguish first four images from the last one, and this difference is well captured by the field.

Hexagonal structures prevail in the ω fields of four ornaments given in Fig. 3.15. All four are of group $p6$, and in contrast to the other ornaments of $p6$ group discussed earlier, these four still exhibit six-fold rotations, even when we consider color symmetries of the ornaments. Along with the hexagonal structures, we can observe six-leaved roses that emerge due to six-fold rotations of some node around the center of rotation. The ornaments of $p6$ group also contain three-fold rotation centers different from the six-fold rotation centers. Therefore, it is no wonder to see three-leaved roses or triangles in the ω fields of those ornaments. Observe the *triskelion* structures in the field of the third ornament in Fig. 3.15.

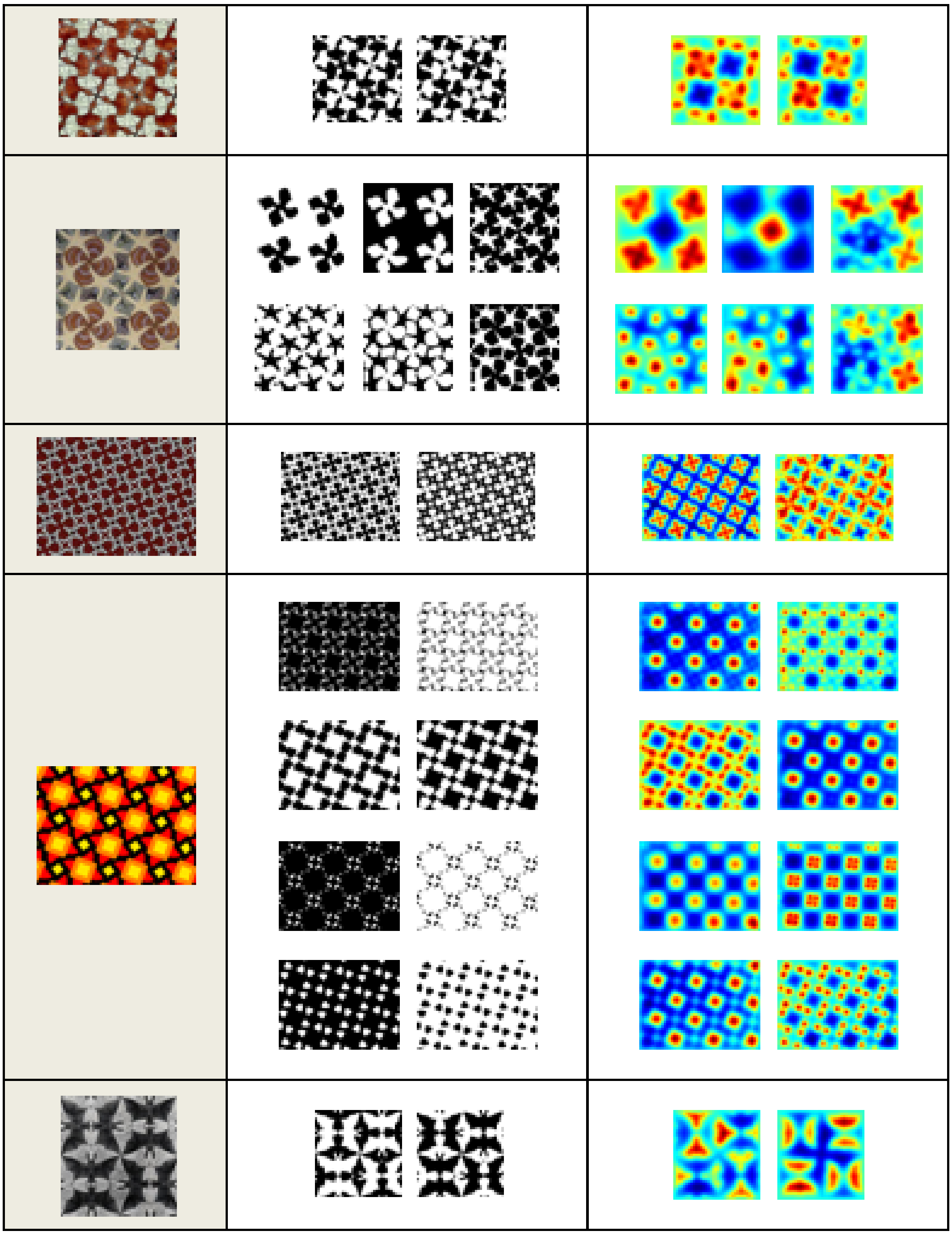

Figure 3.14: Five ornaments with four-fold rotations. First four are of group $p4$, while the last one is of group $p4g$. Four-fold rotation is represented by four-leaved roses and squares in the transform domain. For the last ornament four-fold rotation is represented by swastika-like structure shown in blue on the second mask, and the hour-glass like structures represent mirror reflections.

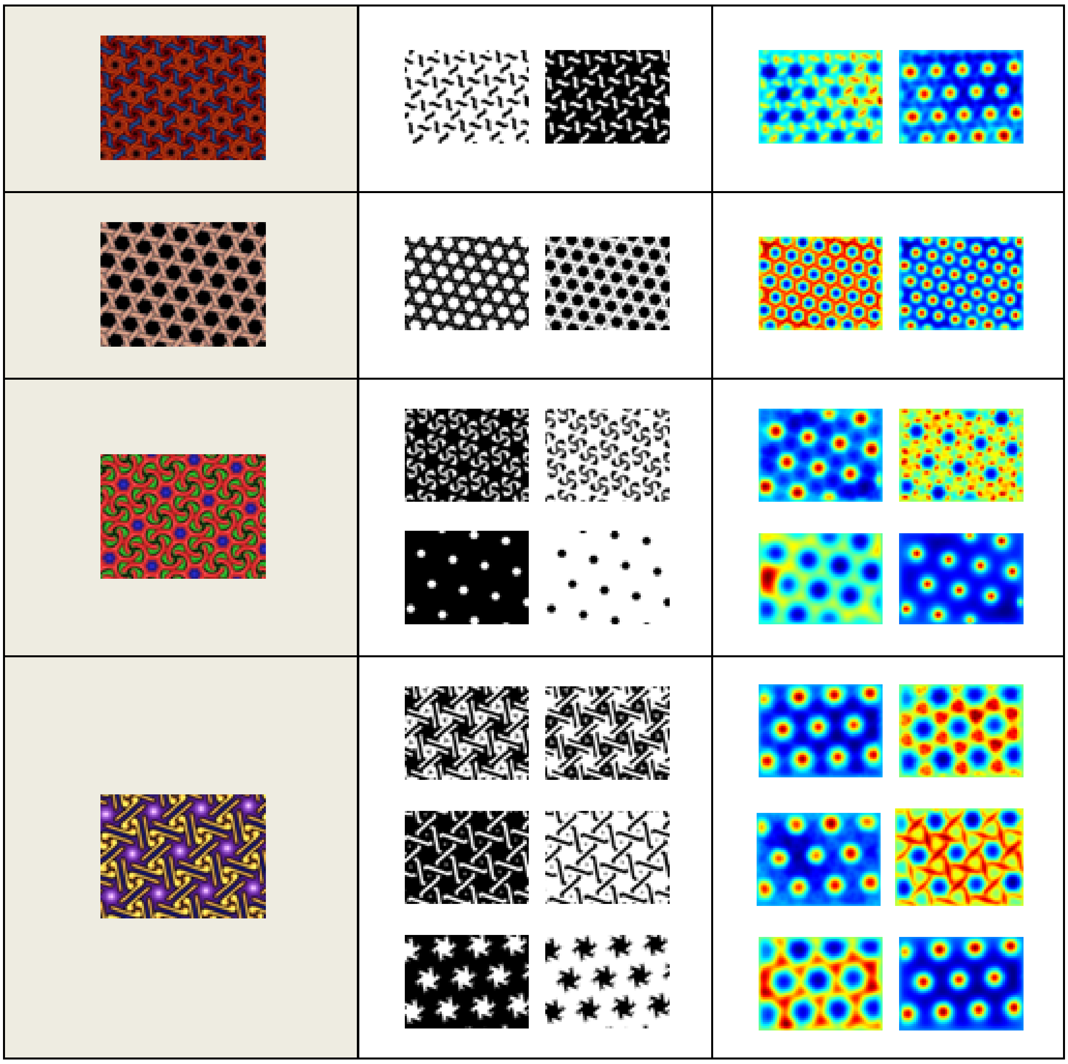

Figure 3.15: Four ornaments of group $p6$. Even when color permutations considered the maximum order of rotation is six. All four exhibit hexagonal structures representing six-fold rotations.

3.5 Abstract Structures

The study of symmetry is not about the explicit forms or colors, but about the motions that are introduced in ornaments by repeating particular nodes. It is the motions we are concerned about, and them we are trying to capture. For that, we perform content suppression in order to separate the content, in terms of explicit forms and colors, from the motions that the ornament exhibit. The content suppression process takes an image with the precise shapes like horses, dogs, birds, as an input. Those precise shapes become unimportant in the process, since our aim is to capture the generalized centers of shapes and their relations only. The output is ω field, which contains abstract structures like triangles, three-leaved roses, four-leaved roses, zigzag structures, swastika-like structures, dumbbell-like structures, hourglass structures, etc, which occur due to relations of coarse structures of nodes. Those abstract structures give clues on what kind of symmetries the ornaments exhibits. We are also able to perceive style-wise similarities between seemingly different ornaments. For each kind of symmetry, we observe a structure that represents it in transformed images. We summarize which structures indicate various symmetries in an ornament.

For ornaments of pure translational group, the ω field of the masks for them exhibit line structures, like shown in Fig. 3.16. Those structures show the arrangement of node centers, suggesting that the nodes are related by translation only, repeating themselves in two different directions. Those line structures might be in vertical, horizontal or diagonal forms.

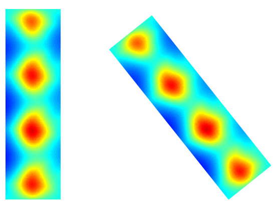

Figure 3.16: Structures representing translational symmetry

Glide reflection is a mirror reflection followed by a translation. Due to reflection, the orientation of a node changes in alternating order to opposite direction. This alternation introduces zigzag structures in the ω fields computed for ornaments of glide groups (Fig. 3.17).

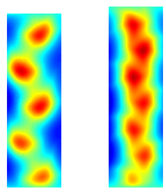

Figure 3.17: Structures representing glide reflection

The ω field for an ornament with rotational symmetries exhibit rosette structures. The rotations of a shape join at some point. When we suppress the boundary details keeping only the coarse structures, we see only a rotation of some node center around that point. As a result, we obtain structures that resemble finite designs, which can be described in terms of rotations and reflections. Finite designs fall into two categories: cn and dn. The first type is known as *cyclic* group of order n, while the second is known as *dihedral* group of order n. Cn group has n-fold rotations, but no mirror reflections. Dn group has both n-fold rotations and mirror reflections. According the symmetries that the ornament exhibit, we will see the abstract structures that are similar to either one of this groups. While for the finite structures n can reach the infinity, in our abstract structures (due to crystallographic restriction mentioned in introductory chapter) it can take values like 1, 2, 3, 4, or 6. Examples for cyclic and dihedral groups is illustrated in Figs. 3.18-3.19.

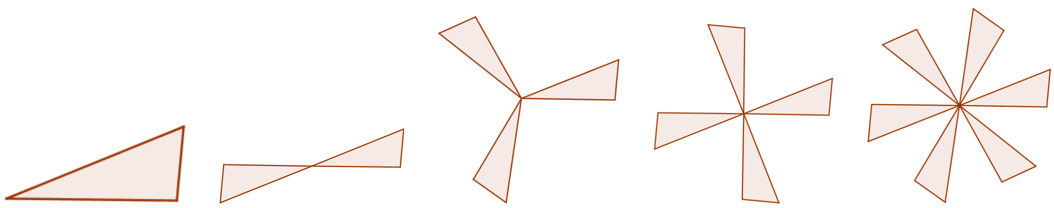

$c1$ $c2$ $c3$ $c4$ $c6$

Figure 3.18: Cn Groups

For the tiles with two-fold rotations, we observe dumbbell-like or hourglass-like structures (Fig. 3.20). Those structures occur when two nodes join at some point due to two-fold rotation. Observe that the dumbbell-like structure on the

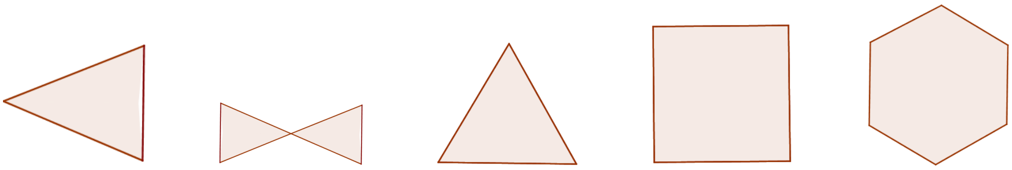

Figure 3.19: Dn Groups

left in Fig. 3.20 is more cyclic, indicating the absence of mirror reflection. This structure falls into $C2$ group, while other two are of group $D2$.

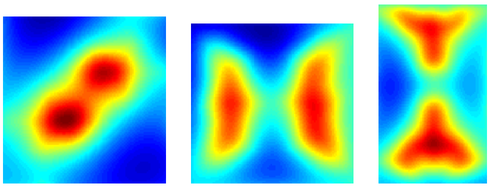

Figure 3.20: Structures representing two-fold rotation and mirror reflections

ω fields for the masks of the ornaments with three-fold rotations and mirror reflections, introduces structures like triangles and three-leaved roses (Fig. 3.21). From those structures, one can infer that the ornaments have three-fold rotations. In addition, those structures exhibit mirror reflections that indicate that the ornaments also contain mirror reflections. Notice that having both rotations and mirror reflections make this structures similar to $D3$ group. There is another type of three-leaved rose structures that show three-fold rotations as shown Fig. 3.22. They are cyclic, representing the absence of mirror reflections in an ornament. The abstract structures of this kind are of group $C3$.

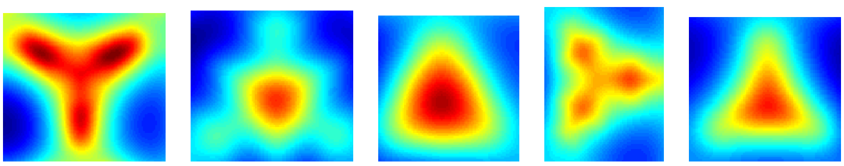

Figure 3.21: Structures representing three-fold rotations with mirror reflections

If three-leaved roses represent three-fold rotations, it would be natural to expect four-leaved roses where four-fold rotations are encountered. However, the struc-

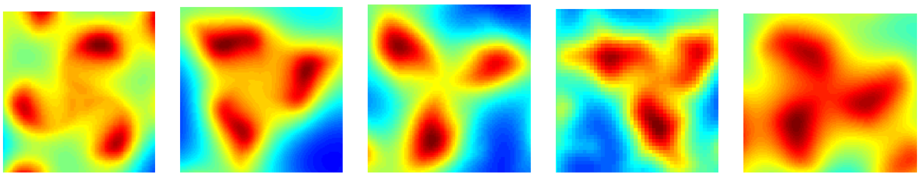

Figure 3.22: Structures representing three-fold rotations without morror reflections

tures for four-fold rotations might be in cross like forms, squares, or swastika like structures as well (Fig. 3.23). When there are no mirror reflections, those structures are more cyclic. Observe that in Fig. 3.23 first two abstract structures resemble $C4$ groups due to its cyclic nature, while three others resemble $D4$ groups.

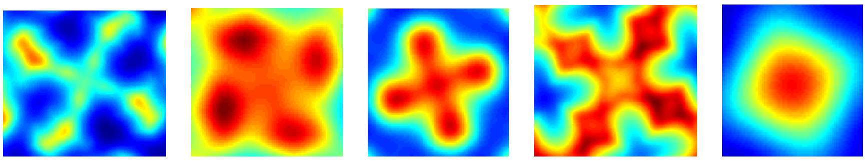

Figure 3.23: Structures representing four-fold rotations

The presence of six-fold rotations in an ornament is indicated by hexagonal structures in the ω fields of mask images. We might also observe six-leaved roses, as shown in Fig. 3.24. First two structures in the figure represent $D6$ group while others are more of $C6$ group.

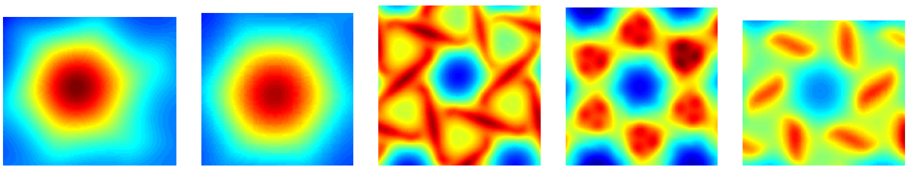

Figure 3.24: Structures representing six-fold rotations

The ω fields computed for ornaments tell more than just the underlying repetition rules. The structures introduced by the field, enable to take into account the continuity of symmetry. Before, we could just classify ornaments according to some predefined groups. Now, we can detect how similar different ornaments or different groups are to each other. For now, we can only perceive the symmetries and similarities between ornament styles. What we need next is to define some method that would measure those similarities. We approach this problem in the following chapters.

CHAPTER 4

CONSIDERING A COLLECTION OF TILES

In Chapter 3, we talked about content suppression in ornaments. As a result, for a given ornament we obtained filtered images with no clues on colors or shapes that are used by artist. What remains, is the underlying structure. It is interesting to observe how complex structures like *mariposas*, after filtering out content information, are left with simple *triskelion* and hexagonal structures. Furthermore, we showed that the ornaments that are created based on same rules, exhibit similar underlying structures. Thus, after content suppression we perceive style-wise similarities and differences in ornaments. However, perceiving similarities or differences in ornaments is not amenable to analysis. That is why; we need to introduce a method that measures pairwise similarities of ornaments. Had we used original ornaments for similarity measurement it would be highly influenced by colors and shapes that the ornaments exhibit. Using content suppressed images, on the other hand, gives style-wise similarities between ornaments. We pursue this result in this thesis. Once we know how to measure pairwise similarities, we can perform clustering of ornaments according to their style-wise similarities. The clustering results are not necessarily in agreement with the symmetry group classification. Given a whole collection of ornaments, we do not cluster them in one-step, identifying groups for whole collection. Instead, we keep in mind the continuous nature of symmetry and perform clustering on the subset of the whole ornament collection. Those clustering results will reveal how different groups are related.

In this chapter, we will talk about context-based continuous labeling, which describes our approach of studying ornaments. We explain the way we compute the pairwise similarities of ornaments, and the ways we visualize the clustering results. Then we show the clustering results for various subsets of our dataset, each conducted as a separate experiment.

4.1 Context-Based Continuous Labeling

The classical approach takes an ornament and labels it with some predefined group. It considers neither continuous nature of the symmetry, nor artistic intention for particular ornament. Recall Fig. 1.19, where two ornaments are given: one of group $p1$ and one of group pg. The repetition rules for those two ornaments are different due to minor changes in the tail part of the $p1$ ornament. Had not the artist introduced this little trick, given two ornaments would be considered of the same symmetry group. If we look at the color symmetries of those two ornaments then, again, both fall into different groups. However, perceptually they look similar. Labeling the ornaments according to predefined groups, does not show the closeness of those two ornaments. On the other hand, consider another example given in Fig. 3.2. It contains two ornaments of $p6$ group according to symmetry group. Further, considering the color symmetry, reveals that the highest order of rotation one of them contains is two, while the other contains three-fold rotations only. This situation introduces ambiguity. Furthermore, according to classical approach, given a set of symmetry groups, we know by the rules what symmetries each group contains, but we cannot say anything about the relations between those groups. However, one symmetry group might be very close to a second symmetry group, and be completely different from a third group. Introducing some kind of measurement of similarities between various ornaments, might reveal that the groups that contain rotations are more close to each other than those that do not contain rotations, or that the pure translational group is closer to the glide group than the rotational group. The same goes for ornaments that are within one group. It sees them as all equal ornaments. For example, for ornaments that are of pg group, in some ornaments a glide reflection of a motif goes to the same color, while in others it goes to the different color. This might indicate that the former ones and the latter ones form two clusters within *pg* group. These relations can only be discovered, when we take into account the continuous nature of symmetry. Instead of labeling the ornaments according to some predefined group, we seek to see how similar or how symmetrical the given ornaments are style-wise. In Chapter 3, we talked about retrieving the style of an ornament. In this chapter, we aim to cluster ornaments according to their styles. The emerging groups from our clustering results are not necessarily in agreement with symmetry group classification. However, taking all the ornaments and clustering them would not reveal the relations between different groups. That is why; we perform the clustering in multiple experiments. For each experiment, we consider only a subset of our dataset. Changing the ornament set, adding one more ornament to the previous collection, or changing the entire group of the previous collection, will reveal relations between groups that are clustered style-based. Thus, if an ornament in a given collection has no pair, which is of the same group, it joins the group, which is the most similar style-wise. Moreover, the ornaments that group in one context, might be in different groups in another context. In this manner, we perform style-based clustering, while also considering the continuous nature of symmetry.

For the dataset, methods and experimental results see subsequent sections.

4.1.1 Dataset

The whole set of ornaments used in our experiments are given in Fig. 4.1. In most of our experiments we use Escher's ornaments, which are listed in Fig. 4.1(a). The first row contains three ornaments with three-fold rotations and mirror reflections. The second row consists of ornaments of group $p6$ according to Wallpaper group. They are internally divided into three groups. The first group is *mariposas* group, which consists of three three-color ornaments. The next two ornaments are also three-color, however, the permutation of colors is different. The third group consists of three two-color ornaments. Ornaments that contain four-fold rotations are listed in the third row. Here, first three ornaments are of group $p4$ and next two ornaments are of group $p4g$. The next group lists six ornaments of glide group. They are also divided internally, so that first two ornaments are of group pgg (two-fold rotations and glide reflections) and last four ornaments are of group pg (glide reflection only). The last row lists six ornaments of pure translational group. Beside Escher's ornaments, we use ornament sets of computer-based creations. The first set is shown in Fig. 4.1(b), where one can observe two different groups. First group consists of five ornaments with three-fold rotations and mirror reflections. The second row lists ten ornaments of group $p4g$. The last set consists of ornaments created by iOrnament application [64]. First row contains a single ornament of cm group. Second row contains two ornaments with three-fold rotations and mirror reflections. Five ornaments of group $p4$ are listed next. Five ornaments of group $p6$ complement the dataset.

4.1.2 Method

In order to be able to quantify how close two images are, we should use some method that measures the similarity between them. Our method is as follows. First, the image features are detected and described using Scale-invariant Feature Transform (SIFT) [50]. SIFT guarantees invariance to scale, rotation and translation while computing pairwise similarities. Then the descriptor of an image is matched to descriptors of other images. Number of matches between the descriptors of images form an intermediate similarity matrix. Next, the number of occurrences of an image in another image's first N (15 in our case) most similar retrievals is calculated. The same image may appear several times since there are several masks of one image. The results are the sum of the occurrences of two images within each other's first N retrieval results. This gives our final similarity matrix.

4.1.3 Visualization of Results

The similarity matrix is not informative on its own, since it cannot be visualized. In order to visualize the similarities of images we turn to dimensionality reduction methods. In our approach two types of dimensionality reduction methods are used: Spectral Multidimensional Scaling (SMDS), introduced by [1], and t-Stochastic Neighborhood Embedding technique, introduced by [77]. Those techniques help to reduce the dimensionality of the similarity matrix, while preserving between-object similarities as much as possible. In all our experiments, the dimensions of similarity matrices are reduced to two and three dimensions. Since two dimensions are easy to visualize, the results for it are plotted directly. However, we do not plot the ornaments themselves. Instead, we use different shapes cut out of ornaments, each shape representing different group. For example, an ornament with four-fold rotations assigned to square shape. See Fig. 4.2 for a sample plot. There, we have triangular, circular, square and inclined rectangular shapes. Triangle indicates three-fold rotation, square indicate four-fold rotation, circles indicate six-fold rotation, and inclined rectangles indicate pure translation or glide reflection. The edge colors on the shapes also represent different groups. For circular shapes, different colors indicate distinct groups with six-fold rotations. Inclined rectangles framed in green color represent pure translational group, while the same shape framed in orange color represents glide group.

Three dimensional results, on the other hand, are mapped to RGB color space. For that, all three dimensions are normalized so that the values are between [0,1]. Since we have three values for each dimension, those values are used to represent RGB colors. Now, ornaments that are close to each other will represent colors similar or close to similar to each other. Observe Fig. 4.3 for an example illustration. The colors are not fixed for some group, in each run every group assigned different color. Note that, the ornaments within one group do not get exactly the same color. Instead, every ornament in a group gets different shades of the same color. Getting exactly the same colors is possible only when two ornaments are reduced to exactly same coordinates. Mapping the coordinates to RGB color space is done solely for visualization purposes, and do not carry any additional information.

For each experiment, we also show a confusion matrix that represents pairwise distances of ornaments. The distances are computed from coordinates obtained after reducing the similarity matrix to three dimensions. See Fig. 4.4(b) for an example of confusion matrix representation. Since the confusion matrix is computed from three-dimensional clustering result, one can look up the ordering of ornaments from three-dimensional result. The ordering of ornaments in confusion matrix is in the order shown by arrows in Fig. 4.4(a). Thus, for this particular example, the confusion matrix shows first six ornaments shown in burgundy, and then come three ornaments shown in pink, then come three ornaments in blue, then green, and the last group is the gray group.

4.1.4 Clustering

Given a dataset we divide the clustering process into multiple experiments. Each time a subset of the dataset is selected for clustering. In each experiment, we add single ornament, add entire group or change one group to another. For each experiment, once we select a collection to be clustered, we construct a similarity matrix. The dimensionality of a similarity matrix is then reduced using one of the techniues described above. Summary of all the steps performed in single experiment is illustrated in Fig. 4.5.

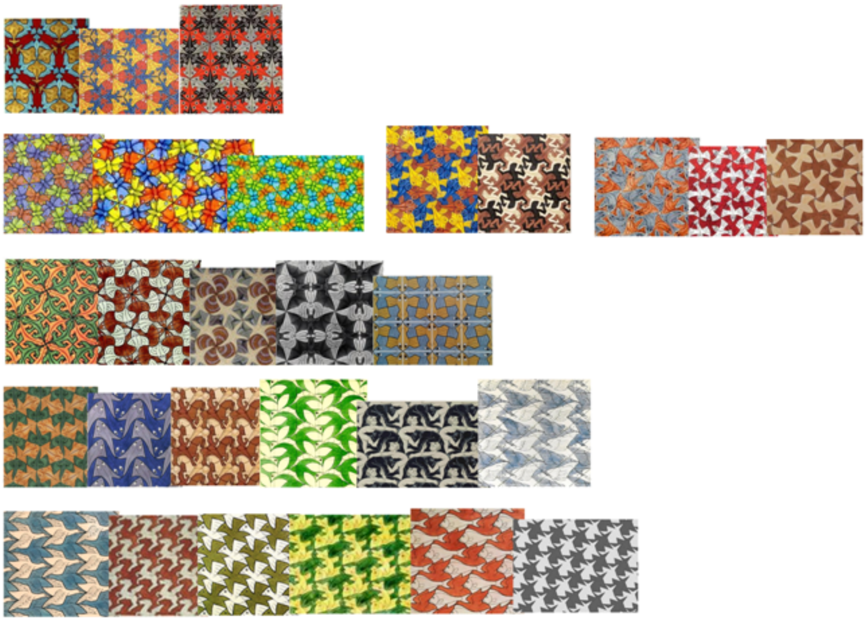

(a)

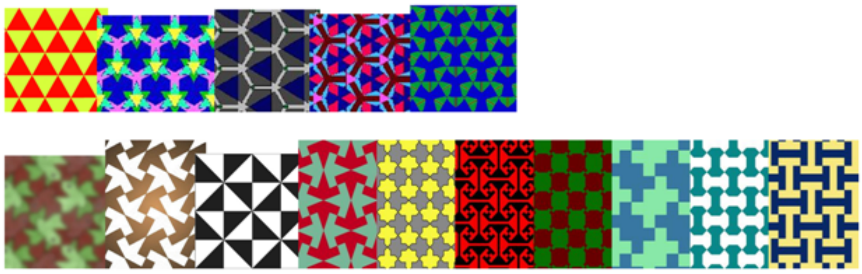

(b)

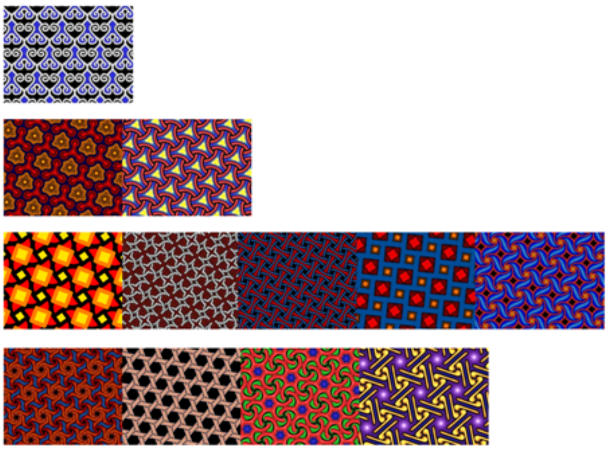

(c)

Figure 4.1: Dataset. Overall fifty-five ornaments are considered. (a) Escher's ornaments. (b) Computer generated ornaments. (c) Computer generated ornaments from iOrnament database.

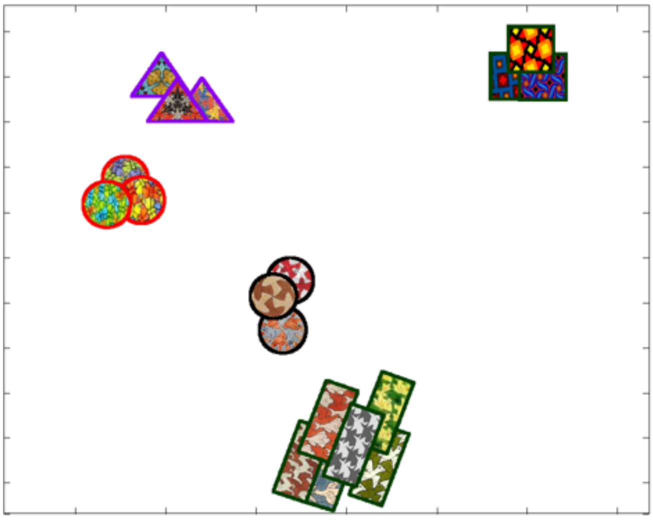

Figure 4.2: An example for visualization of clustering results obtained when the similarity matrix is reduced to two-dimensions. Triangles represent ornaments with three-fold rotations and mirror reflections. Circles represent $p6$ groups: mariposas are framed in red circle and three two-color $p6$ ornaments framed in black circle. Squares represent ornaments with four-fold rotations. Inclined rectangles framed in green represent pure translational group.

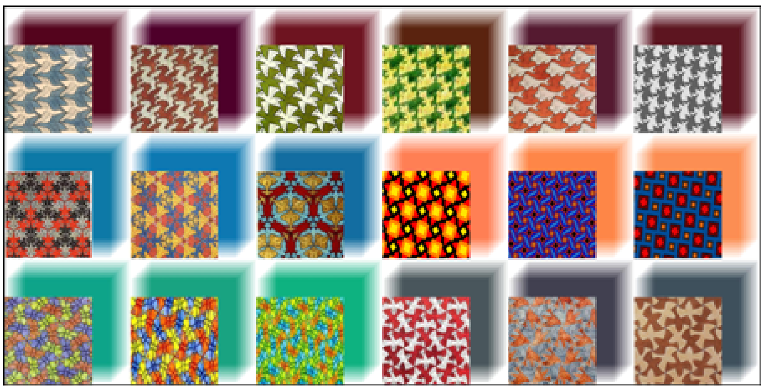

Figure 4.3: An example for visualization of clustering results obtained when the similarity matrix is reduced to three-dimensions. The 3D coordinate positions obtained are mapped to RGB color space. Thus, ornaments that reside close to each other are assigned to similar colors.

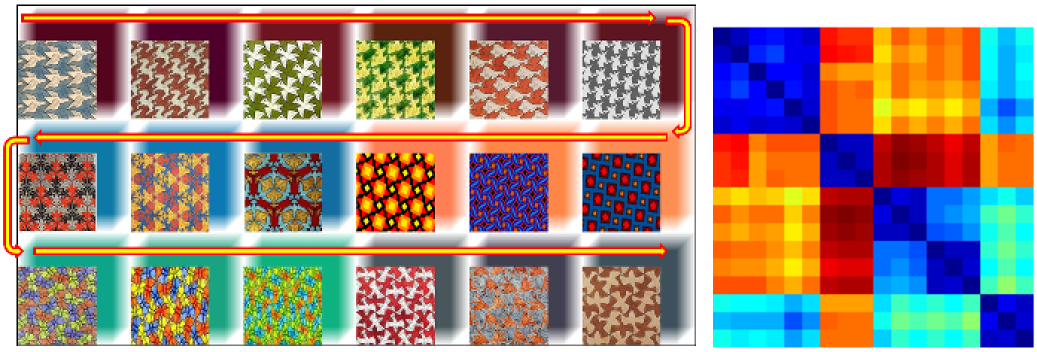

(a) (b)

Figure 4.4: An example for confusion matrix shown on (b). The order based on which the ornaments in confusion matrix reside is shown by arrows in (a).

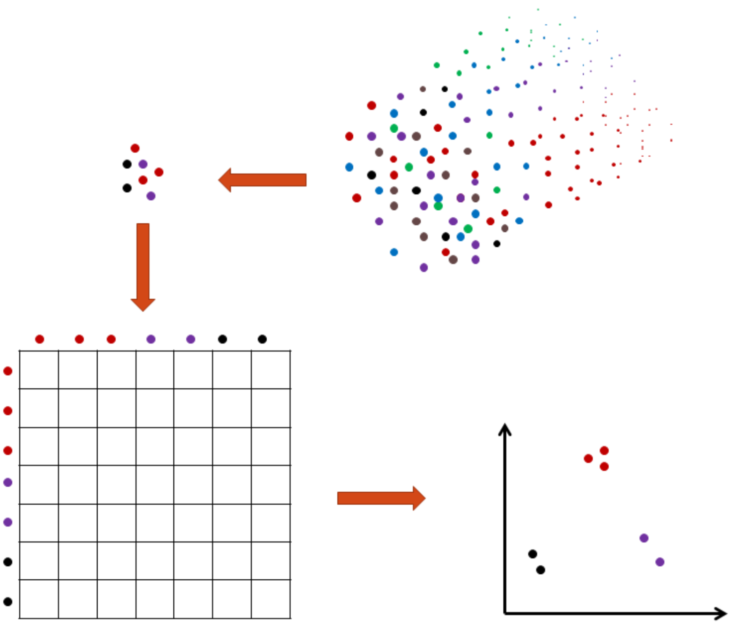

Figure 4.5: Illustration summarizing the clustering process.

4.2 Experimental Results

For the given dataset overall forty-three experiments were conducted. In this section we give clustering results for all forty-three experiments which are illustrated in Figs. 4.6-4.49. For each experiment, we show the results for both tSNE and SMDS dimensionality reduction techniques. For each dimensionality reduction technique, as mentioned above, we show three results: results where the dimensions of similarity matrix are reduced to two and three dimensions, and a confusion matrix, which is based on the three-dimensional result. The tSNE results are illustrated first, and then the SMDS results are shown.

For the first experiment eighteen ornaments are chosen: three ornaments of *mariposas* group, three ornaments of two-color $p6$ group, three ornaments with three-fold rotations and mirror reflections, six ornaments of pure translational group, and three ornaments of $p4$ group from iOrnament collection. We expect exactly these five groups to emerge as a clustering result. The clustering results are illustrated in Fig. 4.6. First row contains tSNE results, while the second row contains SMDS results. All results illustrate expected five groups. Observe that, in two-dimensional results, squares representing $p4$ group are clustered together, triangles representing ornaments with three-fold rotations from another group, two different circle groups are grouped according to the colors on the circle edge (red and black), and finally slightly inclined rectangles with green edges representing pure translational group form another group. The three-dimensional results also give five different main colors for the ornaments. Both two-dimensional results reveal closeness between the three ornaments of $p6$ group and a pure translational group. This closeness occurs because both groups contain ornaments of two colors, indicating that the number of colors also influence the style of an ornament. The closeness of these two groups is also observed from confusion matrices. Also observe the closeness between the *mariposas* group and three ornaments with three-fold rotations and mirror reflections, for both tSNE and SMDS results. The $p4$ group is isolated from all other groups, indicating style-wise difference from the other groups in the collection.

For the next experiment, we replace three ornaments of $p4$ group of the previous

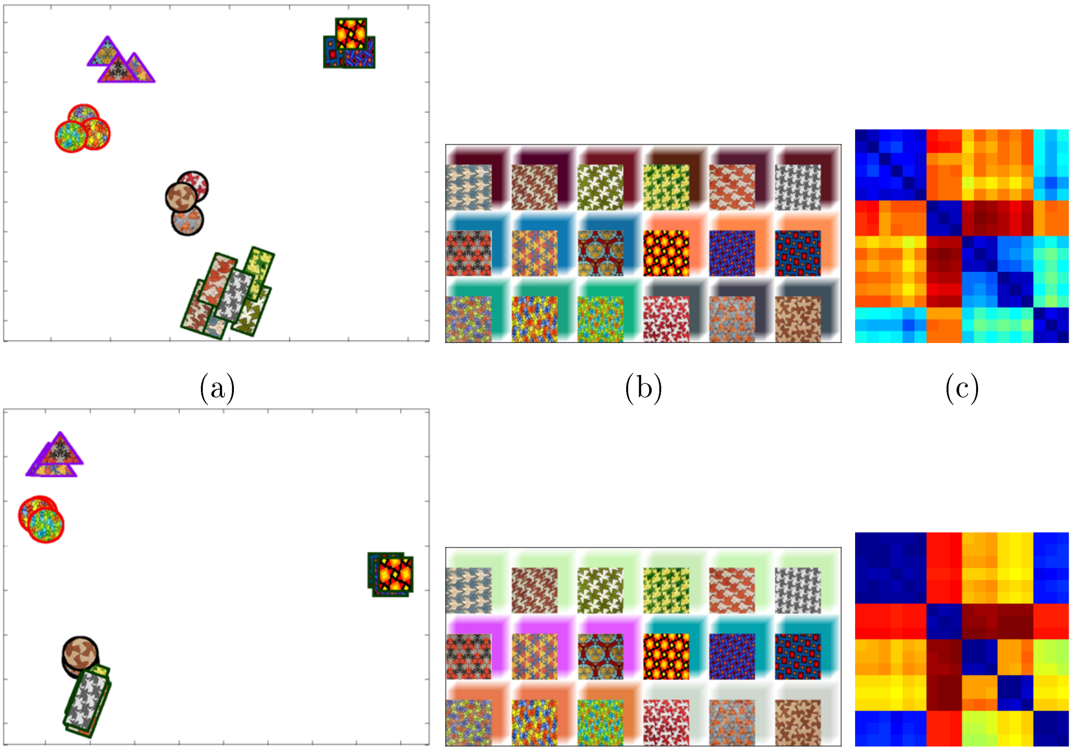

(a) (b) (c)

(d) (e) (f)

Figure 4.6: Experiment 1.

collection, with two other ornaments of $p4$ group. We still expect five groups to emerge as a clustering result. Observe five main colors in three-dimensional results (Fig. 4.7(b) and (e)), just as we expected. While the $p4$ group, in the previous experiment, stayed isolated, in the current context they are shown to be close to a triangular group (Fig. 4.7(c) and (f)). This is mostly due to rosette structures in the latter group, while the former group exhibits mostly square structures when the content is suppressed. The two-dimensional result for tSNE (Fig. 4.7(a)) gives a clear separation between the rotational groups and a pure translational group.

Fig. 4.8 shows the connections of groups in Experiments 1 and 2. The link colors connecting two groups are chosen to be as close as possible to the results of confusion matrices. Thus, the blue links indicate strong connections while red links indicate weak connections. Also, the bolder the link the stronger the connec-

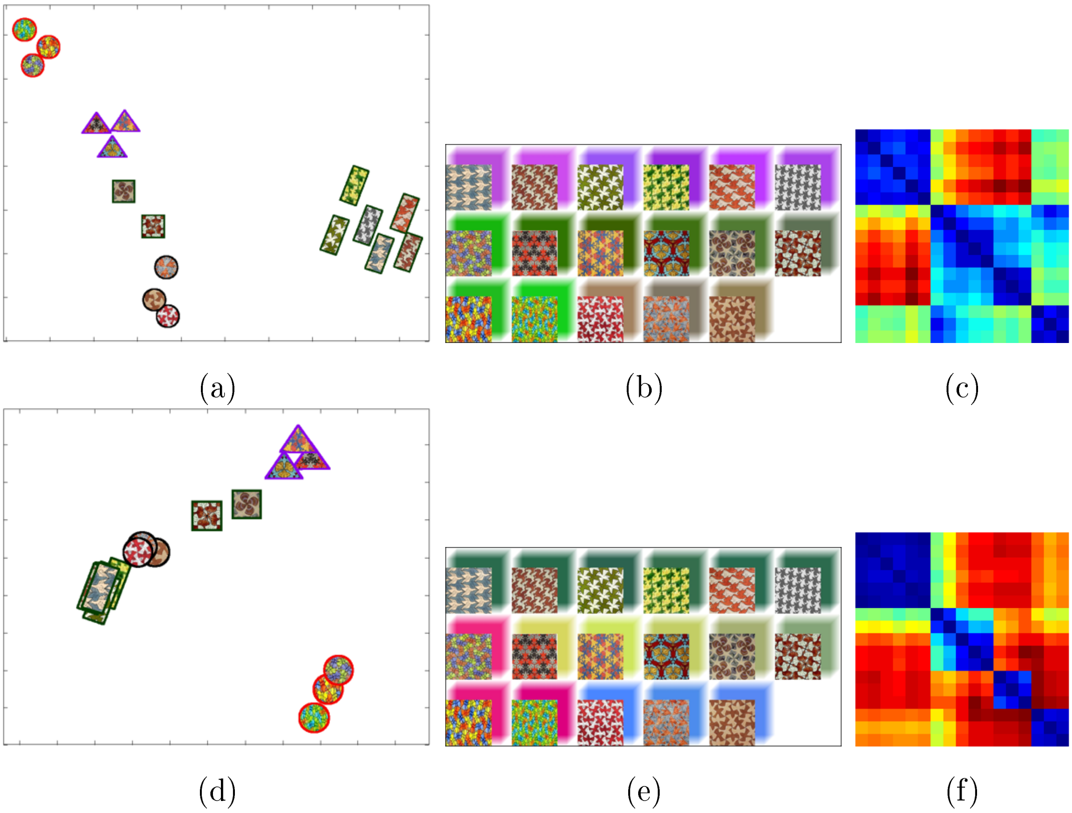

Figure 4.7: Experiment 2.

tion between two groups. Observe that for the first experiment (Fig. 4.8(a)) the $p4$ group has weak connections to all other groups, while in the second experiment (Fig. 4.8(b)) the $p4$ groups has a strong connection to rotational groups due to four-leaved rosette structures in their ω fields. The square structures of the $p4$ group in the first experiment make it style-wise different from all other groups. The relation of pure translational group to other groups is similar in both experiments.

In the next experiment, we replace the pure translational group of the previous collection, with five ornaments of glide group. The glide group is further divided into pg group, where only glide reflection is used, and pgg group, where two-fold rotations come along with the glide reflection. However, in this context, we expect those five to form one cluster.The clustering results are shown in Fig. 4.9. The tSNE results (top row) give five groups, while the SMDS result (second

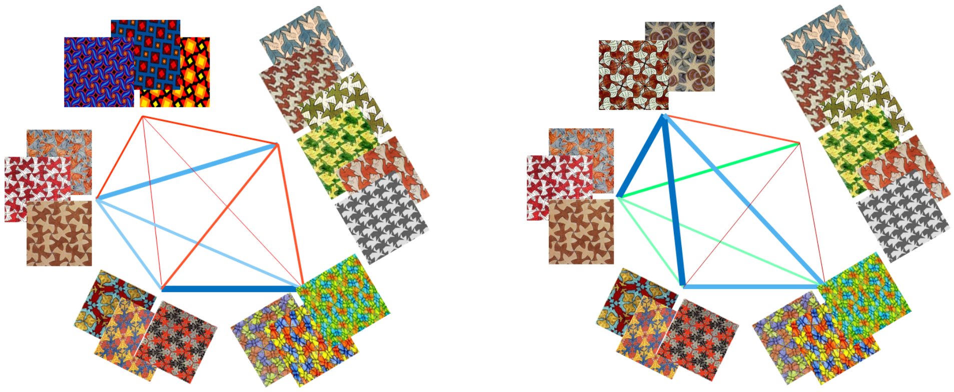

(a) (b)

Figure 4.8: Experiment 1 and Experiment 2: Connections.

row) give four groups clustering the two-color $p6$ group with two ornaments of $p4$ group. Observe that the groups with two-color ornaments (glide, $p4$ and $p6$ groups) are placed close to each other. tSNE clustering result separates the rotational groups from glide group, which is clear from confusion matrix. Two-color rotational groups form a bridge between the glide group and the other rotational groups.

We eliminate two ornaments of $p4$ group from the previous collection and see more scattered groups to emerge (Fig. 4.10). While the confusion matrix for SMDS result (Fig. 4.10(f)) show no relation between groups, the confusion matrix for tSNE result (Fig. 4.10(c)) shows the closeness of rotational groups, and also the two-color groups (glide and two-color $p6$ groups).

Next, we add two three-color ornaments of group $p6$ to the collection in Experiment 4. Although these two ornament are of $p6$ group, they are style-wise different from any other $p6$ group in the collection. When the colors are considered, these two ornaments exhibit two-fold rotations only, while the other groups exhibit three-fold rotations. Therefore, we expect these two ornaments to form a group on their own. Thus, overall five groups are expected. See Fig. 4.11 for clustering results. There are exactly five groups for two-dimensional results. We see four major colors for three-dimensional clustering results. The green color, in the three-dimensional tSNE result, is further divided into two. The darker

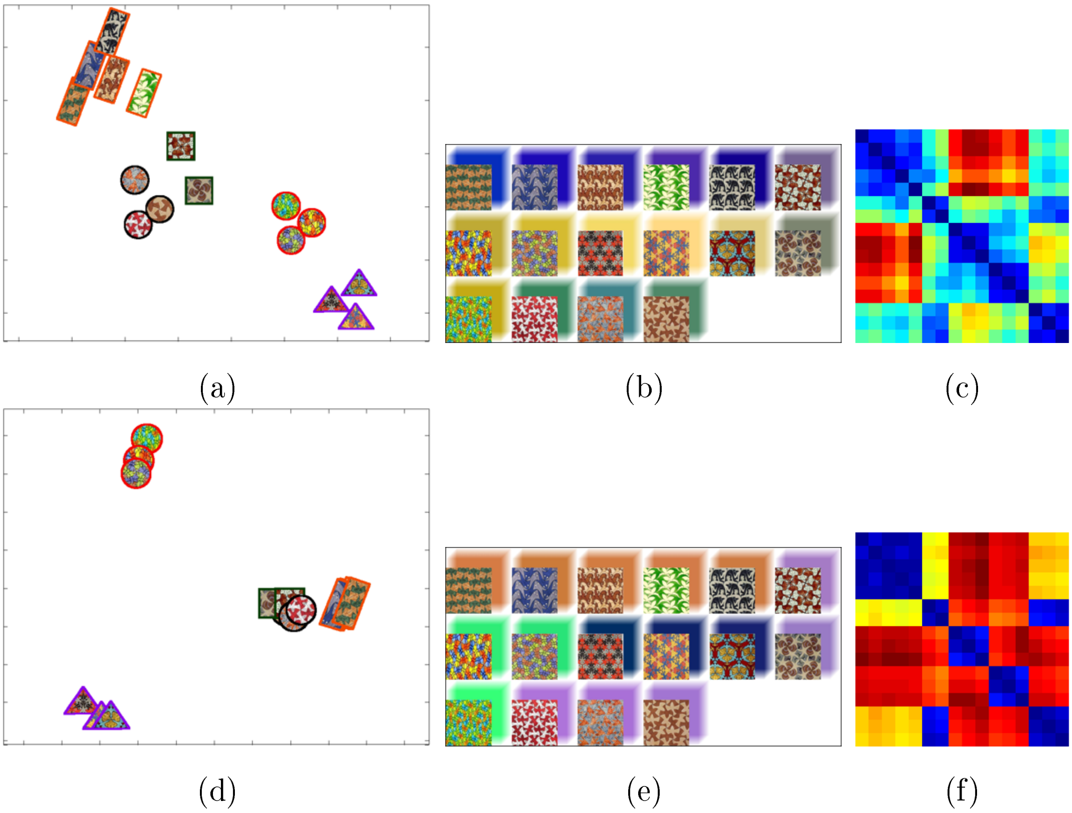

Figure 4.9: Experiment 3.

green indicates two newly added ornaments. The purple color, in the three-dimensional SMDS result, also has two shades, where the lighter one is assigned to newly added ornaments. Observe the closeness of $p6$ groups (represented with circular shapes) against two other groups (glide and three-fold rotational groups), which is also clear from confusion matrix of the tSNE result.

Until now we have been choosing the collection so that each ornament has its style-wise similar pair. In the next experiment, we add a single ornament of pure translational group to the ornament collection of Experiment 5. Since there are no other ornaments of pure translational group, we expect this one to join the closest group in terms of style. From the content suppressed images from previous chapter, we saw that pure translational group is style-wise close to glide group. This is no wonder, both groups have no rotations, hence do not exhibit rosette structure when the content is suppressed. Thus, we expect the newly

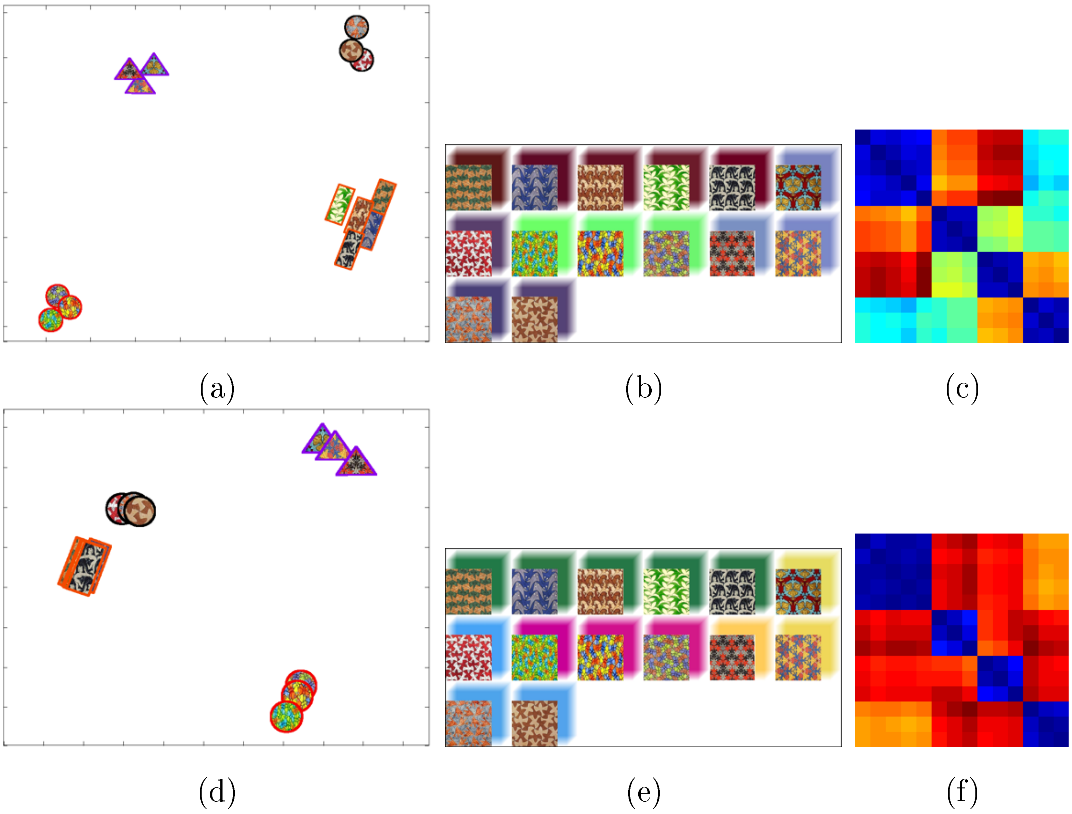

Figure 4.10: Experiment 4.

added ornament of $p1$ group, to join the glide group. Fig. 4.12(d) and (h) show the retrieval results for the standalone ornament for tSNE and SMDS results respectively. Observe that the first closest ornaments are the ones from glide group. Furthermore, both two-dimensional and three-dimensional results show the ornament of $p1$ group (inclined rectangle framed in green) with the glide group (inclined rectangle framed in orange). This example is an illustration for continuous nature of symmetry. Instead of isolating this newly added ornament by saying that it has no similar symmetry, we group it with the ornaments of the closest symmetry.

We reduce the ornament collection from the previous experiment by eliminating two three-color ornaments of $p6$ group. See the clustering results in Fig. 4.13. Observe that the groups become more scattered. These two three-color ornaments of group $p6$ are mostly similar to all groups due to their style-wise

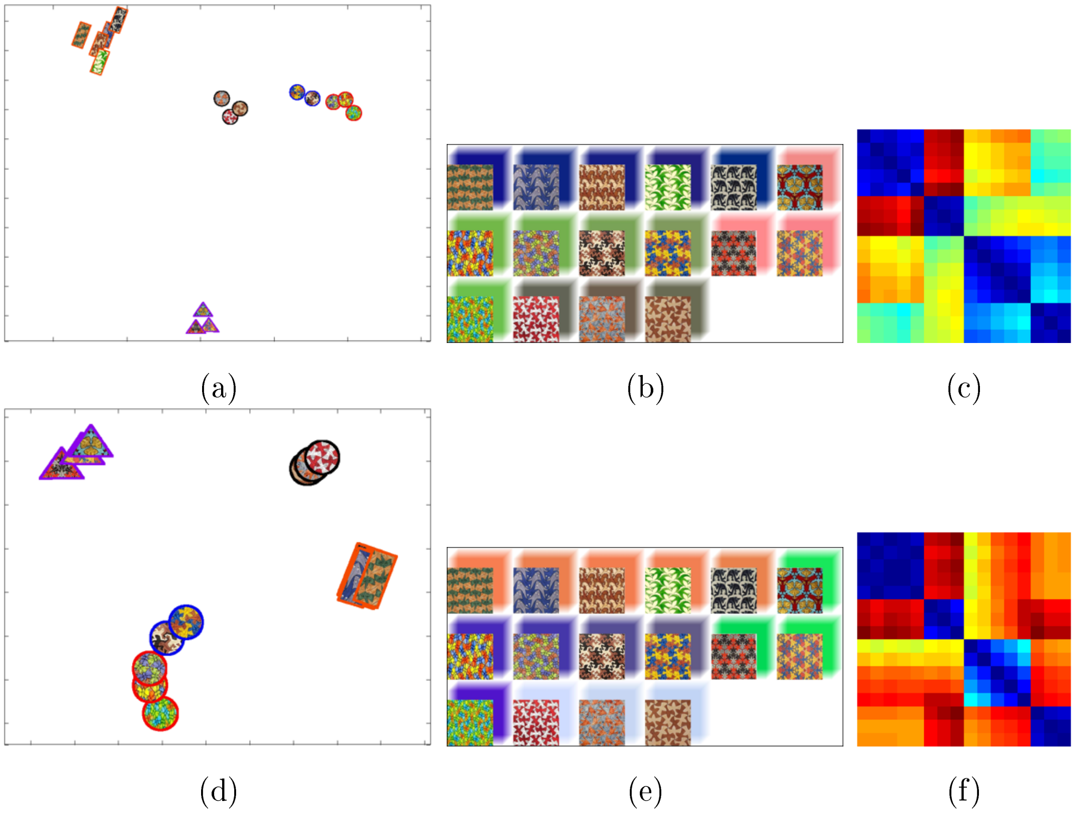

Figure 4.11: Experiment 5.

differences. Hence, they were pulling the clusters together; eliminating which, put gaps between groups.

In the next experiment, we again replace the glide group in the previous experiment, with five ornaments of pure translational group. Thus, taking into account one ornament of $p1$ group which already was in the collection, there are six ornaments of $p1$ group. The expected number of clusters to emerge is four. See the clustering results in Fig. 4.14. Observe that the pure translational group behaves similarly to the glide group in the previous experiments. It is separated from rotational groups, but has some closeness to three two-color ornaments of $p6$ group due to number of colors used in ornaments. The two-dimensional tSNE result separates the rotational group from pure translational group, while the SMDS result fails to do so.

In the ninth experiment, we add two three-color ornaments of $p6$ group to the

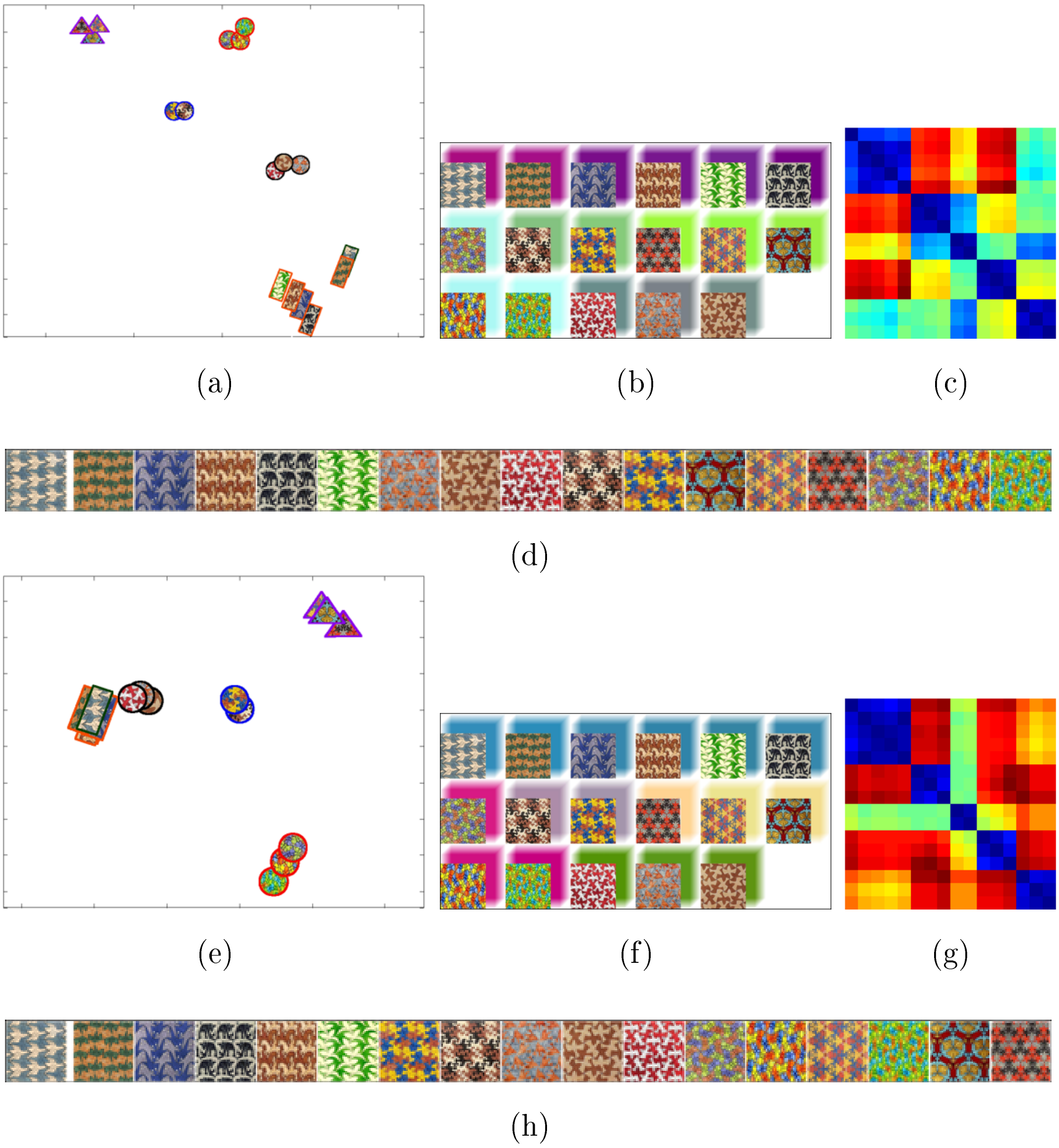

Figure 4.12: Experiment 6.

collection of the previous experiment. Overall, five clusters are observed in Fig. 4.15. Observe the two-dimensional tSNE result in Fig. 4.15(a). The newly added ornaments pull other ornaments of rotational group, giving a clear separation betwen the rotational groups and pure translational group.

Taking the last experiment as a base, we will consider three different cases: adding an ornament of cm group, adding an ornament of glide group, and an ornament of $p4$ group. All newly added ornaments have no pairs in the collection.

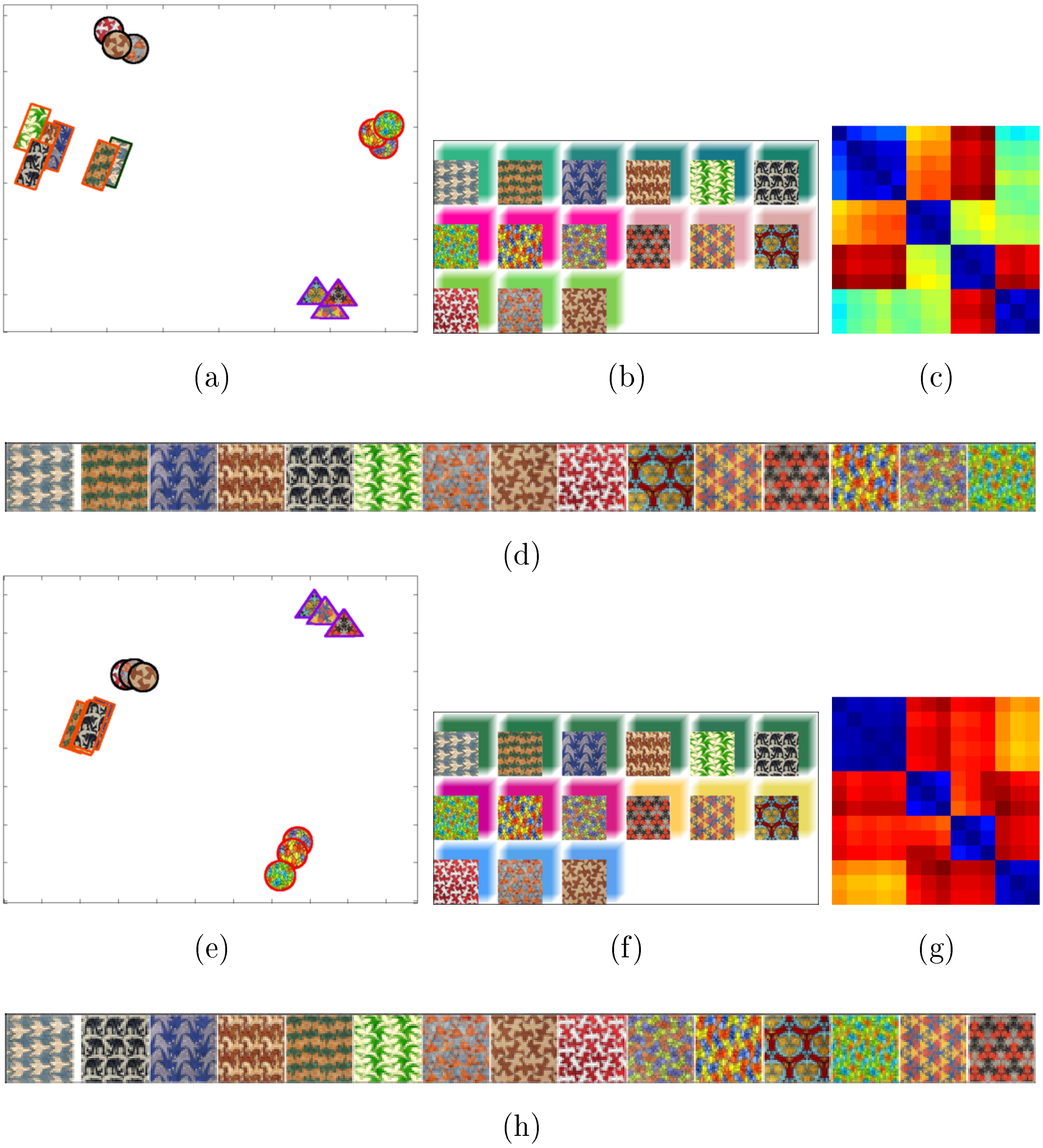

Figure 4.13: Experiment 7.

In the first case, we add an ornament of group *cm*. The symmetry group *cm* introduces ornaments that contain no rotations. There are mirror reflections along one axis and glide reflections in this kind of ornaments. Style-wise the *cm* ornament is more close to $p1$ group in this collection. Thus, we expect it to join the $p1$ group. This is exactly the case, as shown in Fig. 4.16. The topmost similar ornaments in the retrieval results for both tSNE and SMDS (Fig. 4.16(d) and (h), respectively) are the ornaments of pure translational group.

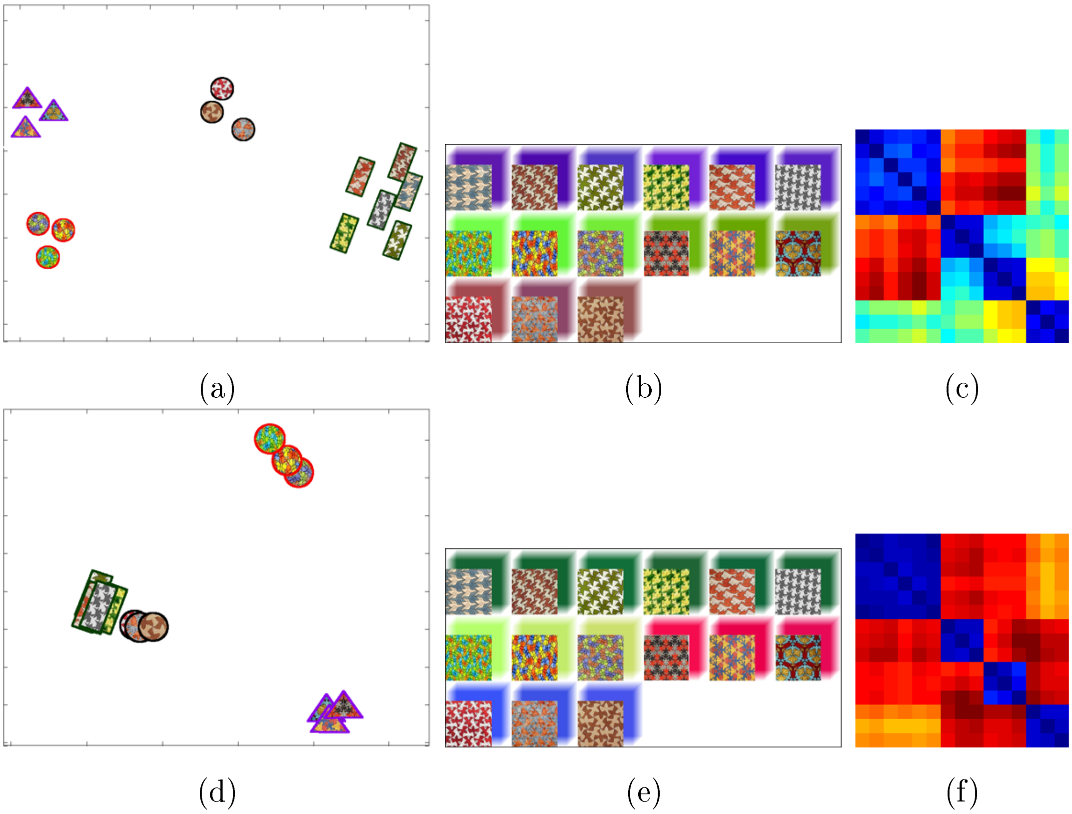

Figure 4.14: Experiment 8.

In the second case, we add an ornament (a bird shown in white and blue) of pg group instead. We again expect this one to join the pure translational group, since no other ornaments of glide group exist in the collection. See the clustering results in Fig. 4.17. Both two-dimensional and three-dimensional results classify the pg ornament with the $p1$ group. Also observe the retrieval results obtained according to distances of three-dimensional results. The ornaments of $p1$ group are the closest ones to the ornament of pg group.

Finally, we add an ornament of rotational group. An ornament is chosen to be of group for which there is no pair in the current collection. The current collection has no ornament of $p4$ group. Thus, we add an ornament of $p4$ group, and expect it to join the group, which is the closest to it style-wise. The closest group is one of the groups among rotational groups. The newly added ornament contains two colors, and since the number of colors is also part of style, we expect

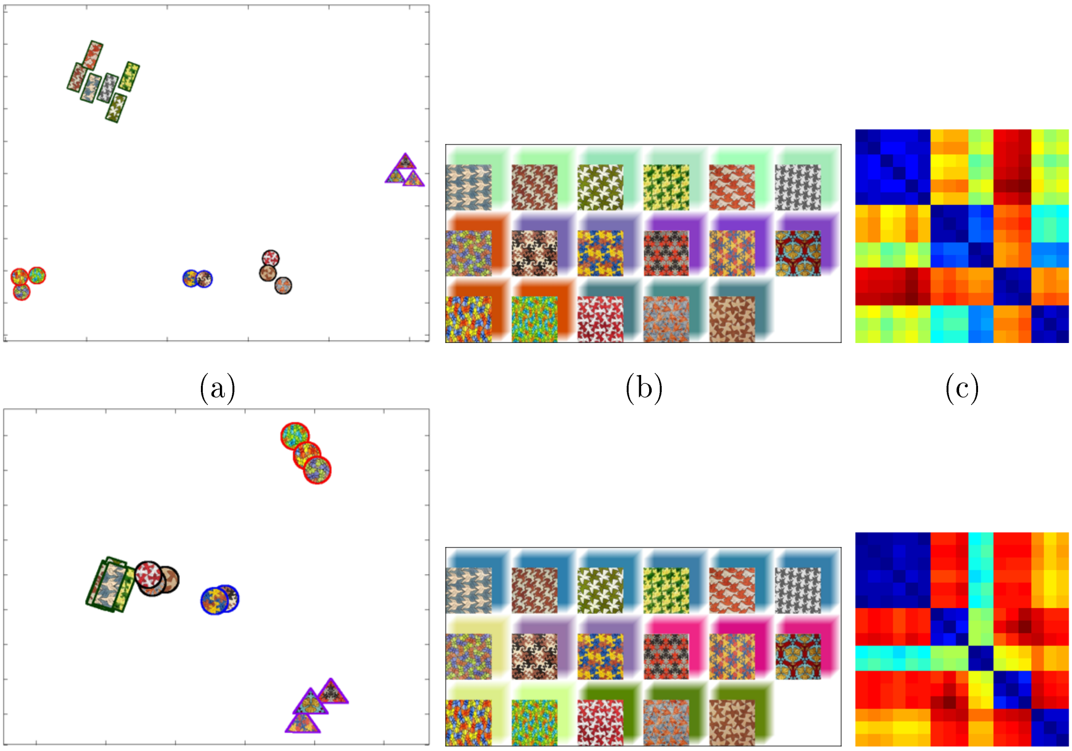

(a) (b) (c)

(d) (e) (f)

Figure 4.15: Experiment 9.

it to join three two-color ornaments of group $p6$. See Fig. 4.18 for the clustering results. In two-dimensional tSNE result (Fig. 4.18(a)) we have five groups, and the ornament of $p4$ group joins a group of three two-color ornaments of group $p6$ just as we expected, while the two-dimensional SMDS result fails to separate the groups properly. In three-dimensional results for both tSNE and SMDS we have exactly five expected groups. Note that the ornament of $p4$ group joins the $p6$ group only because there are no other ornaments of the same group. We add one more ornament of $p4$ group to the collection in Experiment 12. We expect it to join the previous ornament of $p4$ group, and these two to form a group on their own. Observe Fig. 4.19. Six groups emerge from all clustering results, except for the two-dimensional SMDS clustering result Fig. 4.19(d). It again fails to separate the two-color ornaments into proper groups. Also, observe that the two-dimensional tSNE result gives a clear separation of rotational groups from pure translational group in Fig. 4.19(a). It is worth mentioning that the

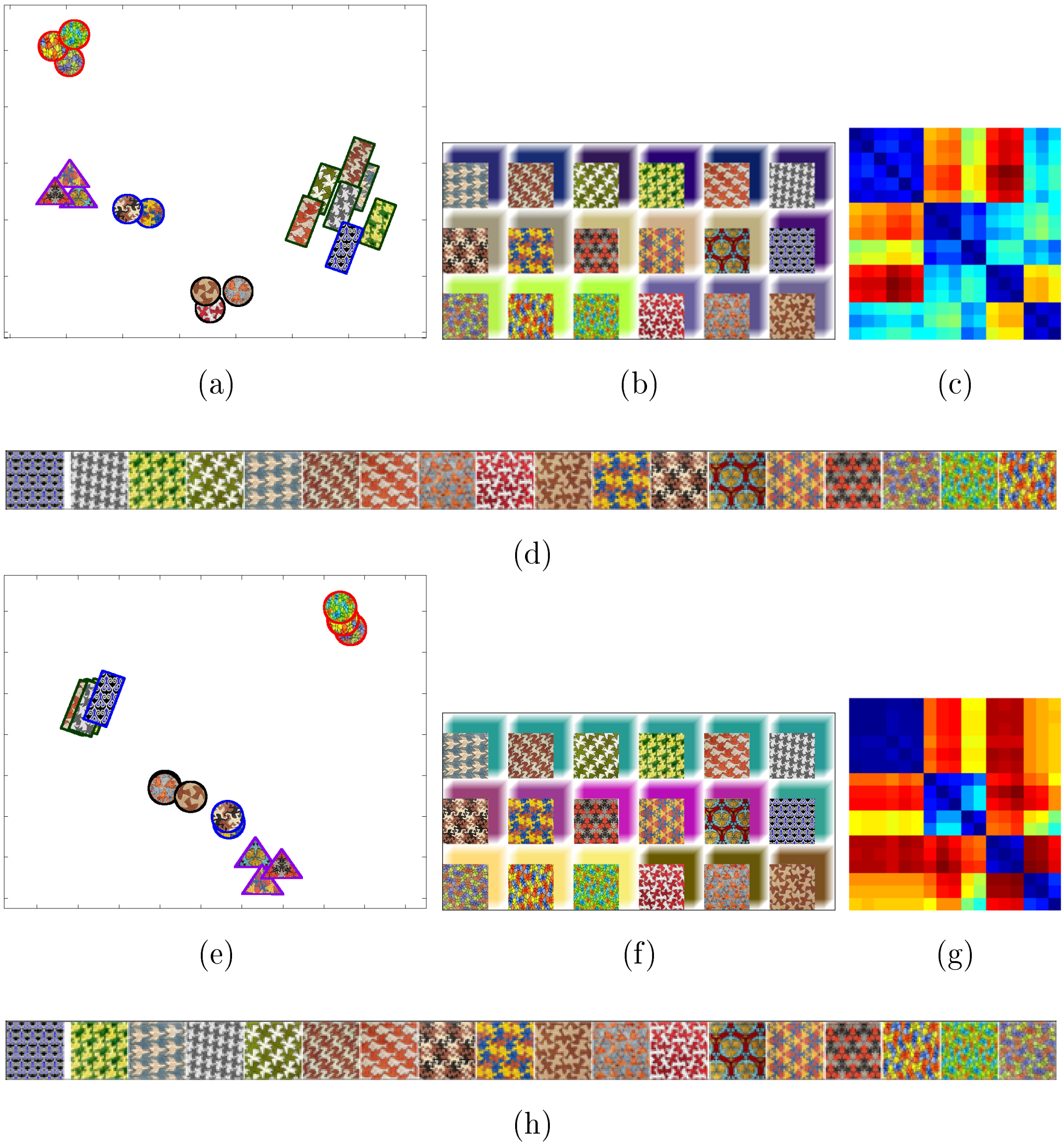

Figure 4.16: Experiment 10.

tSNE generally give a good separation between rotational and pure translational groups, or rotational and glide groups, while SMDS generally cannot recognize this distinction.

Next experiment is another illustration of style-wise closeness between glide group and pure translational group. We have three ornaments of glide group, two ornaments of pure translational group, and three ornaments of *mariposas* group in our collection. The clustering results are shown in Fig. 4.20. We have two major groups in two-dimensional cases. One group is *mariposas* group, the

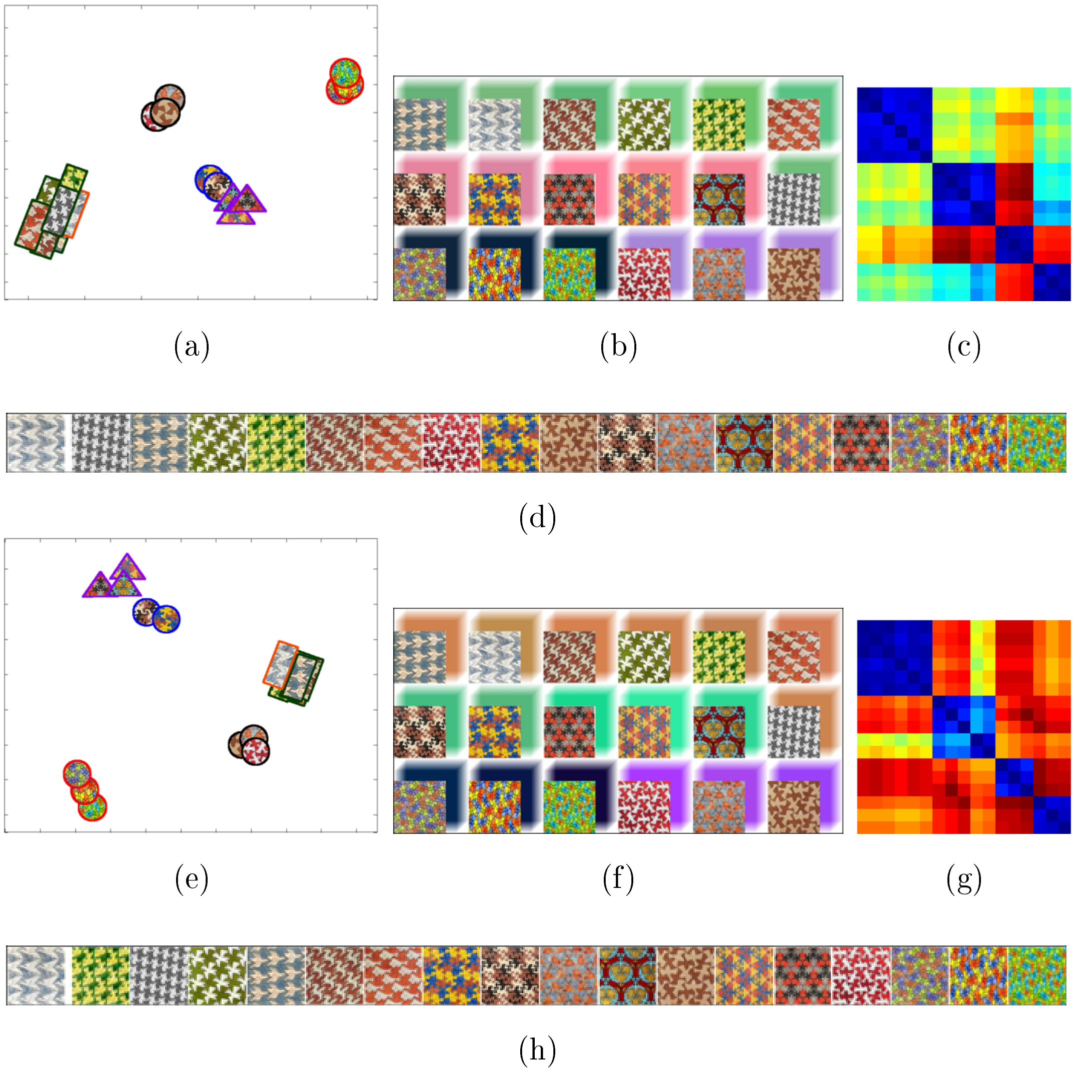

Figure 4.17: Experiment 11.

other is the glide and translational group. The closeness of those two groups (glide and translational) can also be observed from the confusion matrices. However, internally, within this group we observe division into two. Two ornaments of glide group form one cluster; this is also seen from the colors they are mapped from three-dimensional cases. The third ornament joins two ornaments of pure translational group and form another cluster. Recall that, in introductory chapter we were claiming that this third ornament of glide group is perceptually very similar to the ornament of pure translational group, which consists of two different blue and white birds. Since we consider those two ornaments style-wise similar, the clustering results does not seem awkward.

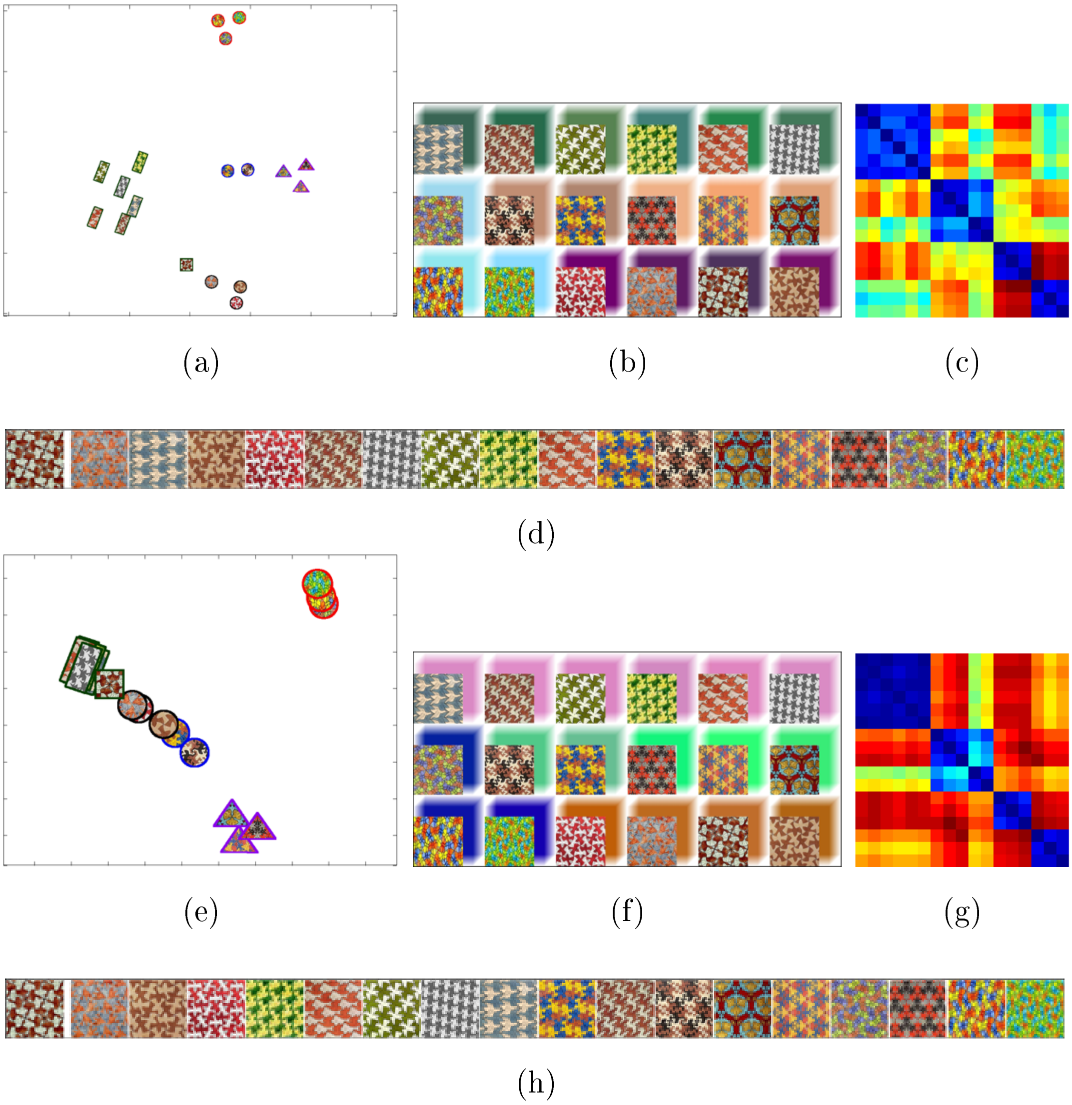

Figure 4.18: Experiment 12.

Up to now, all experiments have shown a style-wise closeness between pure translational and glide groups. A single ornament of glide group joins the pure translational group, or vice versa in the clustering results. Also, in the previous experiment the glide group joined the pure translational group against the rotational group. However, it is equally important to be able to distinguish between those two groups. In the next experiment, we aim to see if the style-wise differences between these two groups are captured via a collection of six ornaments, two of which belong to pure translational group, and four are of glide group. The clustering results give clear separation between those two groups as can be

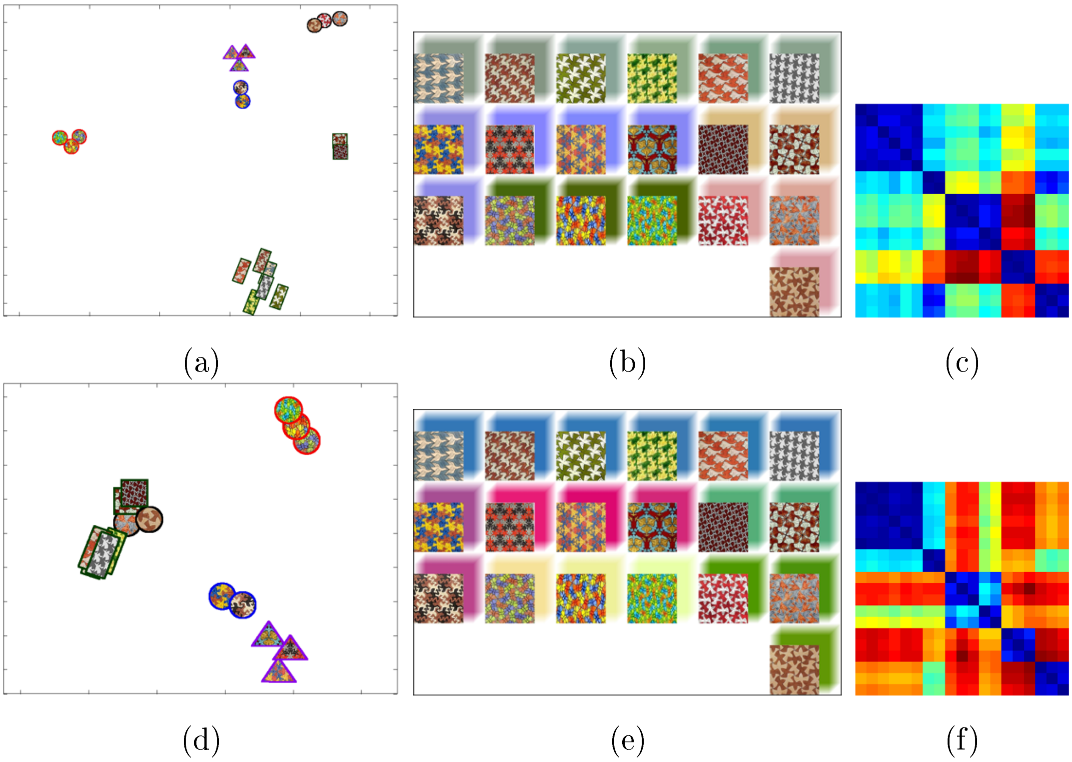

Figure 4.19: Experiment 13.

seen from Fig. 4.21. Observe that both tSNE and SMDS results separate the translational group from glide group.

Consider another collection of six ornaments, where three of them belong to pure translational group and remaining three are of glide group. Again, both tSNE and SMDS results give precisely two groups, successfully separating the glide group from pure translational group (Fig. 4.22).

Previous experiments reveal two big groups within the dataset: a rotational group and a group that contains glide and pure translational groups. Just like an ornament from pure translational group joins the glide group in the absence of other ornaments from the same group, we expect an ornament from rotational group to join any other rotational group against pure translational or glide group in the absence of its own group in the given collection. The next experiment aims to see if this is the case. Consider a collection of six ornaments: three ornaments of pure translational group, two two-color ornaments of group $p6$

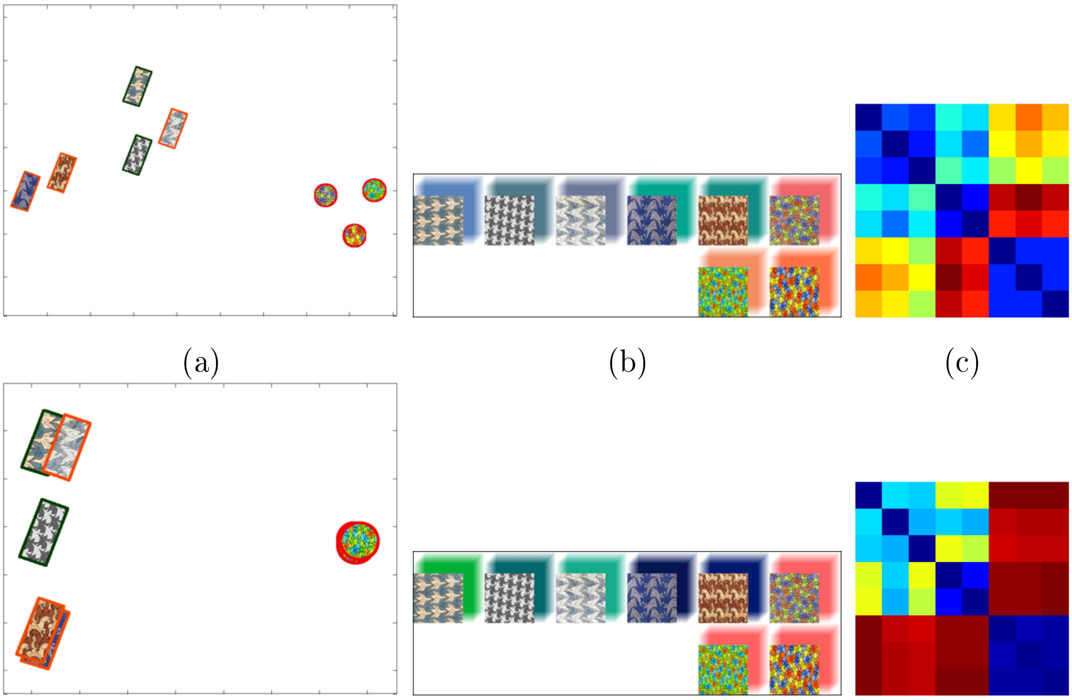

(a) (b) (c)

(d) (e) (f)

Figure 4.20: Experiment 14.

and an ornament of $p4$ group. Since the latter one stands alone, we expect it to join one of two groups. The $p1$ group contains nothing but translations, while both $p6$ and $p4$ groups contain rotations. Thus, we expect the standalone ornament to join the $p6$ group. The clustering results are shown in Fig. 4.23. In all results the collection is divided into two groups: the rotational and pure translational groups.

Consider another collection with six ornaments, where four of them belong to pure translational group, one of them belong to *mariposas* group ($p6$), and the last one is an ornament with three-fold rotations and mirror reflections. We expect two standalone ornaments to join and form a group as a clustering result. When the context is suppressed from images, these two standalone ornaments get three-leaved rosette structures (the ornament of $p6$ group gets three-leaved rosette structures due to color permutations), though structures have some differences. This make them style-wise closer, against the pure translational group,

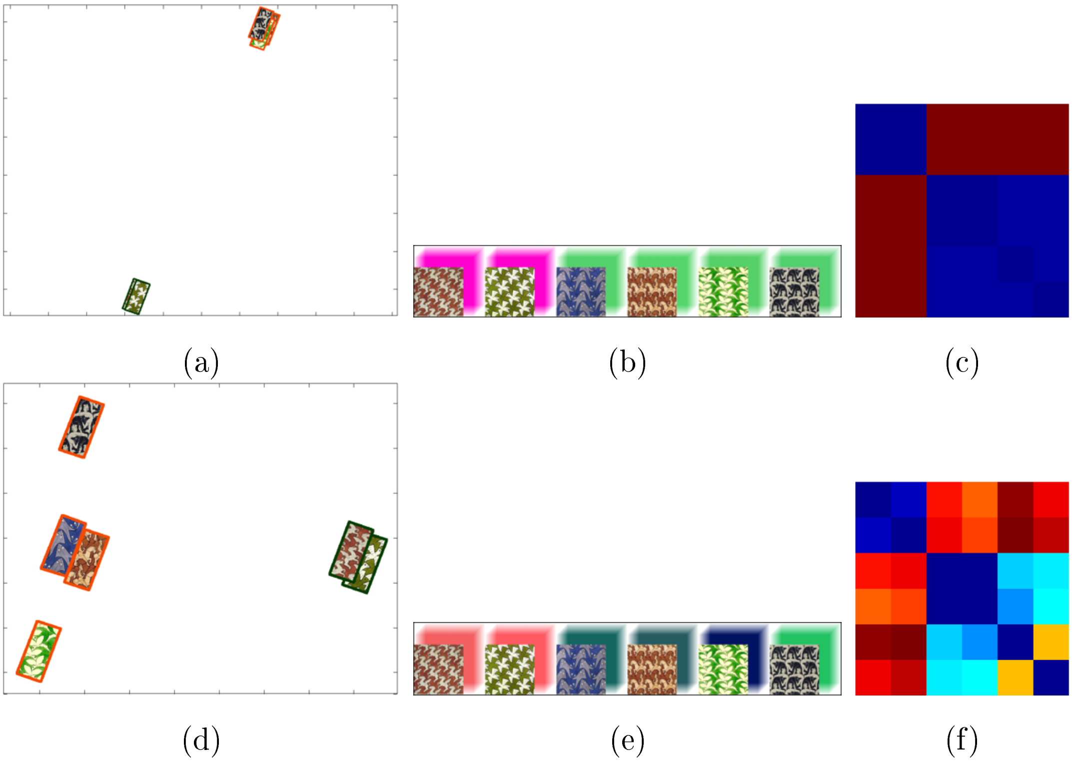

Figure 4.21: Experiment 15.

which has no rosette structures at all. See Fig. 4.24 for clustering results for this experiment. Observe that both two-dimensional and three-dimensional tSNE results give two distinct groups. The confusion matrix reveals no similarity between two groups at all. SMDS results on the other hand give three groups, separating pure translational group into two groups. Yet, the rotational ornaments form one group.

We add one more ornament to the previous collection. The ornament is of group $p4$. Since it has no other ornament that exactly matches it style-wise, we expect it to join the rotational group: the group with an ornament of $p6$ group and an ornament with three-fold rotations. From the clustering results depicted in Fig. 4.25 we can see that the groupings are just as we expected.

We add one more ornament to the collection of the previous experiment. Its symmetry group is pg. We have already discussed style-wise closeness between pure translational and glide groups. Thus, we expect the newly added orna-

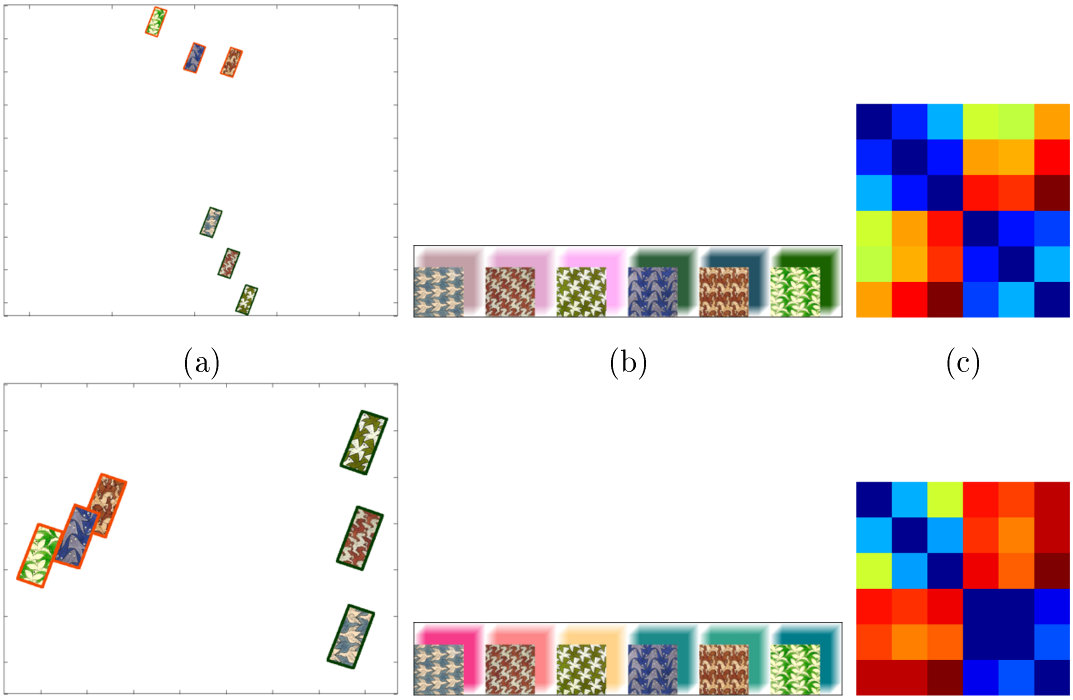

(a) (b) (c)

(d) (e) (f)

Figure 4.22: Experiment 16.

ment to join the pure translational group. The clustering results are shown in Fig. 4.26. The two-dimensional results for both tSNE and SMDS give expected two groups. Three-dimensional results have scattered groups assigning wide range of color shades to ornaments. However, the confusion matrix for tSNE result also reveals two expected groups.

Previous experiments have shown that the rotational groups are closer style-wise, and tend to join against pure translational or glide groups. Next experiments show how the rotational groups are classified internally. The aim is to see if the style-wise differences between different groups are captured from the content suppressed images.

We consider a collection of eleven ornaments: three ornaments with three-fold rotations and mirror reflections, three ornaments of *mariposas* group, three two-color ornaments of $p6$ group and two ornaments of another $p6$ group. Although there are only two groups: those with three-fold rotation and those with six-fold

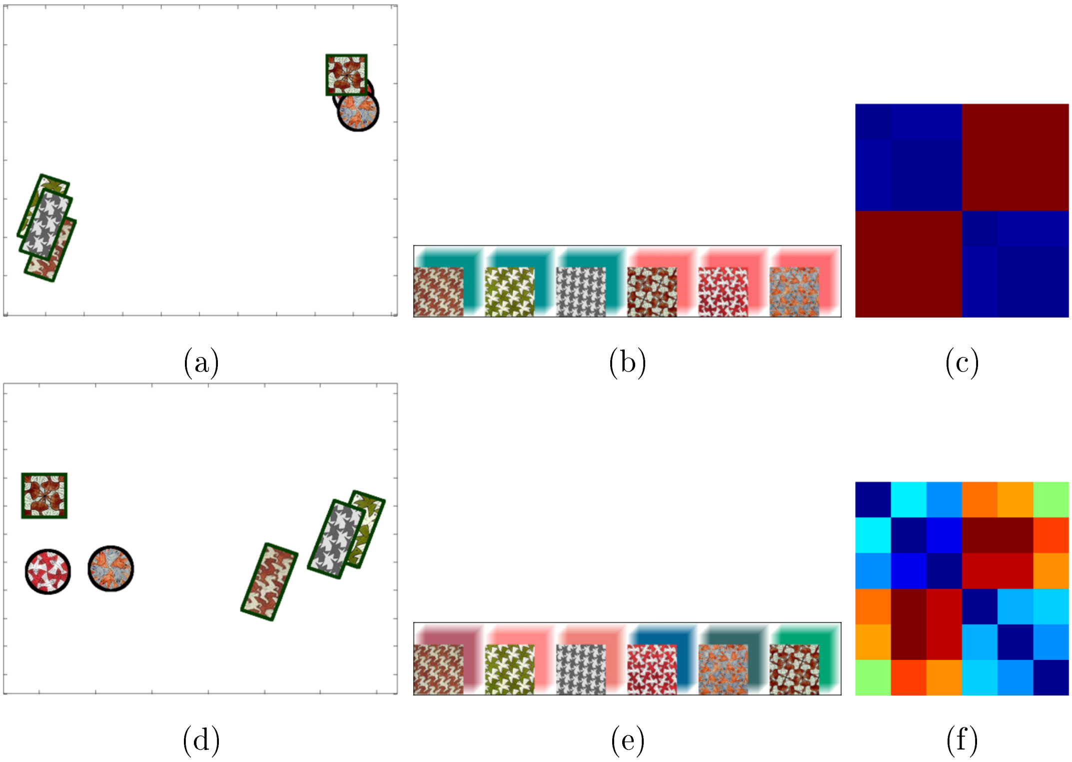

Figure 4.23: Experiment 17.

rotations, there are style-wise differences between ornaments of $p6$ group. The *mariposas* are three-color ornaments, where only three-fold rotation is encountered when we take into account color permutations. The next $p6$ group consists of three two-color ornaments, where the color permutation also introduces only three-fold rotations. The last group consists of two ornaments that preserve the entire six-fold rotation in one color. As one can see, despite being considered as one group according to symmetry group, those ornaments have style-wise differences. We expect four groups to emerge from our clustering results. See Fig. 4.27 for the four clusters. As we expected, suppressing the images enabled to capture style-wise differences within $p6$ groups.

For the next experiment, we take larger set of rotational ornaments: three ornaments with three-fold rotations and mirror reflections, three ornaments of *mariposas* group, three two-color ornaments of $p6$ group, two three-color ornaments of $p6$ group and two ornaments of group $p4$. We expect these five groups

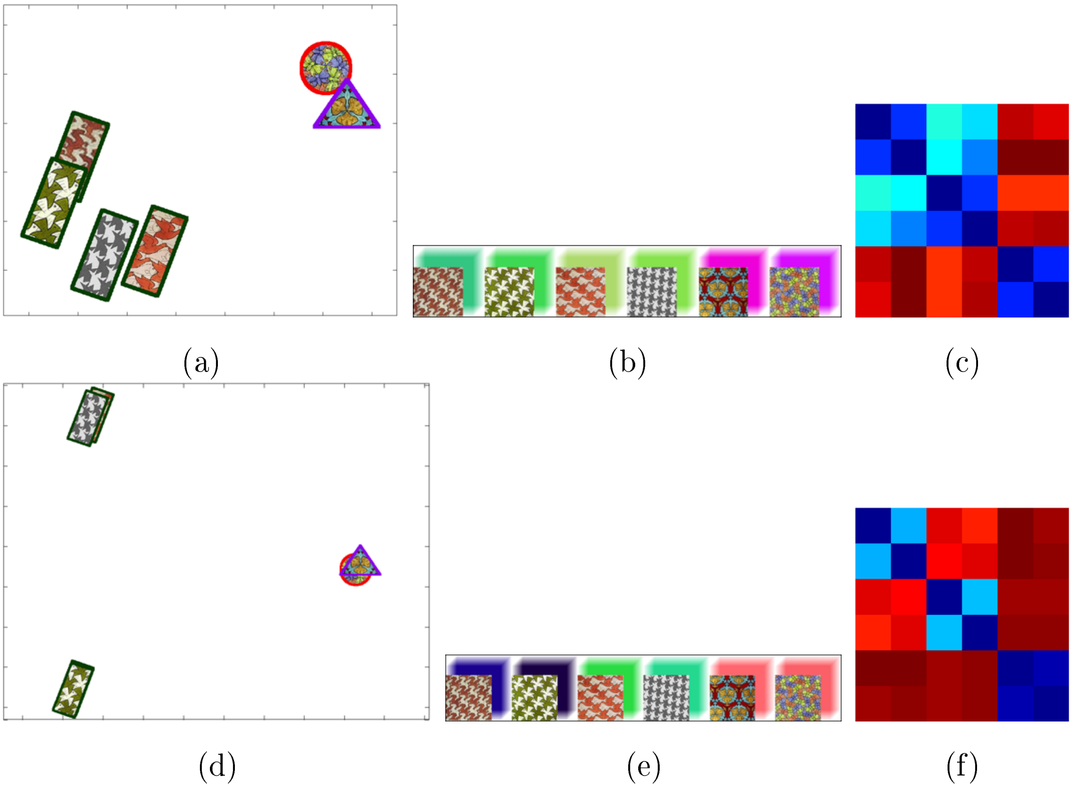

Figure 4.24: Experiment 18.

to emerge. Clustering results for the experiment are shown in Fig. 4.28. We see five groups that we were expecting to see. The two-dimensional results give interesting placement of groups. In two-dimensional result for tSNE the ornaments of $p6$ group are separated from ornament with three-fold rotations. The ornaments with four-fold rotations are right in the middle of these two groups. The order of rotation increases as one goes upward. In two-dimensional result for SMDS the $p6$ groups are separated from other two groups, and the order of rotation increases as one moves from right to left. The confusion matrix of tSNE result illustrates a strong connection between $p6$ groups.

We mentioned above that two three-color ornaments of group $p6$ have some level of similarity to all groups. Thus, they generally pull groups together. For the next experiment, we eliminate these two ornaments from the previous collection. See the clustering results in Fig. 4.29. Observe that the arrangement of groups is now different than it was in the previous experiment. The group with three-

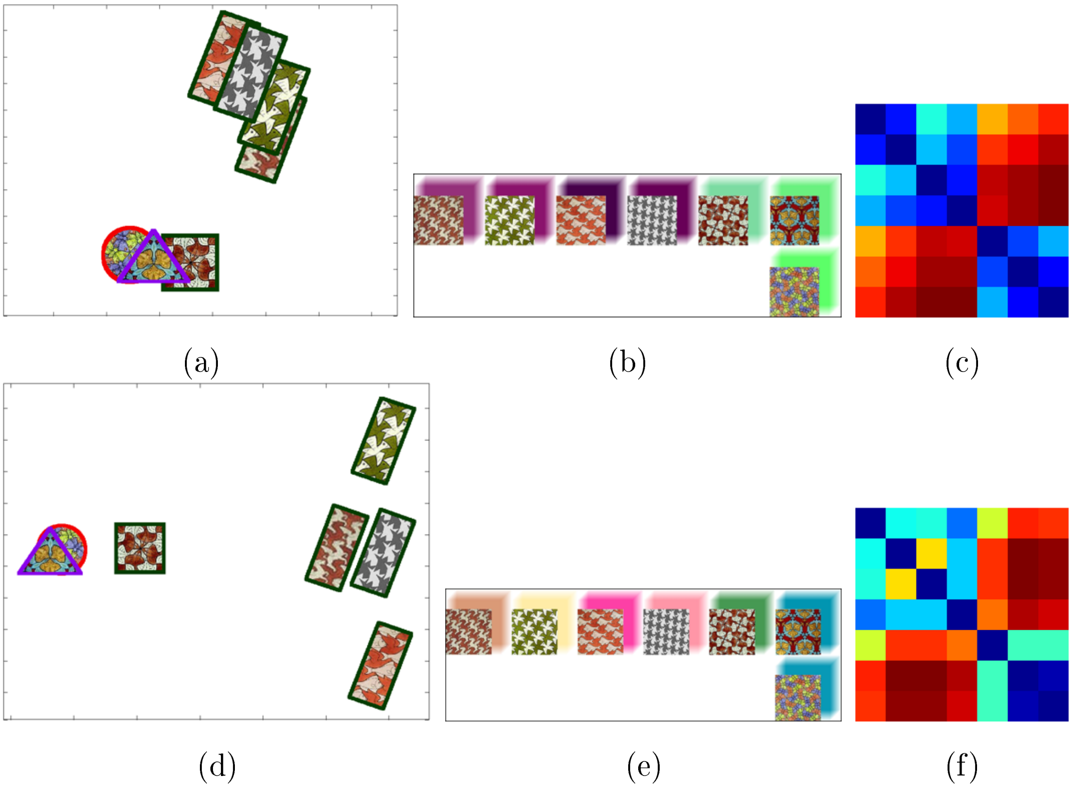

Figure 4.25: Experiment 19.

fold rotation and mirror reflection become isolated. The $p4$ group and two $p6$ groups are on the other side. This is because the group with three-fold rotations exhibit triangular structures along with three-leaved rosettes in their ω fields, while the other groups contain only three- or four-leaved rosette structures. Also the number of colors used for $p4$ group makes it close to the group of two-color $p6$ ornaments.

We further increase our collection to twenty-six ornaments, which combines Escher ornaments with a large collection of non-Escher ornaments. This set contains three ornaments of *mariposas* group, three ornaments of two-color $p6$ group, seven ornaments with three-fold rotations and mirror reflections, two ornaments of $p4$ group, and eleven ornaments of $p4g$. The clustering results for this collection is given in Fig. 4.30. We observe six groups from two-dimensional tSNE result and five groups from two-dimensional SMDS result. In both result the group with three-fold rotations and reflections has separated into two. They

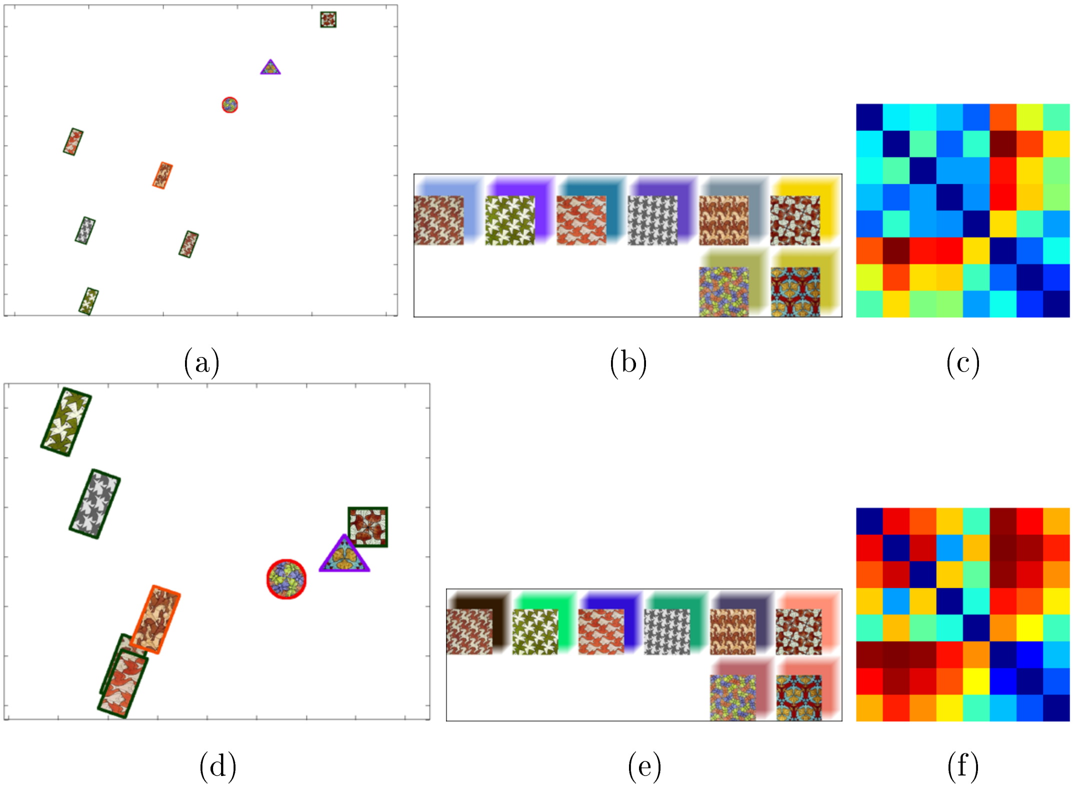

Figure 4.26: Experiment 20.

are separated mostly due to triangular structures in two ornaments that prevail in them. However, from three-dimensional results one can observe that they are mapped to color that is close to the color of their group. The same is with the group with four-fold rotations in two-dimensional tSNE result. However, the colored result gives four major colors. Different shades of blue represent the group with four-fold rotations and mirror reflections. Purple is given to three ornaments of two-color $p6$ group. Burgundy is assigned to *mariposas* group, and there is a big group comprising different shades of brown, which contains seven ornaments with three-fold rotations and mirror reflections. The ornaments from $p4$ group preserve four-fold rotation in one color, while for most of the ornaments of $p4g$ group four-fold rotation is lost due to color permutation, leaving only two-fold rotations. Of course, we should expect those two groups to be separated. However, some ornaments, particularly an ornament with angels and demons have both dumbbell-like structures and swastika-like structures. Thus, it pulls

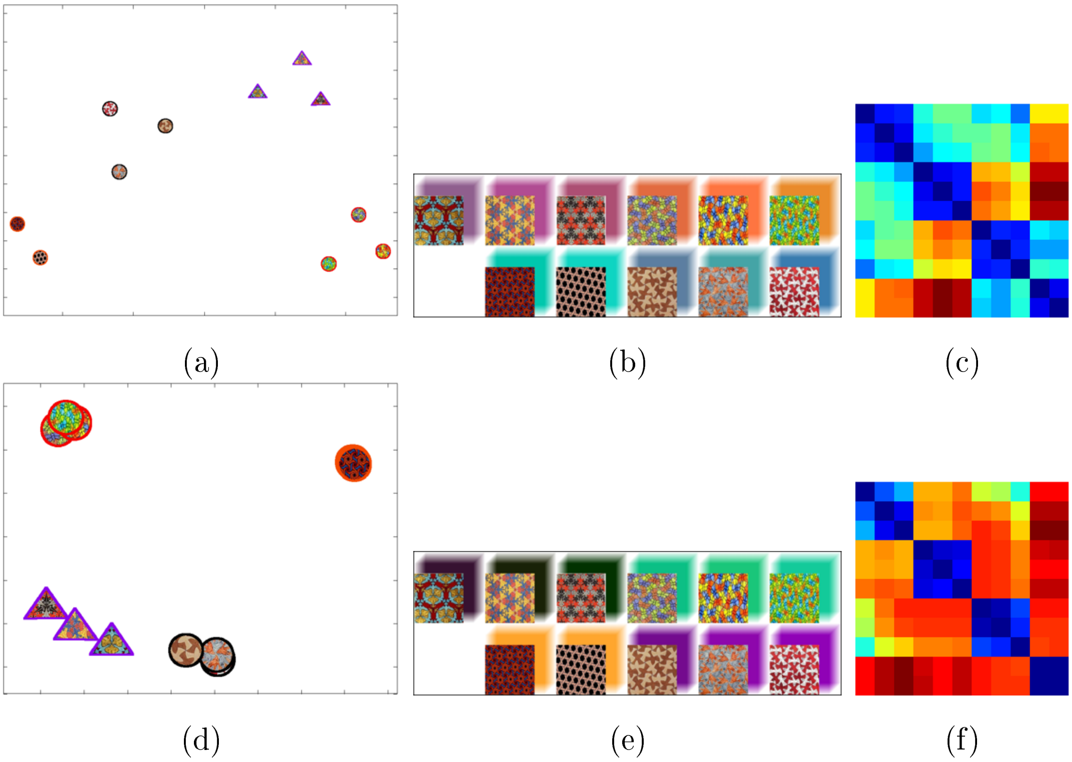

Figure 4.27: Experiment 21.

the ornaments that exhibit dumbbell-like structures, and pulls other ornaments with four-leaved rosette structures to the group.

We add two three-color ornaments of $p6$ group to the previous collection. At a first glance, we see four major groups from both two-dimensional and three-dimensional results (Fig. 4.31). There is a big group consisting of ornaments with four-fold rotations, a group of three two-color ornaments of group $p6$, a *mariposas* group, and another big group consisting of seven ornaments with three-fold rotations and mirror reflections and two three-color ornaments of group $p6$. The last group is further divided into three: five ornaments with three-fold rotations and mirror reflections, two ornaments with three-fold rotations and mirror reflection, and two three-color ornaments of group $p6$. Observe the closeness of two groups: a group with two-color ornaments of group $p6$ and the four-fold rotational group. Again, the number of colors in ornaments is considered as part of style making this two groups similar in that aspect.

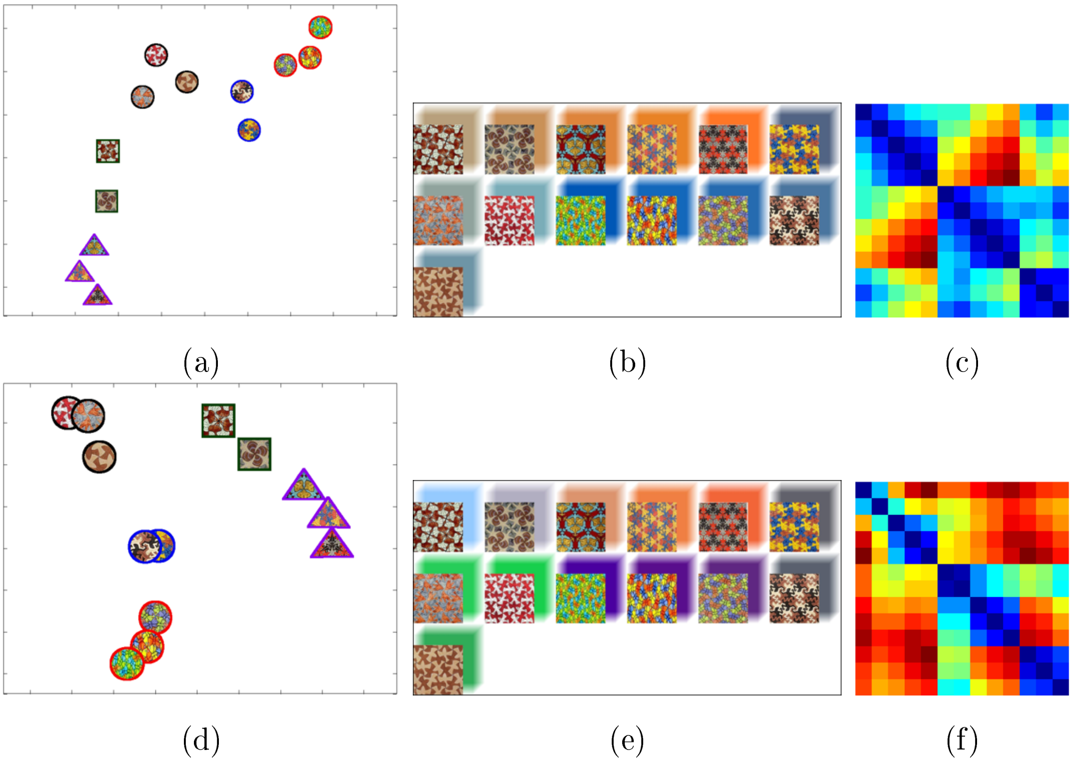

Figure 4.28: Experiment 22.

We add one more ornament with three-fold rotations and mirror reflections to the previous collection. It joins the group of two ornaments with three-fold rotations and mirror reflections, which is separated from the main group of ornaments with three-fold rotations (Fig. 4.32). These three ornaments stay separate from others due to triangular structures that prevail in their content suppressed forms and lack of rosette structures. Observe that in two-dimensional tSNE result the ornaments with three-fold and six-fold rotations stay separate from those with four-fold rotations.

In contrast to pure translational and glide groups, rotational group consists of many different groups. There are groups with three-fold, two-fold, four-fold, and six-fold rotations. There are nuances even for the ornaments that are considered to be in the same group according to symmetry group classification. There are ornaments of $p6$ group that preserve entire rotation in one color, ornaments of $p6$ group that preserve only three-fold rotations in one color (mariposas),

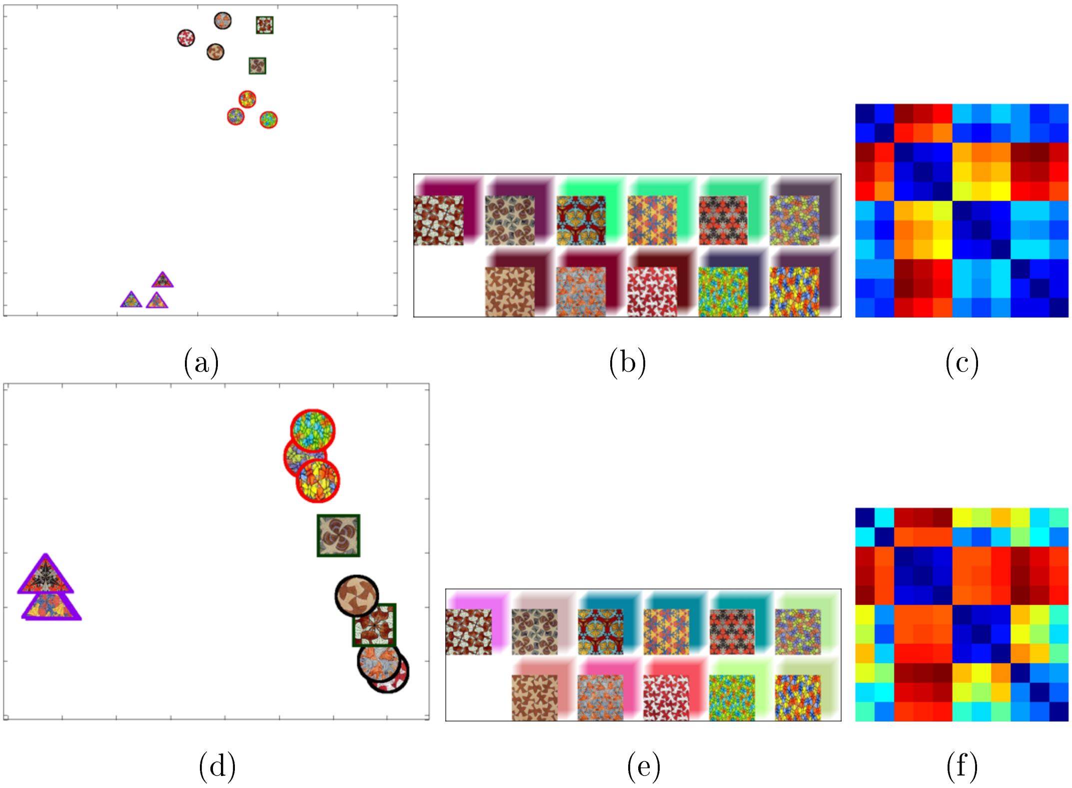

Figure 4.29: Experiment 23.

ornaments of $p4$ group that preserve entire rotation in one color, and those that do not, etc. With the content suppressed images, we can see those style-wise differences, and indeed, we see those groups emerge from our clustering results. Furthermore, those groups do not stand isolated, and we can see the relations between different styles. Generally, relations between the groups are context dependant, and the groups that are close in one experiment might fall apart in the next experiment. Following experiments aim to show the preferences of different clusters. We will see which groups are close to each other style-wise within rotational groups.

We consider an ornament collection of nine ornaments: three ornaments of *mariposas* group ($p6$), three two-color ornaments of $p6$ group, and three ornaments with three-fold rotations and mirror reflections. We expect these three groups to emerge from clustering results. Fig. 4.33 illustrates the clustering results that show three groups we were expecting to see. Observe that in two-

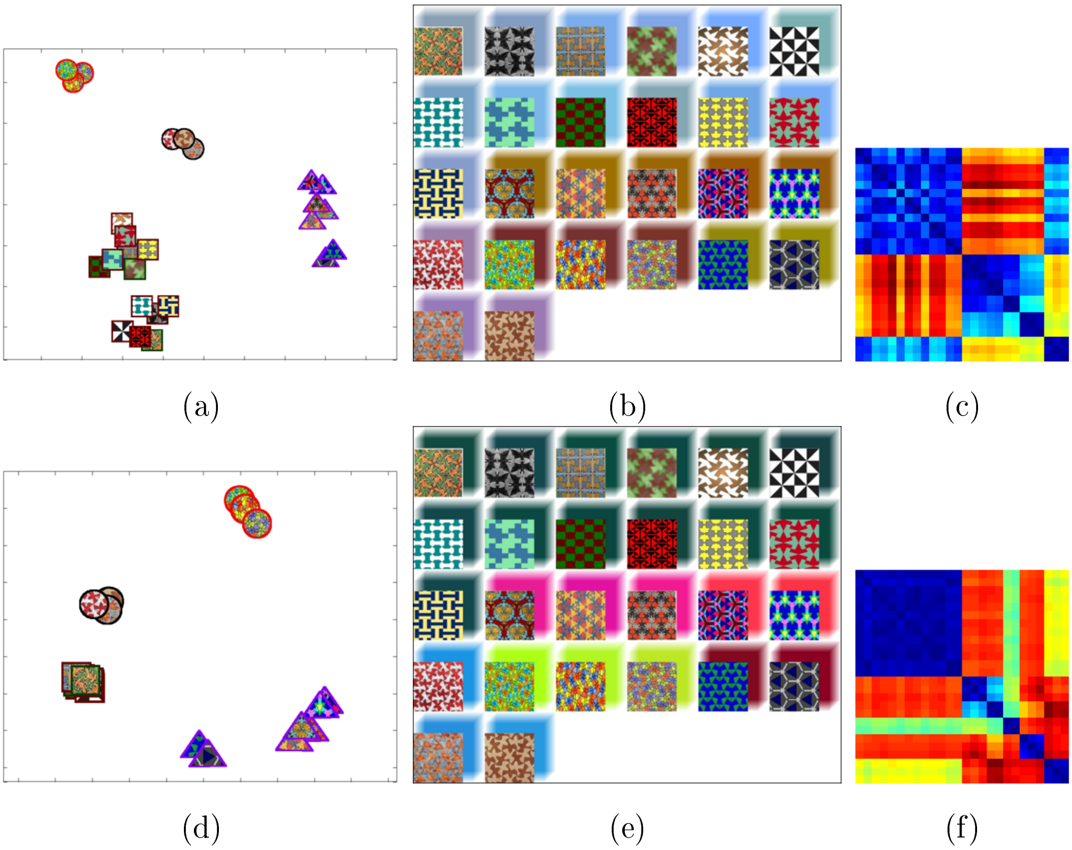

Figure 4.30: Experiment 24.

dimensional results two $p6$ groups are separated from the group with three-fold rotations and mirror reflections.

We add two three-color ornaments of group $p6$ to the previous collection. These two ornaments form a group on their own, so overall four groups emerge (Fig. 4.34). Again, observe that there is a clear separation between the $p6$ groups and the group with three-fold rotations. The same separation is observed in the confusion matrix for tSNE three-dimensional result.

Consider another set of ornaments, where we have five ornaments with three-fold rotations and mirror reflections and three ornaments of *mariposas* group. We expect exactly these two groups to emerge. See the clustering results in Fig. 4.35. All results show two groups that we expected to see. If we add two three-color ornaments of group $p6$ to this collection, we see that it joins the *mariposas*

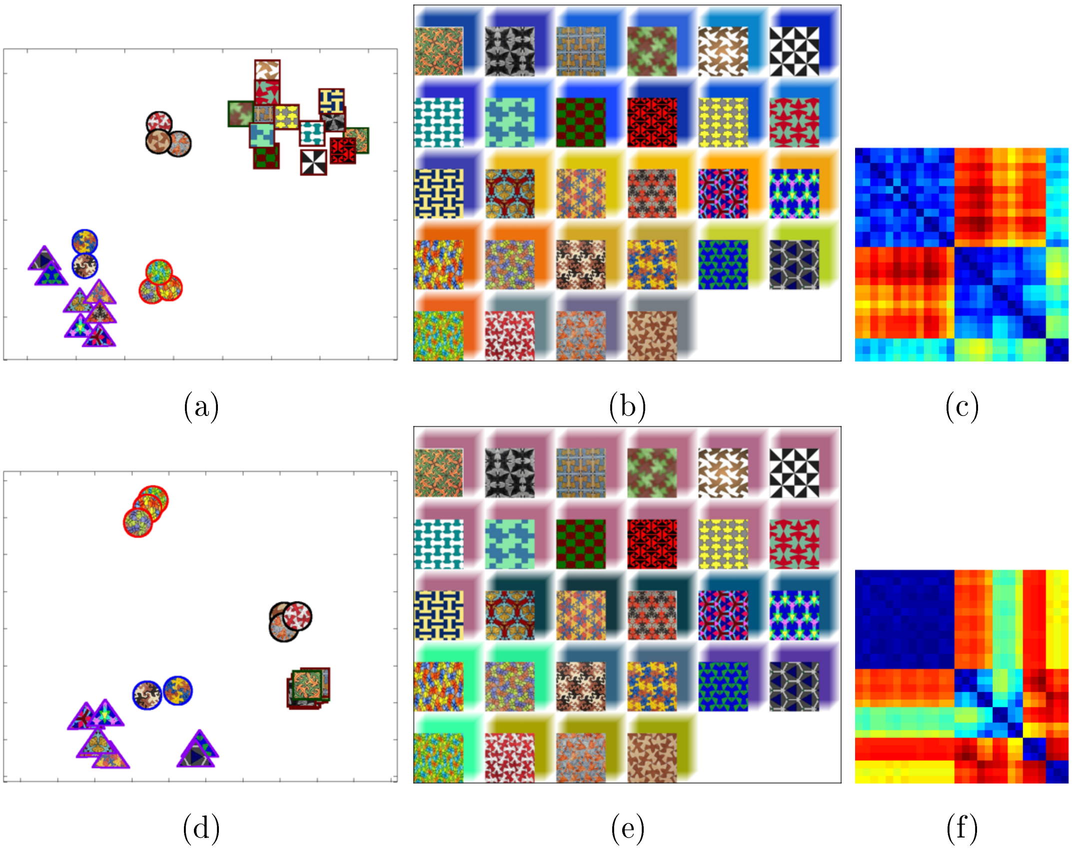

Figure 4.31: Experiment 25.

group (Fig. 4.36). Notice how all results separate the $p6$ group from the group with three-fold rotations and mirror reflections. We add two more ornaments with three-fold rotations and mirror reflections to the collection. They form a group on their own Fig. 4.37. From tSNE results we still observe a clear separation between the $p6$ groups and the groups with three-fold rotations and mirror reflections.

However, the results shown in previous five experiments are not always the case, i.e. three-fold rotational group is not always that distant from the $p6$ group. These two groups join when the four-fold rotational group is introduced. Consider a collection of eight ornaments: three ornaments of $p4g$ group, three ornaments with three-fold rotation and mirror reflections, one ornament of *mariposas* group, and one two-color ornament of group $p6$. Two standalone

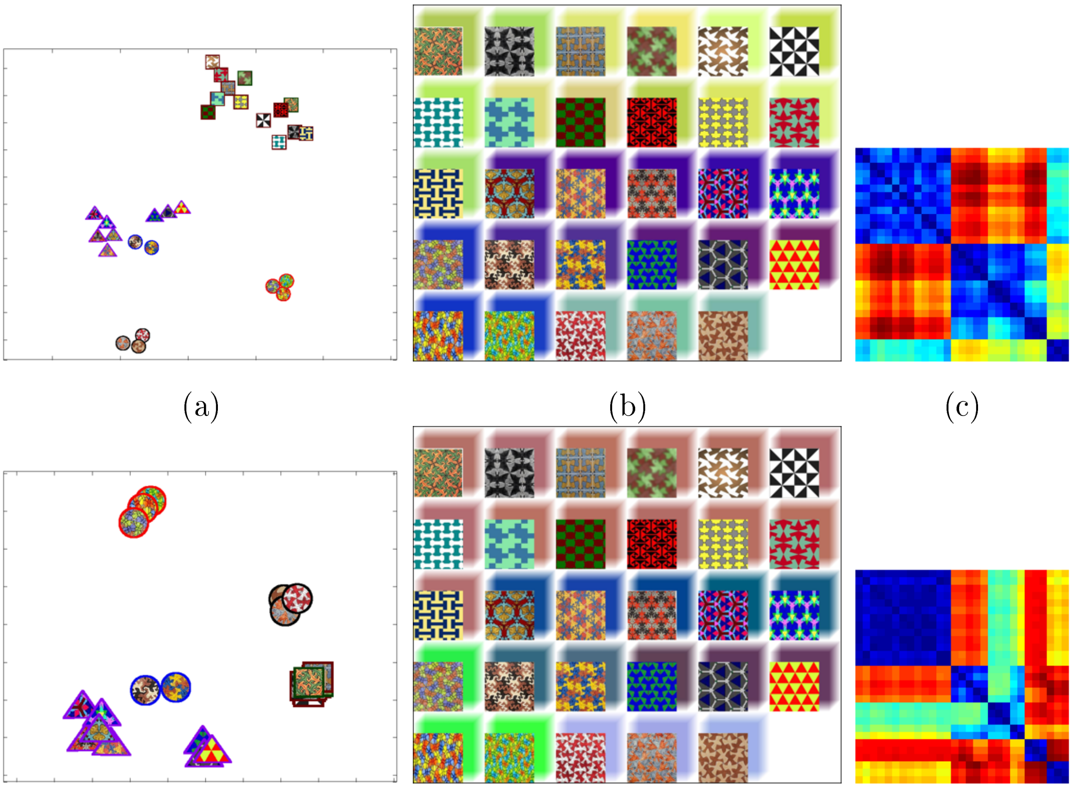

(a) (b) (c)

(d) (e) (f)

Figure 4.32: Experiment 26.

ornaments join the three-fold rotational group, against the $p4g$ group (Fig. 4.38). Thus, those two standalone ornaments are style-wise more similar to three-fold rotational group rather than the four-fold rotational group.

We continue the experiments with the next collection: three ornaments of *mariposas* group, three two-color ornaments of group $p6$, three ornaments with three-fold rotations and mirror reflections, and three ornaments of $p4$ group taken from iOrnament database. We expect exactly those four groups to emerge, as a result of clustering. The clustering results are illustrated in Fig. 4.39. All results give four groups we were expecting to see. Furthermore, observe that the $p6$ groups and the group with three-fold rotations and mirror reflections join against the $p4$ group. This is more obvious from the confusion matrix, which shows almost no connection between the $p4$ group and other groups.

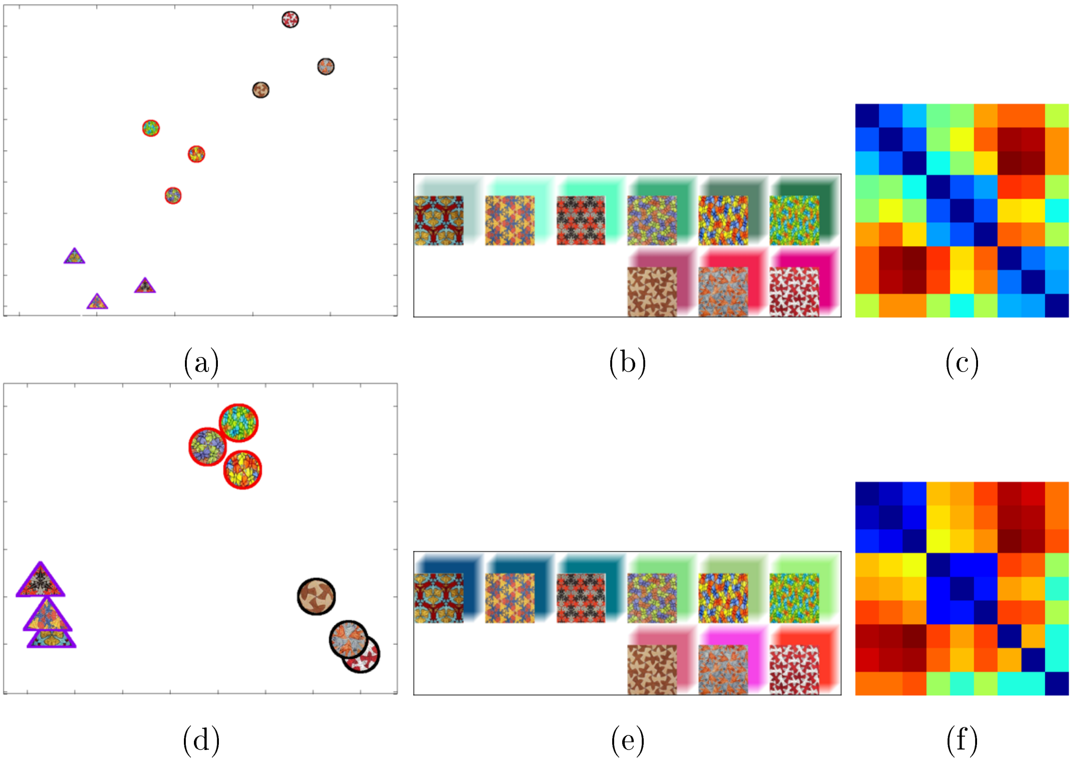

Figure 4.33: Experiment 27.

We consider another collection where five ornaments of group $p4$, three ornaments of group $p6$ and two ornaments of $p3$ group are given. All ornaments are from iOrnament dataset. See the clustering results in Fig. 4.40. We see the same scenario: $p6$ groups join the $p3$ group against the four-fold rotational group. Thus, the clusters that emerge are highly dependent on context. This way of clustering the ornaments preserves continuity of symmetry, and shows relations between the groups. Even within the $p6$ groups we observe internal preferences as shown in Fig. 4.41. Observe that the *mariposas* group and two three-color ornaments of $p6$ group join against the group of three two-color ornaments of group $p6$.

The next experiment is taken as base for subsequent seven experiments. It contains a collection with three ornaments of *mariposas* group, three ornaments with three-fold rotations and mirror reflections, and three ornaments of group $p4g$. See the clustering results in Fig. 4.42. All results contain three groups.

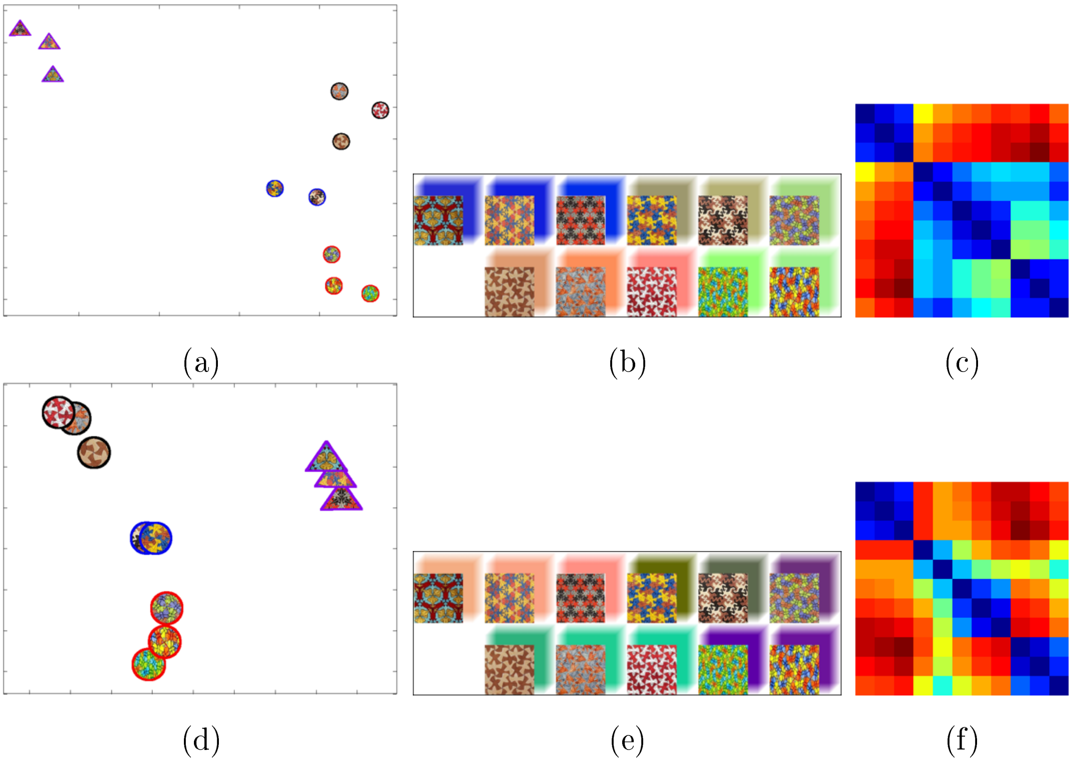

Figure 4.34: Experiment 28.

Notice, also, that the *mariposas* group join the group with three-fold rotations against the $p4g$ group.

We add one more ornament of $p4g$ group (angels and demons) to the previous collection. In contrast to the other ornaments of $p4g$ group, this one retains the whole four-fold rotation in one color. However, from our clustering results we see it joining the other $p4g$ ornaments (See Fig. 4.43). This happens due to dumbbell-like structures that prevail in the ω field of newly added ornament.

Another ornament is added to the collection of the previous experiment. This time the newly added ornament is of pgg group. Recall that there is no other ornament of the same group in the current collection. Thus, we expect it to join the $p4g$ group. The reason behind this is that the $p4g$ group contains two-fold rotations which are represented as dumbbell-like structures in their transform domain. The pgg group contains two-fold rotations followed by glide reflection. Thus, those two-fold rotations also will be represented by dumbbell-

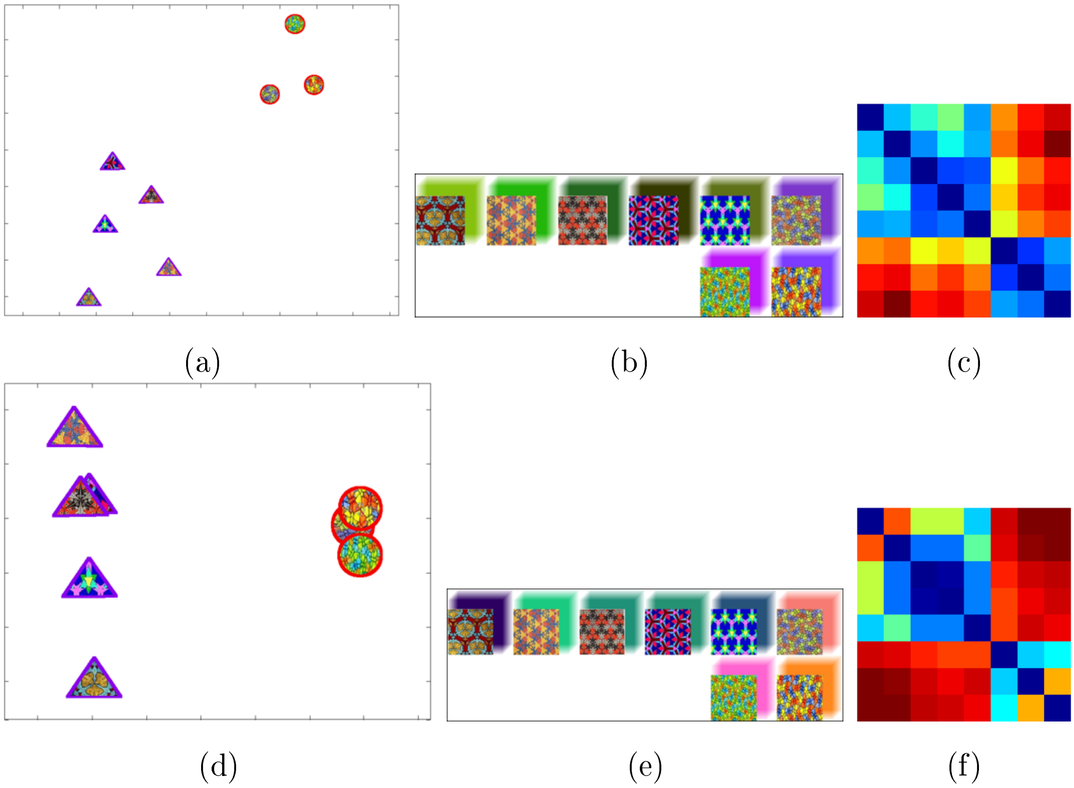

Figure 4.35: Experiment 29.

like structures in their transform domain making these two groups similar in the current context. The *pgg* ornament has more similarity to the *p4g* group than to any other group in the current context. Fig. 4.44 show the clustering results just as we expected. The retrieval results for most similar ornaments show the *p4g* group in the first place both for tSNE and SMDS results (Fig. 4.44 (d) and (h)).

For the next experiment we discard one ornament from the *p4g* group (angels and demons) to see if it influences the clustering result. As shown in Fig. 4.45 we still obtain the same clusters except that for tSNE result the *mariposas* group becomes closer to the group with three-fold rotations and mirror reflections, giving overall two precise clusters.

There is one more case we need to explore using the previous ornament collection. We add one ornament of pure translational group. From the previous

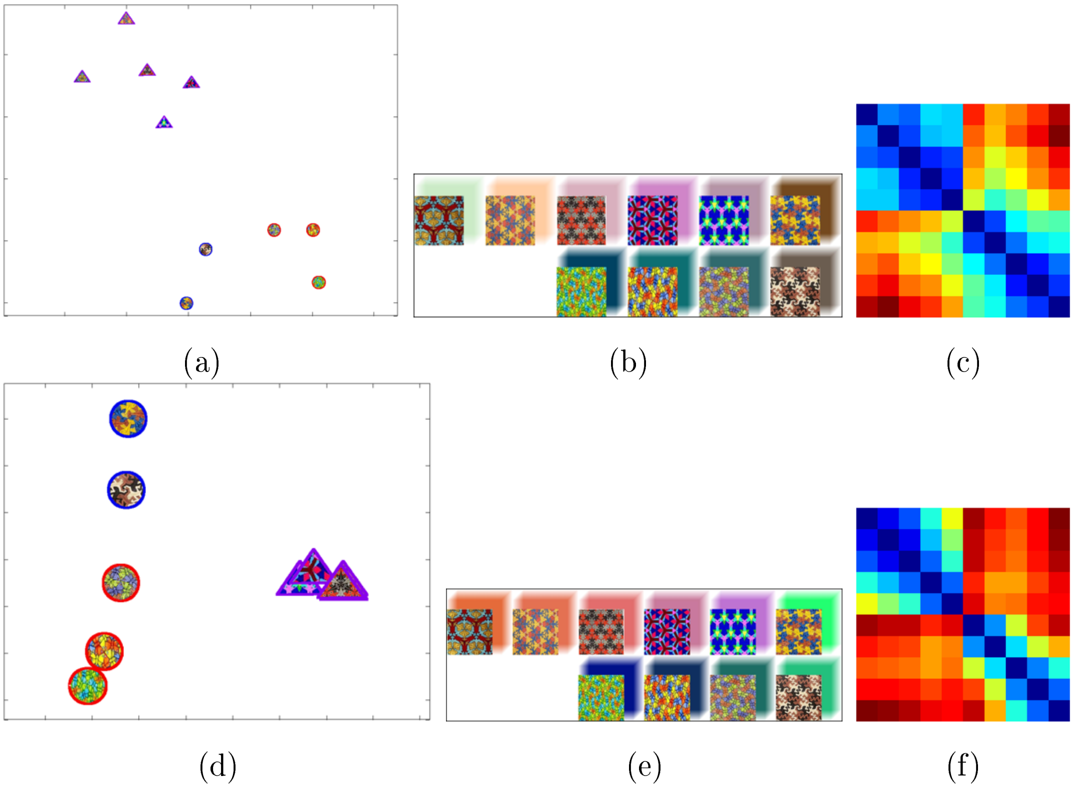

Figure 4.36: Experiment 30.

experiments we saw that the pure translational group is close to the glide group. Hence, we expect the newly added ornament to join the *p4g* group, where the ornament of *pgg* group resides. See the clustering results in Fig. 4.46. Observe that for all results the pure translational ornament comes with the *p4g* group. Also observe from the tSNE results the retrieval for most close ornaments for two standalone ornaments show that they find each other as the most close one in the current context (Fig. 4.46 (d) and (e)).

For the following experiment we return our ornament set to the base state it was four experiments before, i.e. collection with three ornaments of *mariposas* group, three ornaments with three-fold rotations and mirror reflections, and three ornaments of group *p4g*. We add one more ornament with three-fold rotations and mirror reflections. It is not from Escher's collection and is of computer-based creation, just like three other ornaments of *p4g* group. Now, if we do not suppress the content of ornaments, we might get the clustering

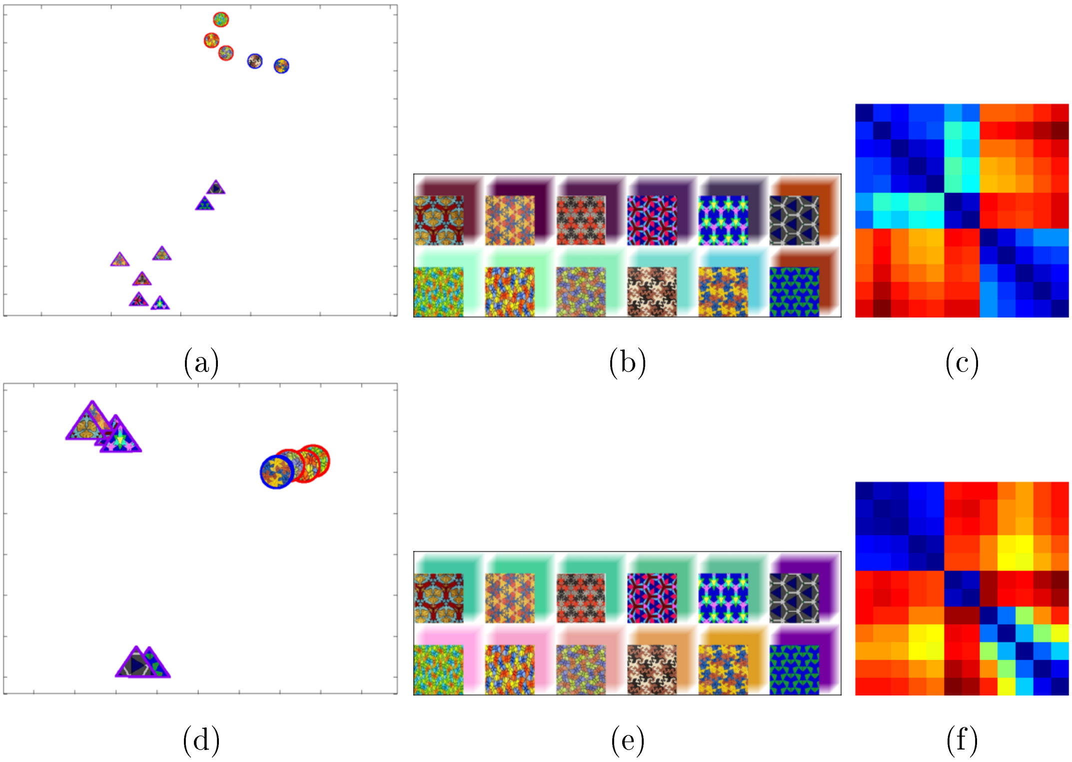

Figure 4.37: Experiment 31.

results where this newly added ornament would join the $p4g$ group. This is because of the colors used in ornaments. Four of them have sharp, unnatural colors in contrast to the ones painted by Escher. However, since we do suppress the content, we expect the newly added ornament to join the ones that have similarity in style, i.e. three ornaments with three-fold rotations and mirror reflections. This is exactly what we see from both two dimensional and three dimensional clustering results (Fig. 4.47).

Again, we take the previous collection and add one ornament of $p4$ group. Retrieval results, based on three dimensional results, for the $p4$ ornament are shown in Fig. 4.48(d) and (h). As one can see, the first three choices of closest ornaments are the ones from group $p4g$. The newly added ornament cannot be seen on the two-dimensional results due to occlusion, and yet it comes with the square group. This can be further checked from three-dimensional result, where the newly added ornament takes the color close to the colors of $p4g$ group. Re-

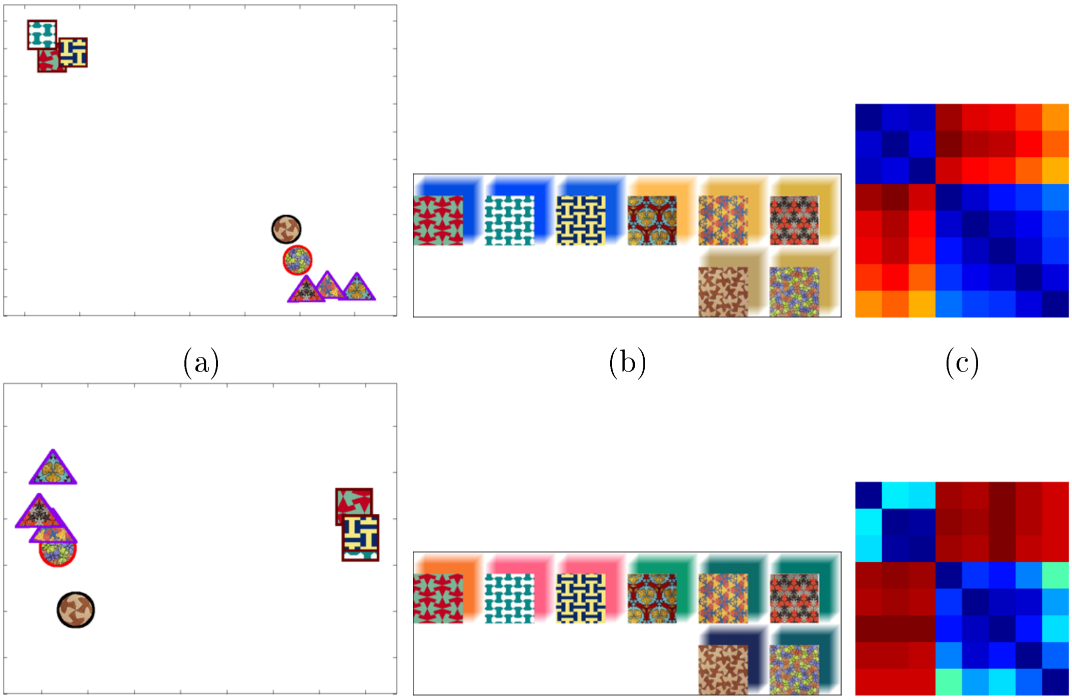

(a) (b) (c)

(d) (e) (f)

Figure 4.38: Experiment 32.

call that for the confusion matrix, we do not consider standalone ornaments. Interestingly, we expected the ornament of $p4$ ornament to join any other group but the $p4g$ group. This is because the ornaments of $p4g$ group in the collection do not preserve four-fold rotations due to color permutations and maximum what we get from this group are dumbbell-like structures, while the ornament we added does preserve four-fold rotations. Therefore, our expectation would be that $p4$ ornament joins other groups, where rosettes introduced due to rotations. The $p4$ ornament might join the $p4g$ group because of the finite nature of our ornament, and of its small size. Because of the cut on the edges of the ornament dumbbell-like structures occur. Nevertheless, for the next experiment we consider another ornament of $p4$ group instead of previous $p4$ ornament, and see if the same scenario occurs. In Fig. 4.49(d) and (h) one can see the retrieval results for this ornament. Observe that the closest ones are the ones with three-fold rotations and the $p4g$ group is the least similar one to the given ornament. In addition, in the clustering results both for two-dimensional and

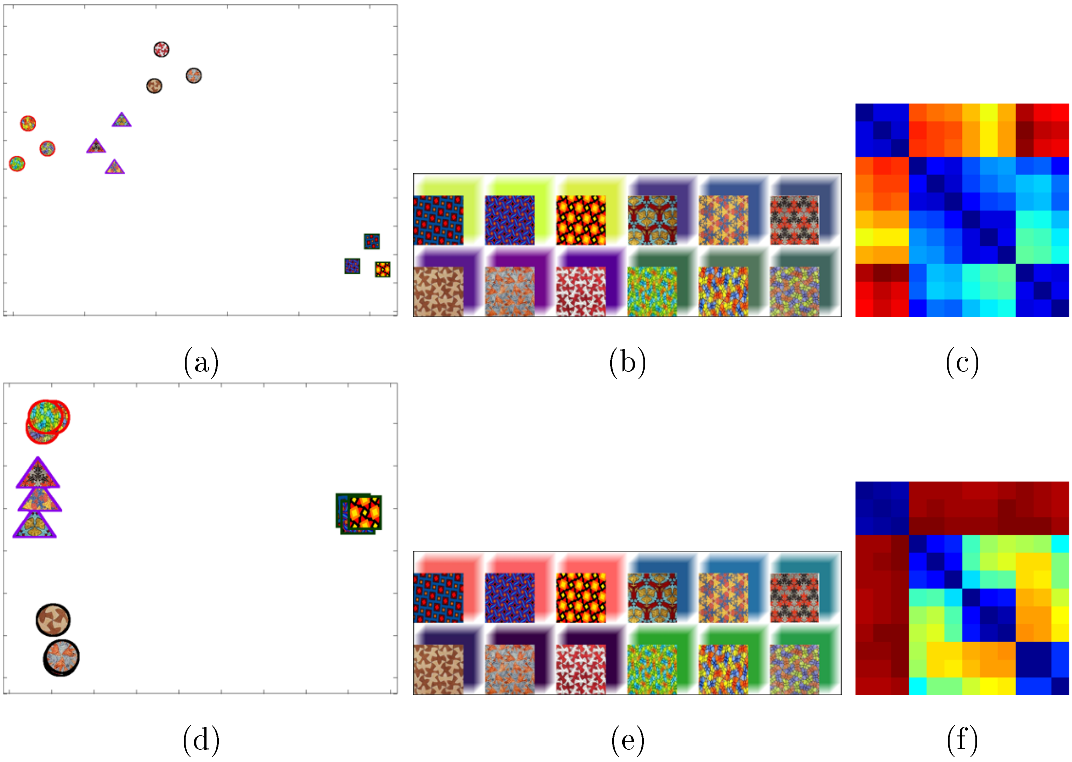

Figure 4.39: Experiment 33.

three-dimensional results, it joins the *mariposas* group.

4.2.1 Groups Hierarchy

Experiments conducted in the previous sections show the relations between different groups. By changing the context in every experiment, we are able to see structural relations of different groups. Fig. 4.50 illustrates the hierarchy inferred from clustering results. Observe that the dataset we consider is separated into two major groups, one containing the rotational groups and the other containing pure translational and glide groups. By changing the granularity of considered ornament set in each experiment, we further see the relations of groups within rotational groups. We highlight the experiments that show this relation between groups.

When rotational groups come with the pure translational group or glide group

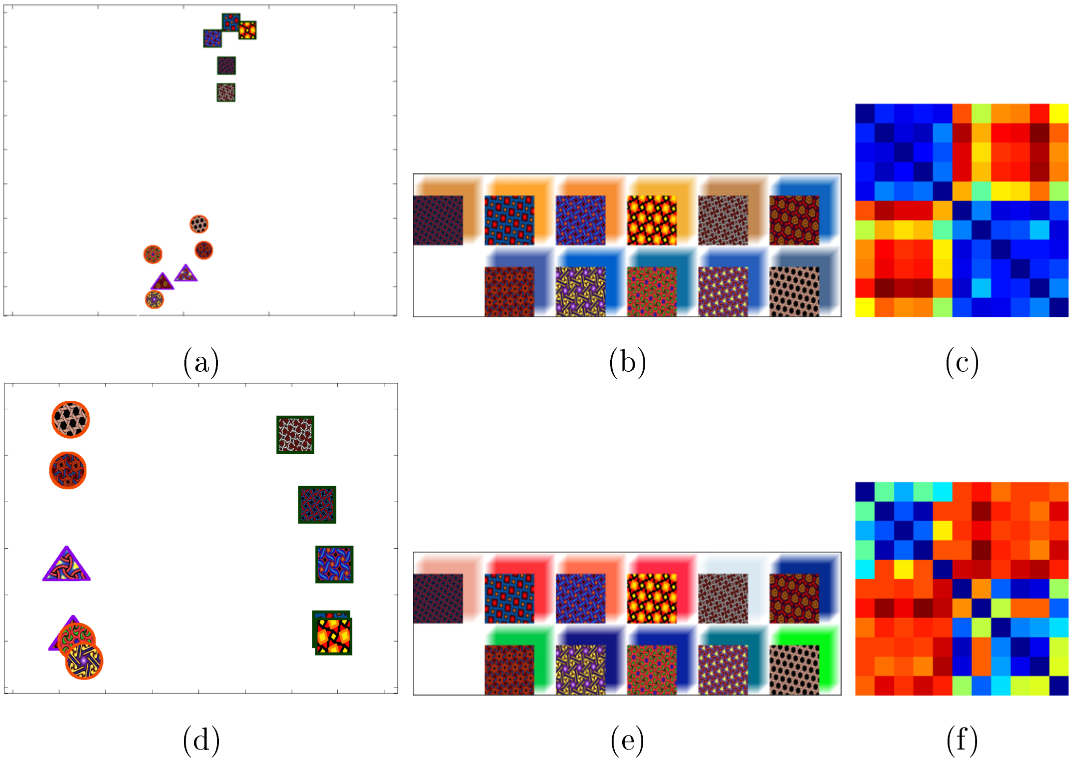

Figure 4.40: Experiment 34.

or both in a context, despite having stylistic differences they join against the other two groups. This situation is illustrated by experiments shown in Fig. 4.51. In the first experiment (Fig. 4.51(a)) there is a clear separation between the pure translational group and rotational groups. In the second experiment (Fig. 4.51(b)) three ornaments from three distinct rotational groups join against the pure translational group. The last experiment shows that the glide and pure translational groups join against the rotational (*mariposas*) group.

By changing the context we are experimenting on, we can change the granularity in group relations. Thus, if we consider only ornaments from pure translational and glide group, we obtain two distinct groups, while in a bigger context these two groups tend to join. See Fig. 4.52 for experiments showing these two groups separated.

If we eliminate pure translational and glide groups from the context, we can observe the relations between different rotational groups. Within rotational groups,

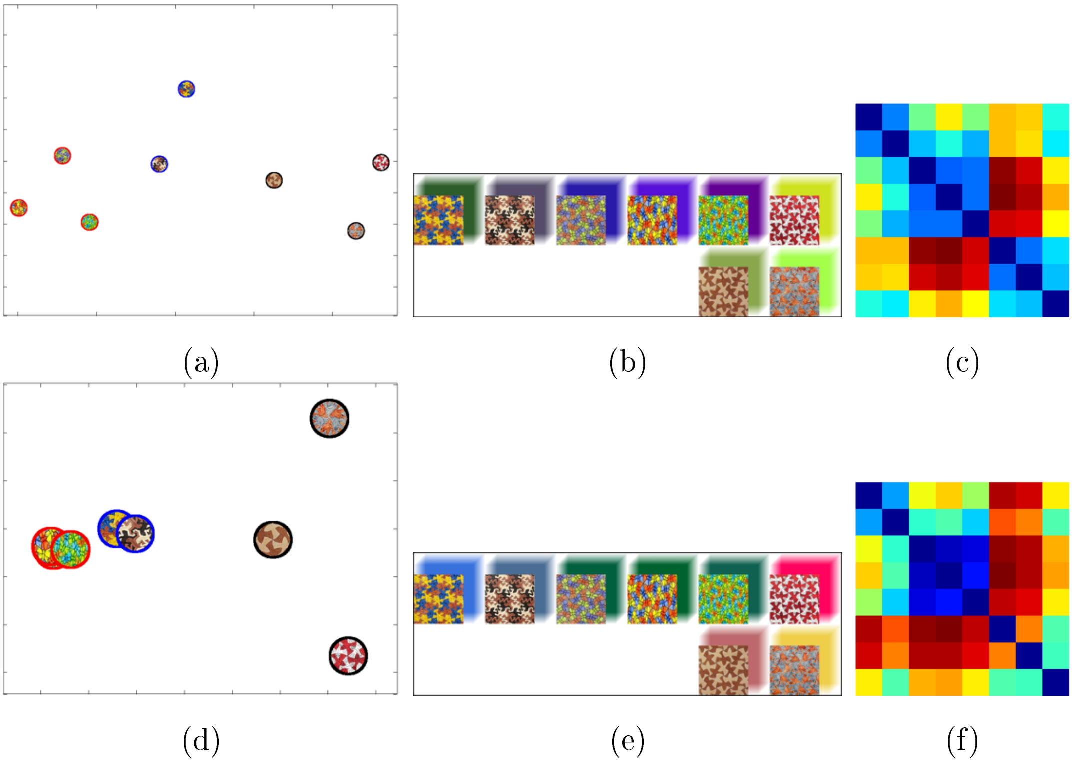

Figure 4.41: Experiment 35.

the ornaments with four-fold rotations differ style-wise from other groups. Experiments in Fig. 4.53 show that the ornaments with three-fold and six-fold rotations are style-wise more similar and tend to join against the ornaments of $p4$ or $p4g$ groups.

While ornaments with three-fold and six-fold rotations join against the ornaments with four-fold rotations, eliminating $p4$ and $p4g$ groups from the context changes the group relations in clustering results. In the context, where only ornaments with three-fold rotations and ornaments with six-fold rotations are considered, another two major groups occur: one consisting of group with three-fold rotations and another of six-fold rotations. Such situations are illustrated by experiments in Fig. 4.54.

If we go further and eliminate ornaments with three-fold rotations from the context, the set will consist of only ornaments of $p6$ group. As we discussed earlier, despite being in the same symmetry group, those ornaments have stylistic

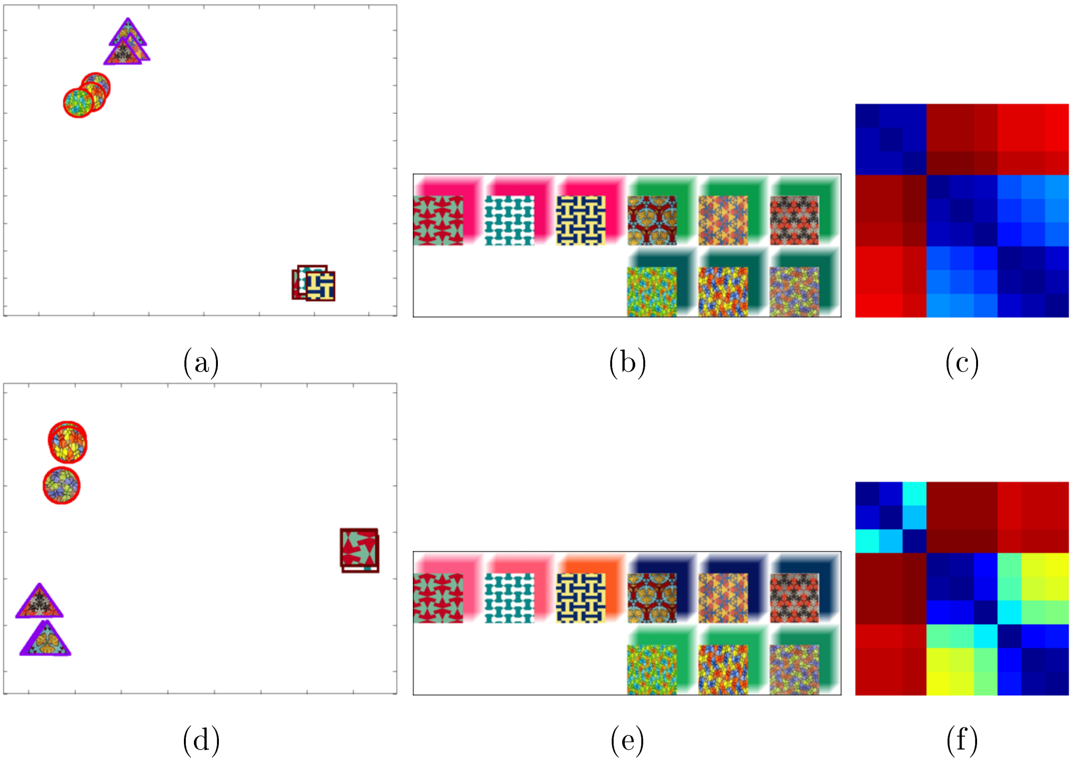

Figure 4.42: Experiment 36.

differences. Thus, if only ornaments of $p6$ group are considered, they are divided into several groups, each group containing the ornaments that are similar style-wise (Fig. 4.55).

4.2.2 Quantification of the Accuracy of Clustering

In our quantitative analysis, we consider forty-three experiments. We divide them into two groups: fourteen experiments are the ones where only two clusters are expected to emerge (like, rotation vs. pure translation, three-fold rotations vs. six-fold rotations, *etc*), and twenty-nine experiments are the ones where emerged clusters are more than two. For the experiments, we compute within and between group average distances. The distances are computed from the three-dimensional reduction results for both SMDS and tSNE. If there are five elements in the group, in order to obtain within group distance, we compute

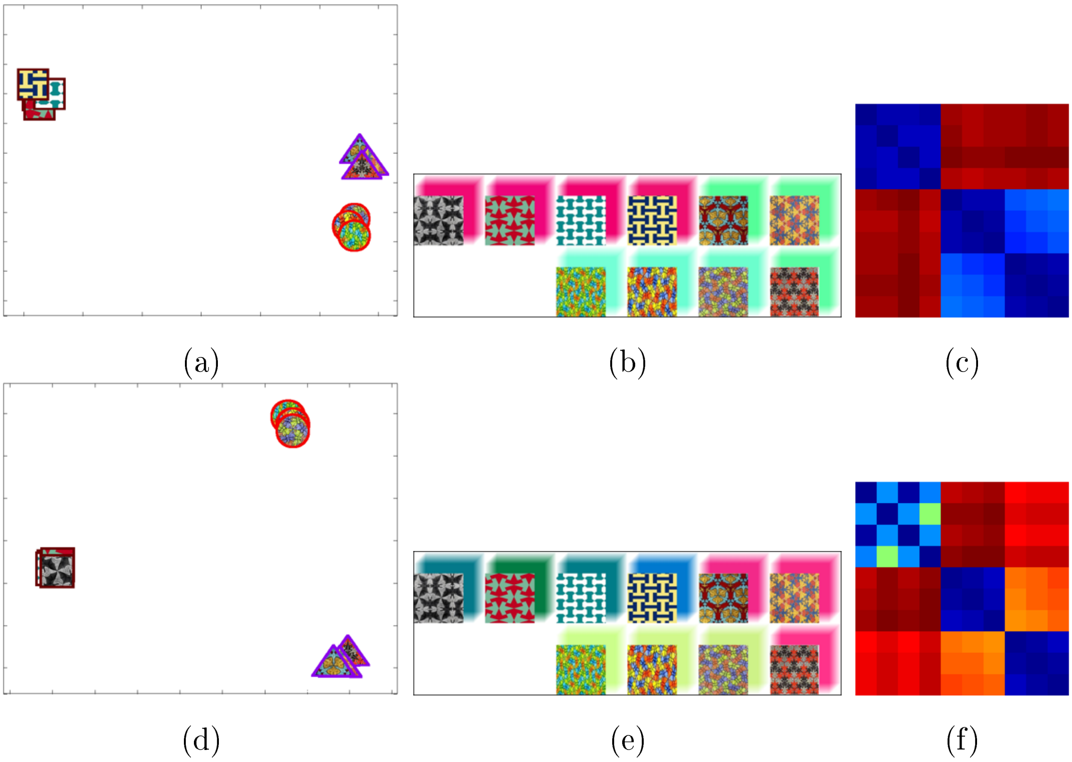

Figure 4.43: Experiment 37.

the average of the distances between these five elements. If there are three groups in the experiment, in order to obtain between group distances for one group, we compute the average of distances of one group to all other groups. For better classification results, it is natural, to expect small within group and large between group distances.

Fig. 4.56 shows within and between group average distances for fourteen two-group experiments for both SMDS and tSNE results. The first column shows which groups are being clustered in the current experiment. For example, first two experiments cluster glide and pure translational groups, the third experiment clusters rotational group (ornaments with six- and four-fold rotations) against pure translational group, and so on. The numbers shown in red represent average within group distances and the blue numbers represent average between group distances. The ratio between within and between group average distances are shown in the middle in black. Notice that the smaller the ratio

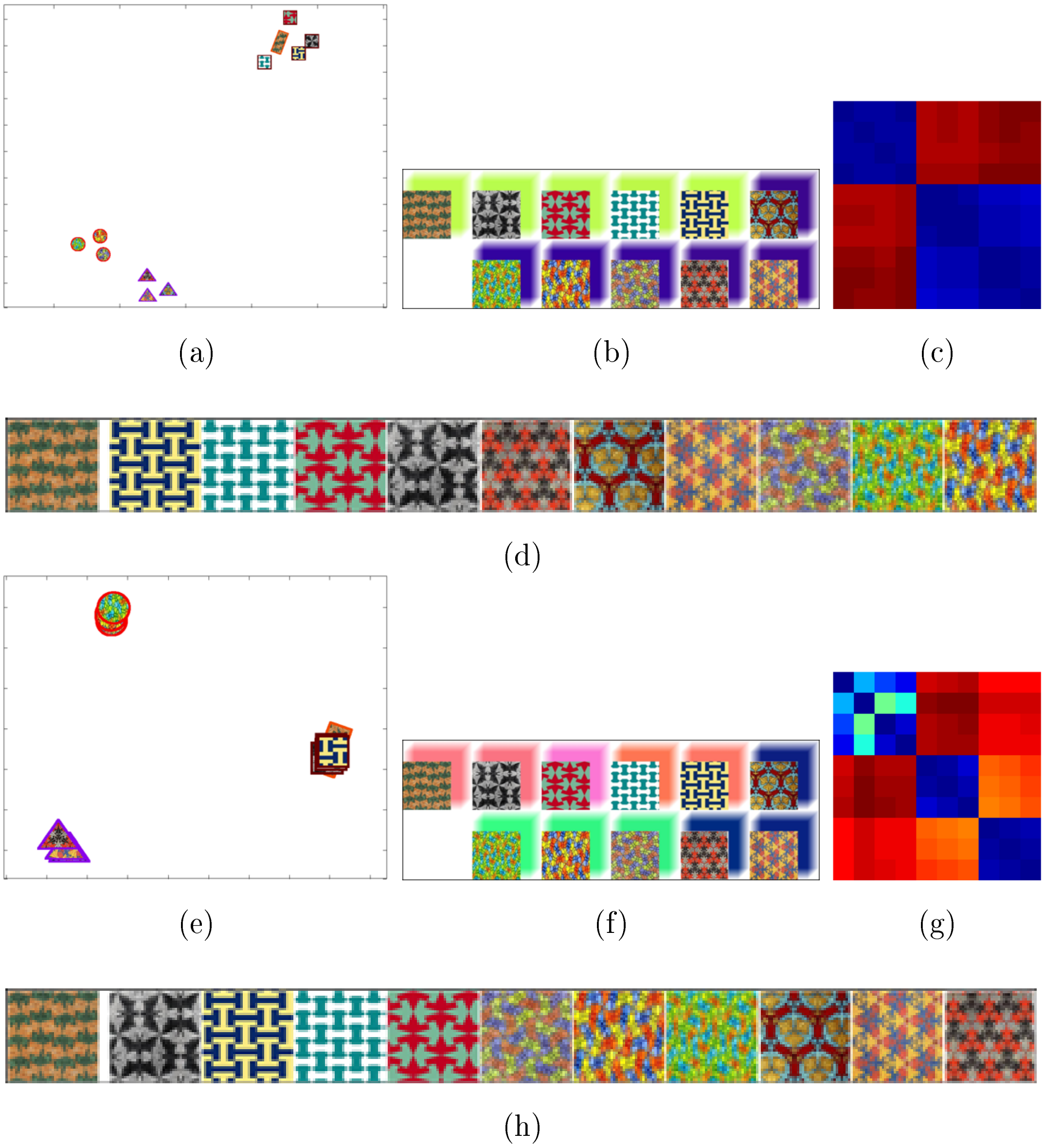

Figure 4.44: Experiment 38.

between within and between group distances, the better the classification, since small values imply that the groups have small within group distances and large between group distances. The last row shows the average of values for all fourteen experiments. Observe that the clustering results for tSNE are better than for SMDS for two-group experiments.

The chart illustrating the ratio between within and between group average distances for all fourteen experiments is given in Fig. 4.57. Observe that for all

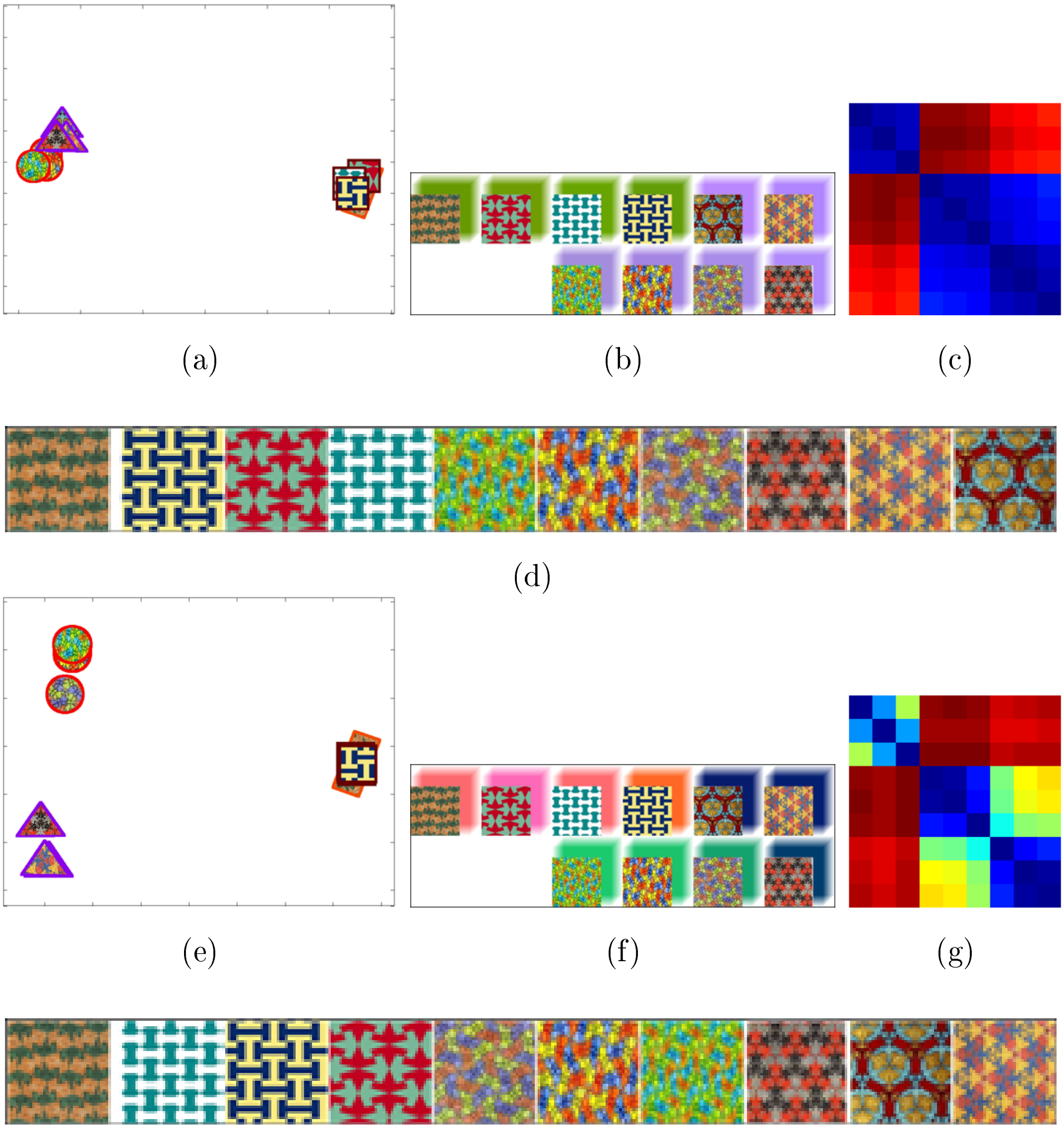

(a) (b) (c)

(d)

(e) (f) (g)

(d)

Figure 4.45: Experiment 39.

experiments the clusters obtain via tSNE have smaller values than the ones obtained via SMDS.

The rest twenty-nine experiments contain more than two groups. There are, overall, seventeen groups that are shown in Fig. 4.58. The same group may occur in different experiments in combination with different ornaments of the same group. We separate those combinations into different subgroups. For example, see $G6$ group, which is further divided into three different subgroups. The first

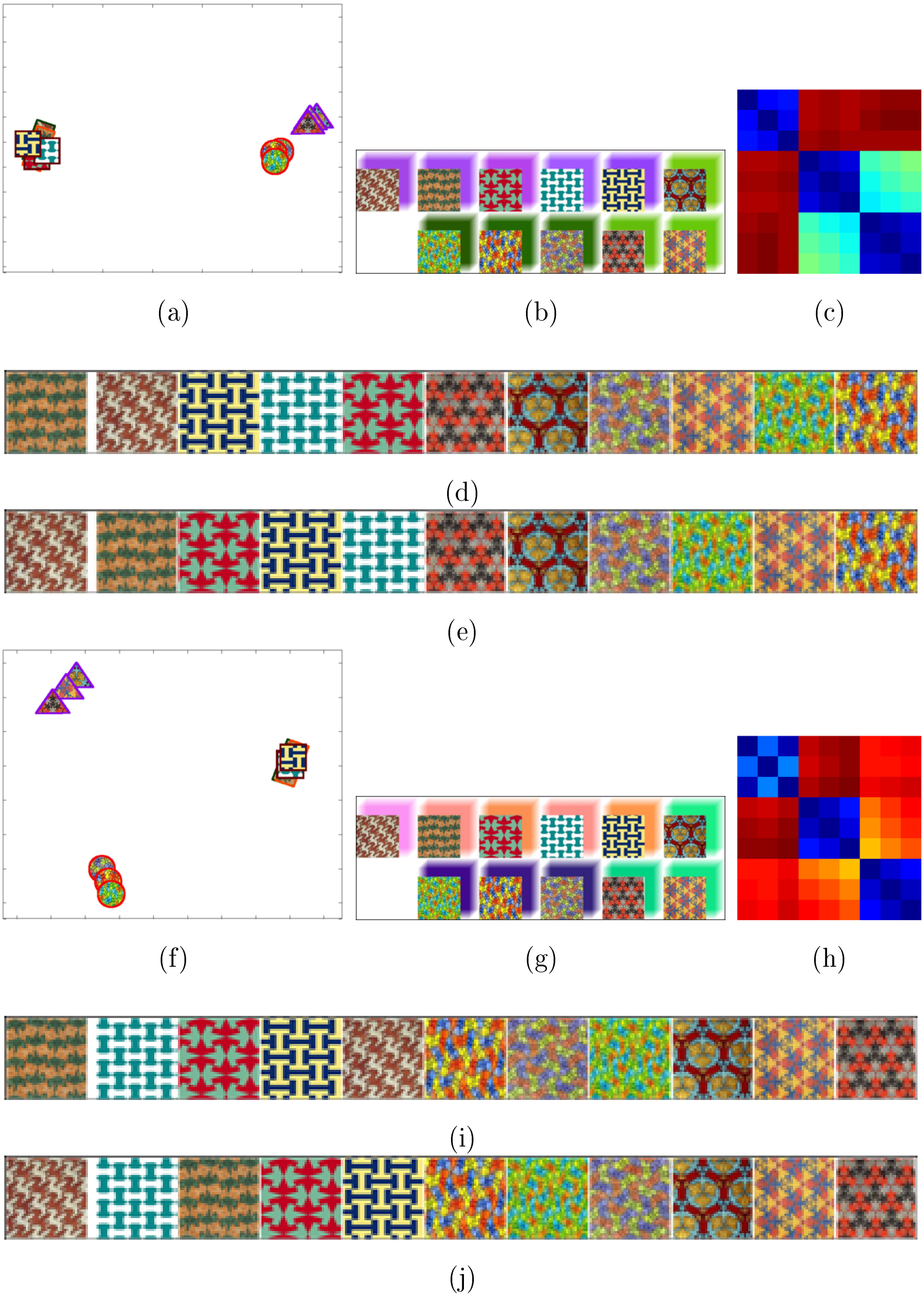

Figure 4.46: Experiment 40.

one contains three commonly occurring ornaments with three-fold rotations and mirror reflections. The other two groups occur when one or two ornaments with

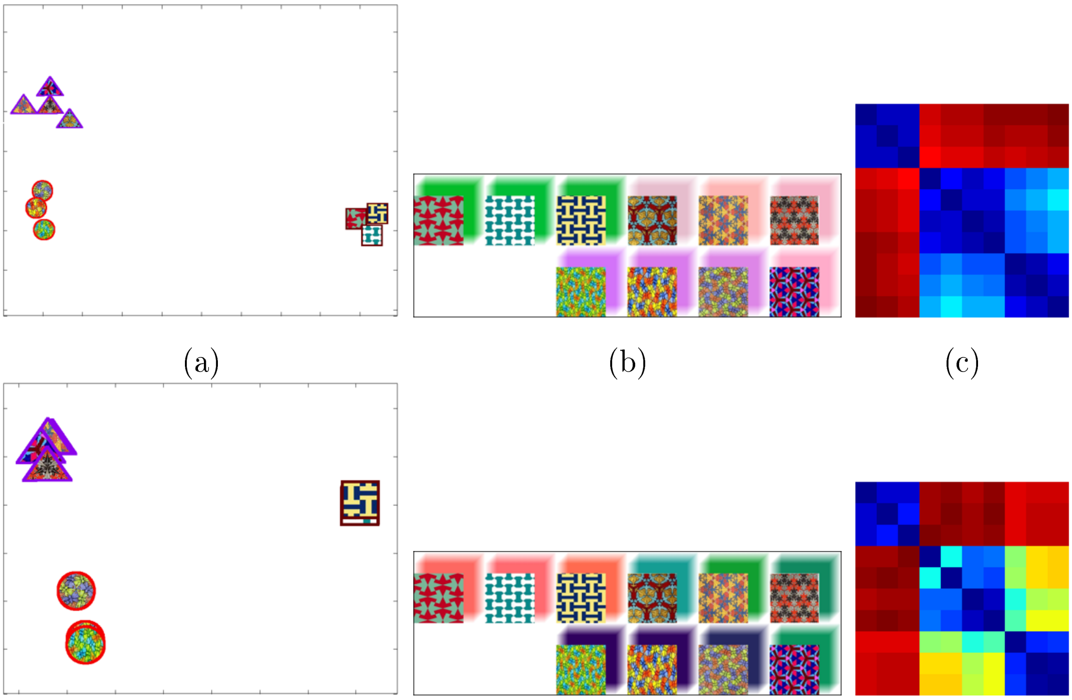

(a) (b) (c)

(d) (e) (f)

Figure 4.47: Experiment 41.

three-fold rotations and mirror reflections are added to the first subgroup. At any given experiment, only one subgroup of the group participates.

The same group may occur in more than one experiment. For each group, we compute the average within and between group distances in one experiment, and then we take the average of those values obtained for all experiments in which the given group took part. See the chart in Fig. 4.59 for average within and between group distances for all seventeen groups for both SMDS and tSNE results. Observe that both SMDS and tSNE have good separation of clusters, which can be inferred from a good separation between within (green diamonds) and between (brown squares) group distances. For both SMDS and tSNE, within group distances lie below 0.2, and between group distances lie above 0.4. Notice the last four groups in both charts have the highest between group distances. Those are group $G10$ and three subgroups of $G11$ group. We infer from the results that these four groups are well separated from all other groups in all

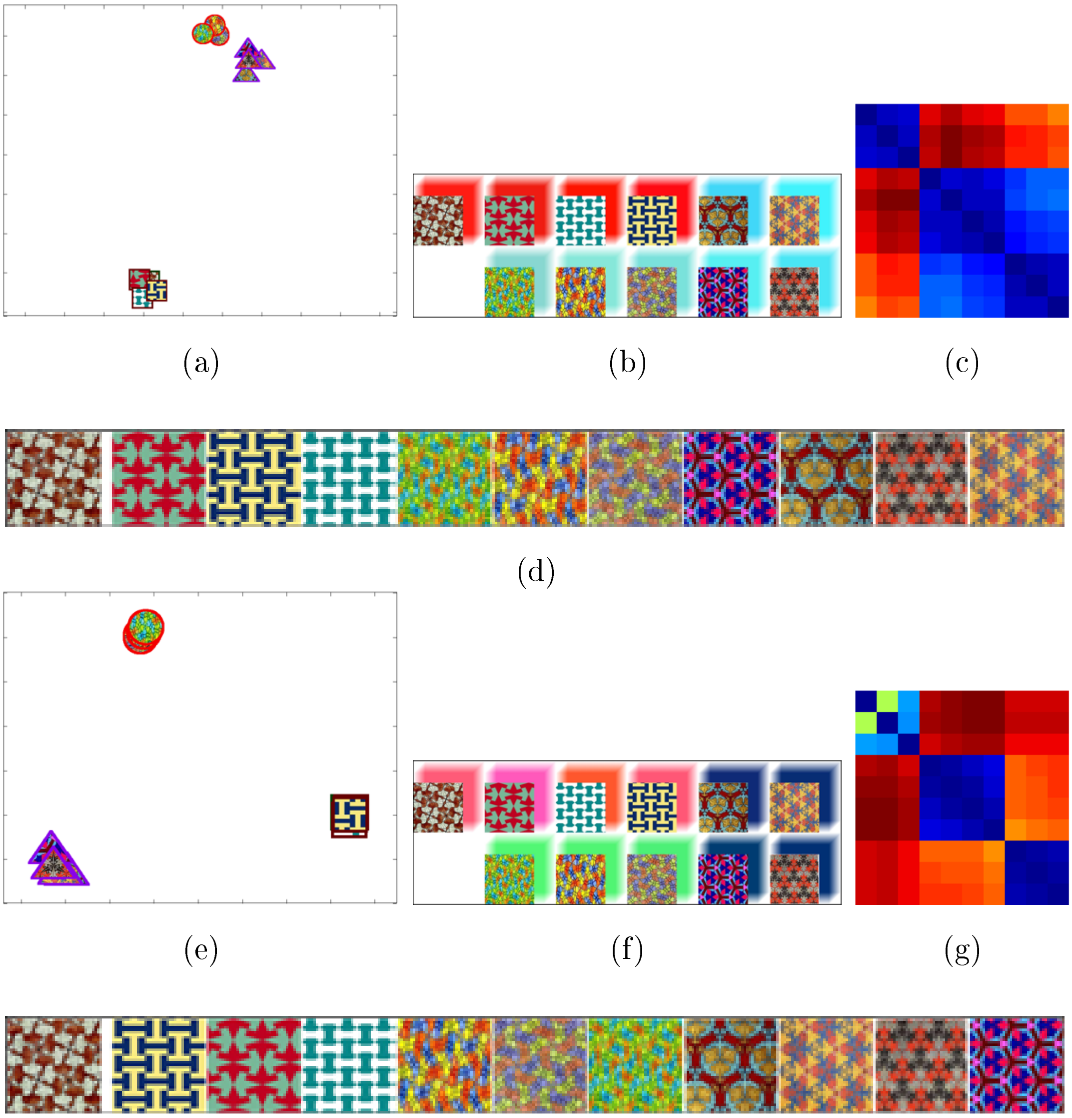
(a) (b) (c)

(d)

(e) (f) (g)

(h)

Figure 4.48: Experiment 42.

experiments they took part.

Just like for two-group experiments, for experiments with more than two groups we show the ratio between the average within and between group distances in Fig. 4.60. While for two-group experiments there was a big difference between SMDS and tSNE results (average of 0.44 and 0.25, respectively), here the average values are close (average of 0.13 and 0.14, respectively). Those results indicate that for two-group experiments tSNE give better clusters, while for ex-

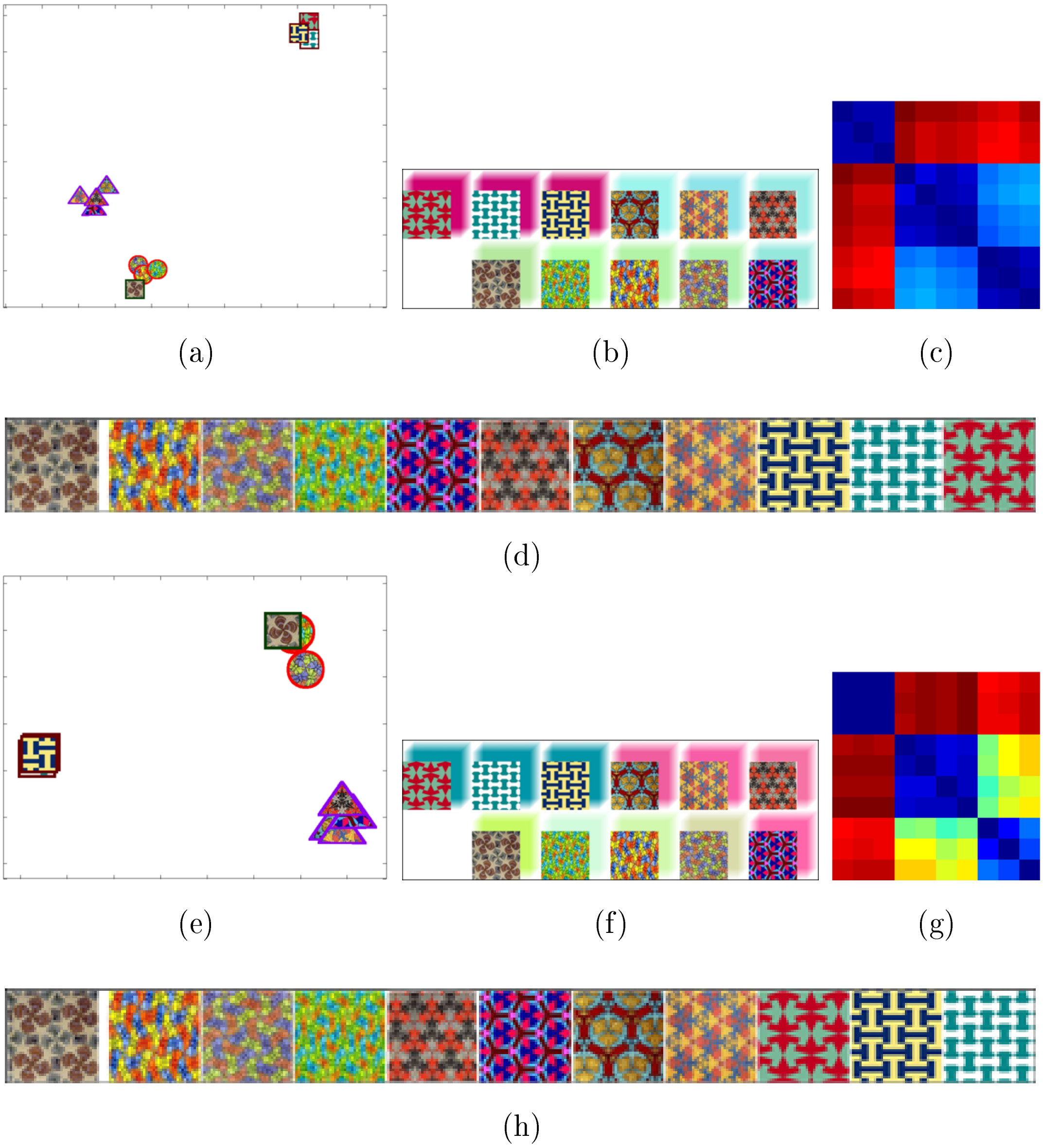

Figure 4.49: Experiment 43.

periments with more than two groups both SMDS and tSNE give almost the same clustering results.

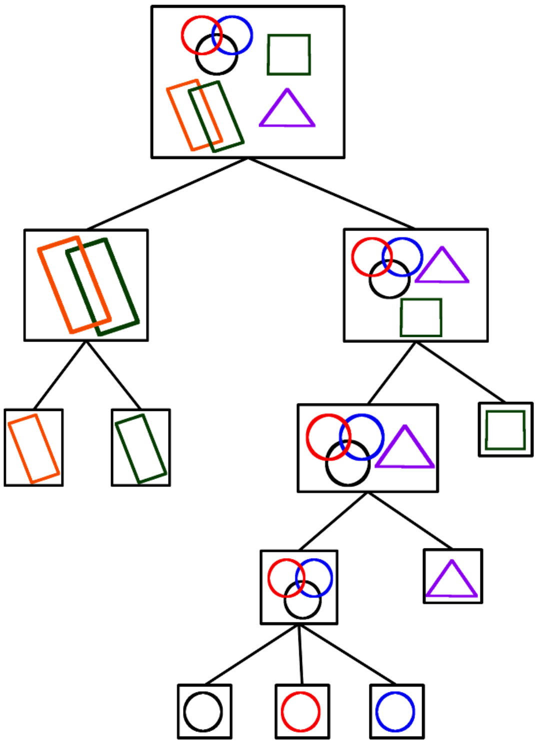

Figure 4.50: Hierarchy illustrating the relations between different groups. Two major groups are observed, the rotational groups and the pure translational and glide groups. These are further separated into groups each time separating the farthest group in the current context.

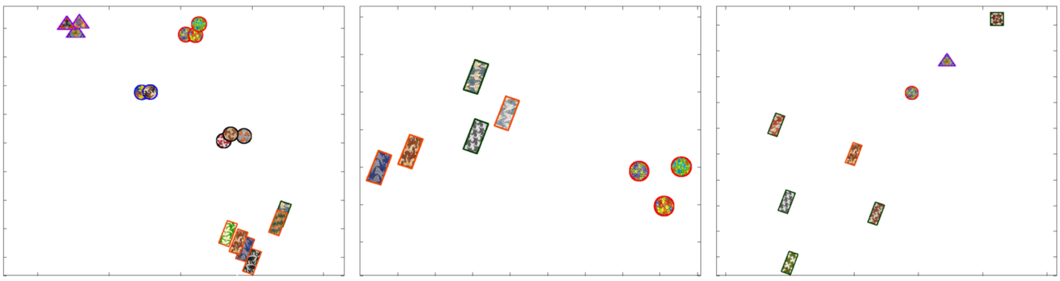

(a) (b) (c)

Figure 4.51: Three different experiments showing that pure translational group is stylisticly close to glide group. These two groups are always separated from rotational groups. Rotational groups tend to join against pure translational and glide groups.

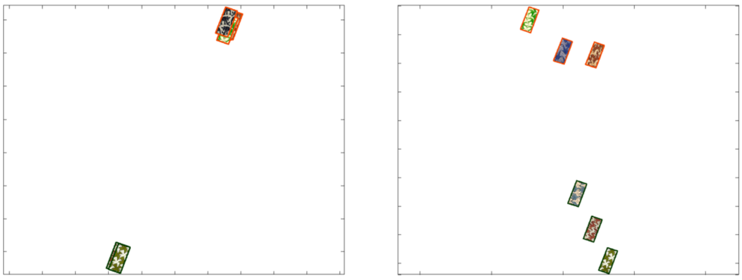

(a) (b)

Figure 4.52: Two experiments indicating that despite being style-wise similar, the glide and pure translational groups are well separated.

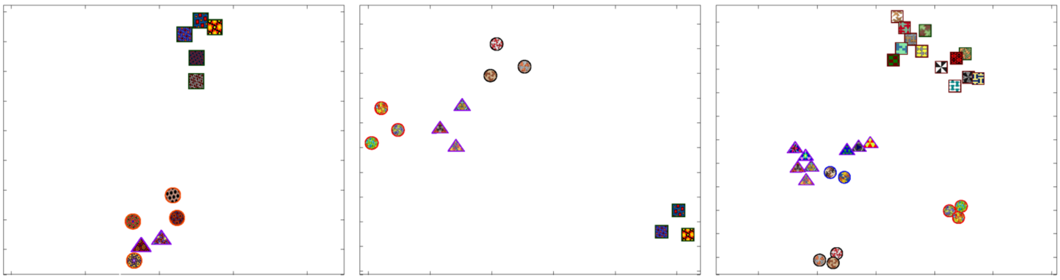

(a) (b) (c)

Figure 4.53: Within rotational groups, the ornaments with tree-fold and six-fold rotations tend to join against the $p4$ and $p4g$ groups.

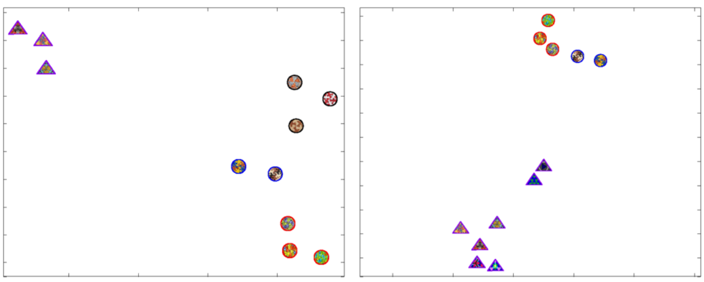

(a) (b)

Figure 4.54: Eliminating $p4$ and $p4g$ groups from the context, shows differences between the ornaments with three-fold rotations and the ornaments with six-fold rotations.

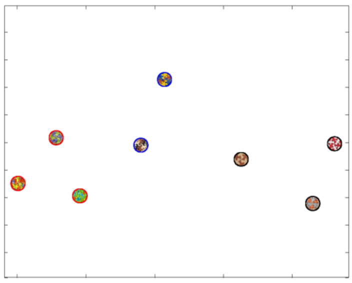

Figure 4.55: The $p6$ group internally is also divided into several groups. Each group contains style-wise similar ornaments.

Experiments	SMDS			tSNE		
	**0.33**	0.22	0.67	**0.02**	0.02	0.99
	**0.28**	0.18	0.64	**0.26**	0.20	0.75
	**0.32**	0.14	0.45	**0.02**	0.02	1.00
	**0.61**	0.47	0.78	**0.29**	0.26	0.91
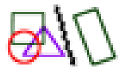	**0.41**	0.20	0.48	**0.25**	0.23	0.89
	**0.33**	0.22	0.67	**0.33**	0.24	0.74
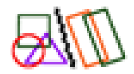	**0.65**	0.34	0.52	**0.46**	0.30	0.64
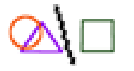	**0.49**	0.31	0.63	**0.20**	0.15	0.77
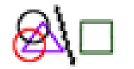	**0.43**	0.34	0.78	**0.28**	0.23	0.80
	**0.22**	0.15	0.67	**0.13**	0.11	0.86
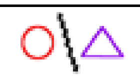	**0.43**	0.24	0.55	**0.36**	0.28	0.79
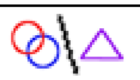	**0.47**	0.25	0.52	**0.37**	0.27	0.72
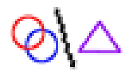	**0.55**	0.31	0.55	**0.26**	0.21	0.82
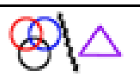	**0.60**	0.36	0.60	**0.31**	0.26	0.83
Average	**0.44**	0.27	0.61	**0.25**	0.20	0.82

Figure 4.56: Experiments containing only two groups. Numbers shown in red represent within group average distances. Between groups average distances shown in blue. The ratio between within and between group average distances shown in balck. Last row shows average values for all values of the experiments.

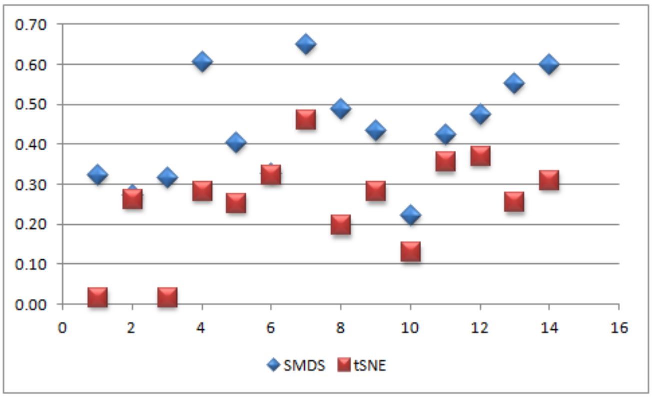

Figure 4.57: Experiments containing only two groups. The ratios between within and between group average distances are plotted. For tSNE results the ratio is below 0.4 for nearly all experiments, indicating a better separation of groups.

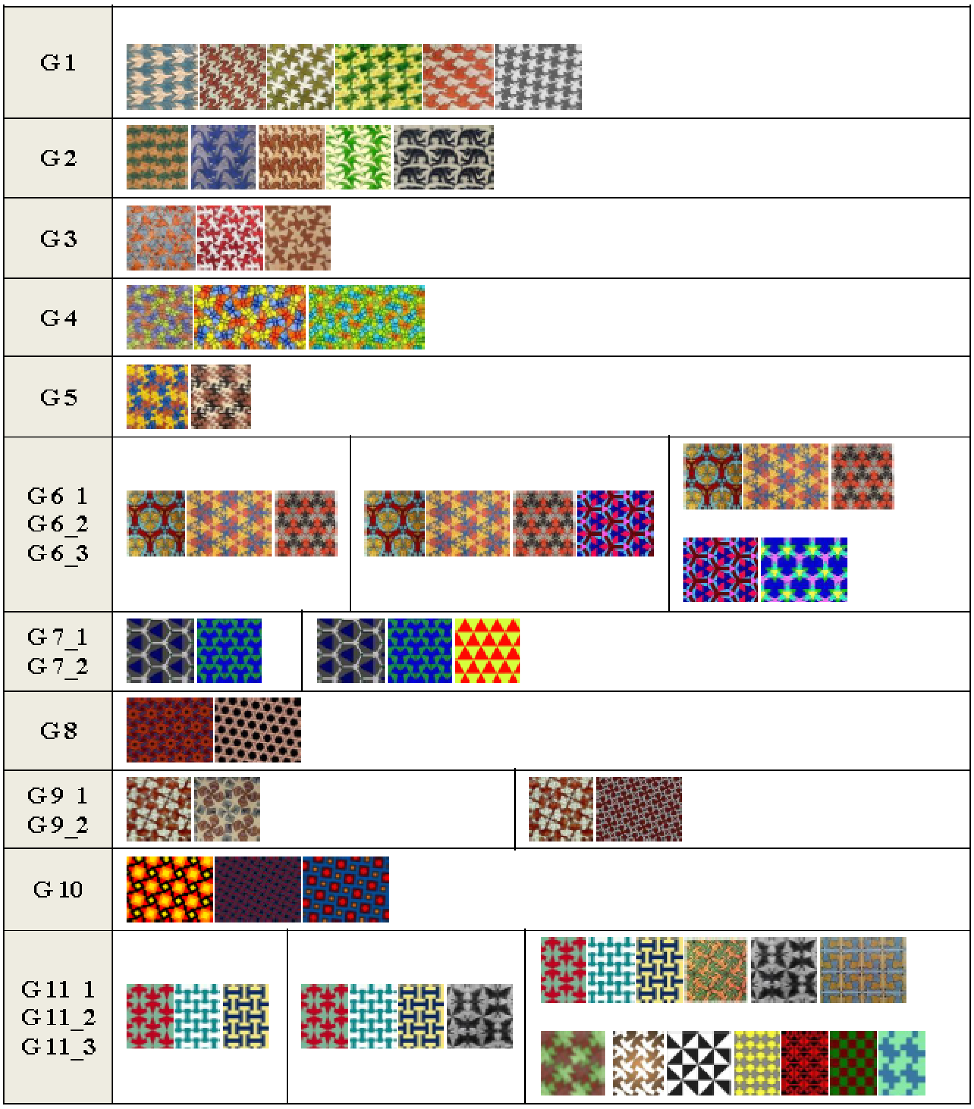

Figure 4.58: Groups that took part in twenty-nine experiments with more than two-groups.

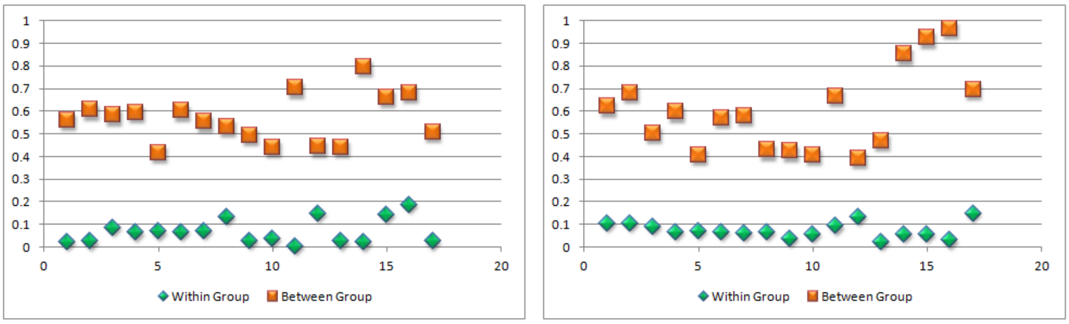

(a) SMDS (b) tSNE

Figure 4.59: Within vs. between group avgerage distances for experiments with more than two groups. Observe that both SMDS and tSNE results give good separation of different groups.

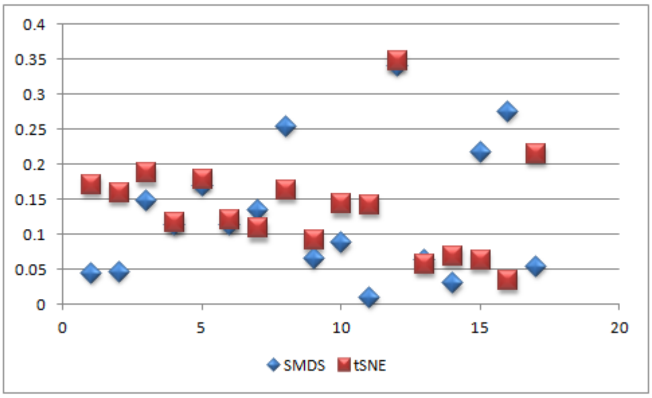

Figure 4.60: The ratio between within vs. between group avgerage distances for experiments with more than two groups. Observe that both SMDS and tSNE give approximately similar results.

CHAPTER 5

COMPARING DIFFERENT LEVELS

In Chapter 3, we introduced content suppression technique as a new way of studying ornaments. We also extensively discussed the levels of content suppression. Starting from original ornament, which is the first level, we go further to the second level, where the binarized images, called masks, are obtained from original ornament. At this stage, we eliminate the color information. We go further to the third level, where we suppress shape information applying a linear transform to the binarized images. We call the linear transform of an image, the ω field of an image. Clustering images of different levels give clustering results based on different factors that are featured in the given image. Thus, clustering raw images yield results where emergence of a cluster is highly influenced by colors and shapes that are present in an image. Clustering according to binary images introduces more style based clustering, since the information on color permutations and the number of colors, which code the style, are present in the given images. However, the clusters to be emerged are also influenced by shapes, since the content is not fully suppressed at this stage. Finally, clustering images where the content is fully suppressed give style-based clustering. The clustering results also show the relation between different clusters depending on the given context.

In this chapter, we analyze each level, comparing the clustering results based on different levels of content suppression. Various clustering results are given. In order for a reader to appreciate the advantages of using content suppressed images, we also present quantitative analysis.

5.1 The Method

For each experiment, we show the clustering results for all levels of content suppression. Thus, in each experiment, given a set of ornaments, we obtain three similarity matrices: one based on raw images, one based on masks, and one based on ω fields of masks. The similarity matrices for masks and ω fields are obtained using the same method described in Chapter 4. When computing the similarity matrix for raw images, we directly detect SIFT features from raw images, since at this stage we do not have masks. We, then, just count the number of matches between different raw images to form a similarity matrix.

All three similarity matrices are then embedded to lower dimension for clustering and visualization purposes. Since in Chapter 4 the tSNE clustering results shown to give better results in this chapter we will be using only tSNE dimensionality reduction technique. Thus, for each experiment we obtain three tSNE results that are illustrated in figures for comparison purposes. Fig. 5.1 gives an overview on the levels we consider in our experiments.

We expect the tSNE results for raw images to group together ornaments with similar shapes and color information. At this stage, no style information exists. When the ornament similarity is measured by measuring the similarities of the respective binary masks, we expect that the similarity measure will place ornaments that use similar shapes as motifs and permute the colors in the same manner. As content suppression proceeds, suppressing any shape and color information, the emerged clusters are expected to be according to style of images.

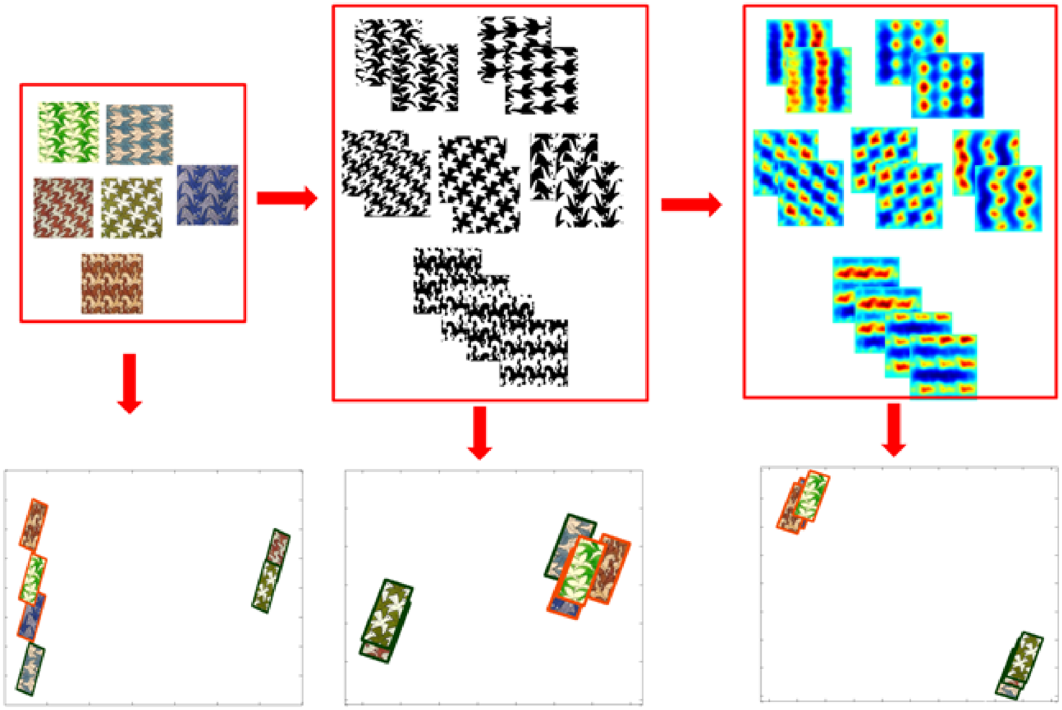

Figure 5.1: Levels of Content Suppression. (Left) Clustering result based on raw images. (Middle) Clustering result based on masks of the images. (Right) Fully content suppressed images and clustering result.

5.2 Experiments

We give experimental results for seventeen selected experiments out of fourty-three experiment set of Chapter 4. We will refer to those forty-three experiment set in this chapter. As it was mentioned earlier, for each experiment we give three clustering results: one based on raw images, one based on masks, and one based on content suppressed images. The results are illustrated in Figs 5.2-5.18. In the following experiments we compare how different levels of content suppression cluster different groups, and analyze how those levels handle group relations in their clustering results. In the next section we give quantitative analysis for all experiments, comparing the clustering results for all three levels of content suppression.

We begin with Experiment 5 of the experiment set, where we have a collection of sixteen ornaments: three ornaments of *mariposas* groups, three two-color ornaments of group $p6$, two three-color ornaments of group $p6$, three ornaments with three-fold rotations and mirror reflections, and five ornaments of glide group. We expect exactly these five groups to emerge as a clustering result. When the clustering is performed on raw images, the emerged clusters (Fig. 5.2 (a)) are not meaningful. Observe that, even the *mariposas* group, which consists of almost the same ornaments, is separated. As soon as we begin suppressing the content by binarizing the images, meaningful clusters begin to emerge. The clustering result for masks, in which the color is suppressed, shows three correct groups (Fig. 5.2 (b)). Notice that, at this stage, the images with motifs that vary significantly could not be clustered correctly. As content suppression proceeds by suppressing also the shape information, all groups are correctly identified showing style-wise similar ornaments in one cluster (Fig. 5.2 (c)).

The next experiment is the Experiment 6 from experiment set, where we add one more ornament to the previous collection. It belongs to pure translational group. Since there are no other ornaments of the same group, we expect the newly added ornament to join the glide group. The clustering result for raw images (Fig. 5.3 (a)) groups all ornaments as one big group, except for two small groups that stand apart. Suppressing the color information gives three correct clusters (Fig. 5.3 (b)). For clustering results for both raw images and masks, we cannot say anything regarding the newly added ornament, because, in both cases, it joins the group, which could not be clustered correctly. When the content is fully suppressed, the newly added ornament finds the group which is the closest to it style-wise (Fig. 5.3 (c)). Observe also in the final clustering result, a group of three-color ornaments of group $p6$ reside very close to the glide group. As we discussed in the previous chapter, this occurs due to similarity in number of colors that the ornaments of both groups contain. The number of colors that the ornaments contain also codes the style, influencing the relations between the groups.

For the next experiment we choose Experiment 9 from experiment set, and replace the glide group of first experiment (Experiment 5), with six ornaments of pure translational group. We still expect five clusters to emerge as a clustering result, the fifth cluster being the group of newly added pure translational group.

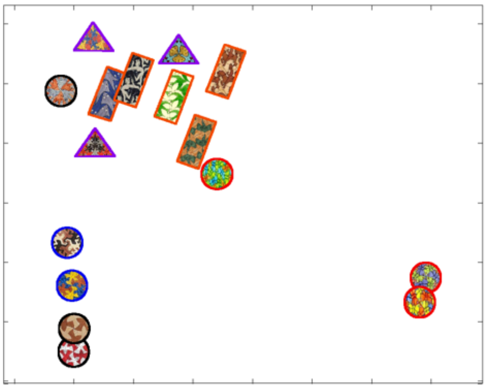

(a) Raw Images

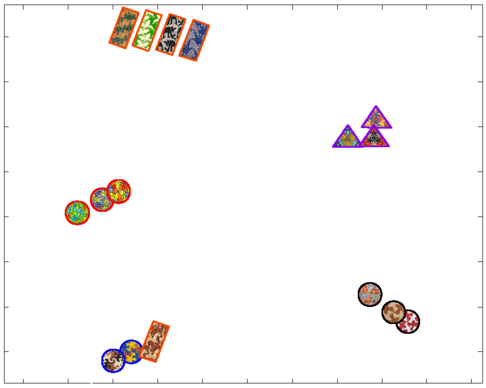

(b) Binary Images

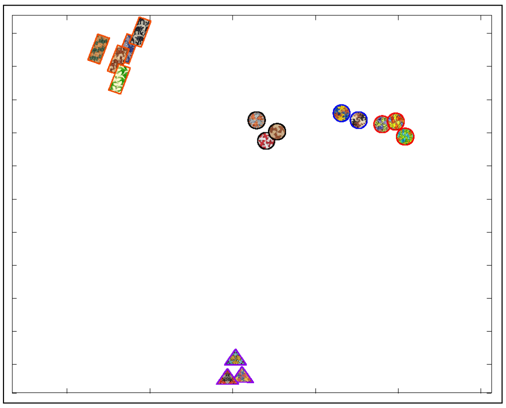

(c) Content Suppressed Images

Figure 5.2: Experiment 5. Sixteen ornaments are considered. Five groups are expected to emerge as a clustering result. We obtain correctly clustered groups only when the content suppressed images are considered (c).

The clustering result for raw images (Fig. 5.4 (a)), just like in the previous experiments, is not meaningful. Just by suppressing the color information in ornaments, we obtain clusters with almost all groups correctly identified, as shown in Fig. 5.4 (b). Here, only the pure translational group is separated into two. This is corrected in the final result (Fig. 5.4 (c)), when the content is fully suppressed. Also, observe how the groups are placed on the plane. The y-axis separates the rotational groups from pure translational group.

We add one more ornament to the previous collection forming Experiment 11 from experiment set. The newly added ornament is of group *pg*, and we expect it to join the pure translational group, which is the closest group style-wise.

(a) Raw Images (b) Binary Images

(c) Content Suppressed Images

Figure 5.3: Experiment 6. Enlarging the ornament set in Fig. 5.2 with an ornament of group $p1$. As expected the newly added ornament joins the glide group, which is the closest group style-wise. The clustering results become more reflective of the style as we move from (a) to (c).

The expected result is seen only from the clustering result for fully content suppressed images in Fig. 5.5 (c). In the clustering result for masks (Fig. 5.5 (b)) the pg ornament joins the group of ornaments with three-fold rotations and mirror reflection, most probably due to shape similarity in ornaments of this group, while clustering of raw images carry no meaning.

We consider Experiment 10 as a next experiment, where we add an ornament of cm group to the ornament set of Experiment 9 instead of pg ornament of previous experiment. We again expect it to join the $p1$ group, since the cm group contains no rotations. See the clustering results in Fig. 5.6. In the clustering results based

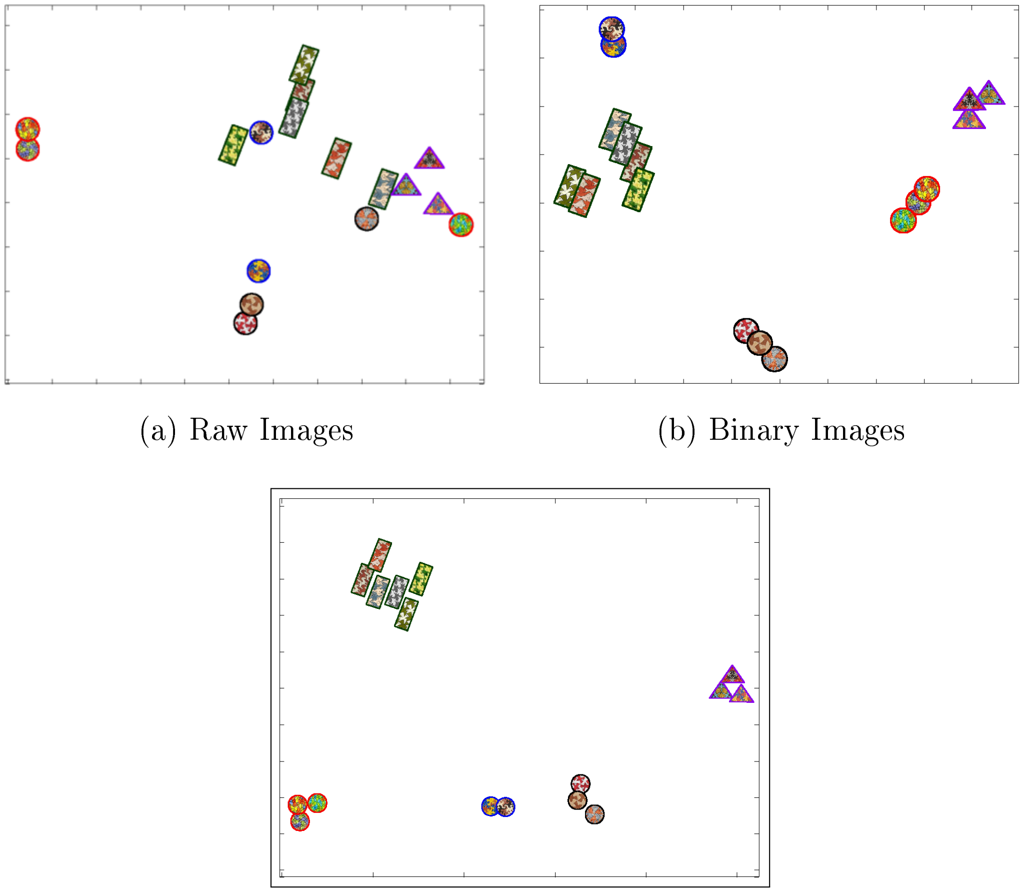

(a) Raw Images

(b) Binary Images

(c) Content Suppressed Images

Figure 5.4: Experiment 9. Five ornaments of glide group in Fig. 5.2 are replaced by six ornaments of pure translational group. Desired five groups emerge only when the content is fully suppressed (c). Observe that the rotational groups are separated from the pure translational group.

on raw images as well as on binary images, the newly added ornament joins the rotational group. The ornament joins the pure translational group only when the clustering is performed on content suppressed images. In Fig. 5.6 (c) we again observe a separation of rotational groups from pure translational group.

We consider another scenario, and instead of the *cm* ornament, an ornament of *p*4 group is added to the ornament set of Experiment 9. A new collection forms Experiment 12. The ornament of *p*4 group contains no pair in this collection, thus we expect it to join one of the rotational groups. Since it is a two-color ornament, we further expect it to join the *p*6 group with two-color ornaments.

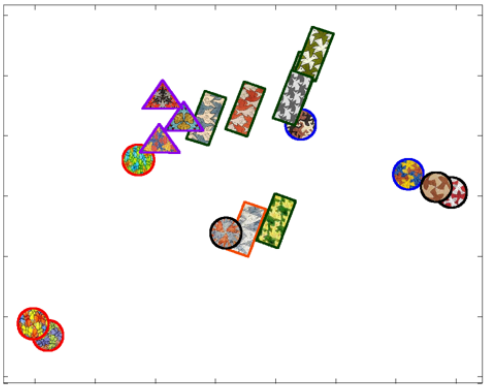

(a) Raw Images

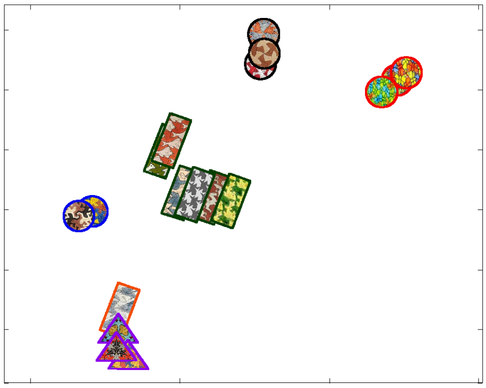

(b) Binary Images

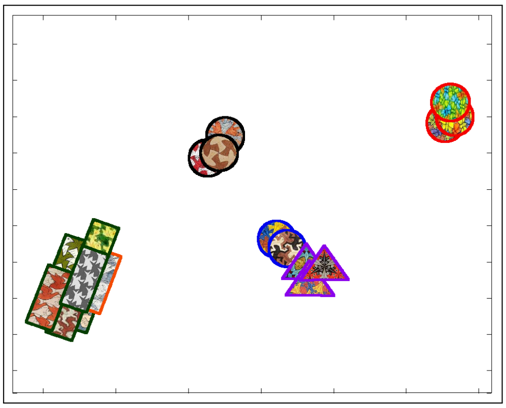

(c) Content Suppressed Images

Figure 5.5: Experiment 11. Exdending the set in Experiment 3 with an ornament of *pg* group. As expected the newly added ornament joins the pure translational group in (c).

We observe the expected clustering result only for content suppressed images (Fig. 5.7).

The ornament of $p4$ group of the previous experiment (Experiment 12) joins the $p6$ group only because it has no other ornament of its own group in the given collection. We, next, perform an Experiment 13 which contains one more ornament of $p4$ group. Now, we expect the ornaments of $p4$ group to form a cluster of their own, thus, forming six clusters. Fig 5.8 shows desired clusters for both binary and content suppressed images, while the result for raw images mixes all groups. Although the clustering result based on binary images give the desired six groups, we cannot infer any meaning from group relations, while

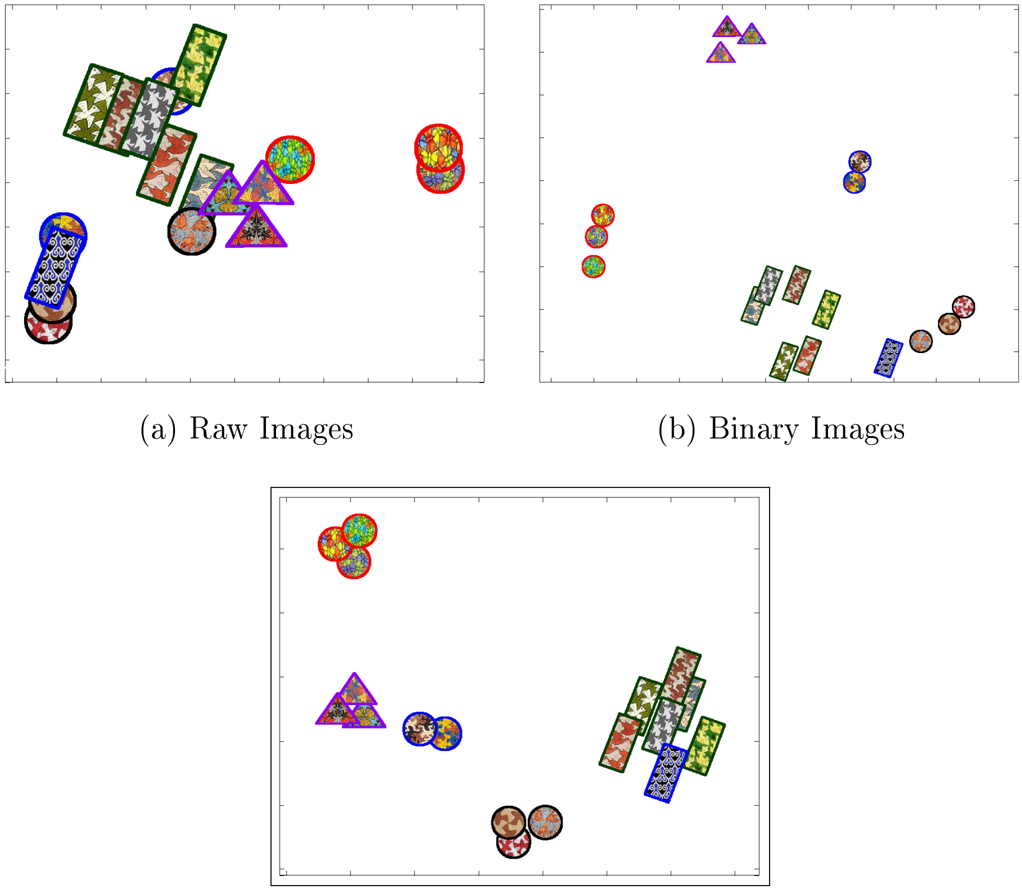

(a) Raw Images (b) Binary Images

(c) Content Suppressed Images

Figure 5.6: Experiment 10. Exdending the set in Experiment 9 with an ornament of *cm* group. As expected the newly added ornament joins the pure translational group (c).

for the content suppressed images the rotational groups are separated from pure translational group. This kind of relation makes more sense than the relations inferred from binary image clustering.

Next, we present the Experiment 14, where we consider eight ornaments, three of which are *mariposas* ($p6$), two are of pure translational group and three of glide group. While we expect three groups to emerge, we also expect the *mariposas* group to reside far from other two groups. The result for raw images shows two major clusters (Fig. 5.9 (a)), the second is further divided into two clusters, one containing pure translational group and the other is a glide group. However, the *mariposas* group is separated. For the mask images we also observe

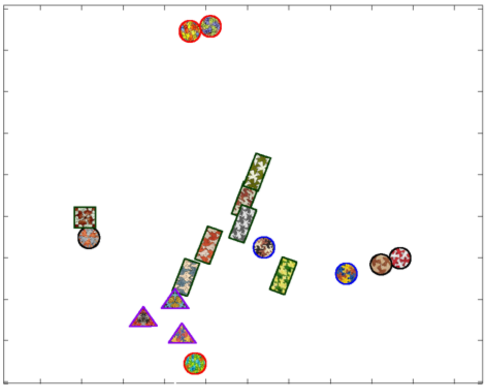

(a) Raw Images

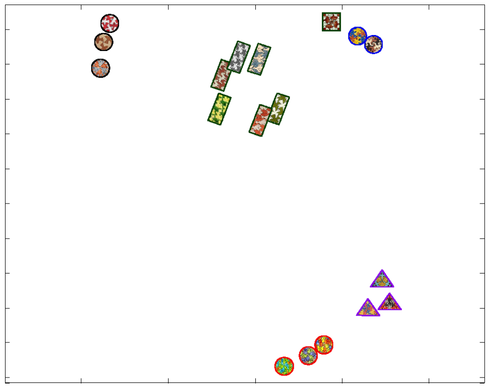

(b) Binary Images

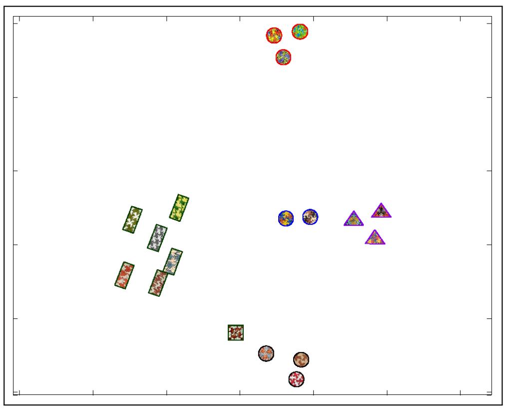

(c) Content Suppressed Images

Figure 5.7: Experiment 12. Enlarging the set in Experiment 9 with an ornament of $p4$ group. Among the rotational groups, it joins the $p6$ group with two-color ornaments.

three clusters, but the rotational group is not well separated from the other two groups (Fig. 5.9 (b)). As we fully suppress the image content we obtain three clusters, and the rotational group is well separated from other two groups (Fig. 5.9 (c)). Observe, however, that one ornament of glide group resides within the pure translational group. In introductory chapter, we talked about the style-wise similarity of this ornament of glide group to the other ornament of pure translational group (an ornament consisting of two blue and white birds translated in two directions). Thus, seeing these two ornaments together does not seem awkward.

While the pure translational group has style-wise similarities with the glide

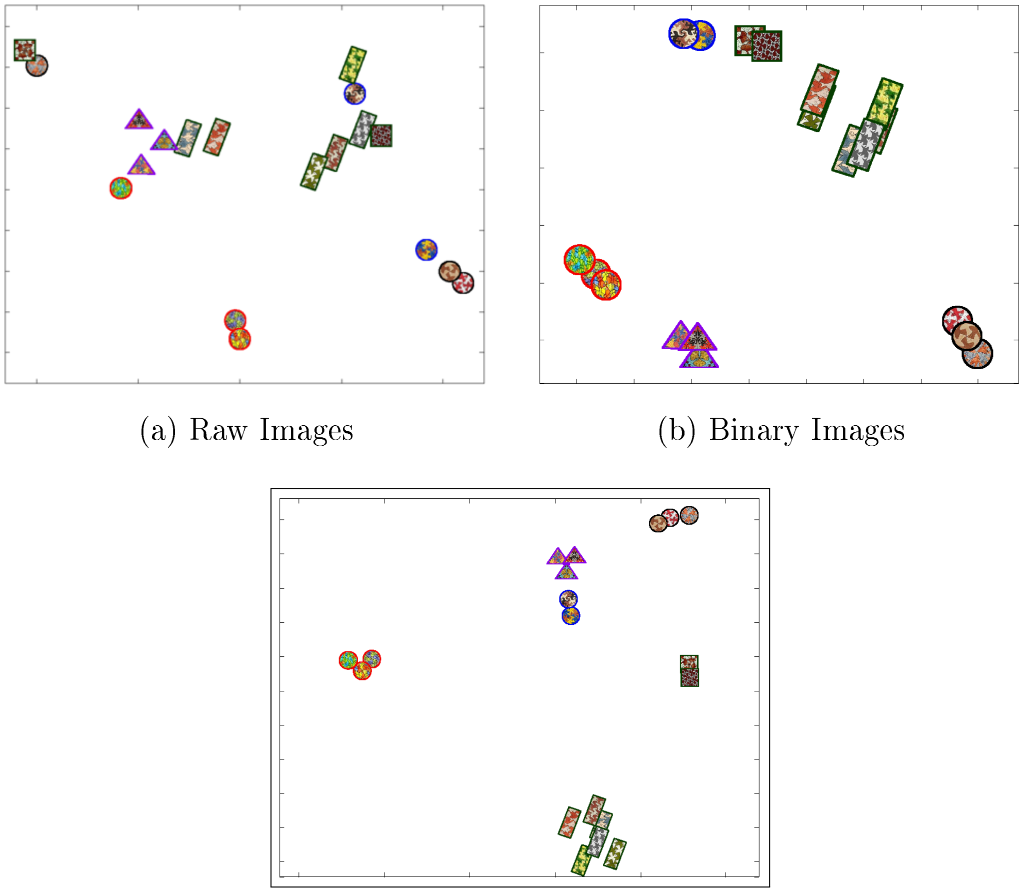

(a) Raw Images (b) Binary Images

(c) Content Suppressed Images

Figure 5.8: Experiment 13. Adding one more ornament to the collection in Experiment 12 introduces new group.

group, we expect these two groups to be well separated when no other groups are considered. We aim to see how different levels of content suppression handle this situation with Experiment 16 of the experiment set, which contains of six ornaments: three ornaments of pure translational group and three ornaments of glide group. We present the dendrograms (clustering hierarchy) of the clustering results for this experiment in Fig. 5.10. Observe that the orange group (glide group) is fully separated from the green group (pure translational group) only when the content is fully suppressed (Fig. 5.10 (c)). This result shows that clustering results based on raw and mask images are not capable of capturing style-wise differences between these style-wise very similar groups.

For the next experiment, we consider the collection set of the Experiment 17.

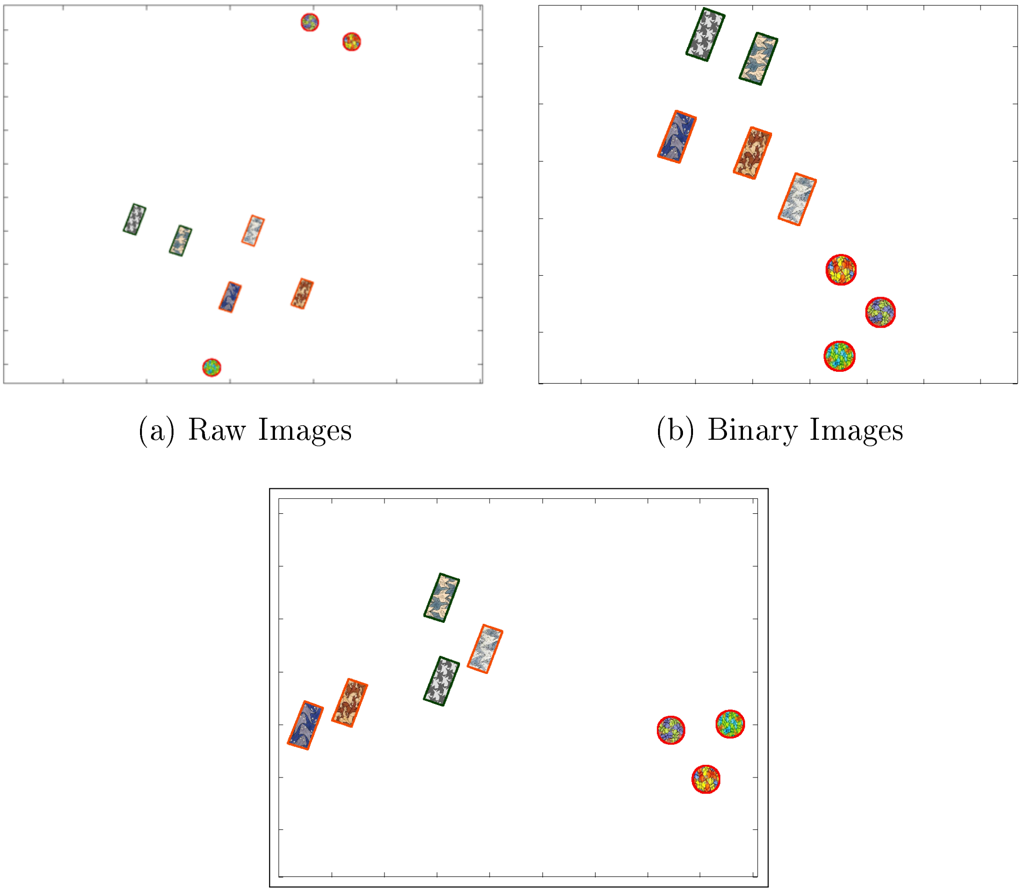

(a) Raw Images

(b) Binary Images

(c) Content Suppressed Images

Figure 5.9: Experiment 14. Considering a rotational groups vs. pure and glide groups. The content suppressed image clustering give precise separation of two groups.

It consists of six ornaments: three ornaments of pure translational group, two two-color ornaments of $p6$ group and one ornament of $p4$ group. Since the $p4$ ornament has no pair, we expect it to join two ornaments of group $p6$. Thus, we expect two clusters to emerge, one translational group and one rotational group. Fig. 5.11 illustrates the clustering results. While the clustering result for raw images (Fig. 5.11 (a)) also shows the desired two groups, the internal relations between the ornaments reveal that the clustering results are highly influenced by the shape similarities. One of the ornaments of $p6$ group is considered to be closer to an ornament of $p4$ group, rather than the ornament of the same group, due to fish shapes that the both ornaments contain. Only after suppressing the

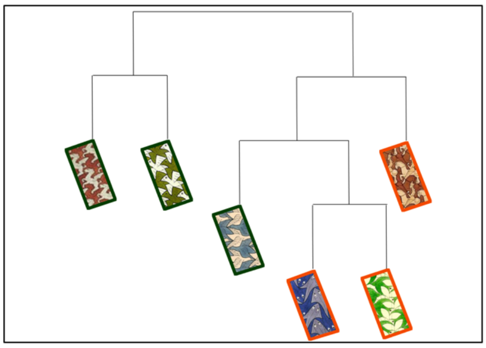

(a) Raw Images

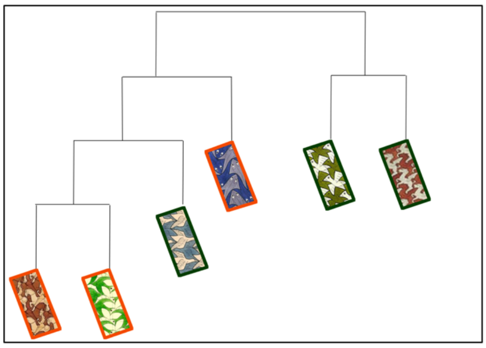

(b) Binary Images

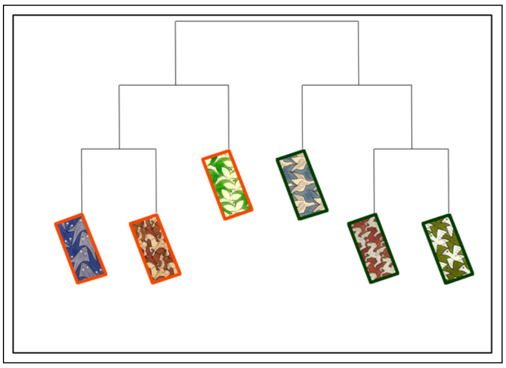

(c) Content Suppressed Images

Figure 5.10: Experiment 16. Dendrograms. Considering pure translational group vs. glide group. Two groups are fully separated only for content suppressed images.

full content, we observe the expected two clusters (Fig. 5.11 (c)). Notice that the internal style-wise ordering also makes sense.

In subsequent seven experiments, we consider the experiments containing a collection set consisting only of rotational groups. Our aim is to analyze how different levels of content suppression capture the style-wise differences between various rotational groups. We start with Experiment 22 which contains an ornament set consists of thirteen ornaments: three *mariposas* ($p6$), three two-color ornaments of group $p6$, two three-color ornaments of group $p6$, two ornaments of group $p4$, and three ornaments with three-fold rotations and mirror reflections. We hope to see exactly these five clusters to emerge. In the clustering result for the raw images (Fig. 5.12 (a)) none of the groups are correctly identified. As we

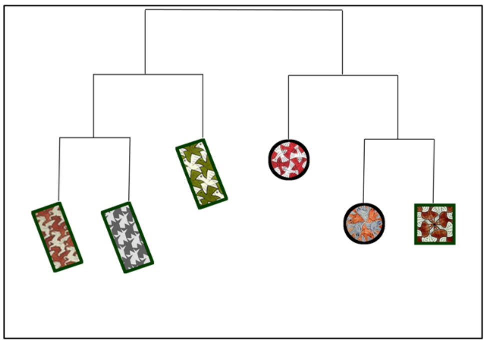

(a) Raw Images

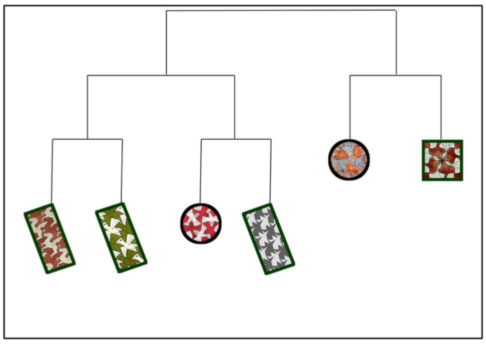

(b) Binary Images

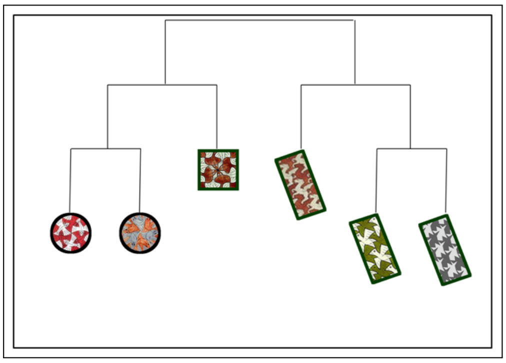

(c) Content Suppressed Images

Figure 5.11: Experiment 17. Dendrograms. Considering pure translational group vs. rotational groups. As expected the ornament of $p4$ group joins the $p6$ group. Also, for the final result, the internal clustering is just as one would expect, in contrast to the result given in (a).

start to suppress the content, ornaments that are style-wise close to each other begin to merge. Three correct groups emerge after suppressing the color information. All five groups emerge when both the colors and shapes are suppressed (Fig. 5.12 (c)). Notice that the groups are located in the 2D plane in a manner implying an increase in rotation order as one moves from right to left.

We further consider the Experiment 24, which contains a larger collection of rotational groups. The collection consists of twenty-six ornaments: three ornaments of *mariposas* group, three ornaments of two-color $p6$ group, seven ornaments with three-fold rotations and mirror reflections, two ornaments of $p4$ group and eleven ornaments of $p4g$ group. Again as we move from (a) to (c) in Fig. 5.13 we see the clusters that are more reflective of the style. The clustering based on

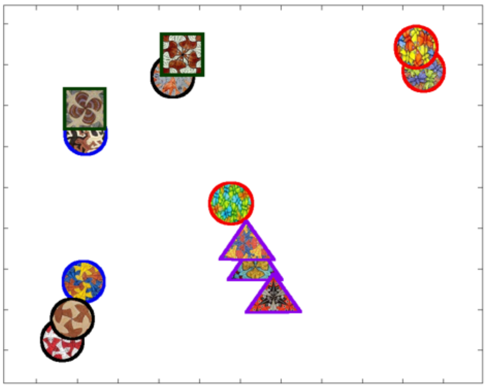

(a) Raw Images

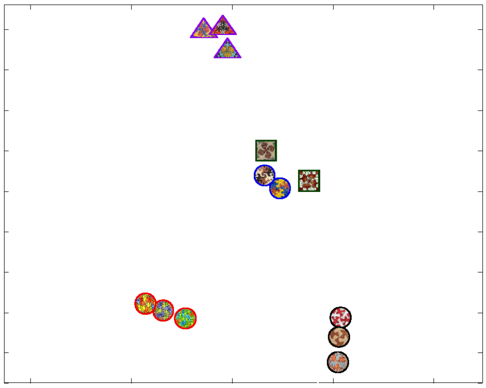

(b) Binary Images

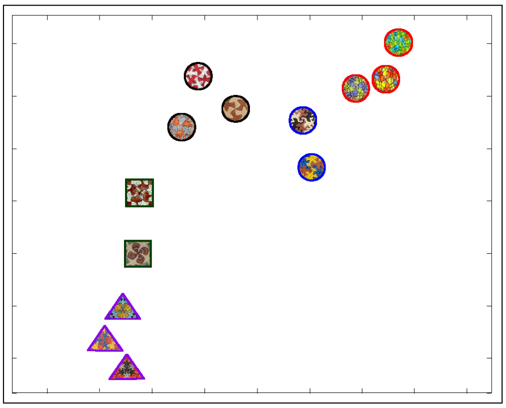

(c) Content Suppressed Images

Figure 5.12: Experiment 22. Rotational groups. The clustering result for content suppressed images gives five groups each containing style-wise similar ornaments. Also, observe the placement of ornament on 2D plane. The order of rotation increases as we move right from left.

raw images mixes different groups giving no meaning regarding the clustering preferences. For both mask and content suppressed images, we obtain similar groups. Note that in this experiment only by suppressing the colors we are able to cluster ornaments according to their styles. Also, observe that for both mask and content suppressed clustering results the four-fold rotational group is separated from other rotational groups. This indicates that this group is style-wise different from the other groups.

The next experiment is the Experiment 25 of the set. Its collection contains two three-color ornaments of $p6$ group in addition to the ornaments of the previous

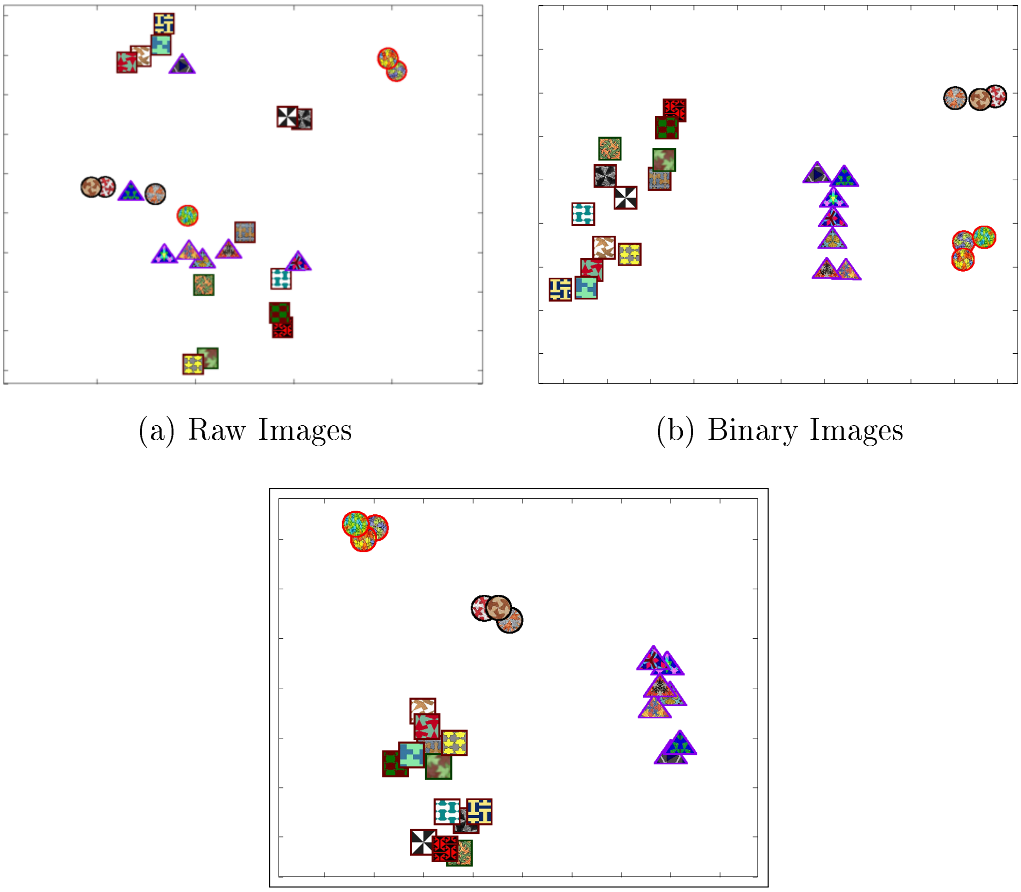

(a) Raw Images

(b) Binary Images

(c) Content Suppressed Images

Figure 5.13: Experiment 24. Considering a larger collection of rotational groups. Only by suppressing the color we obtain the desired groups.

experiment. The ornaments are scattered and no grouping is observed for raw images as shown in Fig. 5.14 (a). While in the previous experiment the clustering result based on masks grouped the ornaments correctly, in the current context it fails to discriminate the newly introduced two ornaments (Fig. 5.14 (b)). Observe that they join the four-fold group. All groups are correctly identified in the last result containing the content suppressed images. Also, observe that the groups with two-color ornaments are separated from the groups with ornaments of more color.

As a next experiment, we consider Experiment 26, which contains one more three-fold rotational ornament with mirrors in addition to the ornament set of the previous experiment. The clustering result for raw images again scat-

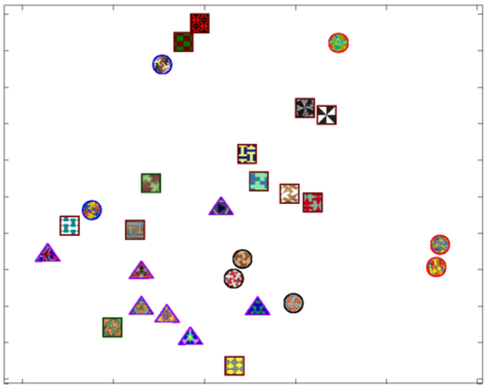

(a) Raw Images

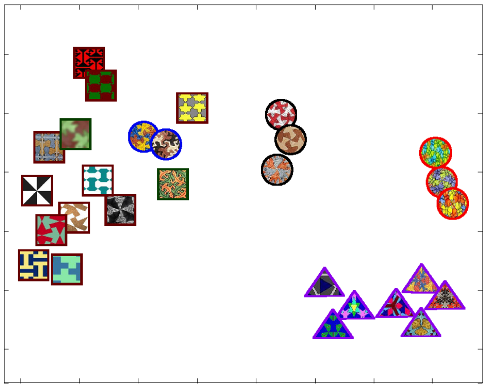

(b) Binary Images

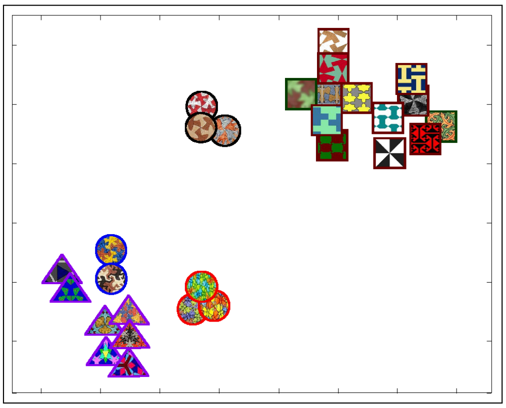

(c) Content Suppressed Images

Figure 5.14: Experiment 25. More rotational groups. Meaningful cluster emerge when the content suppressed images are clustered as shown in (c). The x-axis seems to capture color information discriminating the groups with similar number of colors.

ters all groups, so that none of the emerging groups are correct or meaningful (Fig. 5.15 (a)). As we begin to suppress the content by binarizing images, we begin to obtain meaningful clusters. Two correct groups emerge from binary images (Fig. 5.15 (b)). Once we fully suppress the content information we obtain meaningful clusters, all emerging according to style-wise similarities (Fig. 5.15 (c)). Also, observe that the group with four-fold rotations is well separated from the rest for content suppressed images.

In the last three experiments, we focus on group relations within rotational groups. It was shown in the previous chapter that clustering content suppressed

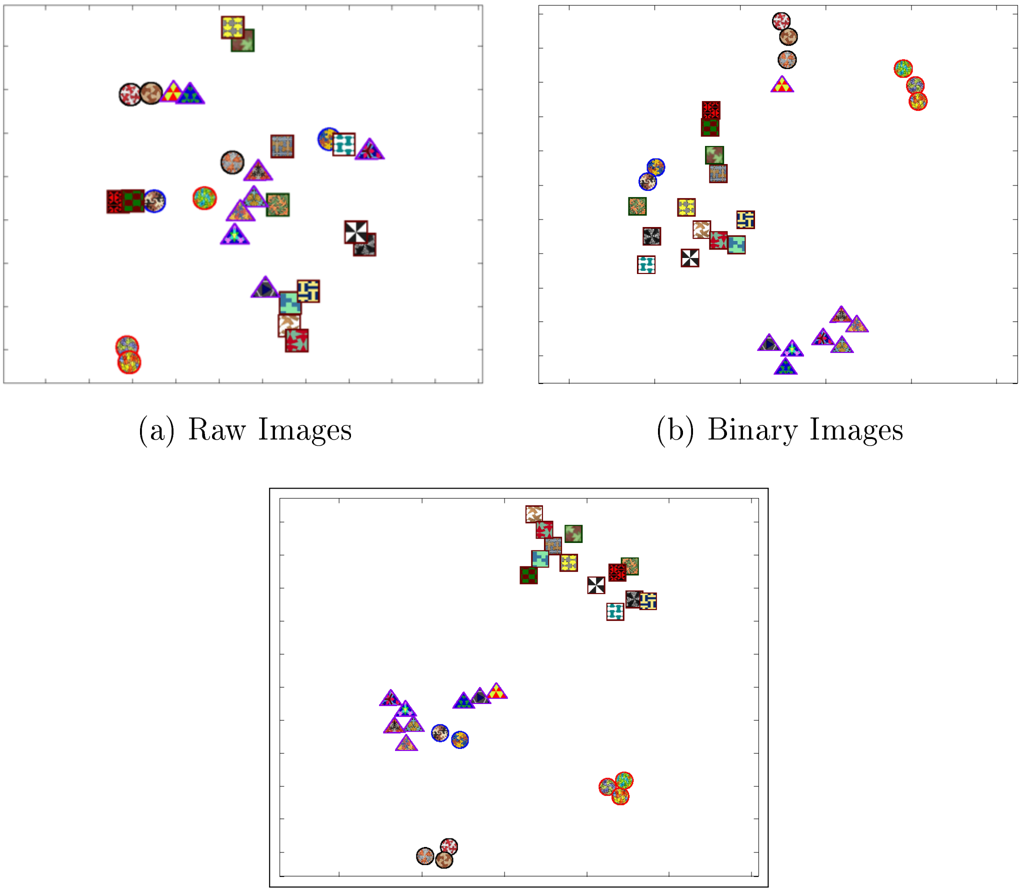

(a) Raw Images

(b) Binary Images

(c) Content Suppressed Images

Figure 5.15: Experiment 26. More ornament of rotational groups. Beside the meaningful clusters emerged for content suppressed images, we observe the relations between rotational groups.

images capture the relations of different groups. We aim to see if this is true for other levels of content suppression. We begin with Experiment 33, which contains twelve ornaments: three *mariposas* ($p6$), three two-color ornaments of group $p6$, three ornaments with three-fold rotations and glide reflections, and three ornaments of $p4$ group. We expect exactly these four clusters to emerge. We also expect the first three groups to be closer against the last group. Although, the first three are of different groups, due to color permutations, the maximum order of rotations they all contain is three. In the presence of pure translational group, all four groups are closely related due to rotations, in contrast to pure translational group, which contains no rotations. However, in the current context we expect them to be separated. See Fig. 5.16 for clustering results. The desired clusters and relations between clusters can be seen only when the context is fully suppressed.

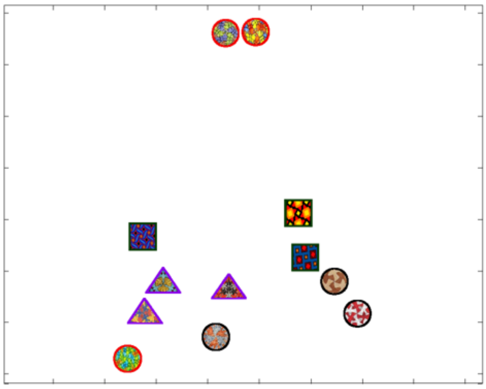

(a) Raw Images

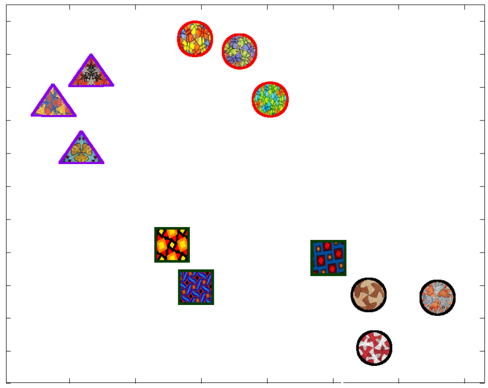

(b) Binary Images

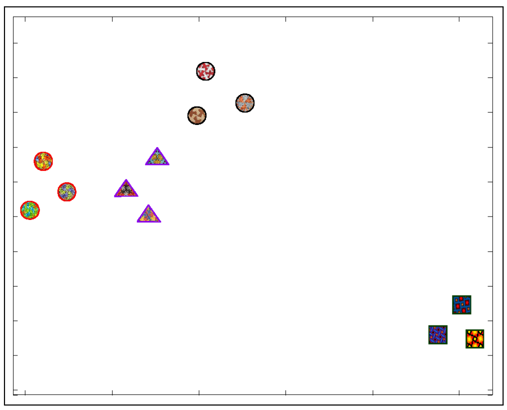

(c) Content Suppressed Images

Figure 5.16: Experiment 33. The correct groups and relations between the groups are observed fo content suppressed images.

In the next experiment, we eliminate the ornaments with four-fold rotations and consider the rest. New ornament collection forms the collection of Experiment 28, which consists of eleven ornaments: three *mariposas* ($p6$), three two-color ornaments of group $p6$, two three-color ornaments of group $p6$ and three ornaments with three-fold rotations and mirror reflections. We expect these four clusters to emerge. Furthermore, we expect the group with three-fold rotations and mirror reflections to be separated from the three $p6$ groups. Constructing a similarity matrix directly from raw images, could not capture style-wise differences between given groups (Fig. 5.17 (a)). Once we suppress the color information, we obtain all clusters correctly (Fig. 5.17 (c)). However, the relations between the groups is not that clear since all groups are scattered on the plane. For fully content suppressed images, all four groups are correctly identified and the relations of groups are well presented. Observe in Fig. 5.17 (c) the closeness of three $p6$ groups against the groups with three-fold rotations and mirror reflections.

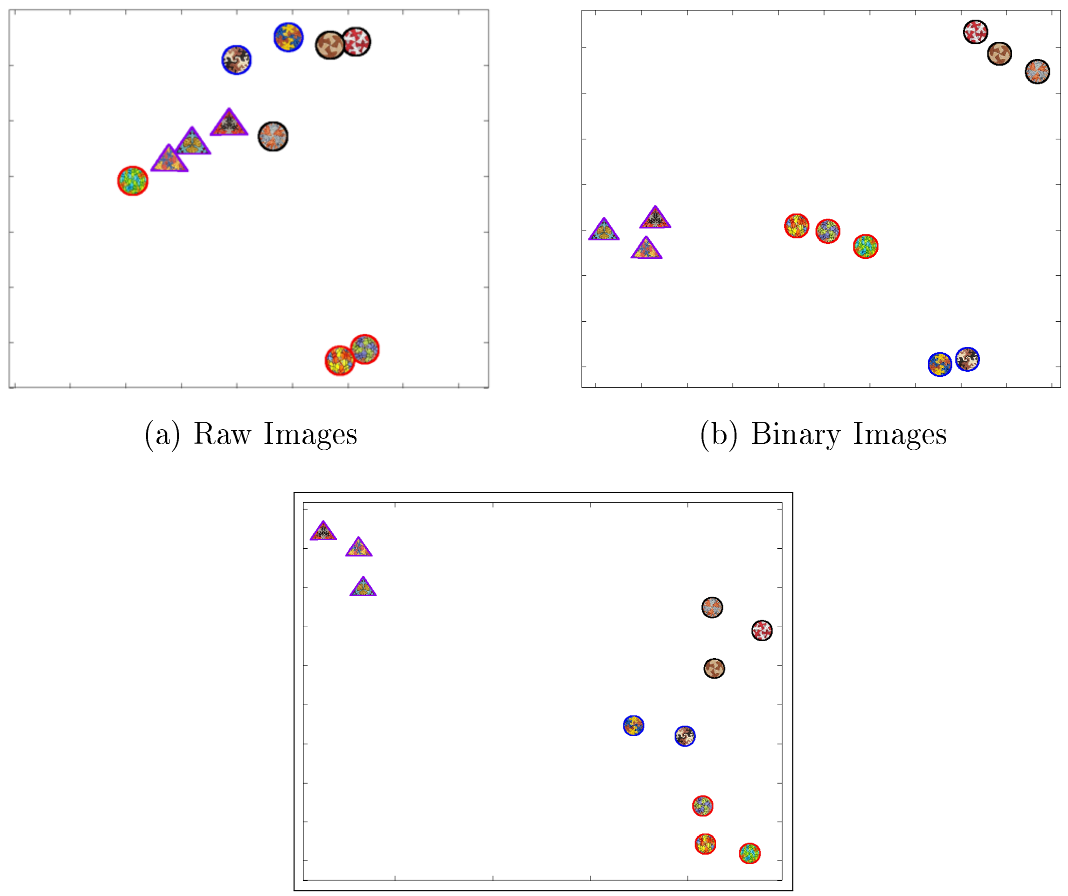

(a) Raw Images

(b) Binary Images

(c) Content Suppressed Images

Figure 5.17: Experiment 28. Rotational groups. Now that there is no four-fold rotational group, the group with three-fold rotations is separated from the $p6$ groups.

In the final experiment, we consider Experiment 31 with a collection of twelve ornaments, seven of which are ornaments with three-fold rotations and mirror reflections, thee of *mariposas* ($p6$) groups and two are three-color ornaments of group $p6$. Again, we expect two major clusters to emerge, separating two $p6$ groups from the group with three-fold rotations and mirror reflections. Clustering of raw images mixes all groups as shown in Fig. 5.18 (a). Clustering result for masks gives only one correct cluster (Fig. 5.18 (b)), that is of *mariposas*. For the fully content suppressed images we observe two major clusters that we hoped to see (Fig. 5.18 (c)).

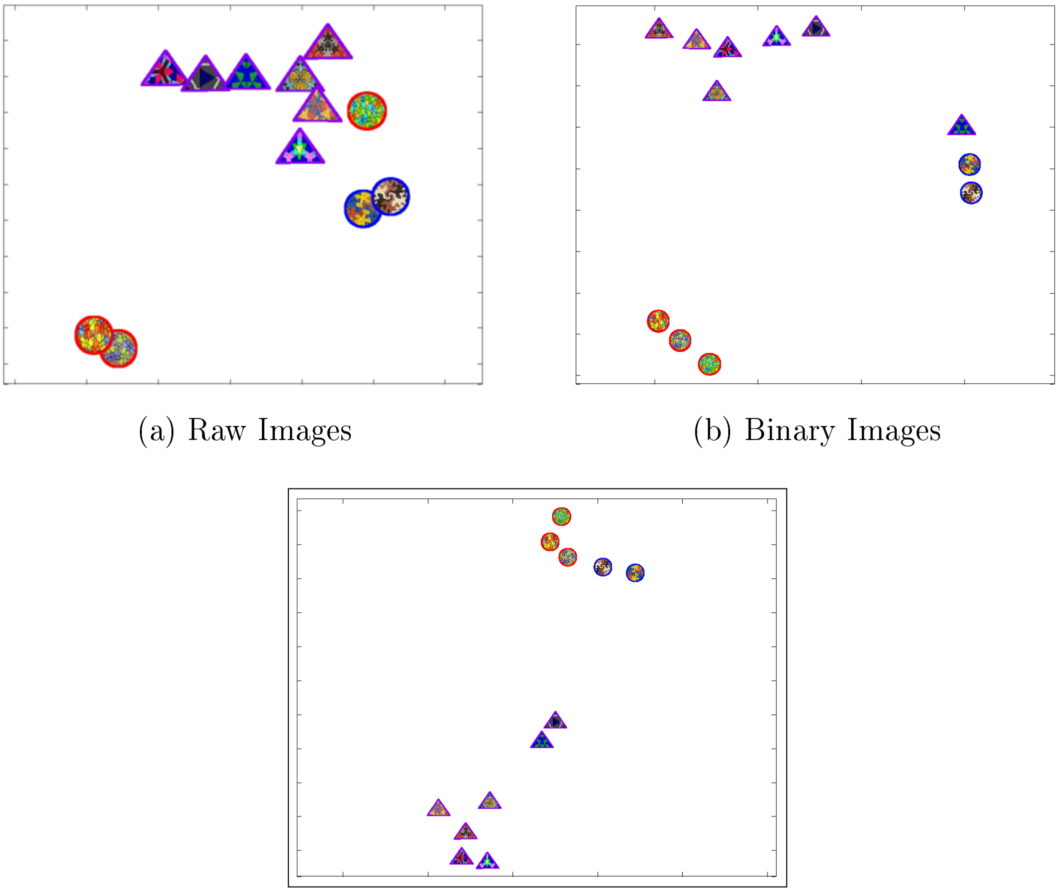

(a) Raw Images

(b) Binary Images

(c) Content Suppressed Images

Figure 5.18: Experiment 31. Rotational groups. As we suppress the content style-wise close groups emerge. Also observe in (c) that the group with three-fold rotations is separated from the $p6$ groups.

5.2.1 Quantification of the Accuracy of Clustering

Just like in the previous chapter, we consider forty-three experiments, where fourteen are two-group experiments and the rest twenty-nine are experiments with more than two groups. We compute within and between group average distances, where the distances are computed from the three-dimensional reduction results. Since tSNE shown to give better clustering results in the previous chapter, for all levels of content suppression we analyze only tSNE results.

Within and between group average distances for fourteen two-group experiments are shown in Fig. 5.19. The first column shows which groups are being clustered in the current experiment, the second, third and fourth columns show computed results obtain from the clustering results of raw, binary and content suppressed images, respectively. The numbers shown in red represent average within group distances and the blue numbers represent average between group distances. The ratio between within and between group average distances are shown in the middle in black. The last row of the table gives the average values computed from all fourteen experiments. Observe that as soon as we start to filter out the content, the separation between groups becomes better. See Fig. 5.20 for comparison of the ratios between within and between group distances for all levels of content suppression. While for raw and binary images the ratio goes up to one and higher, for content suppressed images it is almost for all groups below 0.4.

As we discussed in the previous chapter, the other twenty-nine experiments that contain more than two groups consist of seventeen different groups. Here, again, for each group, we compute the average within and between group distances in one experiment, and then take the average of those values obtained for all experiments in which the given group took part. See the chart in Fig. 5.21 for average within and between group distances for all seventeen groups obtained from clustering results of raw, binary and content suppressed images. As we start to suppress the content, the separation between different groups become more obvious, leading to small within and large between group distances.

However, seeing within and between group distances for each level of content suppression in different charts does not make the differences of the results for different levels obvious. In Fig. 5.22, we combine the results for all three levels of content suppression. Thus, Fig. 5.22 (a) shows average within group distances

Experiments	Raw Images			Binary Images			Content Suppressed		
	Ratio	Within	Between	Ratio	Within	Between	Ratio	Within	Between
	0.02	0.02	1.00	0.05	0.05	0.98	0.02	0.02	0.99
	0.60	0.47	0.79	0.57	0.41	0.72	0.26	0.20	0.75
	0.02	0.02	0.99	0.77	0.41	0.53	0.02	0.02	1.00
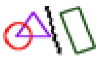	0.31	0.27	0.88	0.58	0.39	0.68	0.29	0.26	0.91
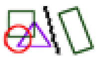	0.17	0.14	0.83	0.49	0.35	0.71	0.25	0.23	0.89
	0.48	0.37	0.77	0.43	0.29	0.67	0.33	0.24	0.74
	0.56	0.37	0.65	0.76	0.47	0.62	0.46	0.30	0.64
	1.07	0.51	0.47	0.26	0.19	0.70	0.20	0.15	0.77
	0.95	0.45	0.47	1.08	0.69	0.64	0.28	0.23	0.80
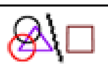	0.27	0.21	0.78	0.32	0.22	0.68	0.13	0.11	0.86
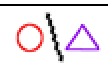	0.54	0.39	0.72	0.34	0.23	0.69	0.36	0.28	0.79
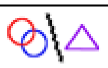	0.77	0.44	0.58	0.29	0.22	0.75	0.37	0.27	0.72
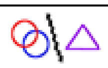	0.65	0.41	0.63	0.45	0.34	0.75	0.26	0.21	0.82
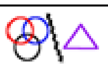	1.18	0.67	0.56	0.53	0.36	0.68	0.31	0.26	0.83
Average	0.54	0.34	0.72	0.49	0.33	0.70	0.25	0.20	0.82

Figure 5.19: Experiments containing only two groups. Numbers shown in red represent within group average distances. Between groups average distances shown in blue. The ratio between within and between group average distances shown in balck. Last row shows average values for all values of the experiments.

for all three levels of content suppression. Observe that from the clustering results of the raw images we obtain high within group distances. Furthermore, in Fig. 5.22 (b), we see that the raw images have small between group distances for almost all groups. Recall that our goal is to have small within groups distances and large between group distances. As can be seen from the charts, we achieve this goal only when we cluster fully content suppressed images.

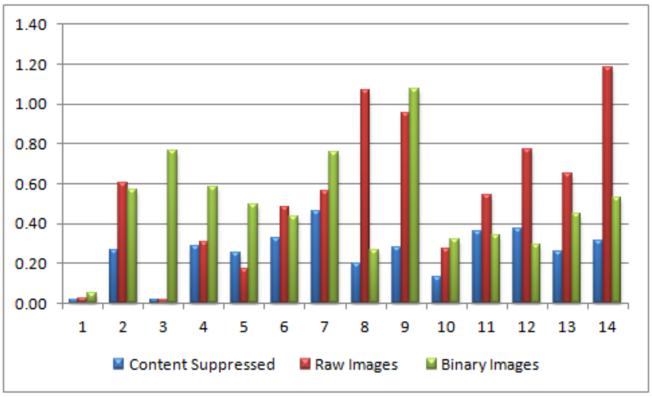

Figure 5.20: Experiments containing only two groups. The ratios between within and between group average distances are plotted. For content suppressed images the ratio for all experiments is below 0.4, indicating a good separation of groups.

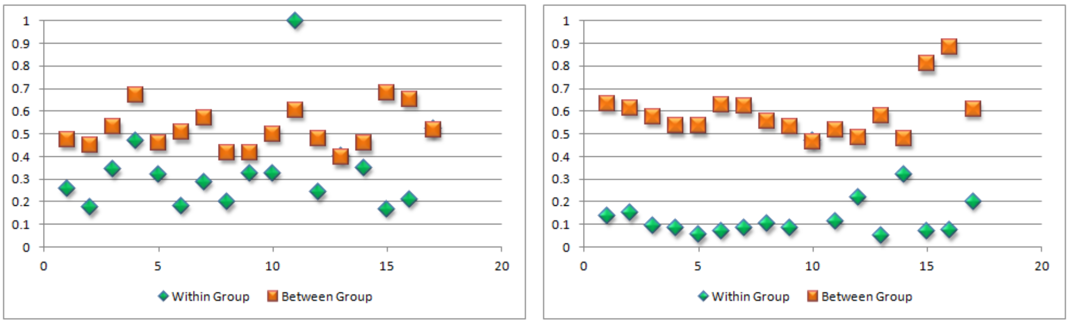

(a) Raw Images

(b) Binary Images

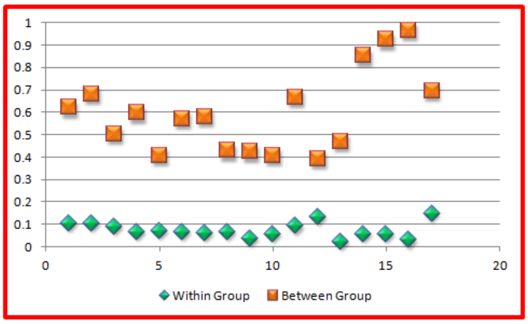

(c) Content Suppressed Images

Figure 5.21: Within vs. between group avgerage distances for experiments with more than two groups. As we suppress the content of ornaments the average within group distances become smaller and average between group distances become larger, giving better separation of clusters.

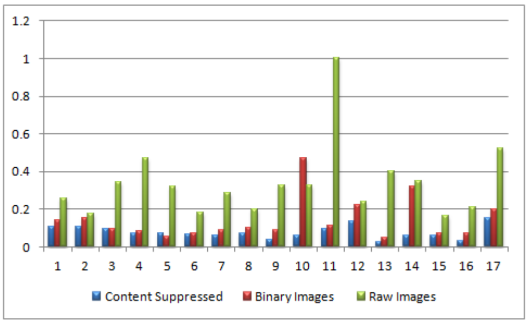

(a) Within Group Distances

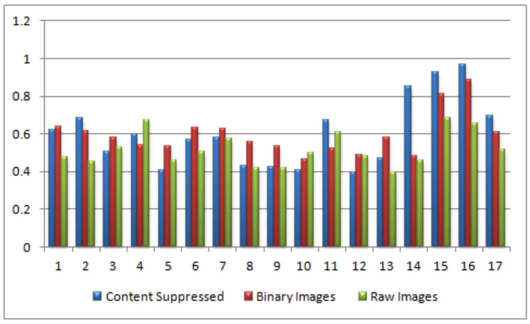

(b) Between Group Distances

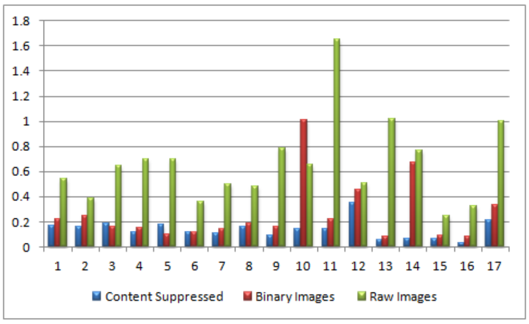

(c) Within Group/Between Group

Figure 5.22: Within and between group average distances and the ratio of these two for experiments with more than two groups. Observe that for content suppressed images in all experiments within group average distances and the ratio between two values are small, while between group average distances are large.

CHAPTER 6

ISOLATED TILES

In Chapter 3, we discussed about content suppression of ornaments. As a result of content suppression the ornaments are converted to their transform domain where individual symmetries that the ornament exhibit is represented by abstract structures. Thus, for instance, if an ornament exhibit three-fold rotations then in their transform domain we observed three-leaved roses or triangles. Using those content suppressed images, we performed clustering experiments in Chapter 4, each time considering a group of ornaments. In Chapter 5, we analyzed the clustering results of images at different levels of content suppression. Up to now, we reported the analysis based on the group of ornaments. In this manner, we were able to see the relations between different symmetry groups and see how clustering results change according to the context. The important aspect of analysis of group of ornaments is that we were able to show the continuous nature of symmetry, which concerns about how similar are the symmetries of two ornaments rather than what symmetry group they belong.

In this chapter, we are going to analyze individual ornaments. For each ornament, we find its nodes and their connections. Clustering the connections that an ornament exhibit reveals the symmetries present in an ornament. Knowing the symmetries enables to find the unit cell for an ornament, which, on the other hand, enables to define the symmetry group of an ornament. We discuss about the detection of ornament nodes and its connections in the following section. We then present the analysis results.

6.1 Extracting Information from Content Suppressed Images

In the previous chapters, we studied the ornaments in a group, observing the relations between different groups and the clustering of ornaments depending on a context. In this chapter, we study individual ornaments. The analysis of ornaments consists of two stages. First, we detect the centers of individual nodes that are repeating throughout the ornament. Afterwards, using those points we obtain different connections. Analysis results show that these connections enable to detect different symmetries present in an ornament. The details of the process are discussed in the following section.

6.1.1 Method

In order to detect node centers we use the content suppressed images for ornaments. Recall that, when the linear transform is applied upon the foreground regions of the mask it reveals the node centers, and reveals the relations between the node centers when applied on entire tile domain. Fig. 6.1 shows a three-color ornament of group $p6$ and the ω fields for its six masks computed both for foreground objects only (Fig. 6.1(a)) and on entire tile domain(Fig. 6.1(b)). Each mask contains the shapes of one color and in its content suppressed form; each mask enhances node centers of one color. Using this information, in the first stage, the node centers for each mask are obtained. First, we look at the fields computed only on foreground objects. Given a field for a mask, we extract positive regions (pixel values that are bigger than zero). If the area of every region is smaller than the twice of the average area, then we extract the centers of the positive regions and mark them as node centers. If, on the other hand, for any region the area is bigger or equal to twice the average area (if positive regions of several nodes overlap), then we look at the fields that are computed over entire tile domain. Again, we extract positive regions and if the regions are all of the same area then mark their centers as node centers. If still different node regions overlap then we divide the field into watershed regions. Each watershed region contains one maximum value, which is in fact the center of some node. Of course, some unnecessary nodes might occur due to noise, especially at the parts close to edges. To eliminate them we introduce some threshold T so that only the nodes with maximal values above T are selected. Some necessary nodes might be below T and, thus, not be included into the set of maximal points. To avoid this, we calculate the average distance between obtained maximal points and then include those points among the discarded points that lie within this distance to any of the selected maximal point. The final set of maximal points defines the node centers for a mask of an ornament. The node centers obtained for six masks in Fig. 6.1 are illustrated in Fig. 6.2.

Ideally, each mask must contain one kind of shape of one color that repeats throughout the mask with equal distances. This occurs when the color permutation is regular. Mask inverses for the given ornament contain nodes with equal distances representing similar colors (Fig. 6.2 second row). However, for non-inverse masks we observe irregular color permutations (Fig. 6.2 top row). Though each non-inverse mask of an ornament contains shapes of one color, the shapes differ. Observe that in the ornament of Fig. 6.2 there are leaves of different size but one color. Also, observe that the small orange (green, violet) leaves form six-fold rotations. The larger orange (green, violet) leaves form three-fold rotations, which are in fact six-fold rotations where orange (green, violet) leaves interchange with green (orange, violet) or violet (orange, green) leaves. Our aim is to further separate the masks so that each mask contains the nodes of one kind only. In order to do so, we pass through an intermediate stage, the second stage. In the second stage, we divide the ω field (computed over entire tile domain) of the mask into regions, so that each region will represent a particular node of the mask. Note that the node centers detected in the first stage and the regions to be detected in the second stage are not the same. A node center represents central point of a shape, while a region represents central body of the shape used in the ornament (after suppressing the peripheral regions we are left only with central parts of the shapes). Recall that the ω field for an image contains maximal values at shape centers and minimal values at shape boundaries. Since the ornaments contain multiple copies of a shape that share boundaries with each other, we cannot directly extract the regions from ω fields. However, we know that in the ω field the points where two shapes meet have

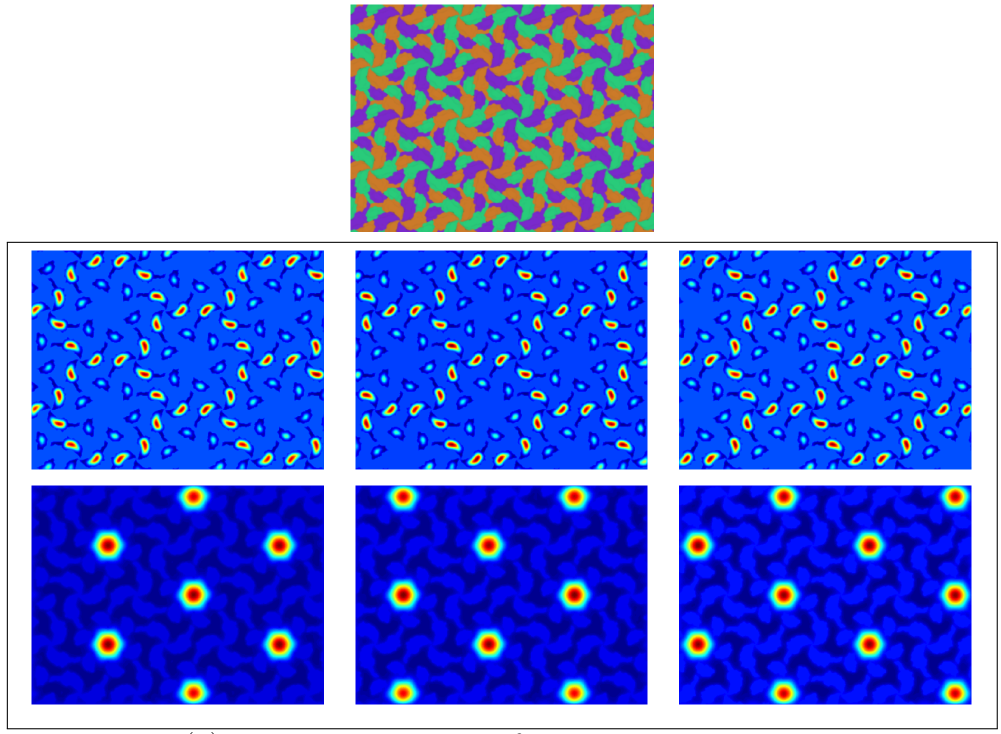

(a) Fields computed on foregroud objects only.

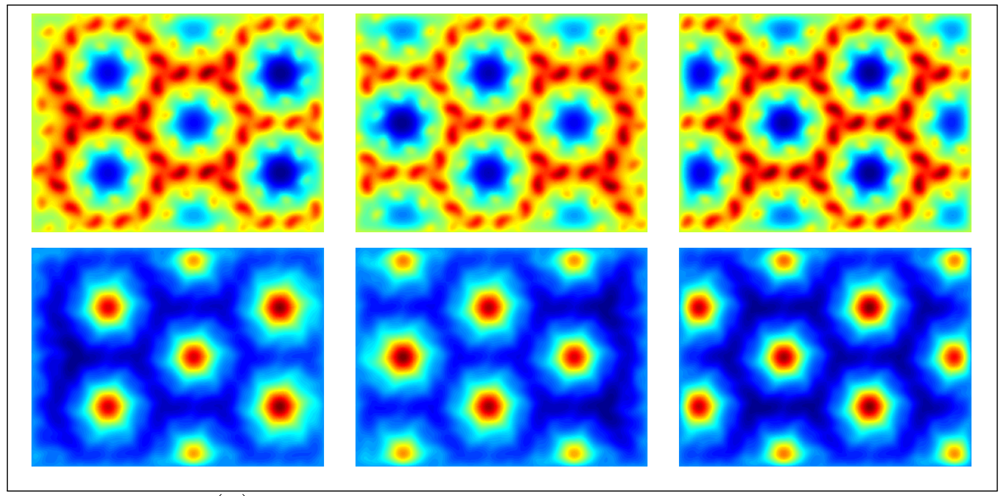

(b) Fields computed on entire tile domain.

Figure 6.1: Three-color ornament of group $p6$ and ω fields of its six masks. Bottom rows contain mask inverses of the masks on the top row.

small values. Using this information, we iteratively find the minimal value bigger than zero in the ω field and set that point to zero. The iteration proceeds until each region contains only one node center. The regions obtained for the six mask of Fig. 6.1 are illustrated in Fig. 6.3. Once the regions are extracted, we proceed with the third stage. For each node center of one mask, we check

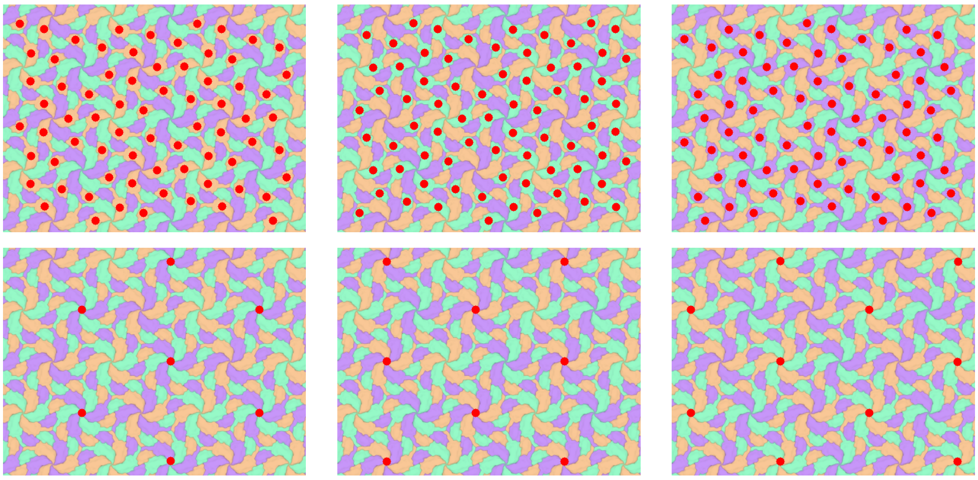

Figure 6.2: Node centers for six masks of the ornament shown in red.

if it attaches or does not attach some region of other masks. In this manner, for each node center of a mask we obtain a vector the size of which is one less the number of masks for an ornament. The entry of a vector is 1 if the node center attaches the region of the mask and 0 otherwise. The node centers that are arranged in the same manner obtain similar vectors. See an example of how node centers for first mask of given ornament behave on other mask regions in Fig. 6.4. We obtain three different point sets for this mask: those having vector [00000], those with vector [00100] and those with [00001]. Fig. 6.5 shows the separation of node centers for three non-inverse masks of Fig. 6.2. For example, the first mask shown in Fig. 6.5 (a) contains the shapes colored in orange. Using further separation we obtain three different masks where the first one contains the small orange leaves arranged in six-fold rotations, the next one contains the larger leaves where the orange leaves interchange with green leaves, and the last one contains the interchange of orange leaves with violet leaves. This introduces six new masks for the ornament. Thus, counting the new mask give overall twelve masks for the ornament. Note that applying this stage to mask inverses does not introduce new masks since the color permutations for mask inverses are regular. This means that all node centers of one mask behave similarly on the regions of other masks and have the same vector.

At the fourth stage, we extract the connections between the node centers of a mask. The first step of this stage iteratively extracts various connections. In

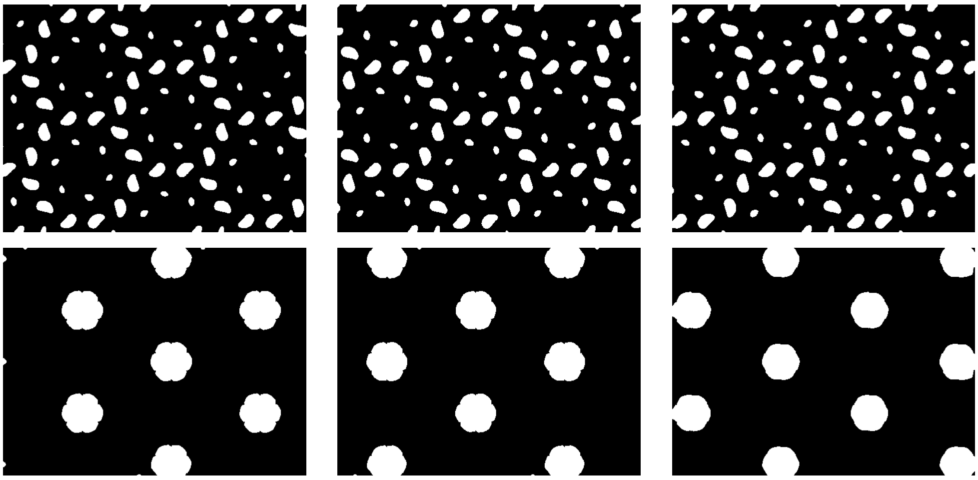

Figure 6.3: Extracted regions for the six masks of the ornament.

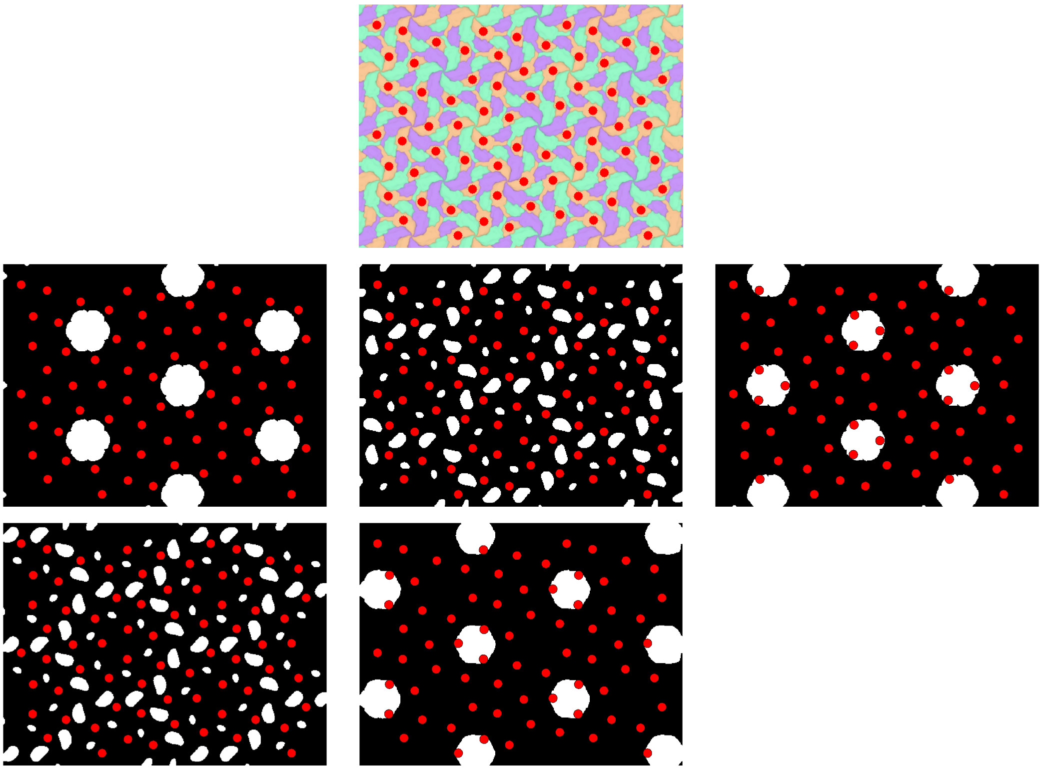

Figure 6.4: Behavior of the node centers for the first mask of the ornament on other mask regions.

the first iteration, we find the minimal distance between two points in a mask and then extract all connections with similar distances. In the next iteration, we discard the connections of the previous iteration and find new minimal distance between points to extract new connections, *etc.*. Of course, when we find the

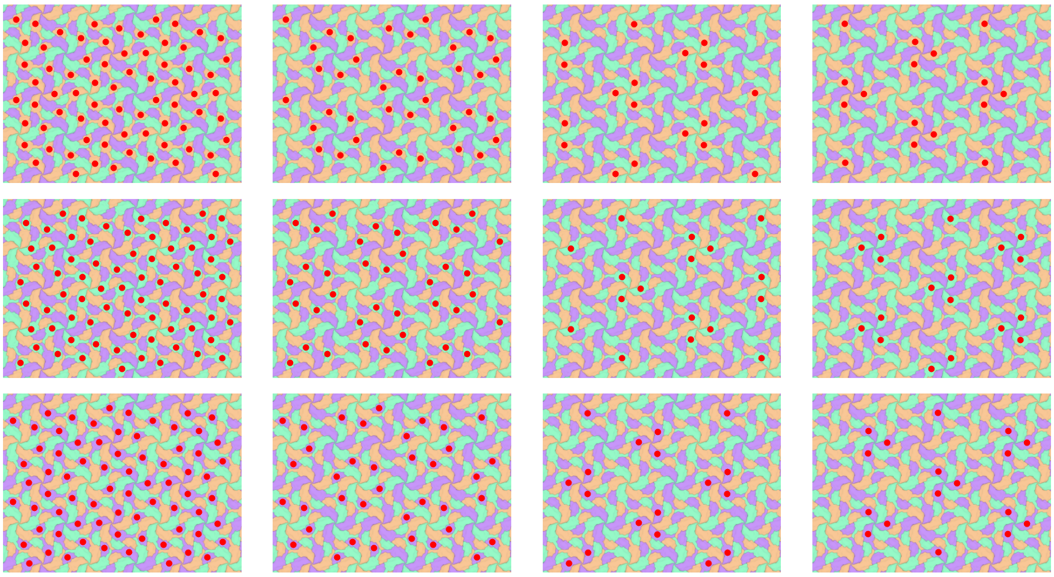

(a) (b) (c) (d)

Figure 6.5: Further separation of non-inverse masks into three masks.

minimal distance the other similar connections might not be exactly equal to this distance. That is why we introduce a tolerance of 2 or 3 pixels. After n iterations we obtain connections of various sizes. Note that this step is done solely to extract different connections between points. In the second step we group these connections into m groups. Initially each connection forms a group itself. We then iteratively join different groups based on sizes and orientations. Orientation is optional and may not be considered. The tolerance for differences in distances among the connections of the same group is set to 1 pixel initially. In each iteration, it joins the closest connections in terms of size and orientation. If no connections join in one iteration, then the tolerance is increased by one. The iteration stops when the number of groups is m. Connections that belong to the same group show similar symmetries of an ornament. As an example see Fig. 6.6 for the connections obtained for twelve masks of the ornament. For each mask, we have shown only the first connection groups. First, fifth and ninth masks in Fig. 6.6 are the mask inverses. Observe that their connections show the lattice of an ornament. Thus, a unit cell of an ornament consists of two equilateral triangles, which join to form a rhombus. The ornament has hexagonal lattice. In contrast to mask inverses, non-inverse masks show the symmetries of ornament. The second, eighth and tenth masks contain six-point connections that form hexagons. In this connection, the points are related by six-fold rotation. The centers of these hexagons fall on the centers of six-fold rotations. The rest of the masks contain three-point connections, where points are related by three-fold rotation. The centers of triangles fall on the centers of three-fold rotations.

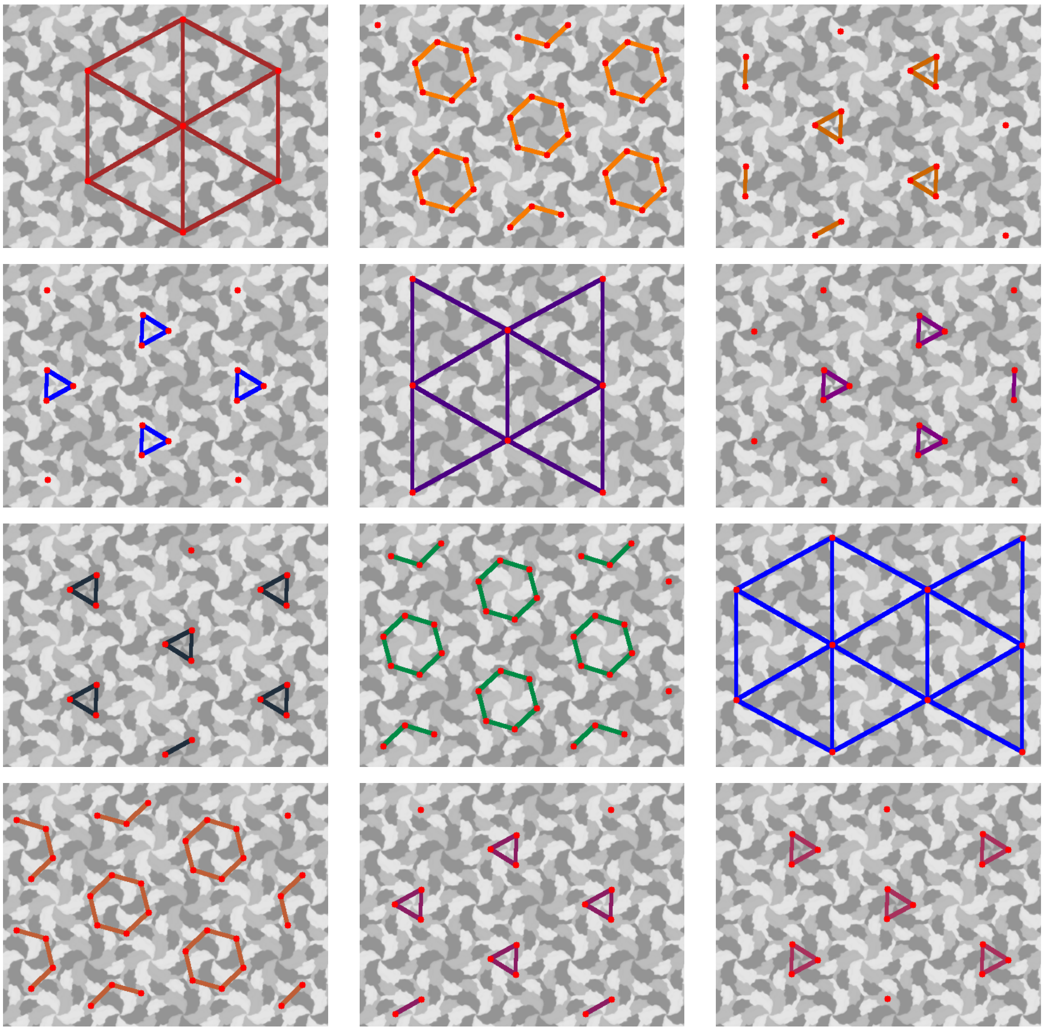

Figure 6.6: Connections of twelve masks of the ornament.

The hexagon connections shown in Fig. 6.6 indicate that the ornament exhibit six-fold rotations. However, this is not true, and we are able to infer it from the triangular connections. The center of each hexagon is also the center of two triangles, which are connections of different masks. Since each mask contains information on different colors, we know that these two triangles represent that there are two three-fold rotations of different color. This become obvious when we put the connections of non-inverse masks on top of each other as shown in Fig. 6.7. In Fig. 6.7 (a) the masks with hexagonal connections are combined. Note that the hexagons of different color represent six-fold rotations of different kind, since they come from different masks. In Fig. 6.7 (b) we add the masks with triangular connections. Observe that each hexagon contains two triangles of different colors. Also, observe that hexagons of one color contain similar two different triangles. This shows that the ornament does not exhibit six-fold rotations. Then we do not consider the masks that have hexagonal structures and proceed with other six masks with triangular structures. If we take any of these masks and increase the connection groups for it, we obtain all the symmetries of an ornament. In Fig. 6.8 we show three connection groups for a third mask of Fig. 6.6. Observe three different triangles indicating three different three-fold rotations. Fig. 6.9 (a) shows all rotation centers inferred from one mask connections. Here, triangles represent the centers of three-fold rotations. Since the lattice points of an ornament are the points with highest order of rotation we connect three-fold rotation centers of same color to obtain the unit cell. Fig. 6.9 (b) separates the unit cell and shows all connections that are incident with unit cell. The ornament can belong to three possible symmetry groups with the highest order of rotation of three. These are $p3$, $p3m1$ and $p31m$ groups. Cell structures for these three groups are shown in Fig. 6.10. The $p31m$ group requires only two different three-fold rotation centers, while we have three different three-fold rotation centers. Then this group can be discarded. The $p3m1$ group implies a reflectional symmetry along the major diagonal of unit cell. However, from Fig. 6.11, one can see that there is no reflectional symmetry along the major diagonal. If there were reflectional symmetry, then the diagonal axis would pass through exactly one point of the green triangle, which is not the case. Then we discard this group, and conclude that the ornament belongs to $p3$ group.

The analyses for the ornament shown above are done by considering the colors. This means, regardless the similarity of two shapes, they considered as different shapes if they have different colors. If, on the contrary, the symmetries of underlying ornament, by ignoring the colors, are needed, we combine the node

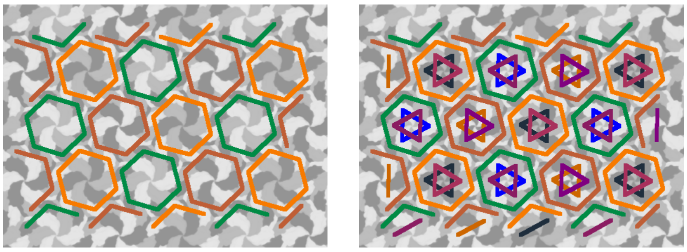

(a) (b)

Figure 6.7: Combining connections of all masks except for mask inverses reveal that there are no six-fold rotations in the ornament.

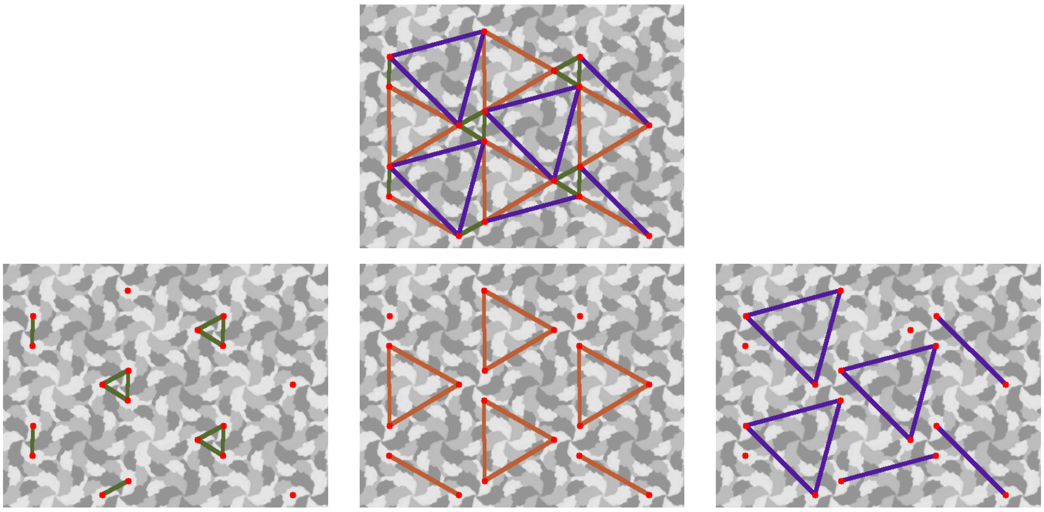

Figure 6.8: Increasing the connection groups of one of the masks of an ornament.

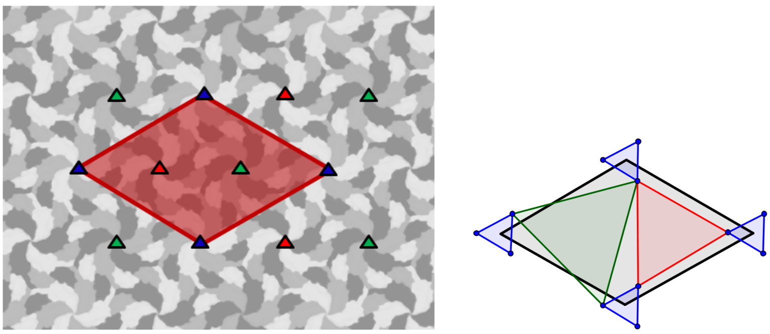

(a) (b)

Figure 6.9: (a) Symmetries and unit cell of an ornament. (b) Connections that are incident with unit cell.

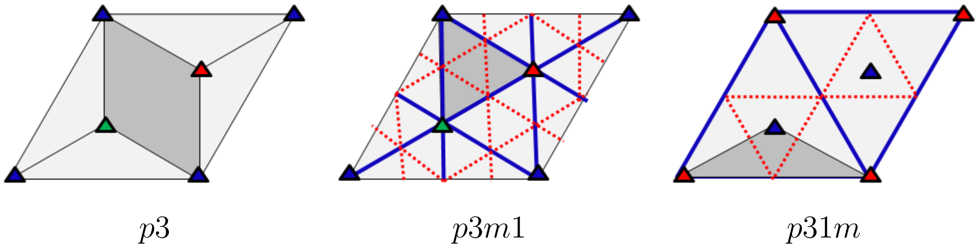

Figure 6.10: Three possible symmetry groups for an ornament. The darker regions represent fundamental domain.

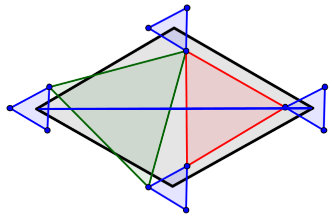

Figure 6.11: The $p3m1$ group implies a reflectional symmetry along the major diagonal of unit cell.

centers of different masks and re-compute the connections going back to the fourth stage. The mask that are combined should be non-inverses, since, as we mentioned before, the mask inverses do not contain the information on ornament symmetries. In addition, the combined masks must contain the centers of similar nodes (*i.e.* of the same shape, colors are ignored). Thus, for the current ornament we can combine the second, eighth and the tenth masks, or the other six non-inverse masks of Fig. 6.5. We combined the node centers of latter six masks. Fig. 6.12 shows six connection groups obtained using the stage four of our method. The first connection group contains six-point connections that form hexagons. They indicate six-fold rotations. The second connection group shows two-point connections indicating two-fold rotations. Two similar three-fold rotations are inferred from the third connection group. The centers of this two three-fold rotation centers coincide with the center of six-fold rotation. Since they are similar, they join to form a six-fold rotation. The fourth connection group represents three similar two-fold rotations the centers of which coincide with the center of six-fold rotation. Again, since they are similar, they join to form a six-fold rotation. Last two connection groups contain three-fold rotations that are different. Collecting all the symmetries inferred from the connections as shown in Fig. 6.13 (a), we obtain a unit cell, and the connections that are incident with unit cell (Fig. 6.13 (b)). There are two possible symmetry groups involving six-fold rotations: $p6$ and $p6m$ (Fig. 6.14). The $p6m$ groups implies a reflectional symmetry along the major diagonal of unit cell. However, from Fig. 6.15 one can see that none of the points of the red triangles lie on major diagonal of the unit cell, which would be required for reflectional symmetry. We discard the $p6m$ group from possibilities. Thus, we conclude that when the colors are ignored, the ornament belongs to $p6$ group.

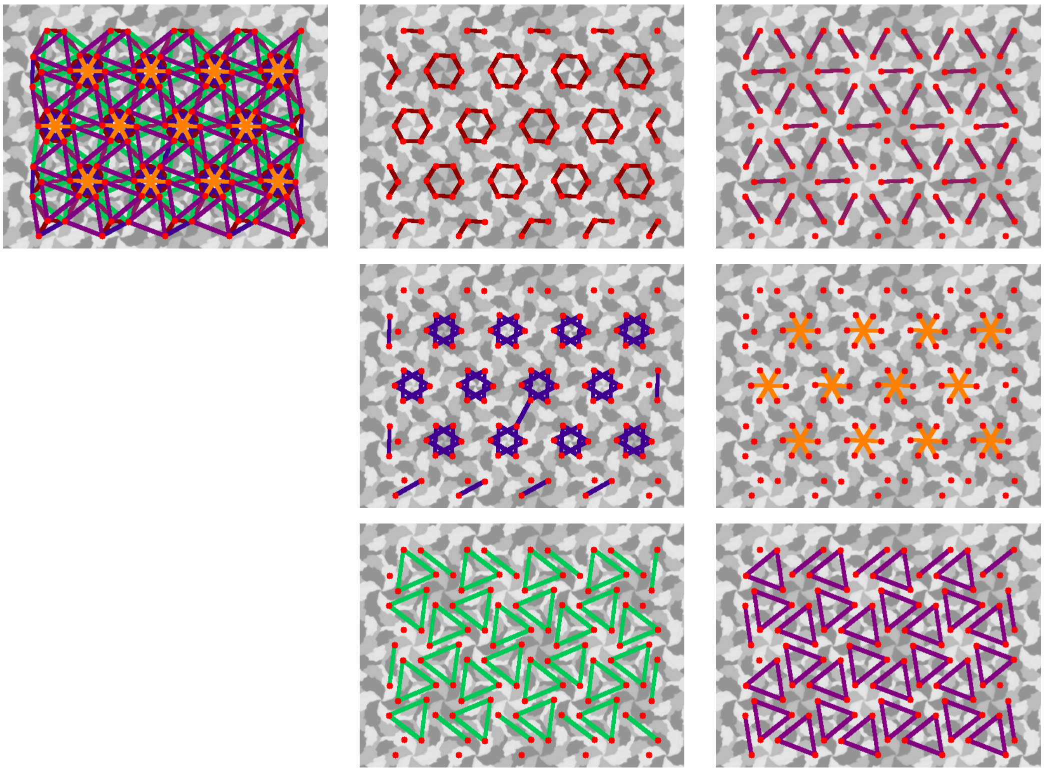

Figure 6.12: Six connection groups obtained for the ornament when we ignore the colors.

The overview of the whole process performed in this chapter is illustrated in Fig. 6.16. Given an ornament, its masks and ω fields for the masks, we detect the node centers for each mask. Using these node centers, we extract various connections and then group similar connections. The connections of one group show one kind of symmetry that the ornament exhibit. We then define the

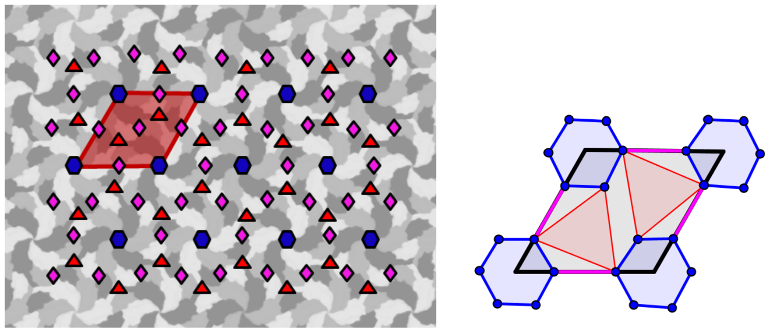

(a) (b)

Figure 6.13: (a) Symmetries and unit cell of an ornament. (b) Connections that are incident with unit cell.

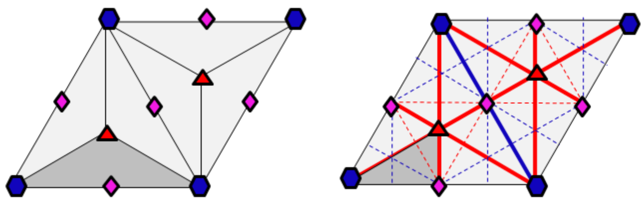

$p6$ $p6m$

Figure 6.14: Two possible symmetry groups for an ornament when colors are ignored.

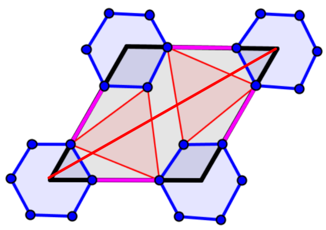

Figure 6.15: The $p6m$ group implies a reflectional symmetry along the major diagonal of unit cell.

symmetries that the ornament exhibit, define its lattice (unit cell) and symmetry group based on the groups of connections obtained for an ornament. Note that the connections for particular mask are searched in interactive process. We are searching for specific symmetries in an ornament. Thus, for example, if we see six-fold rotation from one connection, it is natural to continue searching for two-fold and three fold-rotations, since six-fold rotation also implies these symmetries. We stop searching when we obtain enough information to define the symmetry group of an ornament and when new connections introduce no new information.

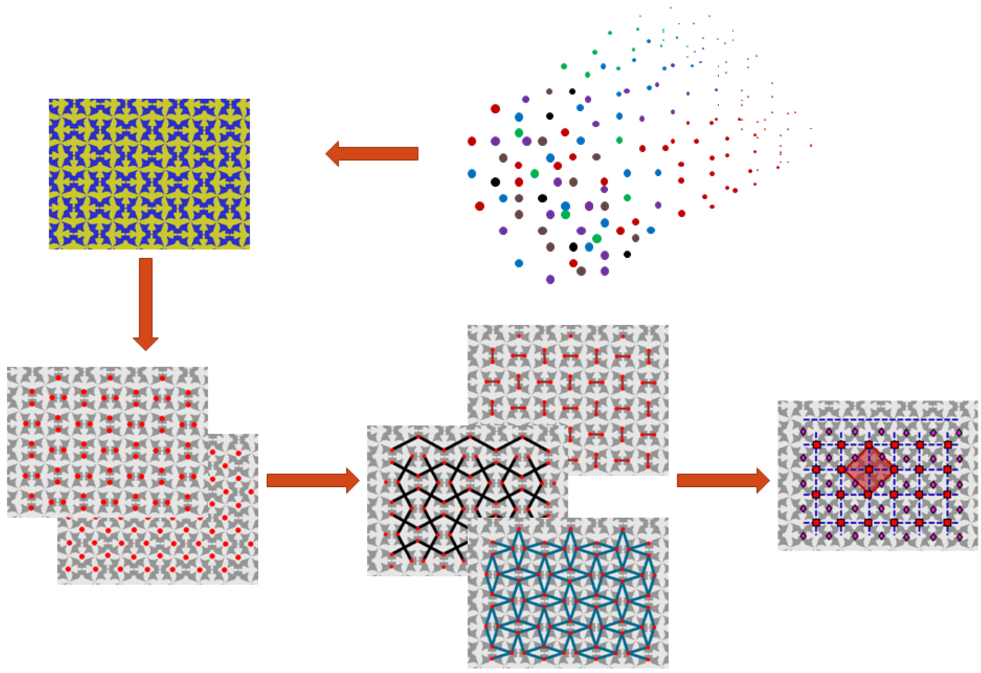

Figure 6.16: Overview of the process.

6.1.2 Dataset

The set of ornaments used in this chapter are given in Fig. 6.17. Overall ten self-generated ornaments are considered, which are created using iOrnament application. Five ornaments out of ten are similar to Escher's ornaments that we recreated. In contrast to the dataset used in previous chapters, this one contains ornaments of larger size with more repetitions. The first row of the dataset consists of two ornaments of pgg group. The next two ornaments are of group $p4$. The third row contains two two-color ornaments of $p4g$ group with no color symmetry. The forth row contains ornaments with six-fold rotations. First three of them have color symmetry. The first one is a two-color ornaments of $p6$ group. The second one is three-color ornament of $p6$ group, while the third one is four-color ornament of $p6$ group. The last ornament is two-color ornament of

$p6m$ group with no color symmetry.

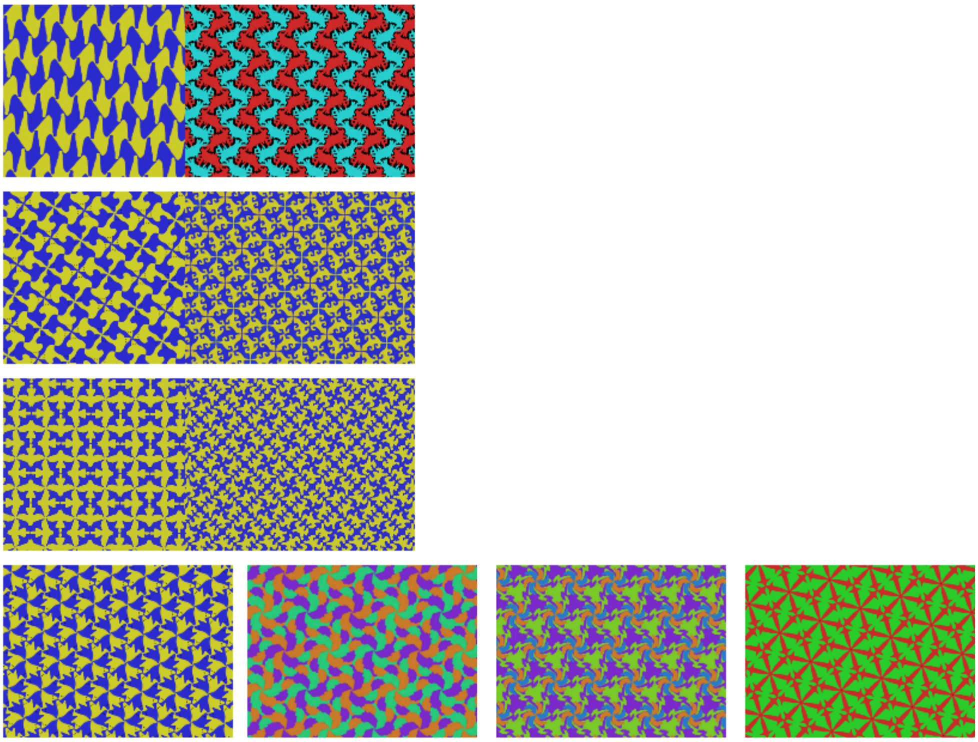

Figure 6.17: Dataset. Overall, ten ornaments are considered. All ornaments are self-generated using iOrnament application. The first row contains two ornaments of group pgg. The second row contains two ornaments of $p4$ group. Two ornaments of the third row are of group $p4g$. Last row contains ornaments with six-fold rotations. First ornament is two-color ornament of $p6$ group. The second ornament is three-color ornament of $p6$ group, while the third one is four-color ornament of $p6$ group. The last ornament is a two-color ornament of $p6m$ group with no color symmetry.

6.2 Results

We analyze the symmetries of nine ornaments in this section. The connections are shown on gray images for clear visualization purposes. For each we show the symmetries inferred from the extracted connections. We put signs on the ornament indicating different symmetries. Table 6.1 defines what signs are used to show particular symmetry on the ornament. Note that the colors of signs change, while the shapes remain fixed.

Table6.1: Signs used to define the symmetry elemets.

◇	A center of rotation of order two
△	A center of rotation of order three
□	A center of rotation of order four
⬡	A center of rotation of order six
——	An axis of reflection
------	An axis of glide reflection

We begin our analyses with a two-color ornament shown in Fig. 6.18, which is of *pgg* group when colors are ignored. The ornament contains two masks each containing the information about one color. Detected node centers for each of the masks of this particular ornament are shown in Fig. 6.19.

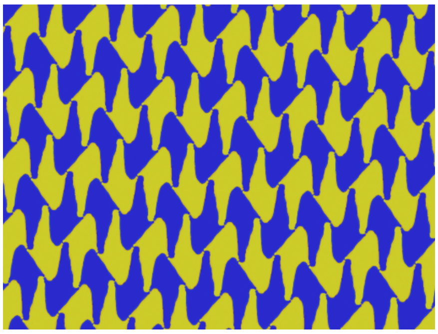

Figure 6.18: A two-color ornament of *pgg* group.

We extract two connection groups for each of the masks of an ornament as shown in Fig. 6.20. Observe that each point of one connection group is connected to two different points. Each point is a glide reflection of the point it is connected to, hence the zigzag structures. If we take the centers of lines connecting two points and connect all the centers of one zigzag structure, we obtain glide reflection axes. By considering two connection groups of the first mask, we infer that

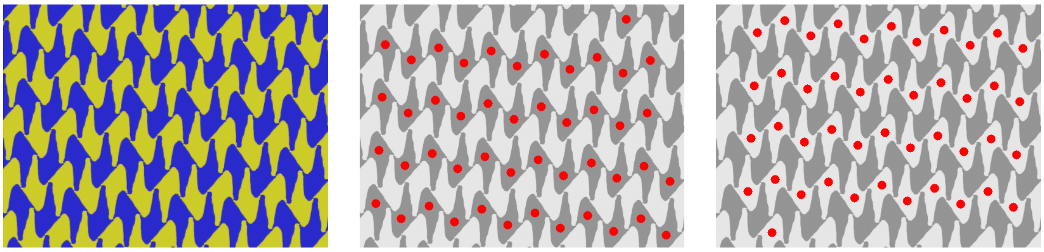

Figure 6.19: Detected node centers for two masks of an ornament in Fig. 6.18.

there are two different glide reflection axes in the ornament and they are parallel to each other. No other symmetries are observed. Fig. 6.21 (a) shows the glide reflection axes on the image. The red rectangle is formed from the closest translations of a point in two directions. Recall that by connecting the translations of a point in two directions we obtain a lattice of an ornament. Thus, the red rectangle in the figure, in fact, represents the unit cell of an ornament. The only possible symmetry group where only two different glide reflections parallel to each other exist is *pg* symmetry group. The cell structure for *pg* group is shown in Fig. 6.21 (b). From this, we conclude that an ornament is of *pg* group.

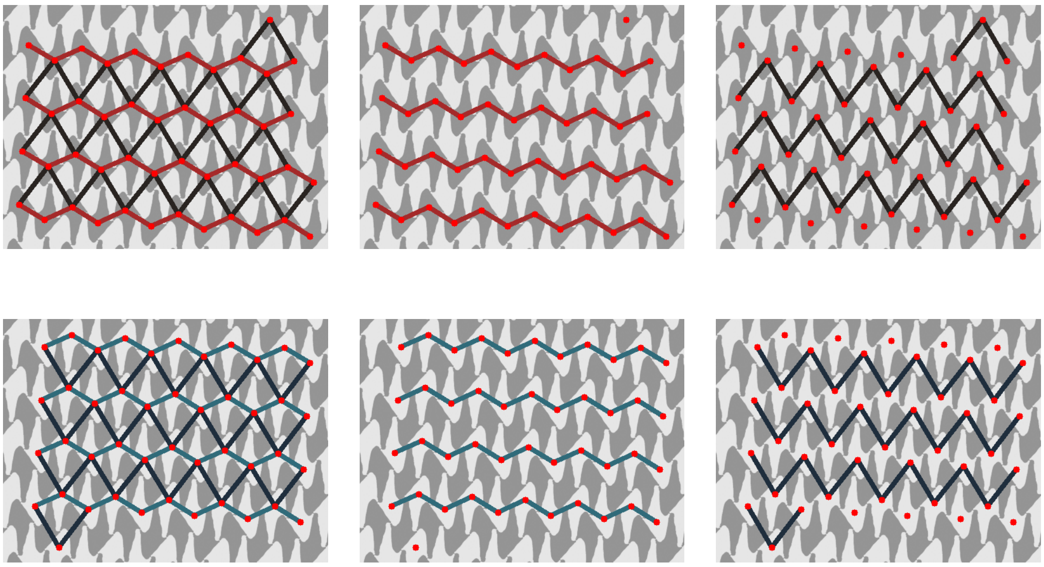

Figure 6.20: Extracted connection groups for two masks of an ornament in Fig. 6.18. First column shows all connections extracted for a mask, and the second and third columns show each connection group of a mask separately.

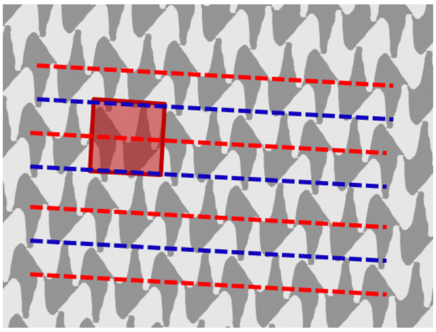

(a)

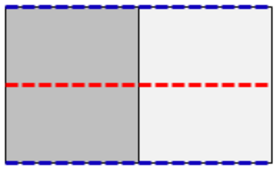

(b)

Figure 6.21: (a) Symmetries of an ornament inferred from the mask connection groups. Connecting similarly arranged points give a rectangular lattice with parallel glide reflection axes. This type of unit cell indicates that the ornament belongs to *pg* group. (b) Cell structure for *pg* group. The darker region indicates the fundamental domain.

By considering the node centers detected for each mask for connection extraction separately, we take into account the color symmetry of the ornament. Recall that introducing colors reduces the symmetries of an ornament. When we ignore the colors, the ornament in Fig. 6.18 is of group *pgg*. In order to see the symmetries of an ornament when the colors are ignored we combine the node centers obtained for two masks and then compute the connections. Four connection groups for an ornament are extracted when the colors are ignored as shown in Fig. 6.22. In the connections when the colors are taken into account for this particular ornament we observed only horizontal glide reflection axes. Now that the colors are ignored, we observe more symmetries. The first and the fourth connection groups contain connections where two points are engaged in two-fold rotation. Each connection group contains the connections of different two-fold rotations. In both cases, one point of one color is a two-fold rotational symmetry of the point it is connected to, which is of other color. The third connection group contains the vertical glide reflections, where a point of one color is connected to the point of other color and they are glide reflections of each other. In fact, when the colors are taken into account, we extracted only the second connection group of Fig. 6.22. All other connections could not be extracted because a particular symmetry of a point goes to the other color. Fig. 6.23 (a) shows all the symmetries inferred from the connections of an ornament when the colors are ignored. We already mentioned that in the detection of ornament lattice the points with maximal order of rotations are chosen as grid nodes. Since the maximal order of rotation that we observe for an ornament is two, we connect translations of any two-fold rotation centers to obtain the unit cell shown in red. The only symmetry groups which contains two different two-fold rotations and perpendicular glide reflections is *pgg* group. Observe that the structure of unit cell for the ornament is similar to the cell structure of *pgg* group shown in Fig. 6.23 (b). Thus, when the colors are ignored, the ornament belongs to *pgg* group.

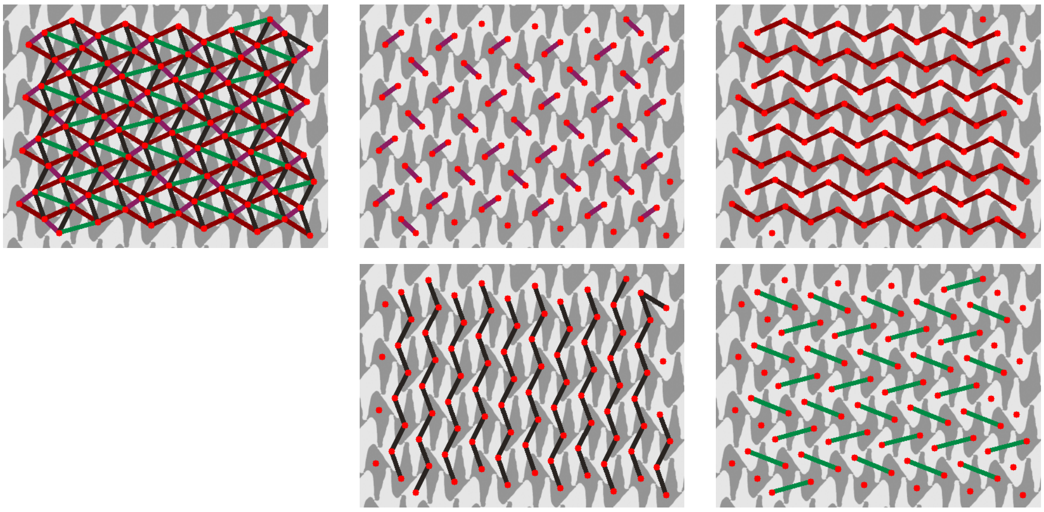

Figure 6.22: Extracted connection groups for an ornament in Fig. 6.18 when the node centers of two masks are combined. First column shows all connections extracted for an ornament, and the second and third columns show each connection group of an ornament separately.

The next ornament to be analyzed is shown in Fig. 6.24, which is also of *pgg* group. Since it is a two-color ornament it contains two masks. The node centers detected for each mask are illustrated in Fig. 6.25.

The connections (See Fig. 6.26) obtained for each mask show similar zigzag structures that we observed on the analysis of the previous *pgg* ornament. However, for current ornament the glide reflections axes are vertical. Just as in the previous ornament, we observe two different glide reflection axes that are paral-

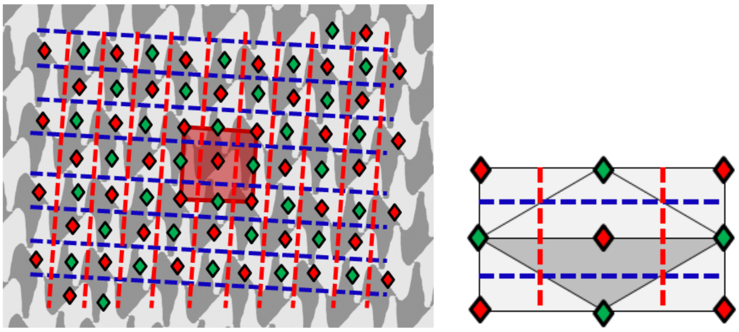

(a) (b)

Figure 6.23: (a) Symmetries of an ornament inferred from the connections obtained from combined node centers. Connecting two-fold rotation centers of similar type introduces a unit cell of an ornament. This type of unit cell indicates that the ornament belongs to *pgg* group. (b) Cell structure for *pgg* group. The darker region indicates the fundamental domain.

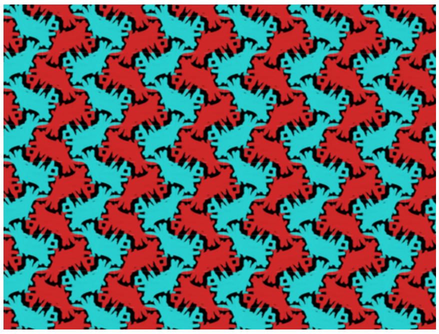

Figure 6.24: A two-color ornament of *pgg* group.

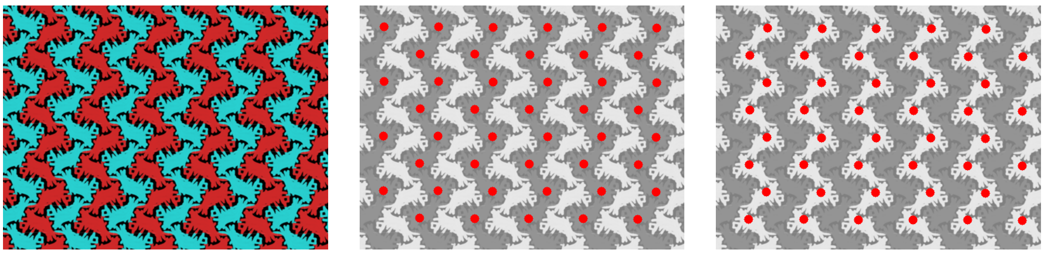

Figure 6.25: Detected node centers for two masks of an ornament in Fig. 6.24.

lel to each other. All symmetries and the unit cell for the ornament are shown in Fig. 6.27 (a). The structure of unit cell is similar to the cell structure of *pg* group, inferring that this ornament also belongs to *pg* group when the colors are taken into account.

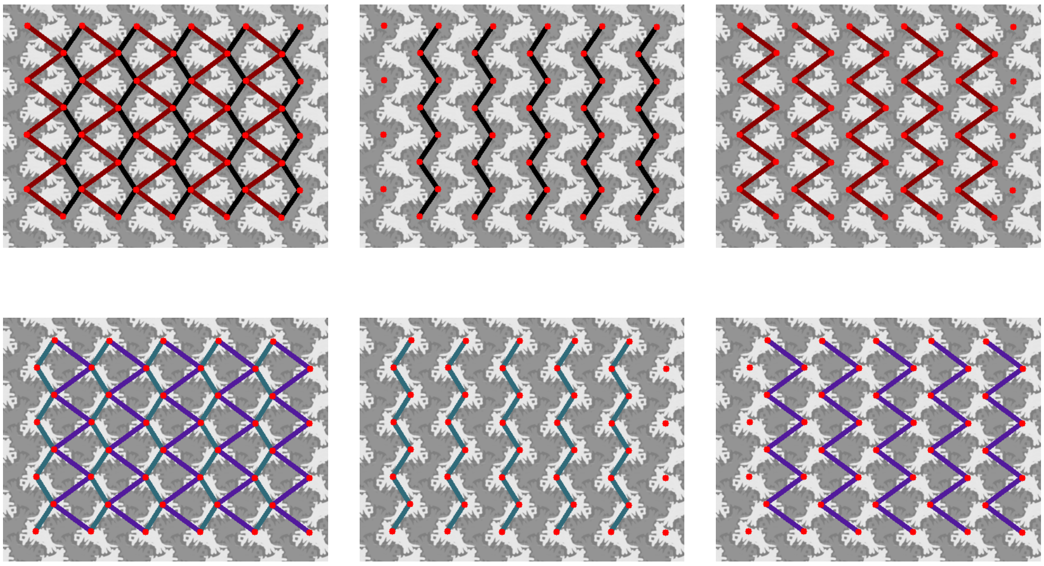

Figure 6.26: Extracted connection groups for two masks of an ornament in Fig. 6.24. First column shows all connections extracted for a mask, and the second and third columns show each connection group of a mask separately.

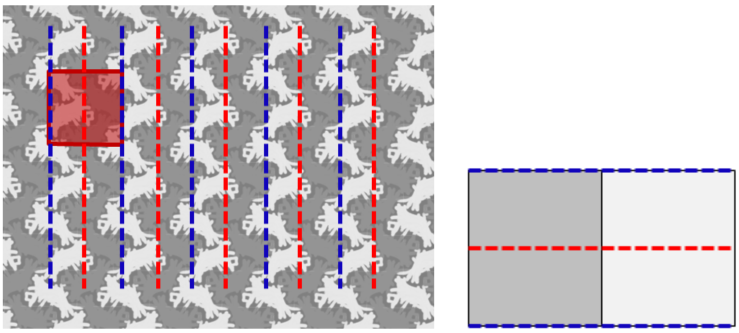

(a) (b)

Figure 6.27: (a) Symmetries of an ornament inferred from the mask connection groups. Connecting similarly arranged points give a rectangular lattice with parallel glide reflection axes. This type of unit cell indicates that the ornament belongs to *pg* group. (b) Cell structure for *pg* group. The darker region indicates the fundamental domain.

Ignoring the colors by combining the node centers of two masks give three more connection groups for the ornament as shown in Fig. 6.28. First and third connection groups contain connections where each node center is connected to only one other point. Such connections indicate two-fold rotations. The second connection group contains horizontal glide reflections, which are indicated by slightly zigzagged almost straight lines. Summarizing all the symmetries of an ornament in Fig. 6.29(a) shows that the symmetries of this ornament is similar to the symmetries of the previous ornament, and that the ornament is of *pgg* group.

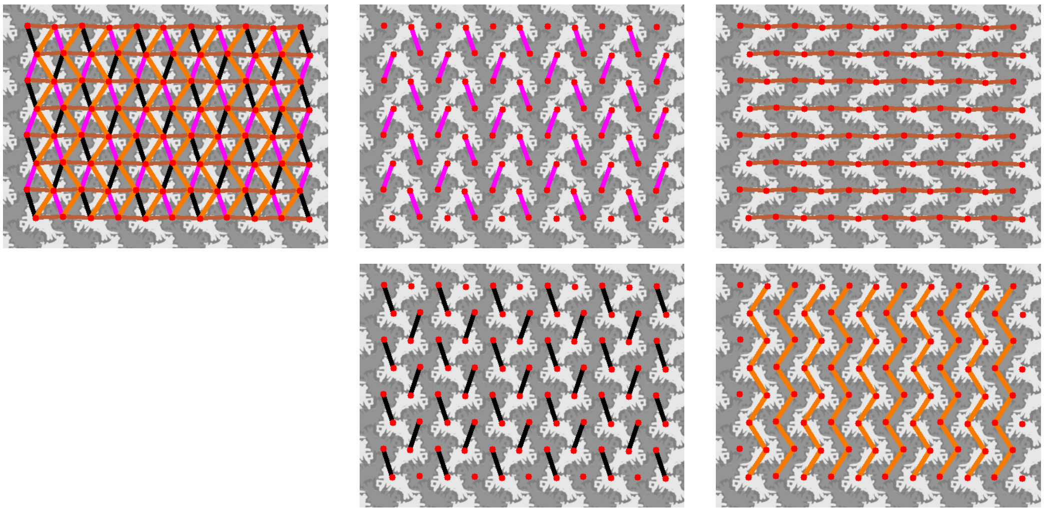

Figure 6.28: Extracted connection groups for an ornament in Fig. 6.24 when the node centers of two masks are combined. First column shows all connections extracted for an ornament, and the second and third columns show each connection group of an ornament separately.

Next, we analyze an ornament with different symmetries. Fig. 6.30 shows an ornament of $p4$ group. When we consider the colors it still belongs to $p4$ group. The ornament contains two masks for which detected node centers are shown in Fig. 6.31.

For each of the masks of an ornament in Fig. 6.30 we show four extracted connection groups in Fig. 6.32. The first connection group for both masks contains line segments, each line connecting two points. These connections indicate a two-fold rotation between two points. For both masks, the second connection group contains square structures. Each point is connected to two different points. Observe that in this manner four points connect to form square structures, which, on the other hand, represent four-fold rotational symmetries of a point. The

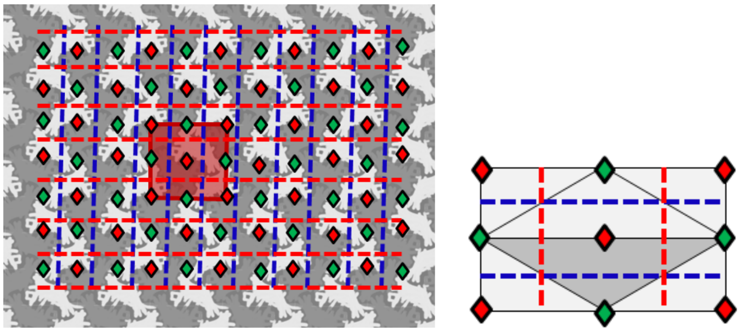

(a) (b)

Figure 6.29: (a) Symmetries of an ornament inferred from the connections obtained from combined node centers. Connecting two-fold rotation centers of similar type introduces a unit cell of an ornament. This type of unit cell indicates that the ornament belongs to *pgg* group. (b) Cell structure for *pgg* group. The darker region indicates the fundamental domain.

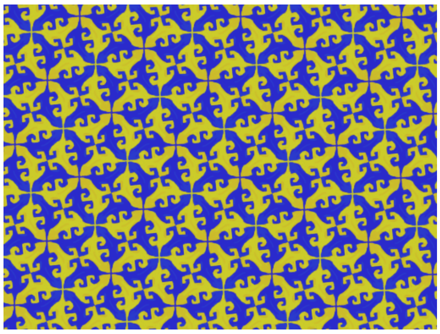

Figure 6.30: A two-color ornament of $p4$ group.

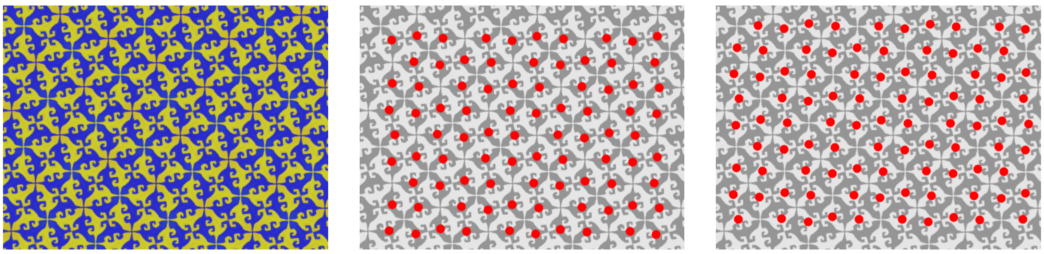

Figure 6.31: Detected node centers for two masks of an ornament in Fig. 6.30.

cross structures shown as a last connection group comprises of two similar connections indicating two-fold rotations. Thus, at the center of the cross structure two two-fold rotation centers reside. This is not surprising, since the center of cross structure is also the center of four-fold rotation, which contains two two-fold rotations in it. The third connection group for both masks again contains square structures indicating four-fold rotations. However, this four-fold rotation is different from the four-fold rotations of the first connection group of the masks. Actually, the centers of squares of third connection group of first mask coincide with the centers of squares of second connection group of second mask, and vice versa. Analyzing all connections extracted for one mask, we conclude that the ornament contains two different four-fold rotation centers and one two-fold rotation center (Fig. 6.33 (a)). Connecting the translations of any of the two four-fold rotation centers give a unit cell. Fig. 6.33 (b) illustrates the unit cell and connections that are incident with it. There are three symmetry groups involving four-fold rotations: $p4$, $p4m$ and $p4g$. The cell structure for $p4g$ group shown in Fig. 6.34 contains only one four-fold rotation center, while the unit cell that we extracted contains two centers. Then we do not consider $p4g$ group any further. The $p4m$ group requires a mirror reflection along the diagonals of the unit cell. However, none of the points of red square in Fig. 6.35 lie on the diagonals, neither the diagonal divides the square equally. Then the diagonal does not divide the four-fold rotation center equally so that the mirror reflection occurs. Thus, we conclude that the ornament is of $p4$ group.

When we ignore the colors and compute the connections for combined node centers, we obtain four connection groups. The symmetries that we obtain ignoring the colors are similar to the symmetries obtained by considering the colors. We observe two different four-fold rotation centers and one two-fold rotation center. Observe that two different four-fold rotation centers obtained for color symmetry now become the translations of the same four-fold rotation center. The two-fold rotation of color symmetry ornament now becomes four-fold rotation. Fig. 6.45 (a) shows the symmetries and the unit cell for an underlying ornament. Observe that the lattice becomes smaller. In general, when we consider the colors the unit cell, hence the fundamental domain is bigger than when we ignore the colors. Again, the ornament can be of three possible symmetry groups: $p4g$, $p4m$ and $p4$. The $p4g$ group can be discarded because it contains only one four-fold rotation center. The $p4m$ group, just as in the previous case, requires a mirror reflection along the diagonals of unit cell. The red square in the unit cell shown

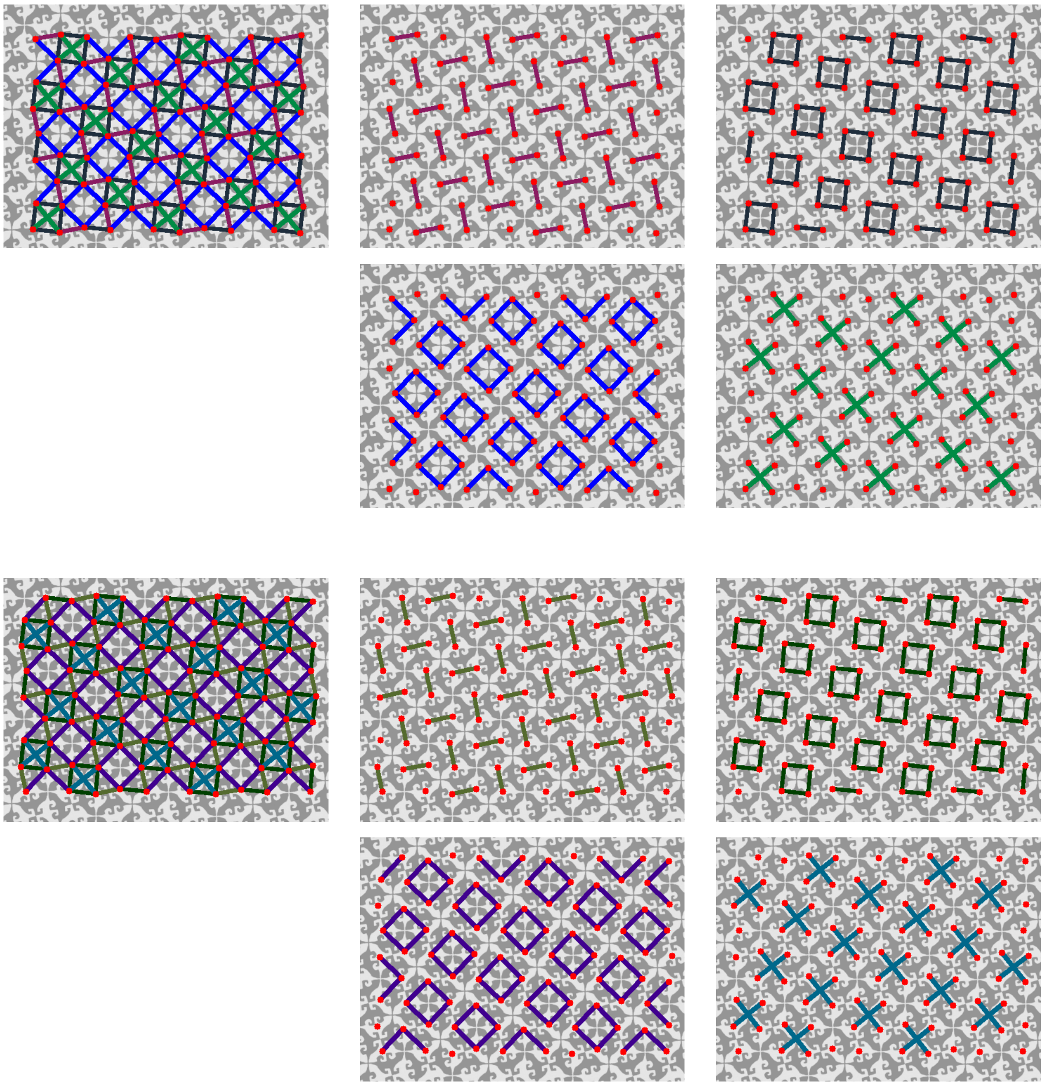

Figure 6.32: Extracted connection groups for two masks of an ornament in Fig. 6.30. First column shows all connections extracted for a mask, and the second and third columns show each connection group of a mask separately.

in Fig. 6.38 is not symmetrical along the diagonals. Then the ornament is still of $p4$ group.

We analyze yet another ornament of $p4$ group, which is shown in Fig. 6.39. Just as the previous ornament, it remains in $p4$ group when the colors are ignored. The ornament contains two masks for which detected node centers are shown in Fig. 6.40. Four connection groups extracted for two masks of the ornament (Fig. 6.41) are the same as the connection groups of the previous ornament. This leads to detection of the same symmetries on the ornament giving the same unit

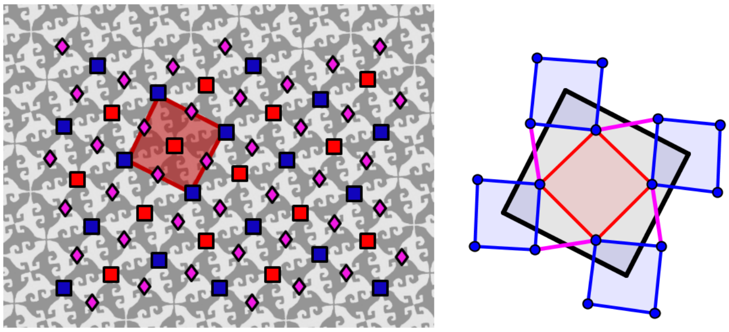

(a) (b)

Figure 6.33: (a) Symmetries of an ornament inferred from the mask connection groups. Red square indicates the unit cell of an ornament. (b) Unit cell and connections incident with it.

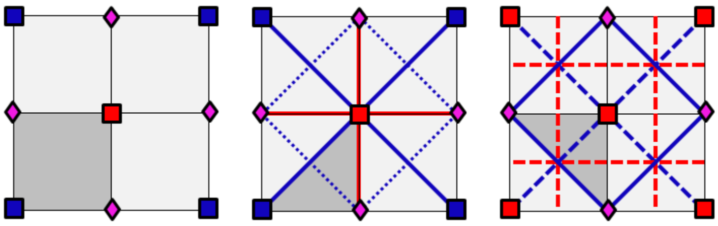

$p4$ $p4m$ $p4g$

Figure 6.34: Three possible symmetry groups for an ornament.

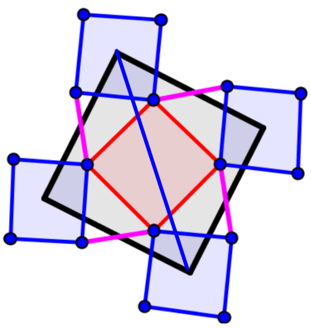

Figure 6.35: The $p4m$ group implies a reflectional symmetry along the diagonals of unit cell.

cell as for the ornament in Fig. 6.30 (See Fig. 6.42). We again have three possible symmetry groups, $p4$, $p4m$ and $p4g$. Since the ornament has two different four-fold rotation centers we discard the $p4g$ group. Furthermore, Fig. 6.43 shows that the unit cell has no reflectional symmetry along the diagonal discarding the

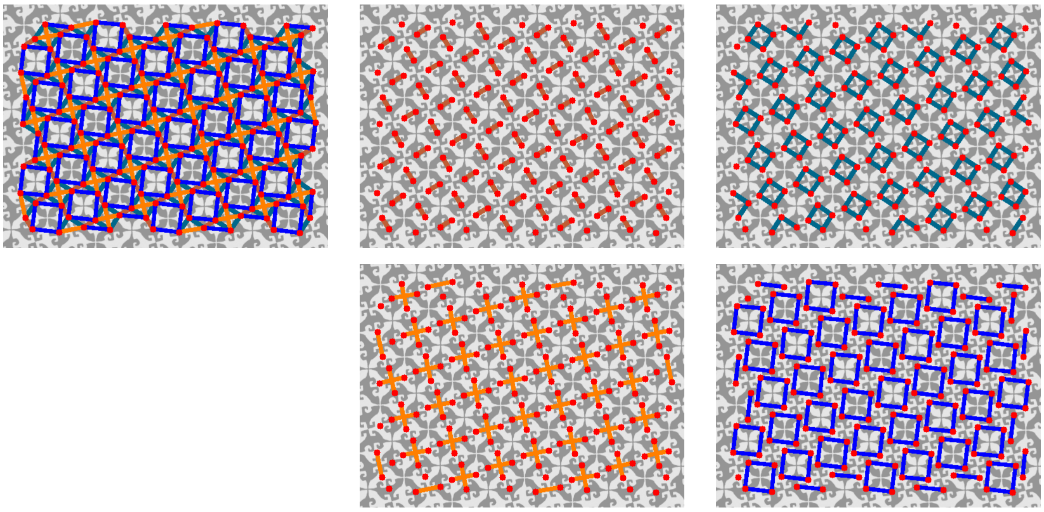

Figure 6.36: Extracted connection groups for two masks of an ornament in Fig. 6.30 when the colors are ignored. First column shows all connections extracted for an ornament, and the second and third columns show each connection group of an ornament separately.

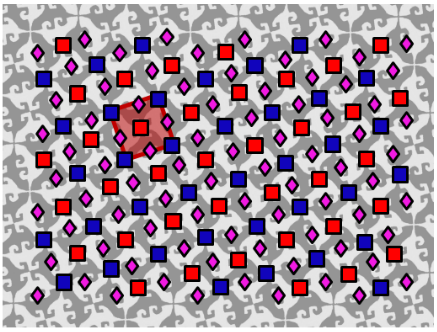

(a)

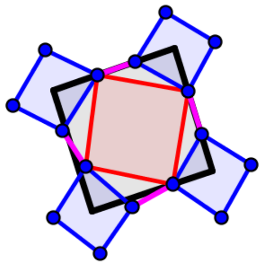

(b)

Figure 6.37: (a) Symmetries of an ornament inferred from the connection groups when colors are ignored. Red square indicates the unit cell of an ornament. (b) Unit cell and connections that each unit cell contains.

$p4m$ group. Thus, we conclude that the ornament belongs to $p4$ groups when colors are considered.

Fig. 6.44 shows four connection groups obtained by ignoring the colors. The symmetries inferred from the connections are similar to those inferred for the previous ornament. Also, the unit cell for the underlying ornament becomes smaller as shown in Fig. 6.45. We again search for the symmetry group of the

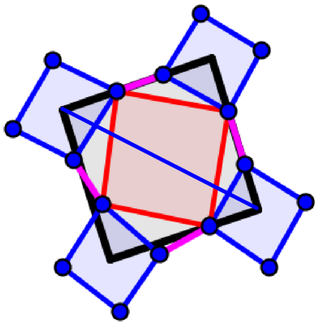

Figure 6.38: The $p4m$ group implies a reflectional symmetry along the diagonals of unit cell.

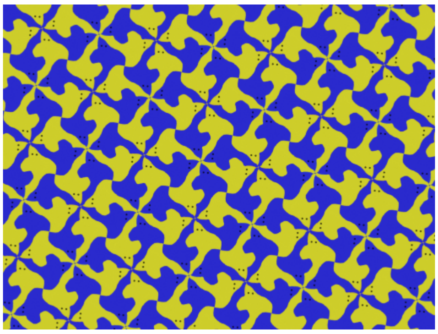

Figure 6.39: Another two-color ornament of $p4$ group.

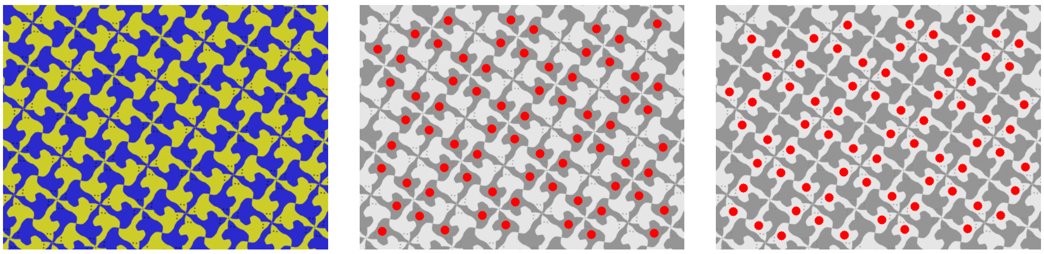

Figure 6.40: Detected node centers for two masks of an ornament in Fig. 6.39.

ornament among $p4$, $p4m$ and $p4g$ symmetry groups. As before $p4g$ is discarded immediately since it have only one four-fold rotation center, and $p4m$ is discarded since it is shown in Fig. 6.46 that there is no reflectional symmetry along the diagonal of unit cell. Thus, we define the symmetry group of an ornament as $p4$ when colors are ignored.

Fig. 6.47 shows first two connection groups for one of the masks of two ornaments of $p4$ group. Observe the structural similarity between the connections of two

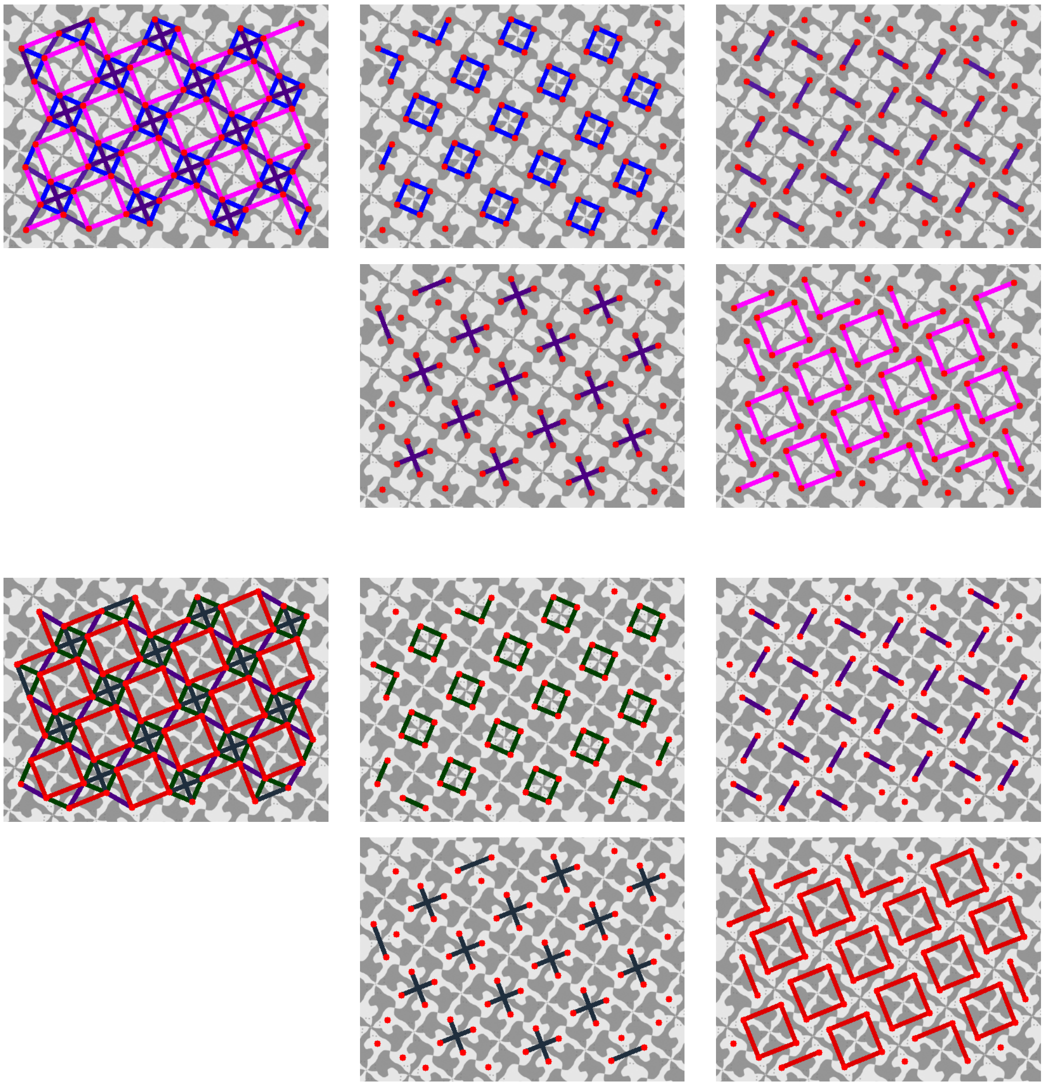

Figure 6.41: Extracted connection groups for two masks of an ornament in Fig. 6.39. First column shows all connections extracted for a mask, and the second and third columns show each connection group of a mask separately.

ornaments. Both contain small square structures indicating four-fold rotations. Each square is connected to the neighboring square indicating two-fold rotations. From the binary representation of connection groups, we observe two different four-fold rotation centers for both ornaments. The difference on the shapes surrounding the second four-fold rotation centers is due to shape variations in two ornaments.

The next two ornaments to be analyzed are of group $p4g$. Both are two-color ornaments with no color symmetry. The first ornament is shown in Fig. 6.48.

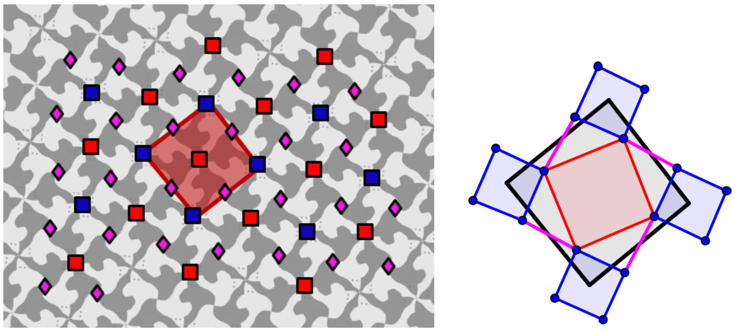

(a) (b)

Figure 6.42: (a) Symmetries of an ornament inferred from the mask connection groups. Red square indicates the unit cell of an ornament. (b) Unit cell and connections within the unit cell.

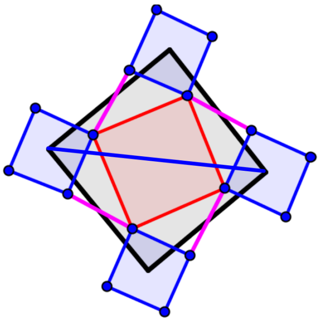

Figure 6.43: The $p4m$ group implies a reflectional symmetry along the diagonals of unit cell.

See Fig. 6.49 for the detected node centers for two masks of the ornament.

Fig. 6.50 show three connection groups for the first mask and four connection groups for the second mask of the ornament. The first connection group of the first mask contains similar connections between two points all indicating the same two-fold rotations. The second connection group connects the points that are related by four-fold rotation, which is indicated by square structures. The last connection group contains zigzag structures in two different directions right where the glide reflection axes of an ornament lie. The first connection of the second mask contains square structures indicating four-fold rotations. However, not all the centers of these squares are truly centers of four-fold rotations. Subsequent connection groups help to discard the incorrectly detected four-fold rotations. For example, the second connection group for this mask shows cross

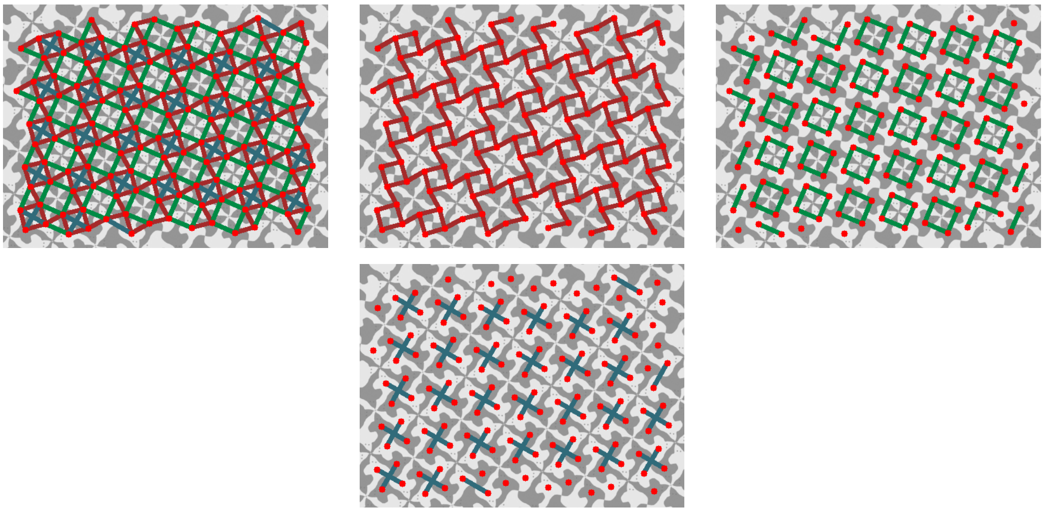

Figure 6.44: Extracted connection groups for two masks of an ornament in Fig. 6.39 when the colors are ignored. First column shows all connections extracted for an ornament, and the second and third columns show each connection group of an ornament separately.

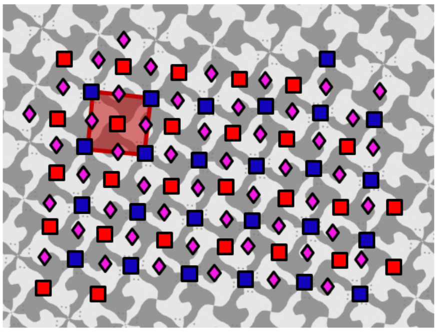

(a)

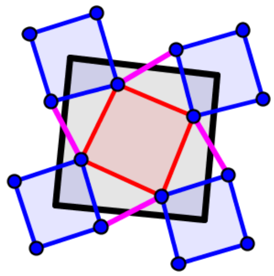

(b)

Figure 6.45: (a) Symmetries of an ornament inferred from the connection groups when colors are ignored. Red square indicates the unit cell of an ornament. (b) Unit cell and connections incident with the unit cell.

structures indicating two similar two-fold rotations on the places where the true four-fold rotations reside. The last two connection groups show that non four-fold rotation centers introduced by first connection group contain two different two-fold rotation centers. In this manner, we are able to distinguish between correct and faulty four-fold rotation centers. The second connection group of the second mask also indicates glide reflections in two different directions. The

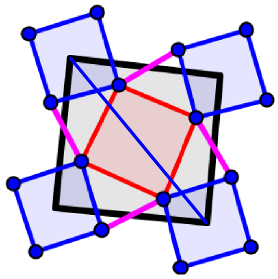

Figure 6.46: The $p4m$ group implies a reflectional symmetry along the diagonals of unit cell.

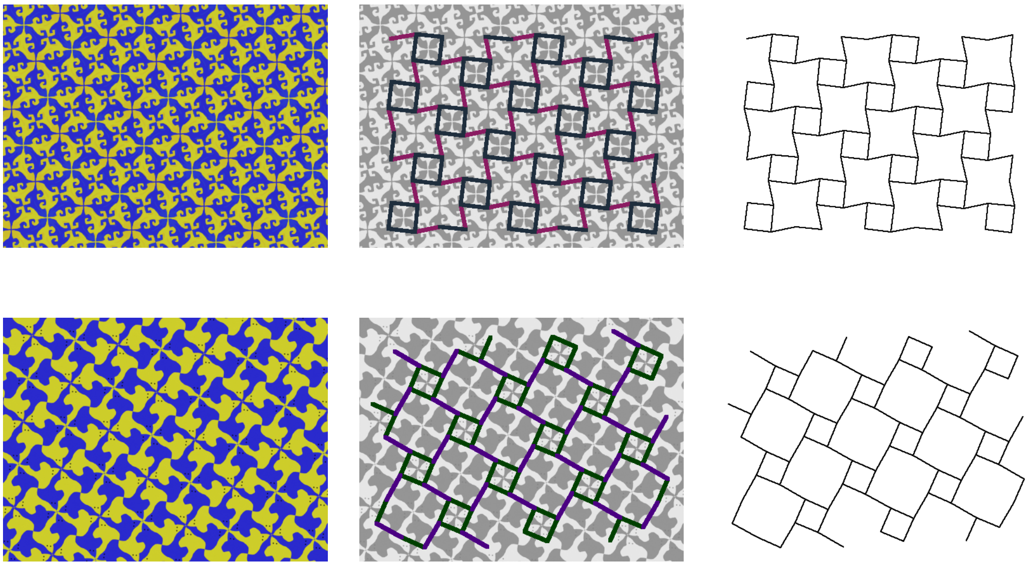

(a) (b) (c)

Figure 6.47: Structural comparison of first two connections of two ornaments of $p4$ group. (a) Original images. (b) First two connection groups of one of the masks of the ornaments. (c) Masks of the connections.

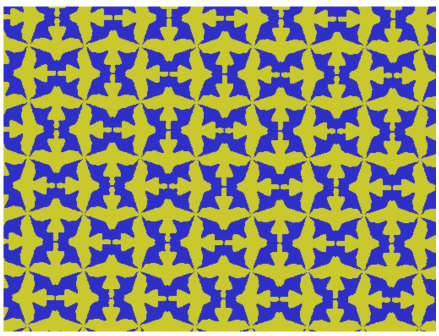

Figure 6.48: A two-color ornament of $p4g$ group with no color symmetry.

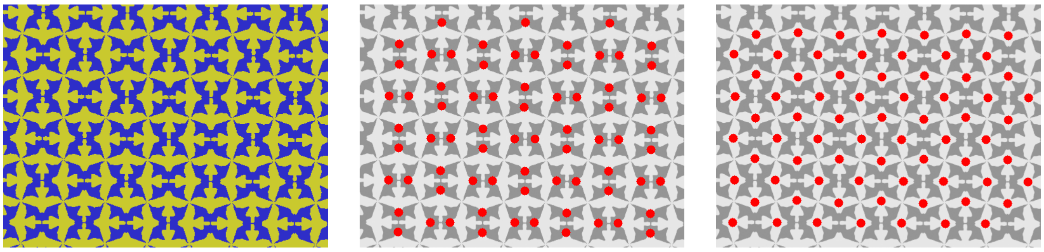

Figure 6.49: Detected node centers for two masks of an ornament in Fig. 6.48.

zigzag structures are hard to see because the node centers lie almost on the same line. Fig. 6.51 (a) shows all the symmetries detected using the connection groups in one place. Overall, the ornament has one four-fold rotation center, one two-fold rotation center and glide reflection axes in two directions. This information is enough to define the symmetry group of the ornament as $p4g$. Note that just by knowing that the ornament contains only one four-fold rotation center repeated throughout is enough to classify the ornament as $p4g$ group, because the other symmetry groups with four-fold rotations ($p4$ and $p4m$) contain two different four-fold rotation centers.

The second two-color ornament of $p4g$ group with no color symmetry is shown in Fig. 6.52. It also has two masks. See Fig. 6.53 for node centers detected for its masks.

Connection groups for the ornament masks are illustrated in Fig. 6.54. The first mask contains four connection groups, while five connection groups are extracted for the second one. The first connections group of the first mask contains three-point connections where one of them is the center of other two points. This type of connection indicates two-fold rotations. Glide reflections in two different directions are shown in the second connection group. The third and fourth connection groups contain square structures representing four-fold rotations. In the third connection group the points that are the centers of four-fold rotation are connected to four other points, while non four-fold rotational centers are connected to six other points. The first connection group of the second mask also contains square structures indicating four-fold rotations. The second and third connection groups indicate two-fold rotations. However, observe that the connections repeat in pairs for both connection groups. This

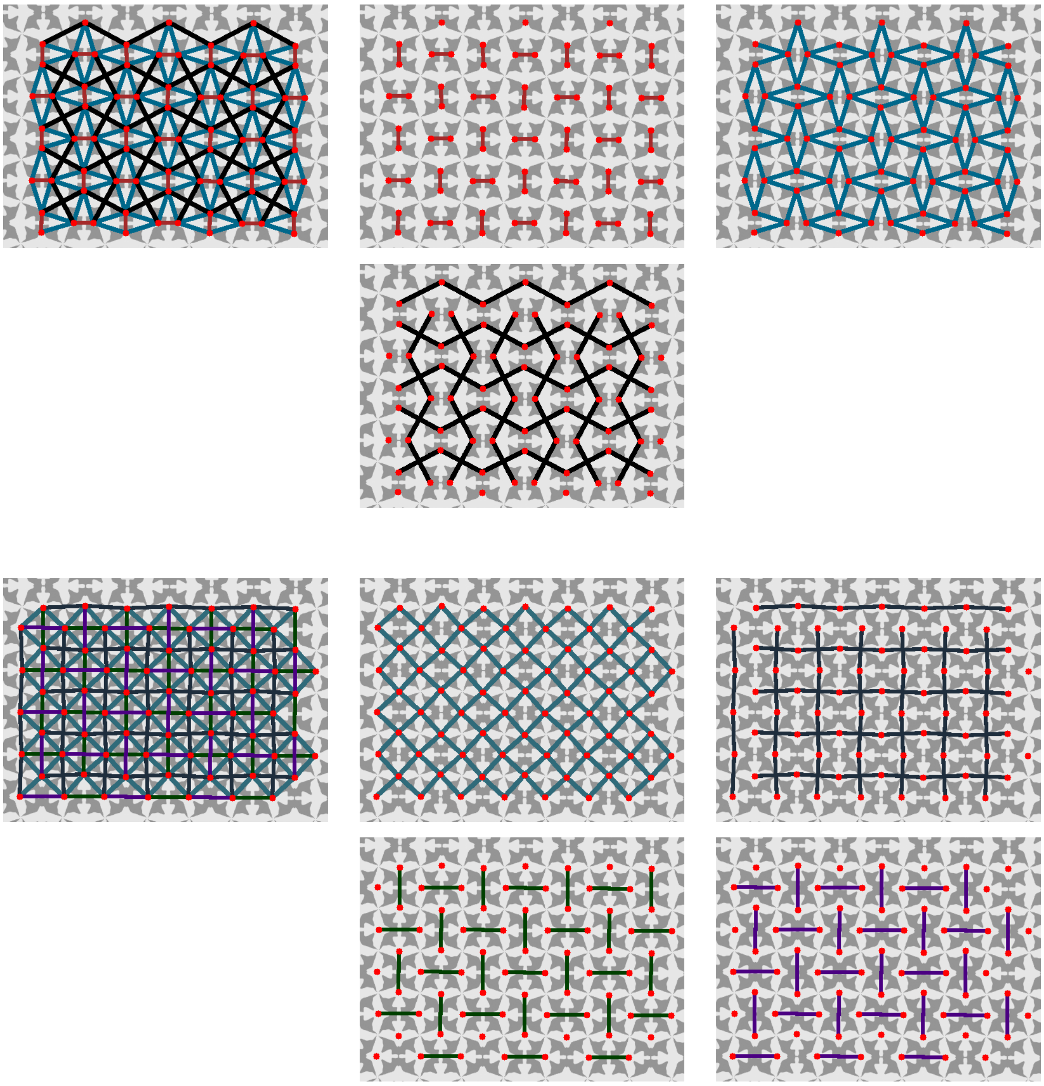

Figure 6.50: Extracted connection groups for two masks of an ornament in Fig. 6.48. First column shows all connections extracted for a mask, and the second and third columns show each connection group of a mask separately.

indicates that two-fold rotation centers do not lie on the center of lines connecting two-points, but on the centers of these two pair lines. This occurs when the two-fold rotation is not done on the individual form of the ornament but on the combination of two forms. Thus, one connection indicates a reflectional symmetry between connected points, and in pair two connections indicate two-fold rotations. An interesting result is obtained for the forth connection group. Here, the cross structures represent two similar two-fold rotations and there are glide reflections in two different directions. Observe that the glide reflection axes are

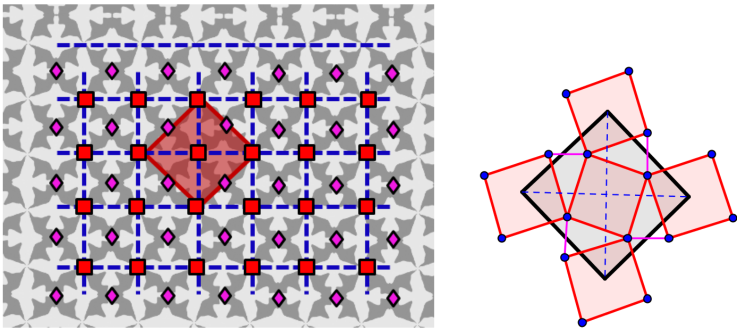

(a) (b)

Figure 6.51: (a) Symmetries of an ornament inferred from the mask connection groups. Red square indicates the unit cell of an ornament. This type of unit cell indicates that the ornament belongs to $p4g$ group. (b) Connections that fall within one unit cell of the ornament.

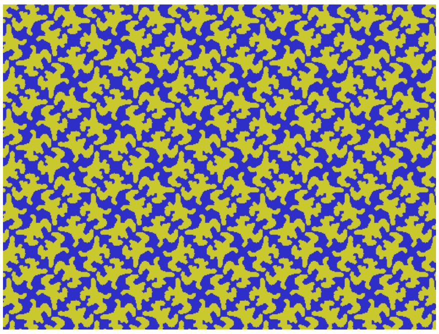

Figure 6.52: A two-color ornament of $p4g$ group with no color symmetry.

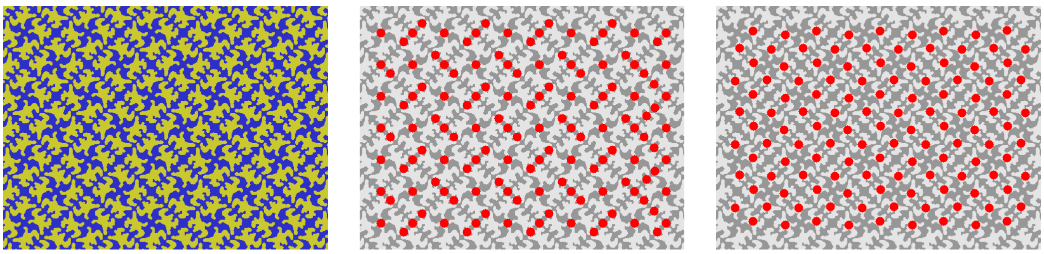

Figure 6.53: Detected node centers for two masks of an ornament in Fig. 6.52.

different from the glide reflections obtained for the first mask. Extracting all the symmetries inferred from the connections of the first masks we obtain a lattice similar to the lattice of the previous $p4g$ ornament (Fig. 6.55). Since we have only one center of four-fold rotation the ornament is of $p4g$ group.

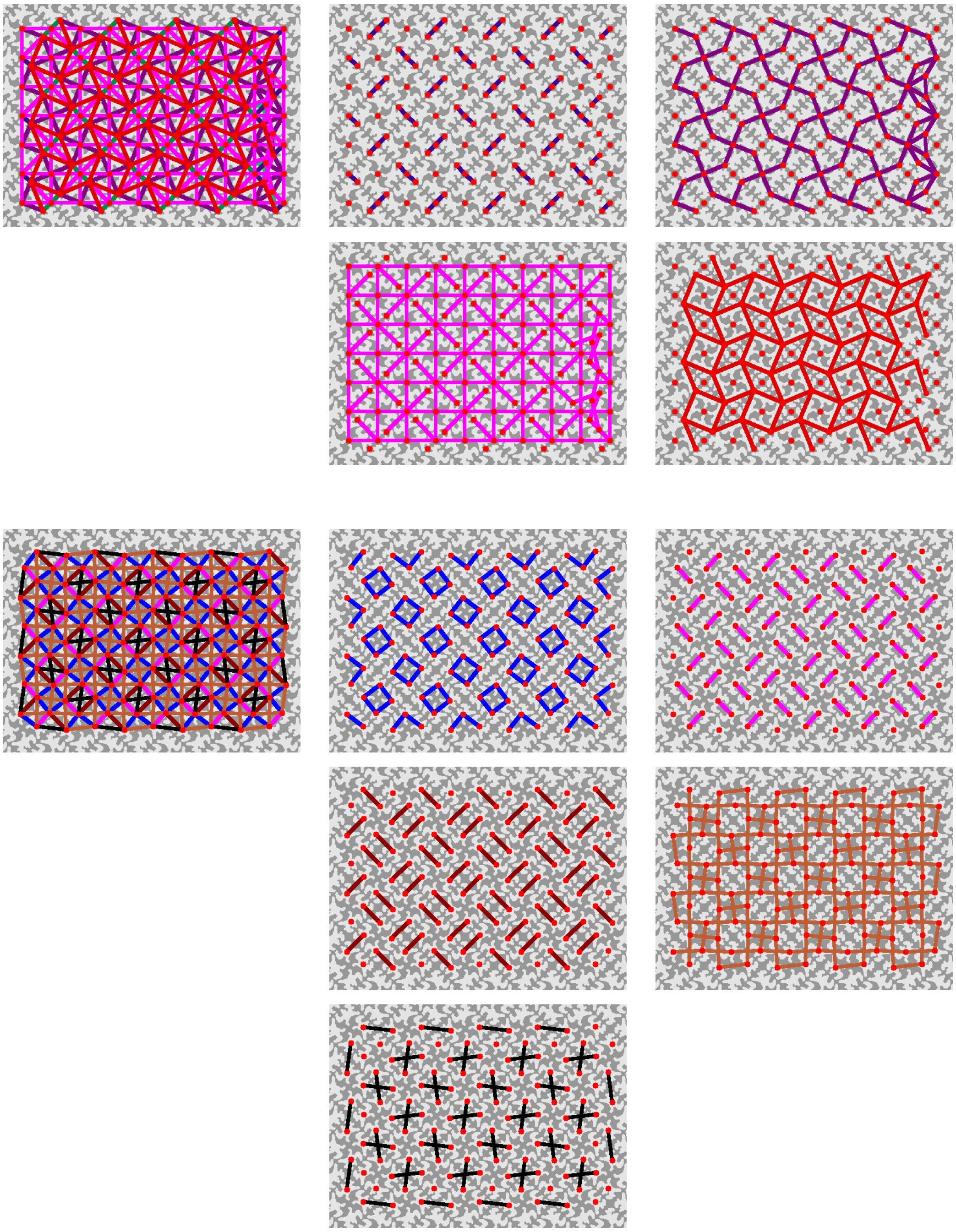

Figure 6.54: Extracted connection groups for two masks of an ornament in Fig. 6.52. First column shows all connections extracted for a mask, and the second and third columns show each connection group of a mask separately.

Fig. 6.56 compares the structures of some of the connection groups of last $p4g$ group ornaments and previous two $p4$ group ornaments. Observe the binary images for the connections of first two $p4g$ ornaments. Both have one type

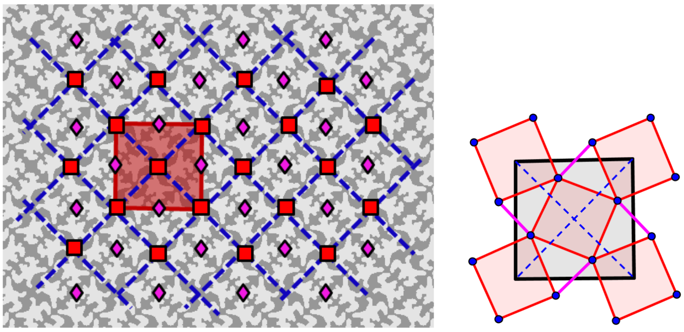

Figure 6.55: (a) Symmetries of an ornament inferred from the mask connection groups. Red square indicates the unit cell of an ornament. (b) Connections that fall within one unit cell of an ornament.

of square indicating one four-fold rotation center and a shape with two-fold rotations in between these squares. This shape varies depending on the forms used in the ornament, but regardless of the forms it contains a two-fold rotation. Also observe that in both cases two squares incline in opposite directions. In contrast to $p4g$ ornaments the connections of last two $p4$ ornaments show two different four-fold rotation centers. However, all four have structural similarity, showing that all are the special cases of a general case for an ornament with four-fold rotations. Thus, both $p4g$ group and $p4$ group have square shapes separated with some kind of shape. The difference is that the in between shape for $p4g$ can only have two-fold rotation while for $p4$ it has both two-fold and four-fold rotational symmetries.

We continue the analysis with a two-color ornament of $p6$ group shown in Fig. 6.57. When the colors are considered the symmetry group of an ornament reduces to $p3$. Detected node centers for two masks are illustrated in Fig. 6.58.

We extract three connection groups for each mask of an ornament, which are illustrated in Fig. 6.59. Observe that all connection groups for both masks contain triangular connections. The symmetries for this ornament can be easily inferred. It contains three different three-fold rotation centers that are obtained by taking the central points of triangles. Marking these central points of one mask on the ornament as in Fig. 6.60 we obtain the lattice for this ornament.

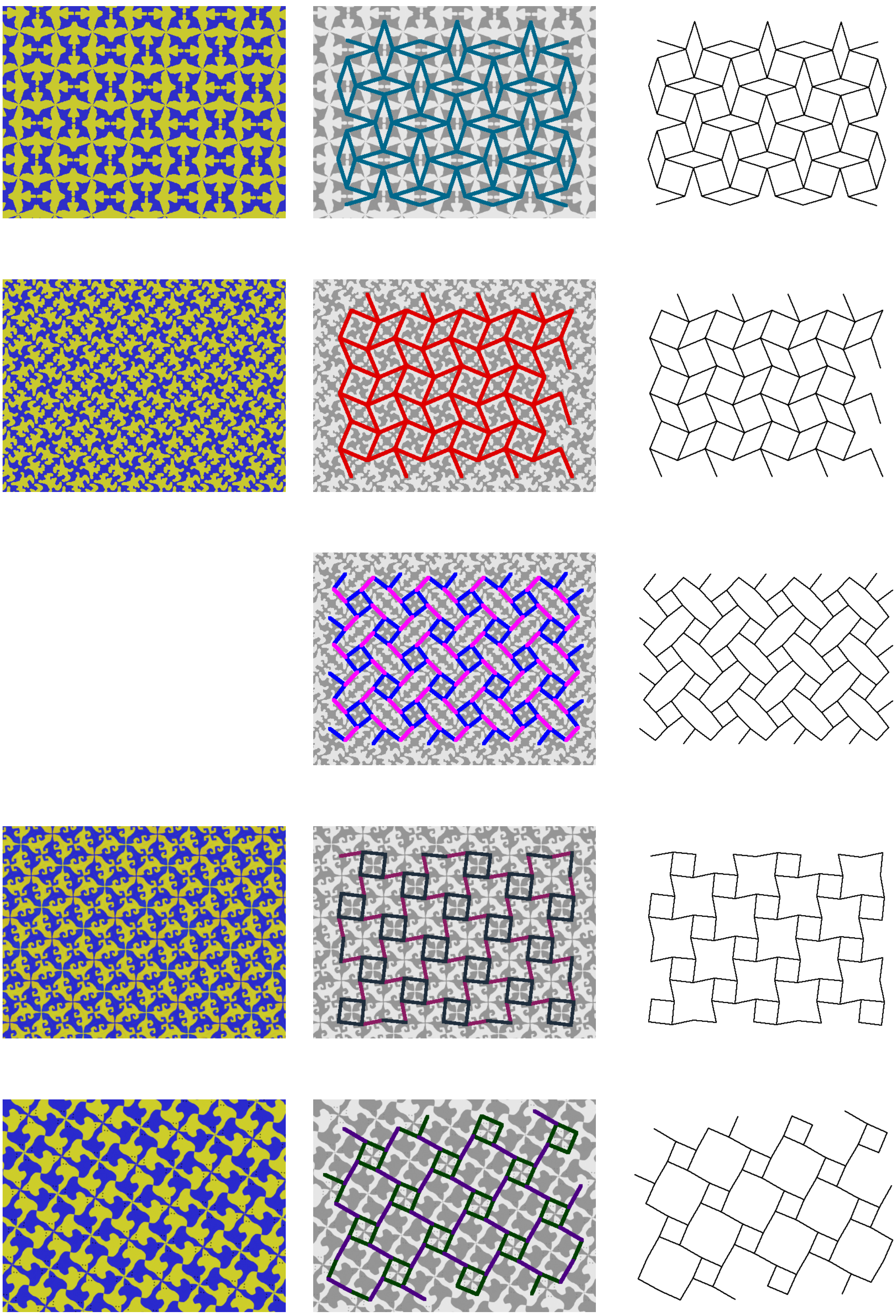

Figure 6.56: Structural comparisons of connections of two $p4g$ and $p4$ ornaments.

Fig. 6.61 shows three possible symmetry groups that the ornament might belong. We discard the $p31m$ symmetry group because it requires only two three-fold

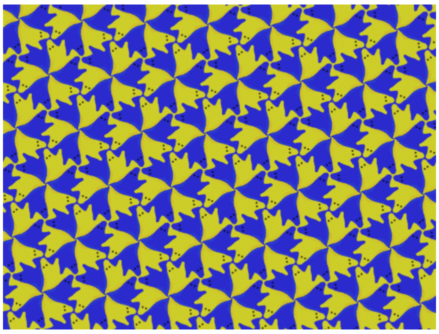

Figure 6.57: Two-color ornament of gorup $p6$.

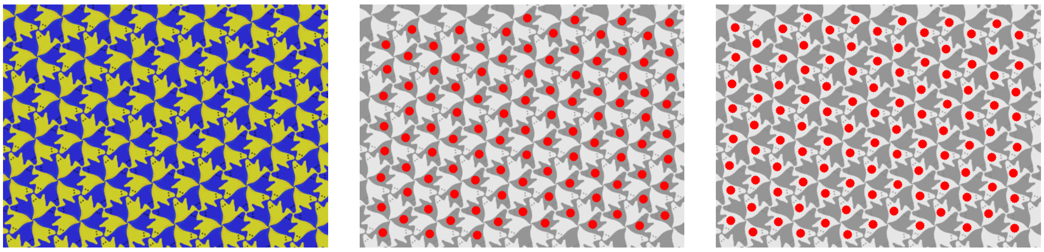

Figure 6.58: Detected node centers for two masks of an ornament in Fig. 6.57.

rotation centers while we have three. The $p3m1$ symmetry group has reflectional symmetry along the major diagonal of the unit cell. This is not true for the ornament that we consider as shown in Fig 6.62. Thus we conclude that the ornament is of $p3$ group when the colors are considered.

Due to color permutations, we do not observe six-fold rotations for this ornament. The six-fold rotations of the ornament are seen when we ignore the colors by combining the node centers of two masks and re-computing the connections. Observe the five connection groups obtained in this way shown in Fig. 6.63. The first connection group contains hexagonal connections the centers of which show the centers of six-fold rotations. The second connection group connects points related by two-fold rotations. The fifth connection group also shows three similar two-fold rotations centered at the same point. The third and forth connection groups indicate three-fold rotations via the triangular structures. The forth connection group contains two similar three-fold rotations centered at the same point. Summarizing the inferred symmetries on the ornament as shown in Fig. 6.64 we obtain the unit cell and connections that fall within the unit cell. There are two possible symmetry groups with six-fold rotations: $p6$ and $p6m$.

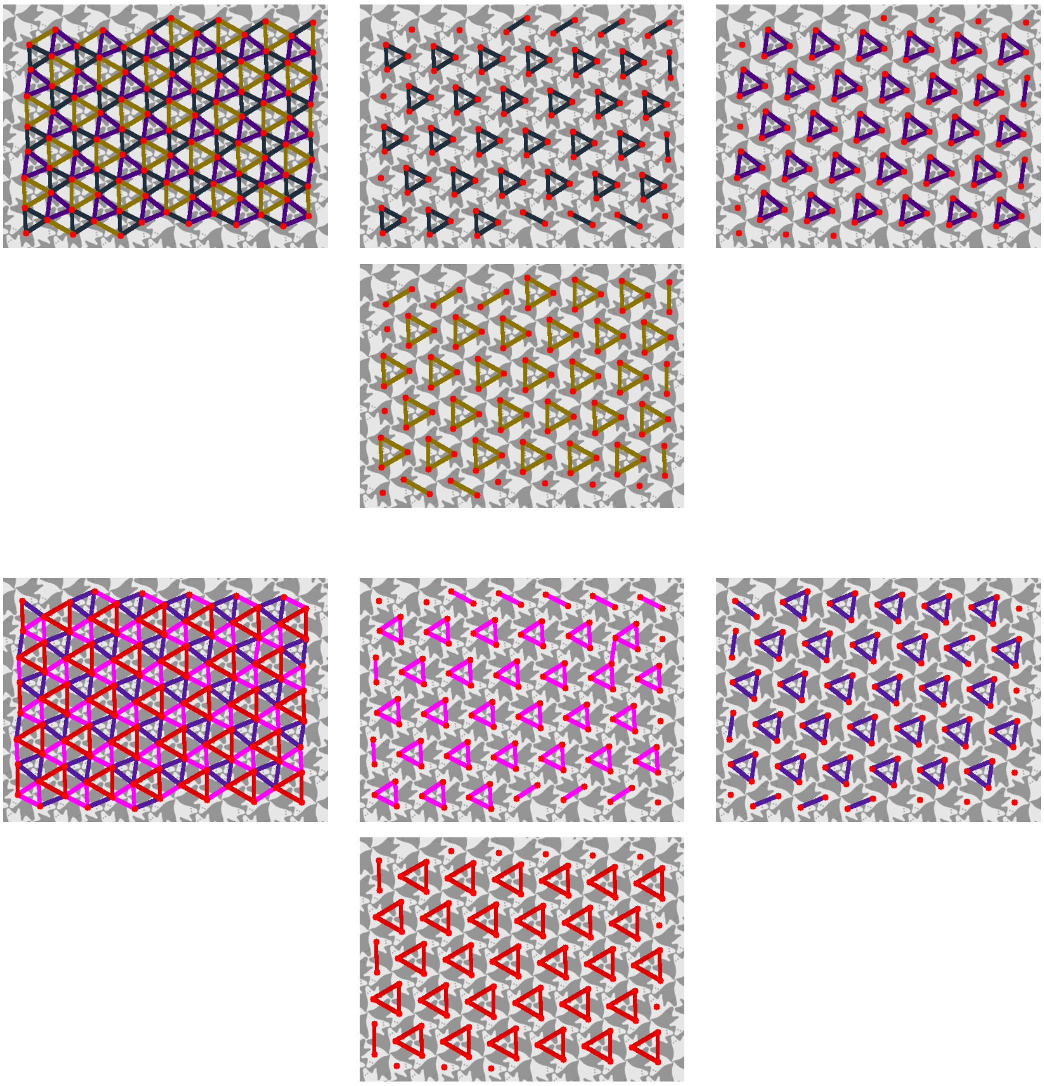

Figure 6.59: Extracted connection groups for two masks of an ornament in Fig. 6.57. First column shows all connections extracted for a mask, and the second and third columns show each connection group of a mask separately.

Fig. 6.66 shows that the ornament does not have a reflectional symmetry along the major diagonal of unit cell. Then the ornament belongs to $p6$ group when the colors are ignored.

We continue analyzing $p6$ ornaments with a four-color ornament of this group. The ornament is shown in Fig. 6.67. Detected node centers for the five masks of the ornament are shown in Fig. 6.68. The other masks are repetitions of the given five masks.

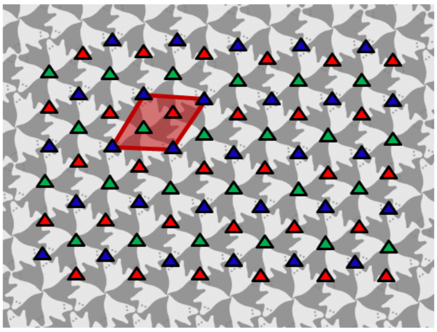
(a)

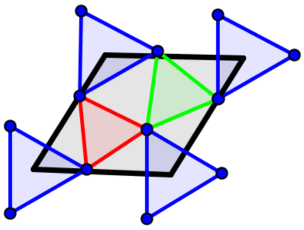
(b)

Figure 6.60: (a) Symmetries of an ornament inferred from the mask connection groups. Red rhombus indicates the unit cell of an ornament. (b) Connections of the ornament that are incident with unit cell.

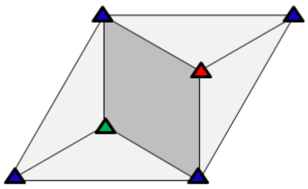
*p*3

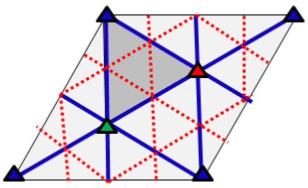
*p*3*m*1

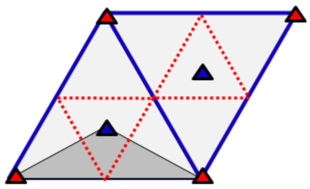
*p*31*m*

Figure 6.61: Three possible symmetry groups for an ornament.

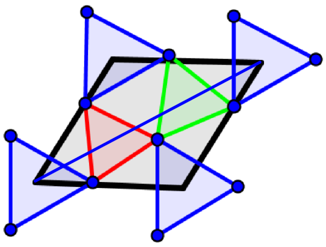

Figure 6.62: The $p3m1$ group implies a reflectional symmetry along the major diagonal of unit cell.

The connections for masks containing only one connection group are shown in Fig. 6.70. Presenting more connection groups for these masks does not introduce additional information. We extract three-connection groups for second and forth masks of the ornament that are illustrated in Fig. 6.69. All connection groups contain triangular connections indicating three-fold rotations. Collecting all the symmetries inferred from these two masks reduces to the symmetries inferred from only one mask connection groups as shown in Fig. 6.69. There are three

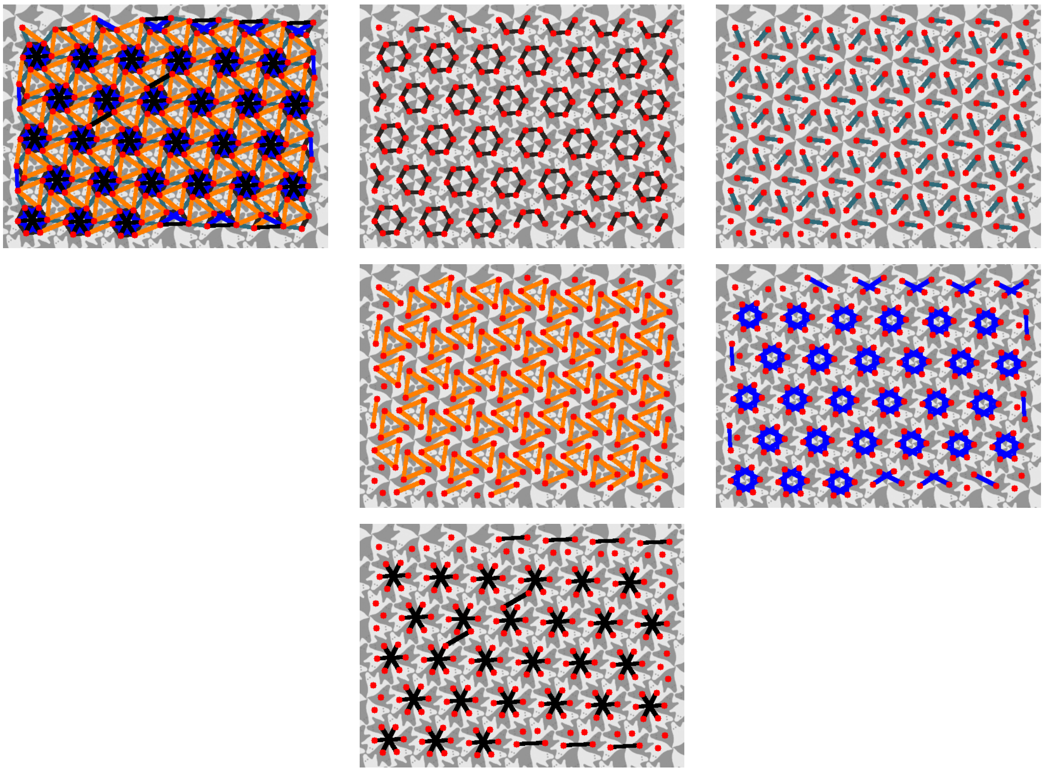

Figure 6.63: The entire six-fold rotation is seen when we compute connections by combining the node centers of two masks.

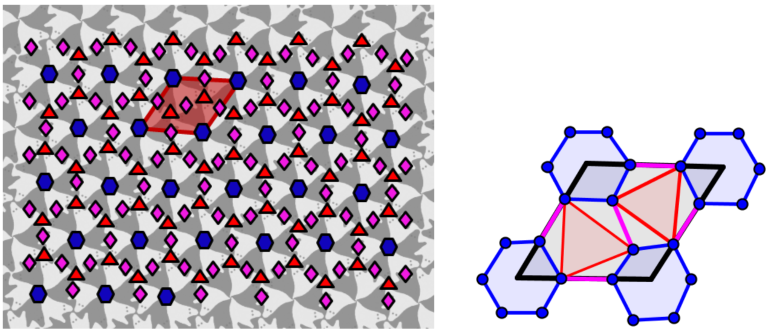

(a) (b)

Figure 6.64: (a) Symmetries of an ornament inferred from the connection groups when they are computed from combined node centers. Red rhombus indicates the unit cell of an ornament. (b) Connections that fall within a unit cell of an ornament.

different three-fold rotation centers in the ornament. Marking all three-fold rotation centers on the ornament (Fig. 6.71) we obtain a lattice unit of an

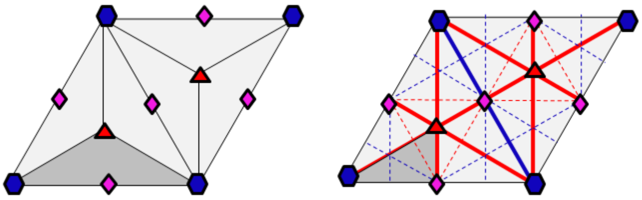

$p6$ $p6m$

Figure 6.65: Two possible symmetry groups for an ornament when colors are ignored.

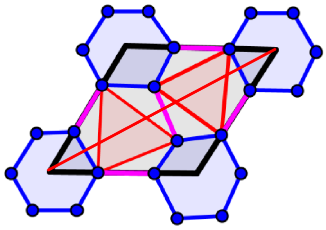

Figure 6.66: The $p6m$ group implies a reflectional symmetry along the major diagonal of unit cell.

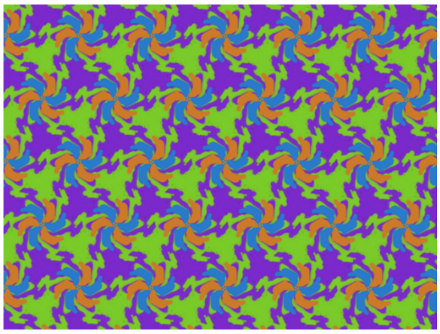

Figure 6.67: A four-color ornament of $p6$ group.

ornament. We have three possible symmetry groups: $p3$, $p3m1$ and $p31m$. We discard the $p31m$ group since it contains only two different three-fold rotation centers. We, then, show that the ornament does not have reflectional symmetry along the major diagonal of the unit cell (Fig. 6.72) and conclude that the ornament belongs to $p3$ group when the colors are considered.

Just like, for the other ornaments with color symmetry for this ornament we also consider the case when the colors are ignored. Combining node centers of two masks given in Fig. 6.69 give five connection groups shown in Fig. 6.73. The

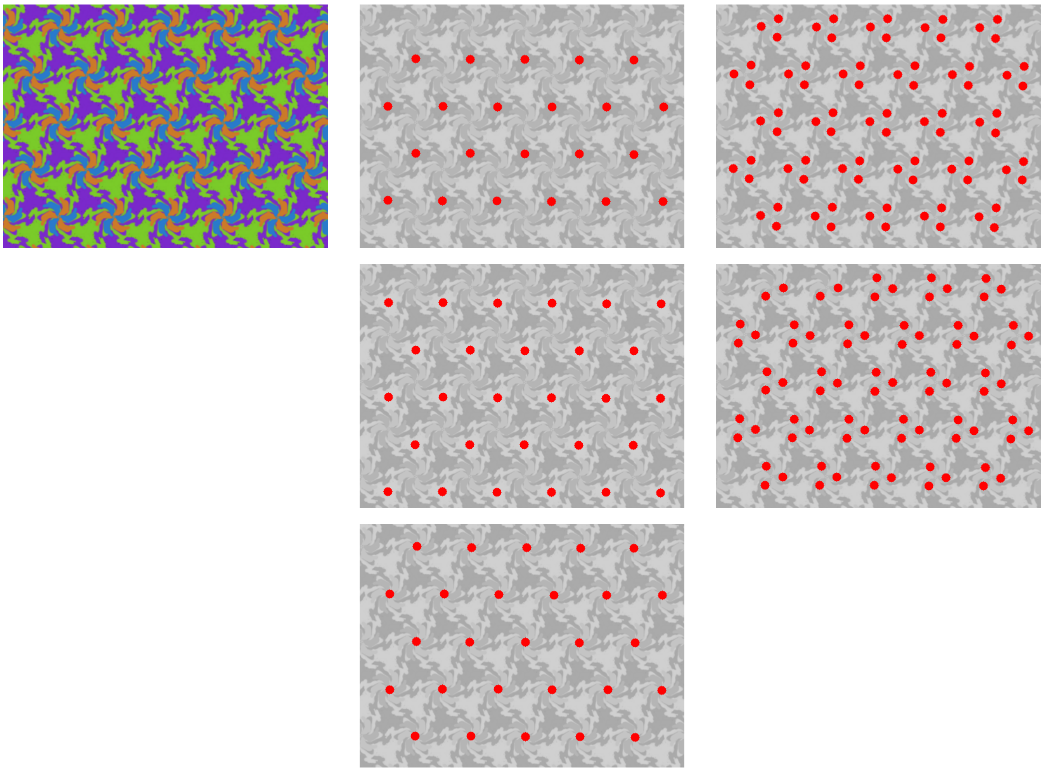

Figure 6.68: Detected node centers for five masks of an ornament in Fig. 6.67.

connections show that the ornament contain six-fold, three-fold and two-fold rotations (see Fig. 6.74). If the ornament is of $p6m$ group then it must contain reflectional symmetry along the major diagonal of the unit cell. Fig. 6.75 shows that there is no reflectional symmetry. Then the ornament is of $p6$ group.

Last ornament we analyze is a two-color ornament shown in Fig. 6.76. It belongs to $p6m$ and has no color symmetry. Two masks of the ornament with detected points are given in Fig. 6.77.

Fig. 6.78 illustrates connection groups for the masks of the ornament. First mask has three connection groups, and the second mask has only one connection. For both masks, we observe hexagonal connection representing six-fold rotations. Triangular connection representing three-fold rotations are also seen for both mask connections. There are also cross structures that occur from the intersections of two-point connections. These represent two similar two-fold rotations. Observe that the triangles in the connections of both masks are mirror symmetries of each other indicating reflection axes passing through the points where

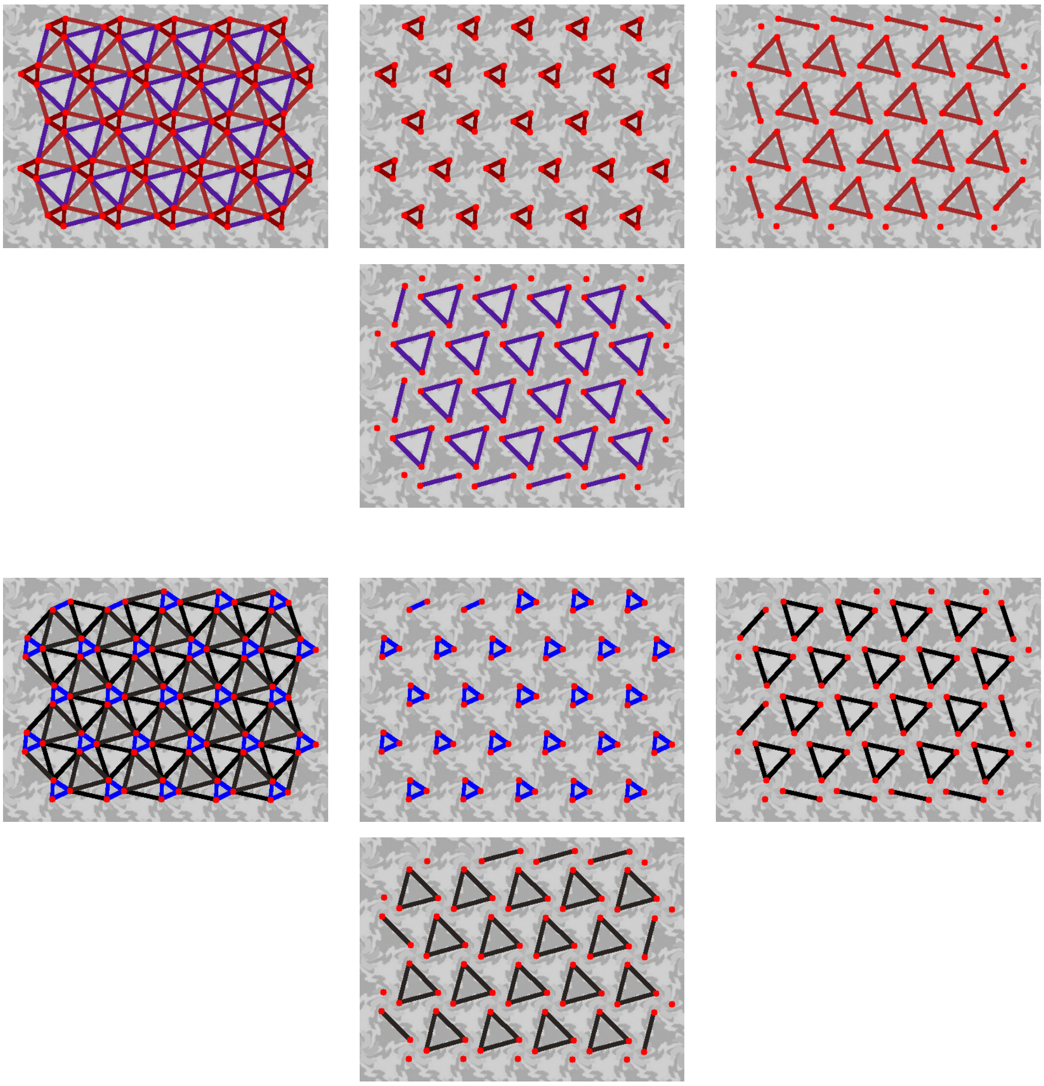

Figure 6.69: Connections of two masks each with three connection groups.

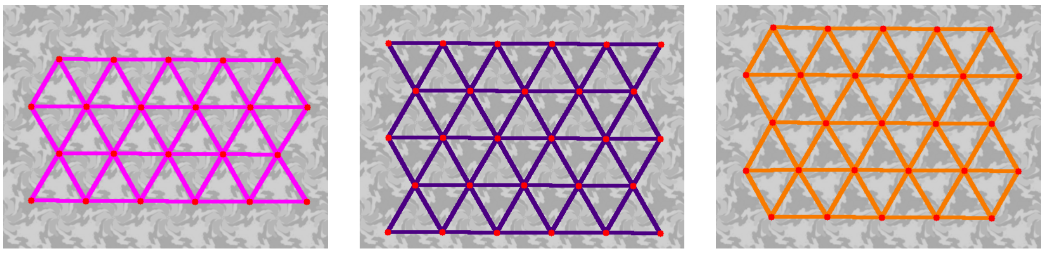

Figure 6.70: Connections of other masks with only one connection group.

two triangles meet. These reflection axes are what make this ornament different from other ornaments with six-fold rotations that we discussed so far. While the ornament contains all the symmetries of $p6$ group it also contain reflection

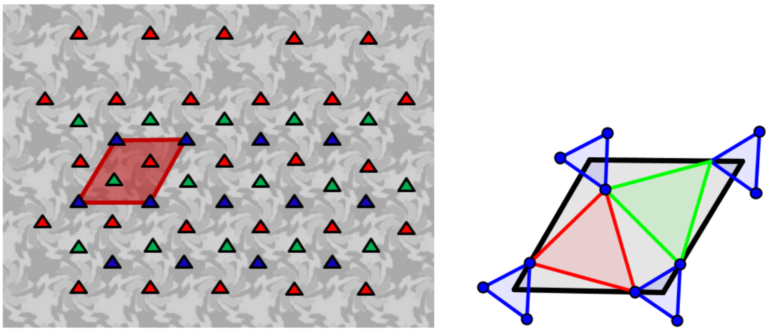
(a) (b)

Figure 6.71: (a) Symmetries and unit cell of an ornament. (b) Connections within unit cell.

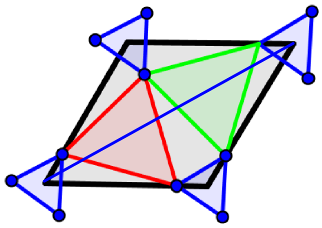

Figure 6.72: The $p3m1$ group implies a reflectional symmetry along the major diagonal of unit cell.

axes which show that the ornament belongs to $p6m$ group (see Fig.6.79).

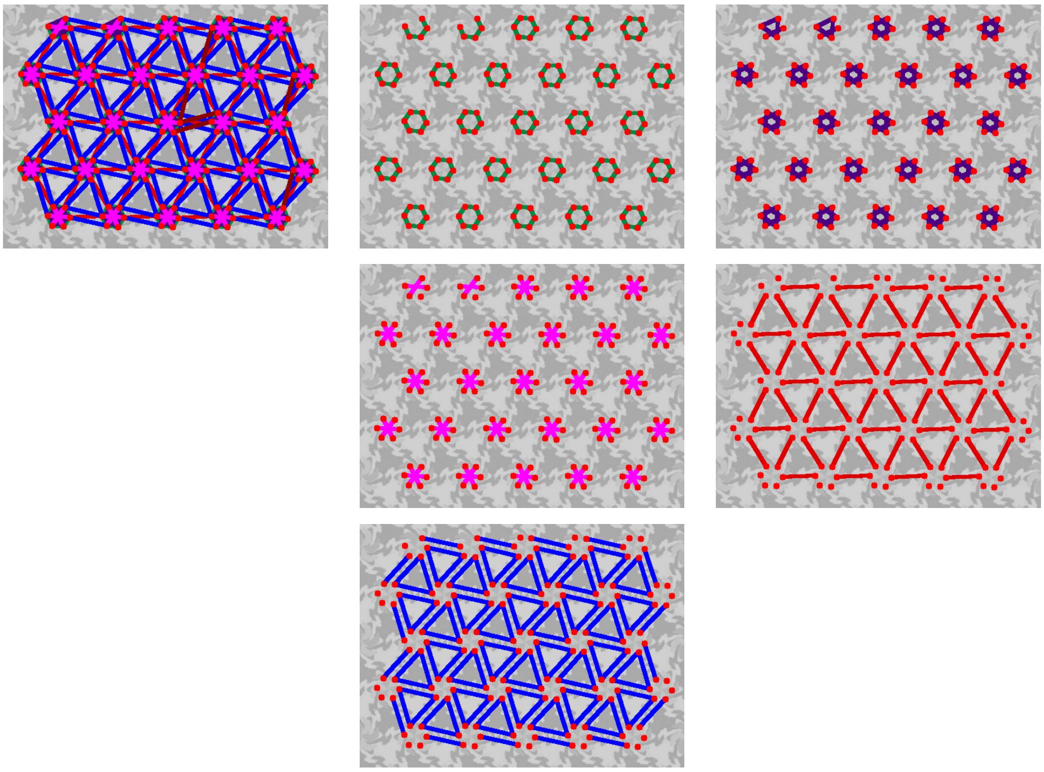

Figure 6.73: Extracted five connection groups ignoring the colors.

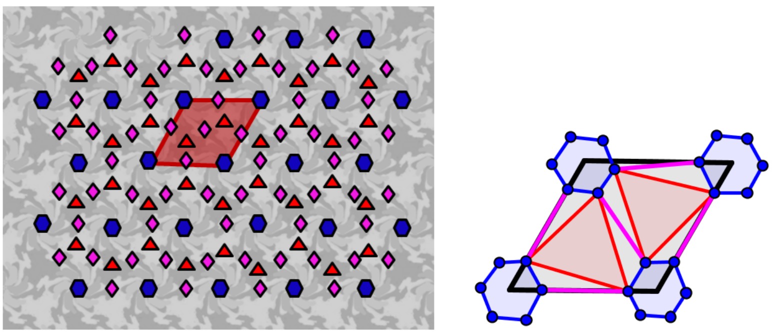

(a) (b)

Figure 6.74: (a) Symmetries and unit cell of an ornament when colors are ignored. (b) Unit cell and connections incident with it.

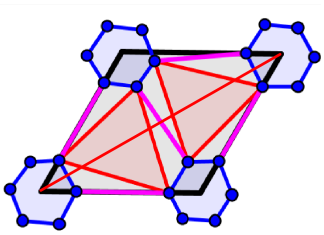

Figure 6.75: The $p6m$ group implies a reflectional symmetry along the major diagonal of unit cell.

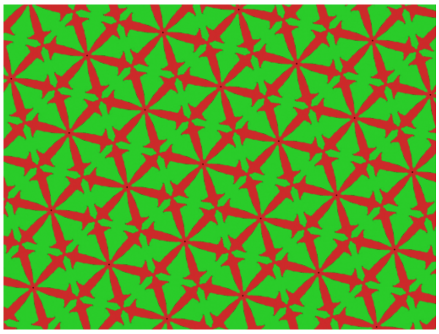

Figure 6.76: A two-color ornament of $p6m$ group with no color symmetry.

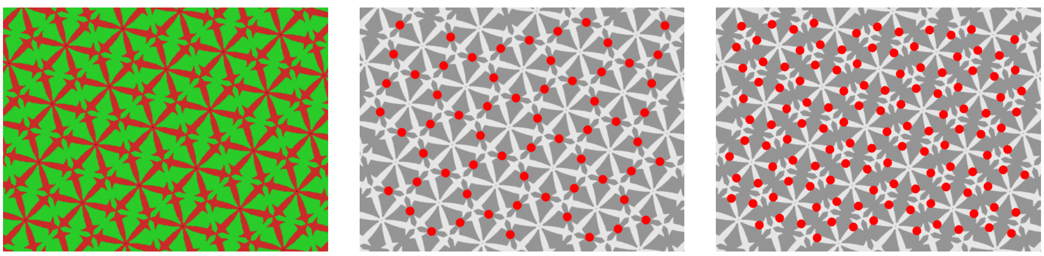

Figure 6.77: Detected node centers for two masks of an ornament in Fig. 6.76

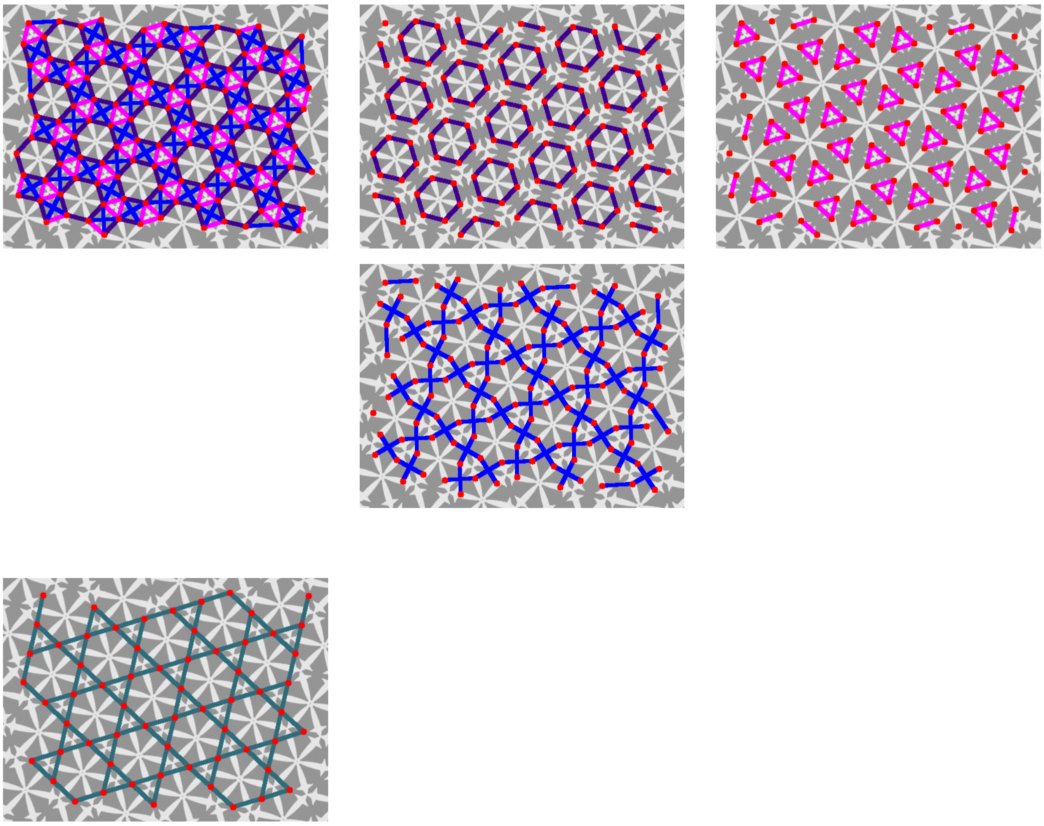

Figure 6.78: Extracted connections for the two masks of an ornament.

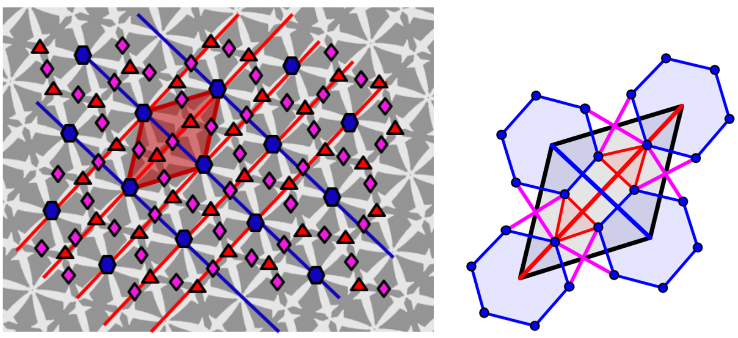

(a) (b)

Figure 6.79: (a) Symmetries and unit cell of an ornament. (b) Connections that fall within one unit cell of the ornament.

CHAPTER 7

CONCLUSION

In this thesis, we approached the problem of studying ornaments from different perspective. We gradually suppressed the content of each ornament in terms of colors and shapes. By suppressing colors, we ignored specific color choices in the ornament, but kept the color permutation information. By suppressing the shapes we ignored the details of specific forms used in an ornament, but enhanced the node centers. As a result, for a given ornament, we obtained the underlying structure, which showed the repetition rules of individual nodes. We showed that, according to the symmetries that the ornament exhibit, the node centers join to form different abstract structures like three-leaved roses, triangles, hexagons, four-leaved roses, *etc.* Moreover, we observed that the ornaments with similar symmetries exhibit similar abstract structures. All abstract structures extracted for an ornament along with the number of colors in the ornament define the style of an ornament. An important advantage that content suppressed images give is the possibility to measure the similarities of different ornaments in terms of style.

Using the content suppressed images, we sought for an alternative way of classifying ornaments, which would give new results with a fresh insight. For that, we performed style-based clustering of ornaments. However, we did not cluster all ornaments at once. Instead, we divided the clustering process into multiple experiments. For each experiment different ornament set were considered. In this manner, we observed style-wise similar ornaments to join in the given context. Such context-based clustering gives information on relations of different symmetry groups. Moreover, clustering ornaments in this manner treats the symmetry as a continuous feature, where the information on how similar are the symmetries of two ornaments is of more importance than what symmetries they have. The analysis comparing the clustering results using raw images vs. content suppressed images showed that in the first case only the images with similar shapes and colors are clustered together, while in the latter case ornaments that are similar style-wise (containing similar symmetries) are clustered together.

Beside the group approach, where we analyzed the clustering solutions for different groups of ornaments, we also analyzed individual ornaments. We took advantage of the content suppressed images that enhance the individual node centers of an ornament. By suppressing the content of an ornament, we detected the node centers. Subsequently, we extracted different connections that are clustered according to their sizes and orientations into different connection groups. These connections showed how different nodes are related, giving information on what symmetries are used in an ornament. Detecting the symmetries of an ornament led to detection of unit cell, hence the fundamental region of an ornament. The symmetries are detected for ornaments both with regular and irregular color permutations. In addition, we showed that it is possible to extract symmetries both when colors are ignored and when colors are taken into account.

Analyzing the ornaments in groups gave some insight on relations of different groups. Thus, for example, we observed that the ornaments of pure translational symmetry group are stylistically more similar to the ornaments of glide group than any other group that we considered. The rotational groups also divide internally. The ornaments with four-fold rotations are shown to be farthest to the groups containing three-fold and six-fold rotations. While the latter ones are also discriminated internally. This is in contrast to group theoretical approach, where ornaments are classified into discrete groups, giving no clues on the relations of different symmetry groups. Moreover, in the group theoretical approach rules for defining the symmetry group of an ornament changes with the number of colors contained in an ornament. In contrast, our approach, be it analyses of group of ornaments or individual ornaments, does not distinguish ornaments according to the number of colors using the same algorithm for all.

REFERENCES

[1] Y. Aflalo and R. Kimmel. Spectral multidimensional scaling. *Proceedings of the National Academy of Sciences of the United States of America*, 110(45):246–247, 2013.

[2] S. Arpa, A. Bulbul, T. K. Çapin, and B. Özgüç. Perceptual 3D rendering based on principles of analytical cubism. *Computers and Graphics*, 36(8):991–1004, 2012.

[3] F. Attneave. Some informational aspects of visual perception. *Psychological Review*, 61(3):183–193, 1954.

[4] F. Attneave. Symmetry, information, and memory for patterns. *The American Journal of Psychology*, 68(2):209–222, 1955.

[5] E. Bae and J. Bailey. COALA: A novel approach for the extraction of an alternative clustering of high quality and high dissimilarity. In *IEEE International Conference on Data Mining (ICDM)*, pages 53–62, 2006.

[6] G. Baloglou. *Isometrica: A Geometrical Introduction Planar Crystallographic Groups*. SUNY, 2007.

[7] N. V. Belov and T. N. Tarkhova. In *Colored Symmetry*, pages 211–219. Macmillan, 1964.

[8] T. Berg and P. N. Belhumeur. How do you tell a blackbird from a crow? In *International Conference on Computer Vision (ICCV)*, pages 9–16, 2013.

[9] T. Berg, J. Liu, S. W. Lee, M. L. Alexander, D. W. Jacobs, and P. N. Belhumeur. Birdsnap: Large-scale fine-grained visual categorization of birds. In *IEEE Conference on Computer Vision and Pattern Recognition*, pages 2019–2026, 2014.

[10] T. L. Berg, A. C. Berg, and J. Shih. Automatic attribute discovery and characterization from noisy web data. In *European Conference on Computer Vision: Part I*, pages 663–676, 2010.

[11] J. Chen, Y. Cui, G. Ye, D. Liu, and S. Chang. Event-driven semantic concept discovery by exploiting weakly tagged internet images. In *International Conference on Multimedia Retrieval*, pages 1:1–1:8, 2014.

[12] H. S. M. Coxeter. In *M. C. Escher: Art and Science*, pages 15–33. North-Holland, 1986.

[13] X. H. Dang and J. Bailey. Generation of alternative clustering using the CAMI approach. In *SIAM International Conference on Data Mining (SDM)*, pages 118–129, 2010.

[14] I. Davidson and Z. Qi. Finding alternative clusterings using constrainsts. In *IEEE International Conference on Data Mining (ICDM)*, pages 773–778, 2008.

[15] I. Davidson, S. S. Ravi, and L. Shamis. A SAT-based framework for efficient constrained clustering. In *SIAM International Conference on Data Mining (SDM)*, pages 94–105, 2010.

[16] C. Doersch, S. Singh, A. Gupta, J. Sivic, and A. A. Efros. What makes paris look like paris? *ACM Transactions on Graphs*, 31(4):101:1–101:9, 2012.

[17] R. Eisenman and J. Rappaport. Complexity preference and semantic differential ratings of complexity-simplicity and symmetry-asymmetry. *Psychonomic Science*, 7(4):147–148, 1967.

[18] U. Fayyad, G. Piatetsky-Shapiro, and P. Smyth. Knowledge discovery and data mining: Towards a unifying framework. In *ACM International Conference on Knowledge Discovery and Data Mining (KDD)*, pages 82–88, 1996.

[19] É. Galois. OEuvres mathématiques d'Évariste galois. *Journal des Mathématiques Pures et Appliquées*, XI:381–444, 1846.

[20] E. Garces, A. Agarwala, D. Gutierrez, and A. Hertzmann. A similarity measure for illustration style. *ACM Transactions on Graph*, 33(4):93:1–93:9, 2014.

[21] D. Gondek and T. Hoffman. Non-redundant data clustering. In *IEEE International Conference on Data Mining (ICDM)*, pages 75–82, 2004.

[22] D. Gondek and T. Hoffman. Non-redundant clustering with conditional ensembles. In *ACM Conference on Knowledge Discovery and Data Mining (SIGKDD)*, pages 70–77, 2005.

[23] B. Grünbaum. What symmetry groups are present in the Alhambra? *American Mathematical Society*, 53(6):670–673, 2006.

[24] B. Grünbaum, Z. Grünbaum, and G. C. Shepard. Symmetry in Moorish and other ornaments. *Computers and Mathematics with Applications*, 12(3-4, Part2):641 – 653, 1986.

[25] B. Grünbaum and G. C. Shephard. *Tilings and Patterns.* Freeman, 1987.

[26] S. Günnemann, I. Färber, M. Müller, and T. Seidl. Asclu: Alternative subspace clustering. In *International Workshop on Discovering, Summarizing and Using Multiple Clusterings (MultiClust 2010) in conjunction with 16th ACM SIGKDD Conference on Knowledge Discovery and Data Mining (KDD)*, 2010.

[27] G. Heidemann. Focus-of-attention from local color symmetries. *IEEE Transactions on Pattern Analysis and Machine Intelligence*, 26(7):817–830, 2004.

[28] N. F. M. Henry and G. C. Lonsdale. *International Tables for X-Ray Crystallography.* Kynoch Press, 1952.

[29] Y. Jae Lee and a. H. M. Efros, A. A. Style-aware mid-level representation for discovering visual connections in space and time. In *IEEE International Conference on Computer Vision, ICCV*, pages 1857–1864, 2013.

[30] Y. Jae Lee and K. Grauman. Learning the easy things first: Self-paced visual category discovery. In *IEEE International Conference on Computer Vision and Pattern Recognition, CVPR*, pages 1721–1728, 2011.

[31] Y. Jae Lee and K. Grauman. Object-graphs for context-aware category discovery, 2012.

[32] C. S. Kaplan. *Introductory Tiling Theory for Computer Graphics.* Morgan & Claypool Publishers, 2009.

[33] C. S. Kaplan and D. H. Salesin. Escherization. In *Computer Graphics and Interactive Techniques*, pages 499–510, 2000.

[34] M. Kazhdan, B. Chazelle, D. Dobkin, A. Finkelstein, and T. Funkhouser. A reflective symmetry descriptor. In *European Conference on Computer Vision (ECCV*, pages 642–656, 2002.

[35] M. Kazhdan, B. Chazelle, D. Dobkin, T. Funkhouser, and S. Rusinkiewicz. A reflective symmetry descriptor for 3d models. *Algorithmica*, 38(1):201–225, 2003.

[36] Y. Keller and Y. Shkolnisky. A signal processing approach to symmetry detection. *Transactions on Image Processing*, 15(8):2198–2207, 2006.

[37] N. Kiryati and Y. Cofman. Detecting symmetry in grey level images: The global optimization approach. *International Journal on Computer Vision*, 29(1):29–45, 1998.

[38] G. Kootstra, A. Nederveen, and B. d. Boer. Paying attention to symmetry. In *British Machine Vision Conference*, pages 111.1–111.10, 2008.

[39] S. Lee, R. Collins, and Y. Liu. Rotation symmetry group detection via frequency analysis of frieze-expansions. In *IEEE Conference on Computer Vision and Pattern Recognition (CVPR*, pages 1–8, 2008.

[40] S. Lee and Y. Liu. Skewed rotation symmetry group detection. *IEEE Transactions on Pattern Analysis and Machine Intelligence*, 32(9):1659–1672, 2010.

[41] S. Lee and Y. Liu. Curved glide-reflection symmetry detection. *IEEE Transactions on Pattern Analysis and Machine Intelligence*, 34(2):266–278, 2012.

[42] H. Li, H. Zhang, Y. Wang, J. Cao, A. Shamir, and D. Cohen-Or. Curve style analysis in a set of shapes. *Computer Graphics Forum*, 32(6):77–88, 2013.

[43] J. Liu and Y. Liu. Curved reflection symmetry detection with self-validation. In *Asian Conference on Computer Vision - Volume Part IV*, pages 102–114, 2010.

[44] Y. Liu and R. Collins. Frieze and wallpaper symmetry groups classification under affine and perspective distortion. Technical report, Robotics Institute, 1998.

[45] Y. Liu and R. Collins. Periodic pattern analysis under affine distortions using wallpaper groups. In *2nd International Workshop on Algebraic Frames for the Perception Action Cycle (AFPAC)*, pages 241 – 250. Springer-Verlag Belin, 2000.

[46] Y. Liu, R. T. Collins, and Y. Tsin. A computational model for periodic pattern perception based on frieze and wallpaper groups. *IEEE Transactions on Pattern Analysis and Machine Intelligence*, 26(3):354–371, 2004.

[47] Y. Liu, Y. Pu, and D. Xu. Computer analysis for visual art style. In *SIGGRAPH Asia 2013 Technical Briefs*, pages 9:1–9:4, 2013.

[48] P. Locher and C. Nodine. The perceptual value of symmetry. *Computers and Mathematics with Applications*, 17(4-6):475–484, 1989.

[49] T. Lombardi. *The Classification of Style in Painting*. VDM Verlag.

[50] D. G. Lowe. Distinctive image features from scale-invariant keypoints. *International Journal of Computer Vision*, 60(2):91–110, 2004.

[51] G. Loy and J. Eklundh. Detecting symmetry and symmetric constellations of features. In *European Conference on Computer Vision - Volume Part II*, pages 508–521, 2006.

[52] L. Lucchese. Frequency domain classification of cyclic and dihedral symmetries of finite 2-d patterns. *Pattern Recognition*, 37(12):2263–2280, 2004.

[53] E. Makovisky. Symmetrology of art:colored and generalized symmetries. *Computers and Mathematics with Applications*, 12B(3-4):949–980, 1986.

[54] P. Niggli. Die flächensymmetrien homogener diskontinuen. *Zeitschrift für Kristallographie*, 60:283–298, 1924.

[55] P. Niggli. Die regelmässige punktverteilung längs einer geraden in einer ebene. *Zeitschrift für Kristallographie*, 63:255–274, 1926.

[56] N. Otsu. A threshold selection method from gray-level histograms. *IEEE Transactions on Systems, Man and Cybernetics*, 9(1):62–66, 1979.

[57] M. Ovsjanikov, J. Sun, and L. Guibas. Global intrinsic symmetries of shapes. In *Symposium on Geometry Processing*, pages 1341–1348, 2008.

[58] J. Podolak, P. Shilane, A. Golovinskiy, S. Rusinkiewicz, and T. Funkhouser. A planar-reflective symmetry transform for 3d shapes. *ACM Transactions on Graphs*, 25(3):549–559, 2006.

[59] G. Polya. Über die analogie der kristallsymmetrie in der ebene. *Zeitschrift für Kristallographie*, 60(1):278–282, 1924.

[60] B. Prasad, V. S. N. amd Yegnanarayana. Finding axes of symmetry from potential fields. *IEEE Transactions on Image Processing*, 13(12):1559–1566, 2004.

[61] V. S. N. Prasad and L. S. Davis. Detecting rotational symmetries. In *IEEE International Conference on Computer Vision - Volume 2*, pages 954–961, 2005.

[62] S. Reddy and Y. Liu. On improving the performance of the wallpaper symmetry group classification algorithm. Technical report, Robotics Institute, 2005.

[63] D. Reisfeld, H. Wolfson, and Y. Yeshurun. Context free attentional operators: the generalized symmetry transform. *International Journal of Computer Vision*, 14:119–130, 1995.

[64] J. Richter-Gebert. Science-to-touch. `http://www.science-to-touch.com/en/index.html`, 2012.

[65] R. M. Rustamov. Augmented symmetry transforms. In *IEEE International Conference on Shape Modeling and Applications*, pages 13–20, 2007.

[66] D. Schattschneider. The plane symmetry groups: Their recognition and notation. *The American Mathematical Monthly*, 85(6):439–450, 1987.

[67] D. Schattschneider. *M.C. Escher: Visions of Symmetry.* Thames & Hudson, 2004.

[68] M. Senechal. Coloring symmetrical objects symmetrically. *Mathematical Association of America*, 56(1):3–16, 1983.

[69] M. Senechal. Color symmetry. *Computers and Mathematics with Applications*, 16(5-8):545–553, 1988.

[70] L. Shamir and J. A. Tarakhovsky. Computer analysis of art. *Journal on Computing and Cultural Heritage*, 5(2):7:1–7:11, 2012.

[71] A. O. Shepard. *The Symmetry of Abstract Design with Special Reference to Ceramic Decoration.* Carnegie Institution of Washington, 1948.

[72] Y. Song, P. L. Rosin, P. M. Hall, and J. Collomosse. Arty shapes. In *Eurographics Conference on Computational Aesthetics in Graphics, Visualization and Imaging*, pages 65–72, 2008.

[73] P. S. Stevens. *Handbook of Regular Patterns: An Introduction to Symmetry in Two Dimensions.* MIT Press, 1980.

[74] C. Sun and D. Si. Fast reflectional symmetry detection using orientation histograms. *Real-Time Imaging*, 5(1):63–74, 1999.

[75] S. Tari. Hierarchical shape decomposition via level sets. In *Mathematical Morphology and Its Applications*, pages 215–225, 2009.

[76] J. B. Tenenbaum and W. T. Freeman. Separating style and content with bilinear models. *Neural Compututation*, 12(6):1247–1283, 2000.

[77] L. J. P. van der Maaten and G. E. Hinton. Visualizing high-dimensional data using t-SNE. *Machine Learning Research*, 9:2579–2605, 2008.

[78] M. von Gagern and J. Richter-Gebert. Hyperbolization of ornaments. *The Electronic Journal of Combinatorics*, 2009.

[79] W. T. W. *The Mathematical Theory of Chromatic Plane Ornaments.* Marcel Dekker, 1982.

[80] D. K. Washburn and D. W. Crowe. *Symmetries of Culture:Theory and Practice of Plane Pattern Analysis.* University of Washington Press, 1988.

[81] M. Wigness, B. A. Draper, and J. R. Beveridge. Selectively guiding visual concept discovery. In *IEEE Winter Conference on Applications of Computer Vision*, pages 247–254, 2014.

[82] K. Xu, H. Li, H. Zhang, D. Cohen-Or, Y. Xiong, and Z. Cheng. Style-content separation by anisotropic part scales. *ACM Transactions on Graphics*, 29(6):184:1–184:10, 2010.

[83] B. Yang and D. Xu. Studying the aesthetic visual style of paintings by multi-cues. *Advances in Information Sciences and Service Sciences (AISS)*, 4(11):193–200, 2012.

[84] H. Zabrodsky, S. Peleg, and D. Avnir. Hierarchical symmetry. In *Pattern Recognition: Image, Speech, and Signal Analysis*, pages 9–12, 1992.

[85] H. Zabrodsky, S. Peleg, and D. Avnir. Symmetry as a continuous feature. *IEEE Transactions on Pattern Analysis and Machine Intelligence*, 17(12):1154–1166, 1995.

[86] M. Zhao and S. Zhu. Sisley the abstract painter. In *International Symposium on Non-Photorealistic Animation and Rendering*, pages 99–107, 2010.

APPENDIX A

NOTATIONS FOR TWO-COLOR TILINGS

TableA.1: Notations for Two-Color Tilings.

Belov and Tarkhova	**Coxeter type-/subtype**	**Grünbaum and Shephard**
p'_b1	$p1/p1$	$p1[2]$
pg'	$pg/p1$	$pg[2]_1$
p'_b1g	pg/pg	$pg[2]_2$
p'_bm	$pm/pm(m)$	$pm[2]_3$
p'_b1m	$pm/pm(m')$	$pm[2]_5$
$c'm$	pm/cm	$pm[2]_2$
pm'	$pm/p1$	$pm[2]_4$
p'_bg	pm/pg	$pm[2]_1$
p'_cm	cm/pm	$cm[2]_3$
cm'	$cm/p1$	$cm[2]_1$
p'_cg	cm/pg	$cm[2]_2$
p'_b2	$p2/p2$	$c2[2]_2$
$p2'$	$p2/p1$	$c2[2]_1$
pgg'	pgg/pg	$pgg[2]_1$
$pg'g'$	$pgg/p2$	$pgg[2]_2$
$pm'g'$	$pmg/p2$	$pmg[2]_5$
$pm'g$	pmg/pg	$pmg[2]_2$
p'_bgg	pmg/pgg	$pmg[2]_3$

TableA.1: Continued.

Belov and Tarkhova	**Coxeter type-/subtype**	**Grünbaum and Shephard**
pmg'	pmg/pm	$pmg[2]_4$
$p'_b mg$	pmg/pmg	$pmg[2]_1$
$c'mm$	pmm/cmm	$pmm[2]_3$
$p'_b mm$	pmm/pmm	$pmm[2]_1$
pmm'	pmm/pm	$pmm[2]_2$
$p'_b gm$	pmm/pmg	$pmm[2]_4$
$pm'm'$	$pmm/p2$	$pmm[2]_5$
$p'_c mm$	cmm/pmm	$cmm[2]_5$
$p'_c mg$	cmm/pmg	$cmm[2]_3$
cmm'	cmm/cm	$cmm[2]_2$
$cm'm'$	$cmm/p2$	$cmm[2]_4$
$p'_c gg$	cmm/pgg	$cmm[2]_1$
$p4'$	$p4/p2$	$p4[2]_2$
$p'_c 4$	$p4/p4$	$p4[2]_1$
$p'_c 4mm$	$p4m/p4m$	$p4m[2]_5$
$p4'mm'$	$p4m/pmm$	$p4m[2]_4$
$p4'm'm$	$p4m/cmm$	$p4m[2]_3$
$p4m'm'$	$p4m/p4$	$p4m[2]_2$
$p'_c 4gm$	$p4m/p4g$	$p4m[2]_1$
$p4g'm'$	$p4g/p4$	$p4g[2]_1$
$p4'g'm$	$p4g/cmm$	$p4g[2]_2$
$p4'gm'$	$p4g/pgg$	$p4g[2]_3$
$p3m'$	$p3m1/p3$	$p3m1[2]$
$p31m'$	$p31m/p3$	$p31m[2]$
$p6'$	$p6/p3$	$p6[2]$
$p6'm'm$	$p6m/p31m$	$p6m[2]_1$

TableA.1: Continued.

Belov and Tarkhova	**Coxeter type-/subtype**	**Grünbaum and Shephard**
$p6'mm'$	$p6m/p3m1$	$p6m[2]_2$
$p6m'm'$	$p6m/p6$	$p6m[2]_3$

CURRICULUM VITAE

PERSONAL INFORMATION

Surname, Name: Adanova, Venera

Nationality: Kyrgyz (KR)

Date and Place of Birth: 16.04.1984, Kyrgyz Republic

Marital Status: Married

Phone: +90 (553) 1585170

EDUCATION

Degree	Institution	Year of Graduation
M.S.	Middle East Technical University	2008
B.S.	Kyrgyzstan Turkey Manas University	2005
High School	Jalalabad KTGS	2001

PUBLICATIONS

1. V. Adanova and S. Tari. Beyond symmetry groups: a grouping study on Escher's Euclidean ornaments. *In SIGGRAPH Asia 2014 Creative Shape Modeling and Design (SA '14)*, ACM, pages 1-8, 2014.

2. V. Adanova and S. Tari. Beyond symmetry groups: A grouping study on Escher's Euclidean ornaments. *Graphical Models* (2015), http://dx.doi.org/10.1016/j.gmod.2015.09.001